Defining Lineage Potential and Fate Behaviour of Progenitors During Pancreas Development

Magdalena Katarzyna Sznurkowska

Clare College

Department of Oncology, University of Cambridge

This dissertation is submitted for the degree of Doctor of Philosophy.

September 2017

For my Grandma, Babcia Gusia.

Dla Babci Gusi.

Declaration

I hereby declare that except where specific reference is made to the work of others, the contents of this dissertation are original and have not been submitted in whole or in part for consideration for any other degree or qualification in this, or any other university. This dissertation is my own work and contains nothing, which is the outcome of work done in collaboration with others, except as specified in the text. This dissertation contains fewer than 60,000 words, and has fewer than 150 figures.

Acknowledgements

Firstly, I would like to wholeheartedly thank my supervisors, Anna Philpott and Ben Simons, who continuously inspired and supported me throughout the four years of my PhD. Scientific discussions with you always made me enthusiastic and motivated to work. I am also truly grateful for the fascinating project I was given a chance to work on.

I would also like to thank Edouard Hannezo, with whom I had the greatest pleasure to collaborate. I really enjoyed your enthusiasm, involvement, inquisitiveness and efficiency. Good luck with setting up your own group, but there is no doubt it will be a great success!

I am also very thankful to have been given the opportunity to collaborate with Steffen Rulands, and for his time explaining to me the principles of single cell sequencing bioinformatics analysis. I would like to thank Prof. Bertie Göttgens and Sonia Nestorowa for the fruitful collaboration on the single cell sequencing project.

I would like to acknowledge all members of the Simons and Philpott group, and the Stem Cell Institute, for creating a great environment. Importantly, I am very grateful to Medical Research Council for funding my PhD.

Furthermore, I would like to thank all core facilities in the WT-MRC Cambridge Stem Cell Institute, for making my work efficient. In particular, Peter Humphreys, the microscopy geek and a friend, with the most sarcastic sense of humour. Thank you for always offering me support, be it help with the microscopy equipment or a drink at the end of a hard week. I am also indebted to the Animal Biofacility for the great help with animal experiments.

A special thank you goes to my fiancé and best friend, Axel, who has been a great support throughout the whole PhD. Apart from all the amazing memories we have had together, you have always made me laugh (even when I didn't feel like laughing at all), you have always critically listened to me, supported me at every step, and made me reach out beyond my comfort

zone. Thank you for your patience with me during this PhD journey, especially when I obsessed about work!

I would like to thank my family, Mama, Tata, Agatka, Babcia Krysia i Gusia, and the cats, Kasa i Amfa. Thank you for all your understanding during the PhD period and respecting the rule that “How is your PhD/publication going?” is a forbidden question. To my loving mum, who always thinks about everyone else but herself. Dziękuję za ciągłą troskę, rady, pomoc w planowaniu nauki na studiach i przed maturą, gdy ogarniała mnie panika, oraz za paczki z dobrym polskim jedzeniem. To my dad, who gave me an example of being an ambitious and constantly seeking self-improvement. To my sister, for always being supportive, listening. You are the coolest, smartest and most independent person, you are like a cat! (and you know that’s a compliment).

I would like to particularly thank my grandma, Babcia Gusia. For our “arguments” about physics and chemistry in secondary and high school. You inspired me to want to become a scientist, in order to try to understand this world better. I admire your intelligence, energy, cheerfulness, wisdom and stoicism. / Szczególnie dziękuję Babci Gusi. Za nasze “kłótnie” o fizyce i chemii w gimnazjum i liceum. Zainspirowałaś mnie, żeby zostać naukowcem, aby móc lepiej zrozumieć otaczający nas świat. Podziwiam Twoją inteligencję, energię, pogodę ducha, oraz mądrość i stoicyzm.

To my wonderful Cambridge friends, Jiho, Karol, Ewelina, Jake, Nick, Dominika, and many others (you know who you are!). You made my time in Cambridge absolutely unforgettable and I could always count on you. Thank you for all the fascinating conversations and all the fun we have had together. And thank you to all my cycling buddies, Jiho, Karol and Aga!

I would like to express my gratitude towards those friends who have critically proofread my thesis for English and common-sense mistakes: Jake, Nick and Axel; for formatting help: Matt; and for scientific content, Elsa, Ola and Tim! I really appreciate your time and insightfulness, and hope I can pay back by reading your theses in the future! Thanks to Carla for lending me her laptop when mine crashed. I would also like to thank the University of Cambridge Writing Group, which enabled me to write this thesis efficiently.

This is also the time to praise Cambridge as a whole, the best place to live, where I have had probably the best time in my life. The place of beautiful scenery, with the highest concentration of smart and fascinating people. I have been extremely privileged to spend four years of my life here. This is the first place besides my hometown, Sopot, that I have instantaneously called “home”. Cambridge, I’ve been mourning leaving you since March (2017), long before I even started writing my thesis, but I’ll be coming back!

Table of contents

List of Figures

List of Tables

Abstract

The specification of the pancreas into lineages has been extensively studied In particular, the focus has lied on molecular cues guiding the differentiation of cells into the endocrine lineage, because of the prevalence of diabetes mellitus. However, the mechanisms of 3D tissue growth and the interaction between the lineages in order to reach an organ of right size and composition are not understood.

In this project, I aim to characterise the dynamics and interaction of three pancreatic compartments, i.e. acinar, ductal, and islet lineage. I carry out clonal lineage tracing, followed by extensive quantitative analysis of clone sizes and tissue parameters. I combine this analysis with whole-mount EdU proliferative assay to study the kinetics during development, as well as single-cell RNA sequencing in order to gain molecular insight of the observed lineage tracing outcomes.

Firstly, I identify a rapid cell fate restriction of the tissue, starting already around E9.5 after the appearance of the pancreatic bud, with the bulk of cells being fully committed by E12.5 with persisting rare tripotent cells, followed by complete replenishment of tripotency beyond E15.5.

I then propose a mechanism explaining a coordinated morphogenesis of acinar, ductal and islet lineage. I identify ductal-ends as a niche proliferative environment carrying acinar-committed, ductal-committed together with rare multipotent precursors. With time, the multipotent precursors replenish. The mechanism of tissue growth involves ductal-end driven morphogenesis with stochastic decision between bifurcation and termination of a branch. Based on clonal data from various timepoints, I find that the most intense branching morphogenesis is taking place until E15.5 after which only a few rounds of branching are taking place.

Lastly, the analysis of islet associated clones and islet parameters enable me to determine some of the cellular mechanisms regulating islet size.

Altogether, I propose a novel model for coordinated lineage growth and development during pancreatic morphogenesis, which complements previous literature.

Chapter 1

Introduction

1.1 The Pancreas: structure and function

The pancreas, located behind the stomach and attached to the duodenum, is an organ essential for controlling nutrient metabolism. It possesses two functionally and morphologically different cell populations – the exocrine and endocrine tissue. The exocrine acinar cells amount to 90% of tissue mass (Benitez et al. 2012) and produce the pancreatic juice with enzymes necessary for the breakdown of proteins, carbohydrates and lipids. This secretion is transported via a system of ductal cells, known as pancreatic ducts, to be released into the duodenum. In addition to performing a digestive enzyme draining function, the mature duct cells produce bicarbonate (which neutralises acidic chyme entering the duodenum from the stomach) and mucins (components of mucus). The endocrine cells, in turn, are located in the Islets of Langerhans, which are embedded within the pancreatic exocrine tissue. The islets are associated with a network of blood vessels, neurons, and stromal components of mesodermal origin. The interaction between endocrine and vascular cells enables hormone release, therefore ensuring the regulation of blood glucose levels. The predominant two endocrine cell types are glucagon-producing α-cells and insulin-producing β-cells, responsible for increasing and decreasing blood glucose levels, respectively. The rarer three endocrine cell types are δ, ε and PP cells producing somatostatin, ghrelin and pancreatic polypeptide respectively – all associated with the control of diet and digestion. The structure and composition of the pancreas is presented in Figure 1.

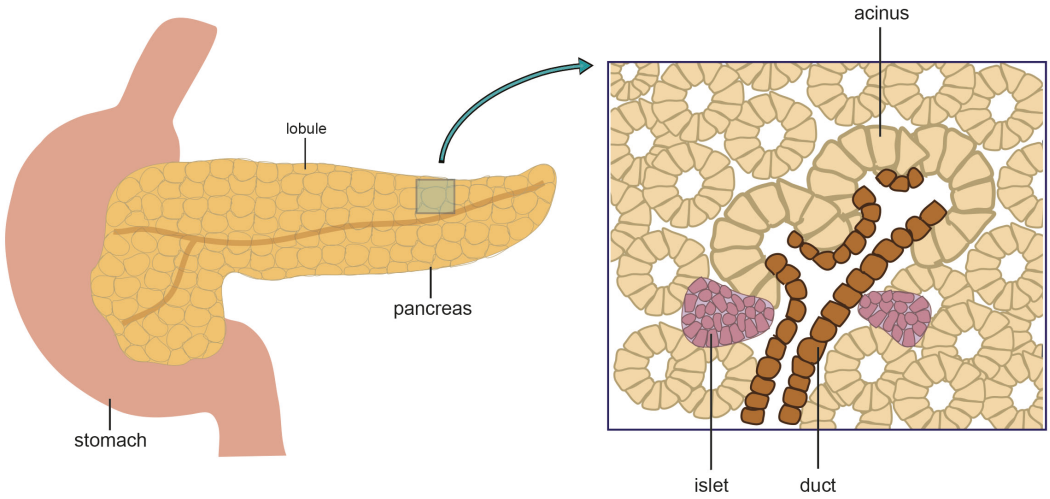

Figure 1. *Pancreatic structure. The pancreas is composed of exocrine and endocrine tissue. Exocrine acinar cells produce pancreatic juice containing enzymes for digestion of proteins, carbohydrates and lipids. The juice is transported via a system of ductal cells into duodenum. Endocrine cells producing hormones are located within the islets of Langerhans, which are embedded in the exocrine tissue.*

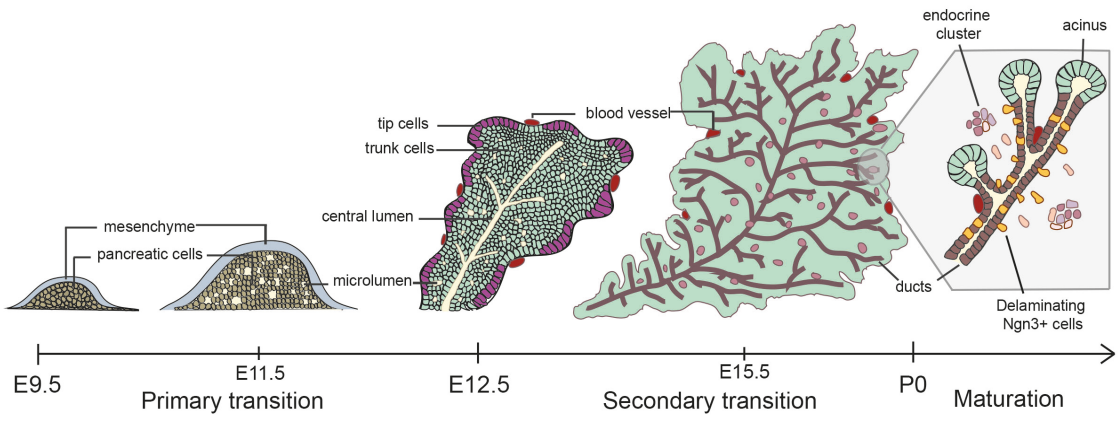

Figure 2. *Pancreas development is composed of two main phases: primary and secondary transition. Primary transition is characterised by rapid proliferation of cells leading to microlumen formation, and eventually specification of tip and trunk domains. Secondary transition is a phase of extensive tissue specification and remodelling, although proliferation continues. Endocrine, ductal and acinar tissues are specified.*

1.2 Pancreatic specification: phases

Pancreas specification is composed of a phase of pancreatic pre-patterning followed by the main developmental phases. Pre-patterning is an essential phase starting at around E8.5, which prepares the local environment for subsequent switching on of the pancreatic specification programmes and emergence of dorsal and ventral pancreas. Pancreatic development itself is composed of 3 phases, as distinguished by morphological and cell specification changes: primary transition between E9.5 and E12.5, secondary transition between E12.5 and birth, as well as maturation between birth and weaning (Fig. 2). Primary transition is characterised by extensive progenitor proliferation leading to microlumen formation. Towards the end of primary transition, the tip and trunk domain begin to appear (details in subsequent sections). Secondary transition is characterised by intense tissue specification and remodelling, concomitant with continued cell proliferation. In this phase the three pancreatic compartments – ductal, acinar and islet – are formed (Fig. 2, reviewed in Shih et al. 2013; Benitez et al. 2012; Pan & Wright 2011).

The growth and development continues in the neonatal pancreas, during the maturation phase in two waves. The first wave lasts until 2 weeks after birth (P15) and is characterised by proliferation of endocrine cells. The second phase, in turn, spans between P15 and P30 and is dominated by the proliferation of exocrine cells (Dore et al. 1981).

1.2.1 Pancreatic pre-patterning

Prior to the outgrowth of ventral and dorsal pancreatic buds, the pre-pancreatic region is specified around E8.5. Even though the two regions arise independently in two distinct locations, similar molecular programmes govern them. They both require Shh signalling exclusion, as well as retanoic acid and VEGF signalling (reviewed in Pan & Wright 2011)

The dorsal pre-pancreatic region formation is promoted firstly by signalling from the adjacent mesoderm during gastrulation, and later on by the signalling from the nearby notochord, dorsal aorta as well as the proliferative signals from the pancreatic mesenchyme. The ventral bud region, in turn, is

established in response to signals from the lateral plate mesoderm, cardiac mesoderm and septum transversum (details of signalling between the tissues in the next Chapter 1.2.1.1) (reviewed in Pan & Wright 2011).

1.2.1.1 Pancreatic pre-patterning: signalling in dorsal region

The notochord is an extrinsic factor absolutely essential for dorsal pancreatic endoderm specification and the two tissues are in close association around E8. The removal of the notochord perturbs dorsal pancreatic development (Apelqvist et al. 1997; Kim et al. 1997; Hebrok et al. 1998). The signals sent from the notochord seem to be permissive rather than instructive, as the tissue is incapable of inducing pancreatic gene expression in non-pancreatic regions (Kim et al. 1997). The notochord is thought to act on the endoderm via the repression of Shh pathway by the release of Activin-β and Tgf2 molecules (Hebrok et al. 1998). It has been shown that Shh is selectively excluded from pancreatic endoderm during normal specification, while removal of the notochord causes ectopic Shh expression (Apelqvist et al. 1997; Kim et al. 1997; Hebrok et al. 1998; reviewed in Pan & Wright 2011).

The influence of notochord is complemented by paraxial mesoderm, which induces retinoic acid (RA) signalling. RA signalling is necessary for proper pancreatic induction, as the absence of RA leads to pancreas agenesis in zebrafish as well as the lack of dorsal pancreas in *Xenopus* and mice (Martin et al. 2005; Molotkov et al. 2005; Stafford & Prince 2002). RA seems to act via Shh independent mechanisms, because loss of RA does not cause ectopic Shh expression in the pre-pancreatic region of mice (Martin et al. 2005).

At E8.5, the fusion of two dorsal aortae displaces the notochord away from the dorsal endoderm. At this stage, the dorsal pre-pancreatic region is in contact with vascular endothelium, which is absolutely necessary for the establishment of the pancreatic domain (Lammert et al. 2001; see Section 1.5.11 for more about the role of blood vessels in pancreas morphogenesis) and may promote the survival of dorsal mesenchyme, which produces Fgf10 and maintains Ptf1a expression and progenitor pool expansion (Jacquemin et al. 2006)

By E10, the mesenchyme has accumulated around dorsal pancreatic region, and the Fgf10 expression is very high, which stimulates the bud outgrowth and proliferation of pancreatic progenitor cells (reviewed in Shih et al. 2013 and Pan & Wright 2011).

1.2.1.2 Pancreatic pre-patterning: signalling in ventral region

The ventral pre-pancreatic endoderm initially receives instructive signals from the adjacent lateral plate mesoderm, which include BMP, RA, or activin (Kumar & Melton 2003). Later, around E8, the region is under inhibitory influence of cardiac mesoderm and septum transversum mesenchyme (reviewed in Pan & Wright 2011).

The cardiac mesoderm induces hepatic differentiation via Fgf signalling (reviewed in Pan & Wright 2011). Indeed, in the absence of the cardiac mesoderm Fgf signalling alone is capable of hepatic differentiation induction in endodermal explants. The prevention of Fgf signalling from the cardiac mesoderm renders the ventral region unable to acquire the hepatic fate, whilst acquiring the pancreatic fate (Jung et al. 1999). Similarly, the septum transversum produces BMP, an inhibitory signal, which then enhances the Gata-4 expression and acts in parallel with Fgf signal from the cardiac mesoderm to induce the liver cell fate (Rossi et al. 2001). Altogether, this suggests that the default fate of cells in that region is to become pancreatic cells, and only active signalling from the cardiac mesoderm can redirect the cells towards the hepatic differentiation pathway.

The important question is then how the pancreas can be formed in the presence of such inhibitory signals. It has been suggested that the proliferation of Hhex positive cells at the leading edge of endoderm promotes the movement away from the cardiac mesoderm (Bort et al. 2004). Indeed, blocking the movement of the lateral ventral endoderm prevents the specification of the ventral pancreas (Bort et al. 2004). Hence, tissue migration might be a mechanism in which cells avoid inhibitory signals.

Additionally, RA and Sonic Hedgehog (Shh) may also play an important role, since differentiation protocols using RA and the inhibitor of Shh and BMP are able to induce pancreatic identity *in vitro* (D'Amour et al. 2006).

Two other factors that may be responsible for decision between pancreatic and hepatic cell fate determination are Sox17 and Hes1. Sox17 is responsible for establishing the boundary between liver, extrahepatobiliary (EHB, including gall bladder primordium, bile and cystic duct) system and ventral pancreas region. Loss of *Sox17* causes biliary abnormalities and ectopic pancreas formation, while *Sox17* miss-expression supresses pancreatic development by promoting the biliary-like tissue formation (Kanai-Azuma et al. 2002). Hence, it appears that Sox17 acts as a pancreas inhibitory and biliary promoting factor. How then can the pancreas be formed from endoderm exposed to Sox17? It has been suggested that Sox17 may up-regulate expression of the key player, Hes1, in Pdx1-expressing endoderm. Hes1 then restricts formation of Sox17+ biliary progenitors in a negative feedback loop to the ventral foregut, in this way creating the boundary between EHB and the ventral pancreas (reviewed in Pan & Wright 2011; Spence et al. 2009).

At E8.5, the gut tube is already formed and the ventral region of prospective pancreas comes in proximity to vitelline veins. The vitelline vascular cells produce VEGF, which induces Pdx1 and Ptf1a expression - transcription factors necessary for acquiring the pancreatic cell fate (reviewed in Pan & Wright 2011)

1.2.2 Primary transition: main developmental events

The primary transition starts with the emergence of ventral and dorsal epithelial buds on two sides of the foregut endoderm – around E9.5 and E10 respectively. It is a phase characterised by huge morphogenic changes – caused by high proliferation of progenitor cells, followed by microlumen formation and their subsequent coalescence (Villasenor et al. 2010; Kesavan et al. 2009). The morphological changes are accompanied by the compartmentalisation of the organ into tip and trunk domain at the end of primary transition.

The tip domain contains the multipotent pancreatic cells (MPCs) that have the potential to differentiate into acinar, ductal or endocrine cells. The trunk epithelium, in turn, is composed of endocrine-duct bipotent progenitors. In this phase already the first differentiated endocrine cells of the dorsal pancreatic bud start to appear and they are mainly the glucagon-producing α-cells (Johansson et al. 2007).

The dorsal and ventral buds elongate along the presumptive duodenum and stomach, and eventually fuse into a single organ by the end of the phase at E12.5 as a result of the coiling of the intestine. At this stage the undifferentiated epithelium is tightly surrounded by mesenchymal tissue (reviewed in Shih et al. 2013).

1.2.2.1 Signalling events in primary transition: establishing and maintaining pancreatic identity

After the ventral and dorsal domains have emerged, several transcription factors specific for the pancreatic region start being expressed. The earliest include Pdx1, Ptf1a and Sox9. Transcription factors *Gata 4*/6, Foxa1/2, Elf2, Onecut 1/2, Hes1, Prx1, Mnx1 are also expressed, but their expression is broader and present throughout the foregut endoderm (reviewed in Pan & Wright 2011). Each individual factor from this group is not essential for the initiation of pancreatic development, i.e. budding still occurs when one of them is not expressed (reviewed in Pan & Wright 2011). However, they play a very important role in determining and maintaining pancreatic cell fate. For example, *Ptf1a* deficient cells reallocate to duodenal and bile duct endoderm fate according to lineage tracing studies (Burlison et al. 2008; Kawaguchi et al. 2002). The gain of function experiments, in turn, reveal an instructive role of Pdx1 and Ptf1a, since their constitutively active expression in the liver redirected these cells to a pancreatic fate (Afelik et al. 2006). The extent to which these factors expression in adult non-pancreatic cells could shift them towards the pancreatic fate should be studied.

Importantly, the transcription factors, mentioned above, function in networks. Even though the deletion might not affect the initial budding of the tissue, it very often affects the general development of the organ. For instance, cross-

talk between *Sox9, Pdx1, Hes1* and *Ptf1a*, as well as the effect of deletion of any of these, has been described (Hale et al. 2005; Seymour et al. 2007; Thompson et al. 2012).

The requirement for specific transcription factors for establishment and maintenance of pancreatic identity is relatively well studied; however less is understood about the control of their expression. Notch signalling is considered a key regulator, as it has been shown to influence Hes1 and Sox9 levels (Kageyama et al. 2007; Shih et al. 2012). Embryos deficient in the Notch effector RBP-jk showed pancreatic growth arrest, with the phenotype similar to *Hes1* or *Sox9* deletion (Apelqvist et al. 1999; Fujikura et al. 2006; Jensen et al. 2000). *Hes1* deletion caused up-regulation of cell cycle inhibitor p57 in pancreatic progenitors (Georgia et al. 2006), which suggests a link between Notch signalling and pancreatic-specific transcription factors as well as the cell cycle control.

Another signalling cue playing an important role in the initial stages of pancreatic development is Fgf signalling. Fgf10 is highly expressed in mesenchyme, while the respective receptor Fgfr2 is present throughout the pancreatic epithelium (Bhushan et al. 2001; Dichmann et al. 2003; Seymour et al. 2012). Gain and loss of function experiments have shown that Fgf10 is required for cell proliferation and thus the growth of the pancreatic bud (Bhushan et al. 2001). Fgf10 regulates Ptf1a and Sox9 expression (Jacquemin et al. 2006; Seymour et al. 2012) and therefore its deletion shows the same phenotype as *Ptf1a* and *Sox9* knockout pancreatic buds (Bhushan et al. 2001; Seymour et al. 2007). In general there is a feed forward loop between Sox9, Fgfr2 and Fgf10. Mesenchymal Fgf10 maintains epithelial Sox9 expression. Sox9, in turn, cell-autonomously controls Fgfr2 levels and hence the receptivity of the cells to Fgf10 (Seymour et al. 2012). If the loop is disrupted at any point during pancreatic development, the cells fail to maintain their identity and liver genes are activated (Seymour et al. 2012; reviewed in Shih et al. 2013).

Lastly, EGF, Wnt and BMP pathways also regulate pancreatic progenitor maintenance. The Wnt and the BMP signalling seem to take place between

pancreatic epithelium and the surrounding mesenchymal tissue (Jonckheere et al. 2008; Ahnfelt-Rønne et al. 2010), but it is not understood if the ligands are secreted by epithelium or the mesenchyme. The importance of mesenchyme has been demonstrated in a study, whereby pancreatic explants *in vitro* do not persist in the absence of mesenchyme, while co-culture of pancreatic cells with mesenchymal tissue leads to progenitor expansion (Bhushan et al. 2001). It appears that multiple factors are involved and work in loops, as co-culture of pancreatic lineage intermediates grown with single factors or combinations of them does not succeed in effective progenitor expansion (Sneddon et al. 2012).

1.2.2.2 Signalling events in primary transition: tip-trunk specification

Before the onset of secondary transition, the epithelial cells of the developing pancreas are multipotent precursor cells (MPCs). At about E12.5 tip-trunk segregation is taking place. The organ grows rapidly, which is accompanied by structural changes, and protrusions from the edges arise. These protrusions are the tips and are Ptf1a+, c-Myc+, Cpa+. The inner cells are referred to as the trunk cells and express Nkx6.1/6.2, Sox9, Tcf2, Onecut-1, Prox1 and Hes1 (see Fig. 3; reviewed in Shih et al. 2013). Lineage tracing has shown that the trunk cells become endocrine and ductal cells predominantly, while the tips will contribute to acinar lineage later on in secondary transition (see Fig. 3; Kopinke et al. 2011; Kopp et al. 2011).

The cell fate decision between becoming a tip or a trunk cell is a process regulated by co-repression of NKx6.1/6.2 and Ptf1a – two transcription factors initially co-expressed in MPCs. Nkx6.1/6.2 promote trunk identity, while Ptf1a directs the cells towards the tip fate (Schaffer et al. 2010) (See Fig. 3).

Importantly, what is the mechanism that makes one master regulator overcome another in a cross-repression and therefore cause the cells to gain either tip or trunk identity? Notch signalling is a candidate pathway for the control of this decision. Repression of Notch causes excessive tip formation at a cost of trunk cells (Afelik et al. 2012). The constitutive activation of Notch, in turn, prevents tip formation and causes the expansion of trunk cells partly by activating trunk marker Nkx6.1 (Afelik et al. 2012; Esni et al. 2004). Hence it

appears that Notch plays a very important role in the tip-trunk decision process. Factors controlling Notch activity, however, are not well understood.

1.2.3 Secondary transition: main developmental events

The secondary transition phase takes place between E12.5 and birth, and is characterised by continued morphogenesis and expansion of pancreatic epithelium as well as endocrine, acinar and ductal specification and tissue remodelling. The potential of the tip compartment is now limited to the production of acinar cells. The trunk domain gives rise to ductal cells and endocrine-committed cells – endocrine precursors delaminate from the emerging ductal structures following Ngn3 expression, while the left-behind cells mature to become functional ductal cells. The process of delamination is poorly understood, but is considered to involve an epithelial-to-mesenchymal transition (Rukstalis & Habener 2007). By the end of secondary transition, the pancreas has acquired the organisation of the adult tissue to a significant extent. The acinar cells are clustered at the ends of the ductal network, while the endocrine cells are located within the Islets of Langerhans and distributed throughout the exocrine tissue.

1.2.4 Signalling events in secondary transition: acinar specification

Tip cells of the secondary transition become unipotent precursors of acinar cells. Acinar differentiation is driven by transcription factors Ptf1a, Rbp-jl and Nr5a2 (reviewed in Shih et al. 2013). Ptf1a interacts with Rbp-jl and this complex establishes the acinar phenotype by activating essential acinar genes, such as those encoding digestive enzymes, proteins required for exocytosis and zymogen granules production, as well as Ptf1a and Rbp-jl themselves as a part of an auto-activation loop (reviewed in Shih et al. 2013).

Nr5a2, on the other hand, is a direct target of Ptf1a. It binds to and activates a similar set of genes as the Nr5a2-Rbp-jl complex. Even though Ptf1a plays a very important role in acinar specification, its forced expression is insufficient to induce acinar cell differentiation (Schaffer et al. 2010). This suggests that other factors acting in parallel may be required. Candidates include Mist1, which is highly expressed in acinar cells but independent of PTF1-L transcriptional activation (Masui et al. 2010). *Mist1* deficient mice show loss of

cell polarity and defective exocytosis in acini (Pin et al. 2001). Genome wide analysis of Mist1 target genes should reveal if there are any overlapping targets between Mist1 and PTF1-L complex and hence whether the two could work in conjunction (Reviewed in Shih et al. 2013).

By E15.5 most tip cells have undergone acinar differentiation and their expansion is mainly driven by proliferation (reviewed in Shih et al. 2013). The molecular mechanisms behind specification of progenitors into the acinar lineage has been studied extensively, however, the factors responsible for rapid divisions of specified cells until birth are not well understood. Mist1 and Ptf1a are considered negative regulators of proliferation. Nr5a2 has been shown to promote divisions (Benod et al. 2011; Botrugno et al. 2004). Other candidates include c-myc ad β-catenin, the inactivation of which in early pancreatic progenitor stage results in acinar cell hypoplasia (Bonal et al. 2009; Murtaugh et al. 2005; Nakhai et al. 2008; Wells et al. 2007; reviewed in Shih et al. 2013).

1.2.5 Signalling events in secondary transition: ductal-islet cell fate choice

Ductal and islet lineages derive from the pancreatic trunk. The key driver of cell fate choice between ductal and islet fate choice is Ngn3, a basic helix-loop helix transcription factor and a master regulator of endocrine differentiation. Only a small fraction of trunk cells express Ngn3. Trunk cells that do not activate Ngn3 stay behind and become ductal tree. Therefore, the control of Ngn3 is critical in the decision between endocrine and ductal cell fate.

It is not fully understood how Ngn3 is repressed in the majority of the trunk cells. One possible mechanism might be via repression by Hes1. One study suggested that Hes1 accelerates the degradation of Ngn3 (Qu et al. 2013). This is in line with the finding of Villasenor et al., whereby Ngn3 mRNA displays a much broader expression than the protein, suggesting post-transcriptional/translational regulation (Villasenor et al. 2008).

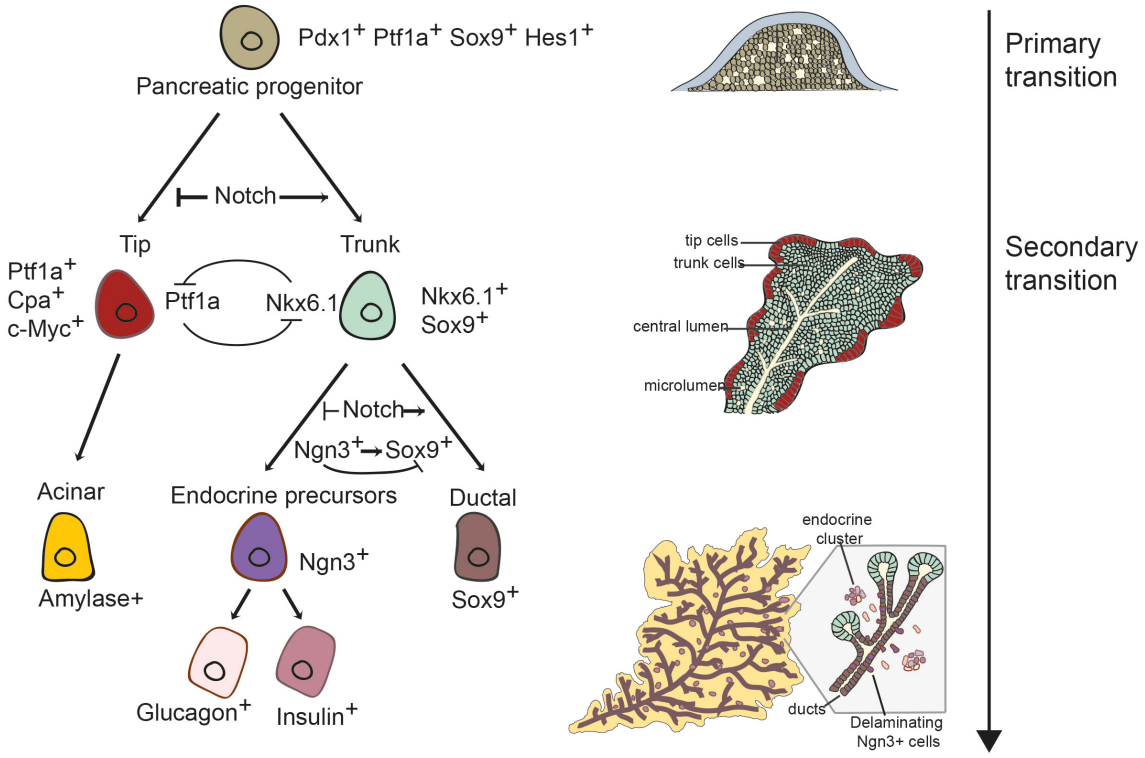

Figure 3. *Signalling events leading to specification of endocrine and exocrine pancreatic lineages are accompanied by morphological changes (adapted from Shih et al. 2013, see Fig. 2). Pdx1+ Ptf1a+ Sox9+ Hes1+ progenitors gradually specify into either tip or trunk domain, regulated by Notch signalling and Ptf1a – Nkx6.1 cross-repression. The Ptf1a+ Cpa+ c-Myc+ cells will later specify into acinar lineage. The Nkx6.1+ Sox9+ cells will later specify into endocrine or ductal cells as regulated by Notch signalling, as well as Ngn3-Sox9 cross-repression. The right side of the schematic presents morphological events accompanying the specification of the pancreas.*

An alternative control mechanism may occur via Notch signalling. Constitutively active Notch signalling prevents *Ngn3* gene activation and enhances ductal differentiation (Greenwood et al. 2007; Murtaugh et al. 2003). This suggests that Notch signalling is switched off in order for endocrine differentiation to occur, however, a set of studies have shown that Notch activates both positive and negative regulators of Ngn3 (Fig. 3; Shih et al. 2012). The solution to this apparent inconsistency may lie in the intensity of Notch signalling. High Notch levels activate Hes1 and Sox9, which inhibit Ngn3. Lower Notch signalling levels, however, activate Sox9 exclusively, which then activates Ngn3 (see schematic in Fig. 3; Shih et al. 2012). How the variable intensity of Notch signalling is regulated during development is not understood.

When the progenitor cells become hormone producing endocrine cells, their gene expression profile changes. Ngn3 dependent factors are expressed, such as Pax4, Arx, Rfx6, NeuroD1, Pax6, Isl1 and IA2, together with the expression of cell specific hormone genes (Shih et al. 2013). For instance, Ngn3 binds directly to promoters of β-cell specific transcription factors B2/NeuroD and Pax4 to promote differentiation into β-cells (Shih et al. 2013). Ngn3 expression ceases or becomes very low as the hormones start being produced (reviewed in Rukstalis & Habener 2009).

1.3 Lineage tracing in the pancreas: establishment of lineage hierarchy and search for multipotent progenitors

1.3.1 Lineage tracing and its contribution to pancreatic developmental biology

Genetic lineage tracing is a novel tool used to follow the progeny of cells during development and tissue maintenance. Lineage tracing provides dynamic information about the fate and the number of cells that descend from the mother cell and their localisation within a tissue. The temporal understanding of cell fate cannot be achieved with the aid of "traditional techniques" such as transcriptional profiling of cell populations or the use of fixed samples to quantify gene and protein expression levels. Importantly, lineage tracing has shed light on some aspects of pancreatic developmental biology, prominently the fate of Pdx1 and Ngn3 expressing cells, the role of Ptf1a transcription factor in progenitor cell contribution to exocrine and endocrine lineages, the role of Notch signalling in pancreatic development, the origin and maintenance of β-cells, as well as the search for multipotent progenitors. The contribution of lineage tracing studies to each of these areas is outlined below.

1.3.2 All pancreatic cells differentiate from *Pdx1* expressing precursors, while endocrine islet cells arise from *Ngn3* expressing precursor cells

Gu et al. used *Pdx1*-Cre-based and *Ngn3*-Cre-based lineage tracing to prove that *Pdx1* expressing cells give rise to all pancreatic cell types, while the *Ngn3* expression restricts the cells to the endocrine lineage (α, β, δ, ε and PP cells) (Gu et al. 2002).

Desgraz and Herrera investigated the potential of individual Ngn3+ cells (Desgraz & Herrera 2009) as opposed to the previous studies, which treated Ngn3+ cells as a population of cells capable of differentiation into all endocrine cell types (Gu et al. 2002). They used the MADM system (mosaic analyses with double markers) to label Ngn3+ cells at a low mosaic frequency. The authors found that in newborn mice the labelled islets frequently contain a single marked Ngn3+ cell, suggesting that one Ngn3+ cell

gives rise to one type of endocrine cell by differentiation without division. In adult mice, clusters of marked cells within an islet were found, suggesting that the single endocrine cell originating from a single Ngn3+ cell re-enters the cell cycle after birth. According to this data, Ngn3+ cells are committed to a specific endocrine subtype and can be considered unipotent precursors (Desgraz & Herrera 2009).

Although it has been shown that all endocrine cells arise from Ngn3+ cells, it does not mean that all *Ngn3* expressing cells eventually differentiate into endocrine islet cells. In fact, some studies found that different amounts of Ngn3 transcription factor may result in different cell fates. Wang et al. postulated the existence of a threshold of Ngn3 (Wang et al. 2010). The lower Ngn3 levels shift the cells towards the exocrine lineage, while higher *Ngn3* expression results in endocrine differentiation. They lineage traced Ngn3+ cells in the pancreases of 3 genetically engineered mice: a) $Ngn3^{TGBAC\text{-}Cre}$; $R26R^{EYFP}$ wild type pancreas expressing normal amounts of Ngn3, b) $Ngn3^{+/-}$; $Ngn3^{TGBAC\text{-}Cre}$; $R26R^{EYFP}$ pancreas of lower *Ngn3* expression, and c) $Ngn3^{F/-}$; $Ngn3^{TGBAC\text{-}Cre}$; $R26R^{EYFP}$ pancreas whereby Ngn3 is immediately inactivated when its own transcription is activated. Analysis performed at E14.5 revealed that only 15% of the labelled cells developed into exocrine cells in the wild type pancreas, 45% in the pancreas with decreased expression of Ngn3, while almost all EYFP reporter label was located in the exocrine tissue in the pancreas of mice with inactivated *Ngn3*. This suggests that pancreatic progenitors, in which Ngn3 levels are decreased, maintain a degree of plasticity to revert to the exocrine progenitor state.

Beucher et al. went further on to investigate the fate of those “failed” endocrine progenitors. They lineage traced the failed endocrine progenitors in *Ngn3* deficient mice at different stages and found that their ability to become duct or acinar cells depended on a particular stage these cells were in (Beucher et al. 2012). At an early bud stage, before E12.5, the failed endocrine cells are capable of differentiation into acinar or duct cells, however, after E12.5 in the branching pancreas they are limited to differentiation only into duct cells. This indicates a higher degree of plasticity at early developmental stages.

1.3.3 Ptf1a (AKA PTF1-p48) transcription factor switches on the differentiation of pancreatic cells from endodermal epithelium

Kawaguchi et al. showed that *Ptf1a*-inactivated cells differentiated to the duodenal and bile duct cell lineages, whereas the *Ptf1a* expressing cells were capable of differentiation into all pancreatic cell types (Kawaguchi et al. 2002). This suggests that Ptf1a plays an important role in the switching on of the pancreatic cell fate in the undifferentiated endodermal epithelium.

Similarly to what has been showed for Ngn3, the study by Fukuda et al. revealed that the level of *Ptf1a* expression influences cell fate determination (Fukuda et al. 2008). The authors traced the cells and their progeny with diminished *Ptf1a* expression and they managed to show that there was a threshold above which the cells would differentiated into pancreatic cells and below which only the bile duct or the duodenal cell fates could be achieved.

1.3.4 Notch signalling plays an important role in pancreatic development

Notch signalling is known to regulate various developmental processes. Its role in the pancreas is not well understood. Generally, it is thought to inhibit exocrine and endocrine specification, but it is not clear how exactly Notch signalling regulates pancreatic progenitors at different stages of development.

A study by Fukuda et al. showed that Notch signalling is necessary for region appropriate specification of pancreas in the foregut (Fukuda et al. 2006). They used *Hes1* knockout mice, Hes1 being a downstream target of Notch signalling, and carried out *Ptf1a*-Cre lineage tracing. They found that Ptf1a, a pancreatic determinant, was misallocated to distinct regions of the primitive stomach and duodenum as well as the bile duct. These mislocalised Ptf1a+ cells were able to differentiate into endocrine, exocrine or duct pancreatic cells, resulting in ectopic pancreas development. This shows that Notch signalling is required for correct pancreas development by spatial regulation of Ptf1a expression.

Kopinke et al. aimed at finding out the differentiation potential of pancreatic progenitors in response to Hes1-mediated Notch signalling at different developmental stages (Kopinke et al. 2011). They used *Hes1*-Cre^{ERT2} knock-

in allele, whereby *Hes1* expression was induced and Hes1+ cells traced. The authors found that in embryonic pancreas, Hes1+ cells are multipotent progenitors, the differentiation of which seems to be inhibited by Notch signalling. Late Hes1+ cells are exocrine restricted and respond to elevated Notch signalling by becoming ductal cells. In adults, in turn, Hes1 expression is restricted to differentiated cells, mainly the presumptive centroacinar population at the interface of ductal ends and acini. These Hes1+ cells in adults do not normally serve as progenitors for β-cells, even after pancreatic duct ligation injury. Hence, the results of this group reveal a shift in the differentiation potential of Notch-responsive cells from multipotent progenitors to exocrine restricted progenitor cells.

1.3.5 β-cell maintenance and the possible existence of multipotent progenitor compartments have been studied by lineage tracing

Much interest has been given to the study of the origin and maintenance of β-cells, as understanding the natural mechanisms of these cells' derivation would be a huge step forward in the creation of potential replacement therapies for diabetic patients. Opinions concerning the regeneration of β and other pancreatic cells from duct or duct associated progenitor populations have been divided, with studies supporting and contradicting this hypothesis. Although the matter remains unresolved, lineage tracing has helped elucidate this challenging aspect of pancreatic biology by providing a new type of evidence.

Dor et al. suggested that adult β-cells are maintained by self-duplication rather than differentiation from progenitor cells (Dor et al. 2004). In their experiment, the fraction of *insulin*-Cre labelled cells stayed constant over time. The authors of the article reasoned that the proportion should decrease, if the insulin-positive β-cells were to be maintained by endocrine neogenesis from insulin-negative progenitors. On the contrary, the constant proportion of insulin+ cells observed suggests the maintenance of islet mass in adults by duplication of pre-existing endocrine precursors specified during development. This conclusion, however, is based on the premise that all the insulin+ cells are mature β-cells. It is possible that the insulin+ cells could retain the

multipotency despite expression of differentiation-associated marker, as it is the case for the expression of differentiated astrocyte marker GFAP in a neural stem cell population in the brain (Doetsch et al. 1999).

Contradictory evidence was provided by Xu et al., whereby they proposed that β-cell neogenesis from the pancreatic ducts after recovery from pancreatic duct ligation (pancreatic injury model) was taking place (Xu et al. 2008). However, the authors of this paper did not provide the evidence of lineage tracing *in vivo*.

The hypothesis, whereby duct cells might be a source of progenitors in the adult and developing pancreas capable of the generation of β cells and other cells (usually of lesser interest), has been supported by some lineage tracing studies. Inada et al. performed *Carbonic anhydrase II*-Cre transgene lineage tracing (using a human promoter that marks only duct cells), and they observed that cells positive for this duct cell marker were able to give rise to β-cells and acinar cells (Inada et al. 2008). Furthermore, their results suggest that duct progenitors may play a role in pancreatic tissue regeneration, as a quarter of β-cells were labelled after pancreatic duct ligation. However, the quantification of the reporter-labelled β-cells in the non-injected control was not well characterised, leading to potential error in the assessment of the quantity of newly arising β-cells.

Furthermore, the results of Solar et al., Kopp et al., and Furuyama et al. question the conclusion of Inada et al. about the possibility of β-cell regeneration in adults. By lineage tracing Sox9+ (Kopp et al. 2011; Furuyama et al. 2011) and Hnf1β+ duct cells (Solar et al. 2009) the groups showed that endocrine cells can be differentiated from ductal cells during embryogenesis but not after birth. Only one study shows a minor production of endocrine cells within the first three weeks post-birth (Kopp et al. 2011). Furthermore, pancreatic duct ligation suggests that β-cell regeneration from ductal cells is not taking place in the adult (Solar et al. 2009).

The existence of multipotent progenitors, that can give rise to all pancreatic lineages, has been proposed by Zhou and colleagues. The authors identified another multipotent compartment in the early tip domain based on expression

analysis and lineage tracing (Zhou et al. 2007). This population of cells co-expresses Pdx1, Ptf1a, c-Myc (high), and Carboxypeptidase A1 (Cpa1) and was shown to be capable of differentiation into exocrine, endocrine and duct cells. However, the switch from multipotent cells into exocrine-fated cells occurs at E14, during secondary transition, consistent with the differentiation of the tip domain. Hence, no multipotent domain persisting beyond E14 has been identified in this study.

Furthermore, one group has suggested a hypothetical multipotent domain based on transcription factor expression (Kopp et al. 2011). The early pancreatic bud expresses a set of transcription factors such as Pdx1, Sox9, Ptf1a, Hnf1b, Hes1 and Nkx6.1 (Seymour et al. 2007; Hald et al. 2008; Haumaitre et al. 2005), the domains of which separate at later stages (Schaffer et al. 2010). Kopp et al. identified a rare area of tissue at the interface of ducts and acini at later embryonic stages, where these transcription factors are still co-expressed (Kopp et al. 2011). This could be the potential site of multipotent progenitors. Interestingly, the location of these cells highly resembles that of centroacinar cells, previously reported to be multipotent *ex vivo* (Rovira et al. 2010). Unfortunately, the question of multipotency of the cells expressing this specific combination of factors cannot be assessed functionally with lineage tracing experiment due to current technological limitations. It should be the focus of future studies, when more refined cell-fate mapping of cells expressing multiple markers has been developed.

Finally, the question of the acinar compartment hosting the potential multipotent progenitor domain has been debated. The acinar tissue cells seem to contribute to acinar tissue maintenance, with a possibility of acinar to ductal trans-differentiation, however, it has not been reported as a potential source of progenitors for the endocrine lineage cell regeneration (Desai et al. 2007; Strobel et al. 2007).

Overall, the existing literature outlined above studies the behaviour of cells which may include the specific subset of Pdx1+ Sox9+ Ptf1a+ Hnf1b+ Hes1+ and Nkx6.1+ cells, however, the observed tripotency in embryos may be

associated with merging of multiple lineage-restricted progenitors due to non-clonal levels of reporter induction in these studies (Zhou et al. 2007; Kopinke et al. 2011; Kopp et al. 2011; Inada et al. 2008; Solar et al. 2009).

1.3.6 It is not clear if β-cells may originate from α-cells during development

It has been postulated that the insulin producing β-cells may derive from α-cells. The reasoning behind this was that the early primordial epithelial cells express more than one pancreatic hormone, hence the idea of a common precursor for all five islet cell types (α, β, δ, ε, PP). Since the glucagon-containing cells are the first to differentiate in early buds and because cells that co-express insulin and glucagon exist (Johansson et al. 2007), this encouraged the hypothesis that β cells may be derived from α-cells. Several experiments have focused on determining whether such conversion is possible, including the lineage tracing studies.

By lineage tracing, Herrera showed that adult glucagon producing α-cells and insulin producing β-cells derive from cells that never transcribed insulin or glucagon respectively (Herrera 2000). In their genetic construct, they placed a reporter under the control of insulin-2 or glucagon promoter, so that cells expressing these hormones could be traced. They found no cells expressing the two hormones at any time during the time-course of analysis. This suggests that neither of the two cell types descend from another.

On the other hand, Thorel et al. reported that the conversion of α to β-cells was possible after extreme β-cell loss (Thorel et al. 2010). Targeted β-cell destruction together with the tracing of α-cells was performed, and a very low conversion rate was observed.

1.3.7 Summary of lineage tracing studies in the developing mouse pancreas

In summary, genetic lineage tracing enables the study of gene function in a novel way – the role of genes in cell differentiation, proliferation and migration can be investigated. This has helped to identify the role of certain transcription factors in pancreatic development, as summarised in Figure 4. It needs to be

emphasised, however, that the studies outlined in this part were all based on high induction levels of lineage tracing. This may lead to inaccuracy in the apparent potency outcome, as multiple independent labelled cells could merge together. Hence, while the studies discussed here have helped to elucidate the role of various transcription factors in pancreatic development, the lineage hierarchy model and potency assessment based on them is hypothetical and needs to be confirmed with clonal density lineage tracing. Furthermore, only specific cell lineages have been traced, therefore, a more unbiased approach in the search of multipotent precursors and in the inference of lineage hierarchy should be undertaken in the future.

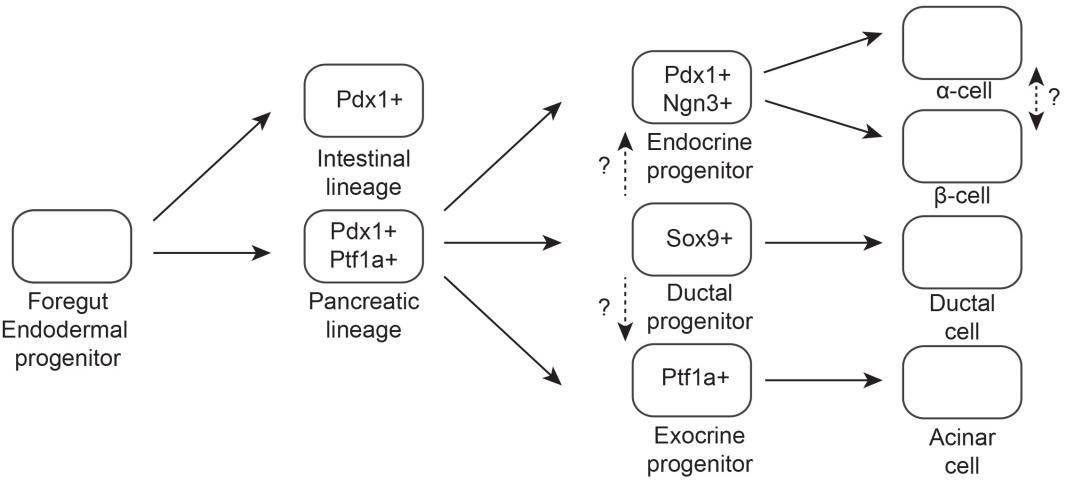

Figure 4. *Role of different transcription factors as revealed by genetic lineage tracing (adapted from Herrera et al. 2002). Ptf1a switches on the differentiation of pancreatic cells from endodermal epithelium. All pancreatic cells arise from Pdx1 expressing precursors, while endocrine islet cells arise from Ngn3-expressing precursor cells. It is not clear if β-cells may originate from α-cells during development, and until what stages the Sox9+ domain retains tripotent precursors.*

1.4 Non-lineage tracing based search for evidence of multipotent progenitors

Besides the lineage tracing approach, a key role in understanding the potency of pancreatic progenitors has been played by experiments involving fluorescently activated cell sorting (FACS) followed by seeding of cells *in vitro* to study their potential. The premise behind these *ex vivo* studies has been the reasoning that even though certain lineages might not give rise to endocrine cells in the tracing studies *in vivo* under physiological conditions, they may retain the potential to do so when they are provided with sufficient signals.

For instance, Rovira and colleagues FACS-sorted a centroacinar population of cells based on their stem cell-associated aldehyde-dehydrogenase-1 (ALDH-1) activity and E-cadherin expression (Rovira et al. 2010). These cells were capable of sphere formation *in vitro* – the phenomenon that has been associated with progenitor cell activity in the nervous system and other organs (Lawson et al. 2007; Dontu et al. 2003). The expression of endocrine markers in the spheres was initiated, while the expression of the ductal Sox9 was retained throughout. These cells differentiated into endocrine and acinar cells upon transplantation into embryonic pancreatic explants (Rovira et al. 2010).

Another study by Seaberg et al. identified the so called pancreas-derived multipotent precursors (PMPs) in the adult pancreas (Seaberg et al. 2004). They showed that a single PMP is capable of in vitro proliferation to form a clonally-derived sphere, which expresses neural and pancreatic precursor genes. After differentiation, these spheres contain differentiated cells coming from both the nervous and pancreatic lineages. Functional β-cells were generated, which were capable of a glucose stimulated Ca^{2+} response, and insulin secretion.

A follow up study was then carried out by Smukler et al., whereby they showed that transplanted PMP cells express insulin and those insulin+ cells are capable of producing pancreatic and neural cells in normal adult pancreas (Smukler et al. 2011). To confirm the pancreatic origin of PMPs and exclude

their neural crest derivation, pancreatic Pdx1 and neural crest labelling were performed.

Altogether, these studies have been useful in identifying facultative progenitors, which show multipotency in *ex vivo* conditions. However, FACS isolation does not always result in pure populations of cells, and it is possible that the colonies described above contain cells of non-ductal or even of non-epithelial origin. Furthermore, the *ex vivo* behaviour does not necessarily recapitulate the *in vivo* cell fate potency.

Interestingly, a study by Stanger et al. has shown that the persistence of multipotent progenitors in the developing pancreas may indeed be very limited. Deletion of cells until E12.5 for various periods of time results in a significantly reduced pancreatic mass (Stanger et al. 2007), indicative of pre-determination of pancreas size by the early progenitor pool. This could mean that the cells have an autonomous restriction of the amount of tissue they are capable of generating, suggesting that there are no ‘stem cell-like’ progenitors present which can compensate the tissue loss by proliferation.

1.5 Link between pancreas morphogenesis, specification and molecular signalling

Specification of cells during pancreatic development has been extensively studied, and the understanding of molecular pathways guiding the lineage differentiation and maturation is becoming progressively more complete. In particular, β-cell differentiation protocols *in vitro* have been developed to a great extent due to an increasing understanding of molecular cues guiding their specification *in vivo* (D'Amour et al. 2006; Pagliuca & Melton 2013; Pagliuca et al. 2014). However, these signalling events are accompanied by morphological changes leading to the formation of adult topology of tubular ductal structures with acini at ductal ends and islets in between them by the end of secondary transition. The understanding of how the morphological events are linked to cell signalling and specification is very limited at present. The key unanswered question in the field of pancreatic biology regards the way in which the pancreas reaches its final size and composition.

In this section, I focus on the main morphological processes such as cells acquiring early polarity, primordial central tube formation, plexus remodelling, branching morphogenesis and islet formation, detailing the cellular mechanism and the influence of molecular signals on the tissue 3-dimensional development.

1.5.1 Establishment of early tissue polarity

The pancreas emerges at E9.5 as a morphologically homogenous bud (reviewed in Shih et al. 2013) composed of multipotent precursors (Shih et al. 2013; Pan & Wright 2011; Zhou et al. 2007; Solar et al. 2009; Gu et al. 2002; Kopp et al. 2011; Pan et al. 2013).

First distinguished pancreatic polarity arises due to the presence of a central lumen following stratification of cells during bud emergence from pre-pancreatic endoderm between E7.5 and E10.0 (Villasenor et al. 2010). Even though the placode is originally 1 layer thick, it stratifies into 6-8 layers surrounding the primary central lumen (PLC) between E8.75 and E11.5 (Villasenor et al. 2010).

Initially, the epithelium is highly polarised with cells in the lumen displaying apical polarity and cells in contact with basement membrane displaying basement polarity. Around E10.5, when the bud becomes more stratified, the inner cells, which constitute the majority of cells, are not in contact, directly nor via thin extensions, with either the PLC nor the basement membrane encasing the pancreatic bud (Villasenor et al. 2010). Once the pancreas is fully stratified (around E10.5), the cells organise into 3 main layers, with an outer layer of 'cap' cells, internal 'body' cells and the lumen-lining cells. The cap cells maintain their polarity by being in direct contact with basement membrane and by receiving signals such as laminin and collagen. However, they show no apical polarity as evident by the lack of aPKC, Par3 or ezrin expression (Villasenor et al. 2010). The body cells show no polarity as they are not in contact with either apical or basal membrane. The lumen-lining cells, unlike the cap cells, show only apical polarisation, as they are in direct contact with the lumen, and accumulate apical markers such as Par3, aPKC, ezrin, ZO (Villasenor et al. 2010).

Even though the cap progenitors are highly motile and rearrange frequently during mitotic divisions in the cap compartment (Shih et al. 2016), the cap and inner body cells tend to stay within their compartment and not intermingle at E10.5 (Shih et al. 2016). This suggests that the initial axis for pancreas growth and development may already be established by this stage. Even though the progenitors are considered to be multipotent at this stage (Shih et al. 2013; Pan & Wright 2011; Zhou et al. 2007; Solar et al. 2009; Gu et al. 2002; Kopp et al. 2011; Pan et al. 2013) there may be some morphological and mechanical differences related to positional effects. This could possibly have an effect on the future fate potential of cells in these distinct regions.

Specifically, cap cells are likely to receive pro-proliferative signals from the ECM and mesenchyme and may therefore contribute to the formation of tip protrusions during the tip-trunk specification (see Chapter 4.3). Additionally, mechanical cues arising from the mesenchyme exerting local pressure on the pancreatic bud may also play a role in regulating the local proliferation and movement of cells and hence the emergence of tips.

Around E11.5, the dorsal and ventral pancreatic buds come in contact and fuse due to the rotation of the gut. The mechanism of fusion and how the process affects the global pancreatic polarity are not understood.

1.5.2 Plexus formation and remodelling

Around E11, the first pancreatic ductal plexus starts to appear and remodel. The origin and mechanism of its formation is not fully understood (Iber & Menshykau 2013). The central lumen formation, described in the previous section, appears to serve as the origin of the ductal plexus. The PCL, which is initially a prominent central cavity, is progressively and very quickly thinned as the bud elongates. In parallel, new lumen emerge in the pancreatic epithelium. At E10.75, the pancreatic bud consists mainly of the forming lumen and links and networks established between those lumens (Villasenor et al. 2010). Even though at E10.5 the body cells were shown to lack polarity (see previous section), by E10.75 they regain this polarity as assessed by the expression of ZO-1 protein (Villasenor et al. 2010). The reason for the re-appearance of polarity in body cells, associated with ZO-1 expression, is not clear. It could be due to cells receiving a different concentration of signals from the mesenchyme such as Fgf10 from that of cap cells.

Villasenor et al. show that individual body cells express aggregates of ZO-1 expression, and in some cells the expression pattern is distinguishable by an O-ring pattern forming a collar on the apical side (Villasenor et al. 2010). These cells have a ‘constricted apical side of a bottle-shaped body cell’ and they appear scarcely in random locations, with a tendency to cluster together and form ‘rosettes’. Once together, these rosettes re-localise the expression of ZO-1 to the apical side in the centre of a ‘rosette’. As a consequence, the rosettes start to open up the microlumens between them. These lumen-rosettes appear to connect together progressively during development around E12.5 (Villasenor et al. 2010). As a consequence of microlumen fusion and coalescence, the initial plexus is formed. Hence, the authors of this article present the cellular mechanism of microlumen formation within the body cells of the pancreas, which leads to the formation of a framework for ductal structures. Other than the correlative evidence of lumen formation and the

appearance of polarity within the rings of cells, the authors do not provide a cellular mechanism of the microlumen formation. For instance, it is not clear whether the lumen appear independently of apoptosis.

The process of lumen formation is believed to be additionally mediated by cdc42 (Kesavan et al. 2009). The protein is suggested to play a key role in the establishment of the apical-luminal polarity, and it could act either via the targeting of vesicles to luminal surface or the targeting of tight junctional complexes. However, the upstream molecular regulatory pathways affecting the protein expression and/or activation are unknown.

Overall, the initial central plexus is a convoluted structure with intermingled modules and disconnected clusters not joined to one another in a clear tubular fashion. How the conversion of this plexus into the mature structures of branched ductal epithelium observed by the end of secondary transition takes place is not understood and has been a focus of very few studies (Bankaitis et al. 2015).

An important molecular mechanism suggested to play a key role in both the microlumen formation and plexus remodelling involves EphB2/B3 signalling. EphB2/B3 receptors are expressed in the pancreatic epithelium, while the ligands are expressed in the mesenchyme around E12 and arteries around E11.5 (Villasenor et al. 2010). Mutant mice lacking the expression of EphB2 and B3 show disrupted microlumen and rosette formation, together with delayed plexus remodelling (Villasenor et al. 2010). The mutant pancreata produce fewer of the multipotent Ptf1a+ progenitors, which results in a reduced total pancreatic mass. Hence, it appears that EphB2/B3 is required for normal pancreatic epithelium morphogenesis, including the formation of microlumen.

The mechanism of EphB signalling and its effect on plexus formation and remodelling seems to act independently of the cdc42-related lumen formation mechanism (Kesavan et al. 2009), as it involves decreased epithelial adhesion evident by the decreased expression of β-catenin and E-cadherin.

This mechanism may be similar to plexus remodelling during vasculogenesis and angiogenesis (Oike et al. 2002).

Deletion experiments described above (Villasenor et al. 2010; Kesavan et al. 2009) have proved very useful in gaining certain degree of understanding about the key molecular players involved in plexus remodelling. However, a cellular mechanism of the process is still missing. Pan and Wright in their review propose a model in which the remodelling of the internal plexus pushes the outgrowth of the pancreas, consistently with the formation of tip protrusions during tip-trunk segregation (Pan & Wright 2011; Schaffer et al. 2010). Plexus remodelling seems to occur in an outside-in fashion, because central immature plexus domains seem to be retained until later in gestation, when already side ductal branches have formed (Bankaitis et al. 2015). Plexus structures and remodelling may persist even by E15 (Pan & Wright 2011; Bankaitis et al. 2015).

It is not understood how plexus remodelling into epithelium of the right size and shape takes place, and should be the focus of future studies. The possible clues as to the cellular and molecular mechanism might lie in the analogy to vascular plexus based on structure similarities, which have been suggested (Risau & Flamme 1995). In the case of the latter, the hemodynamic flow of blood within the primitive vessels (Jones et al. 2006) might play a key role, but it is unresolved whether exocrine secretions would be significant enough to drive the remodelling.

1.5.3 Establishment of tip-trunk polarity

At around E12.5, the tip and trunk domain arise with distinct potencies of the two populations. The origin and mechanism of their appearance, as well as the relationship between the specific location within these domains and the potency are not fully understood.

The emergence of tips might be a result of basal constriction of scattered cap-associated progenitors and integrin-mediated signalling from the surrounding ECM (Shih et al. 2016). Tip cells retain multipotency until E13.5, while trunk cells are ductal-islet bipotent progenitors (Shih et al. 2013; Pan & Wright

2011). Later on, the initially tripotent tip domains become restricted to the acinar lineage. However, a significant proportion of cells both within the tip and trunk domain retain tripotency until E14.5 (Kopp et al. 2011; Kopinke et al. 2011; Solar et al. 2009; Furuyama et al. 2011; Zhou et al. 2007), with some lineages retaining tripotency even until birth (Kopp et al. 2011). Hence, it is not understood how despite the morphological separation of the two domains, tripotency is maintained. The symmetry and sharpness of tip trunk separation, and the existence of potential intermediate zones, is therefore not clear.

The separation of domains has been suggested to be guided by Nkx6-1 and Ptf1a cross-repression, which are initially co-expressed in multipotent progenitors (Schaffer et al. 2010). However, it is not clear if more factors could be involved in the regulation of the tip-trunk polarity generation given the intermediate cell states reported. Such a candidate molecule is Prox1. *Prox1*-deficient mice lack the second phase of endocrine production and the pancreata display enhanced acinar specification (Westmoreland et al. 2012; Wang et al. 2005). This could be due to imbalanced tip-trunk separation and hence Prox1 could have an impact on the separation of domains and determine the sharpness of the two boundaries, perhaps leaving a more plastic zone in between.

Notch signalling is also transiently employed in orchestrating tip versus trunk decisions at the beginning of branching morphogenesis. During segregation, Notch-responsive cells were shown to contribute to the trunk domain, while cells expressing dominant negative mastermind like 1 (MAML1), which supresses transcriptional activation downstream of Notch signalling, contributed to the tip domain (Horn et al. 2012; Esni et al. 2004). Overexpression of Notch intracellular domain (NICD), on the other hand, prevents acinar and endocrine differentiation leaving pancreatic cells in a progenitor-like state even after birth (Murtaugh et al. 2003; Hald et al. 2003). Altogether, this suggests that multiple factors may be involved in the generation of tip and trunk domains, which may result in a less symmetrical domain separation and existence of intermediate regions of a more multipotential character than previously suggested (Shih et al. 2013).

Currently, it is not clear whether the tip-trunk polarity is a separate step or occurs in parallel with plexus remodelling. Pan and Wright in their review propose a model in which the remodelling of the internal plexus pushes the outgrowth of the pancreas, consistently with tip trunk segregation (Pan & Wright 2011). Furthermore, it is not clear if tip-trunk separation is a single step process, which occurs only at the onset of secondary transition or if it is conveyed during generation of side branches in the process of mature ductal tree formation.

1.5.4 Branching morphogenesis

Branching morphogenesis has fascinated biologists and theoreticians, as it is a process underlying the basis of organogenesis. Branching morphogenesis is the formation of tubular ductal network with associated other tissues. The process maximises surface area of an organ and its compartments in a limited space within organisms. A remarkable conservation of tools applied during branching morphogenesis between different organs has been described (Andrew & Ewald 2011; Iber & Menshykau 2013) such as communication between tissues and the use of common branch regulating genes and pathways. The regularity of the process and the existence of stereotypical branching patterns in certain organs such as lung suggest that branching may not be random, but controlled by genetic information (opinion from Iber & Menshykau 2013).

How the pancreatic branches achieve their specific branching pattern is not clear. Branching morphogenesis of pancreas appears to be partially stereotyped with the framework branches being conserved and giving rise to conserved tissue pattern such as the formation of heel and ridge (Villasenor et al. 2010). However, large variation in the branches within subtrees with stochastic variability between individuals has been reported (Dahl-Jensen et al. 2016; Villasenor et al. 2010). The highest variation in the protrusion/branch number was reported for E12.5-E13.5, however, between E13.5 and E17.5 the morphology of pancreata converges in appearance (Villasenor et al. 2010).

Generation of tip protrusions during the tip-trunk separation mediated by

Nkx6.1-Ptf1a cross-repression could be considered the onset of branching morphogenesis. The tip domains would undergo a process of extension and branching, accompanied by maturation into ductal structures. This has not been demonstrated directly *in vivo* however, as it would require live imaging, which is not currently technologically possible in embryos, *in utero*.

What controls the process of branching morphogenesis is not clear. Mesenchyme and the factors it produces, such as Fgf10 and Bmp4, have been reported to induce the first pancreatic protrusions and affect correct pancreatic development (Bhushan et al. 2001).

To start with, Fgf signalling provided by mesenchyme is a key pathway thought to play an important role in branching morphogenesis. *Ex vivo* organoids fail to grow without Fgf10 (Bhushan et al. 2001), while sustaining it uniformly in the medium maintains the branching (Miralles et al. 1999). However, it is plausible that mesenchyme is necessary for pancreatic bud growth induction but not branching *per se* (Dahl-Jensen et al. 2016). Indeed, SU5402 inhibition of Fgf signalling prevents organoid formation and expansion, but does not affect the expansion in the branching phase (Greggio et al. 2013). This is consistent with the fact that FGFR2IIIb inactivation leads to hypoplasia at E12.5 and the hypoplasia is maintained but does not worsen as development proceeds (Pulkkinen et al. 2003). Therefore, it is not clear if inhibition of Fgf signalling could affect the variability of subtree branch size, and should be the focus of future studies.

Additionally, BMP signalling in addition to its role in early pancreatic budding (Pan & Wright 2011; Shih et al. 2013), may also play a role in influencing pancreatic branching besides its role in early budding. Its inhibition via either noggin overexpression or the expression of dominant-negative BMP receptor causes pancreatic hypoplasia in mice combined with reduced branching and excessive endocrine differentiation (Ahnfelt-Rønne et al. 2010).

ECM has also been shown to play a significant role in regulating branching morphogenesis. In addition to its effect on cell adhesion of cap cells via ECM-integrin signalling (Shih et al. 2016), which may result in the generation of the tip protrusions, the ECM secretes molecules such as laminin-1. Blocking

laminin-1 in pancreatic explant cultures, impaired branching and reduced the expression of acinar markers (Li et al. 2004). The role of ECM in regulating acinar differentiation could work in a concentration-based fashion, whereby initially the exposure to ECM is low but with subsequent rounds of branching, increased exposure causes more cells to adopt acinar identity.

Cdc42, in addition to its pivotal role in microlumen formation, also has an important function in branching morphogenesis. Firstly, tubulogenesis is disrupted in *cdc42* deletion mutants, and the maintenance of the tubes fails, as the branch structure is impaired when cdc42 is deleted from E12.5 onwards. This shows that cdc42 not only plays a key role in plexus formation and the initial tubule formation which could result from its role is contribution to the plexus, but also in the maintenance of branches (Kesavan et al. 2009).

Similarly to cdc42, EphB3/B2, which plays a role in microlumen formation (described in Section 1.5.2), is also very important in branching morphogenesis. *EphB3*-null/*EphB2*-dominant negative mice develop a hypobranched pancreas with fewer and shorter branches, and an overall lower exocrine mass (Villasenor et al. 2010). However, none of the single mutants, *EphB3*-null or *EphB2* dominant negative, showed defects in pancreatic morphology and branching, suggesting that both receptors are required in the coordination of pancreatic branching. Whether the branching is disrupted as a consequence of the initial microlumen formation and hence plexus generation, or whether EphB3/2 has an effect on branching morphogenesis from E12.5 onwards, is not clear.

The EGFR pathway also seems to be a requirement for normal pancreatic development. Branching morphogenesis is impaired in *EGFR* (-/-) mice (Miettinen et al. 2000). Therefore, the search for EphB and EGF inhibitors expressed in the epithelium might be an important focus for future studies, as it could explain localised inhibition of branching and the resulting stochastic variability of subtree branch number within different regions of pancreas (Dahl-Jensen et al. 2016)

Ephrin and EGF could act by affecting the Rho GTPase activity in the pancreas as in other organs it has been shown that Rho GTPases are

regulated by Ephrin, EGF and ECM integrin signalling (Heasman & Ridley 2008; Huveneers & Danen 2009; Poliakov et al. 2004). GTPases are believed to be important in tubulogenesis (Heasman & Ridley 2008). It has been reported that tubulogenesis of pancreas is prematurely arrested in the absence of RhoA GTPase inhibitor Stard13 (Petzold et al. 2013) and that it acts via the regulation of cytoskeleton organisation and ERK signalling.

Another signalling molecule, which could control the ductal branch formation in the pancreas, is the hepatocyte growth factor (HGF), as it controls branching of prostate through the Hedgehog pathway (Lim et al. 2014). Both the Hedgehog and HGF are expressed during pancreatic development, however, conditional inactivation of HGF receptor has not been associated with any defect in pancreas morphogenesis (Sonnenberg et al. 1993; Mellado-Gil et al. 2011). On the other hand, HGF mediated migration of progenitors has been observed and this process could contribute to correct morphogenesis in mouse pancreas, as this has been previously shown in zebrafish (Anderson et al. 2013).

In addition to studying the effect of various pathways on the branching patters, the cellular mechanism of pancreas morphogenesis has also been the focus of numerous studies. Enhanced proliferation of cells in the tip area at E12.5 has been observed both *in vivo* and *ex vivo* (Zhou et al. 2007; Dahl-Jensen et al. 2016; Petzold et al. 2013). However, contradicting evidence has also been provided recently (Marty-Santos & Cleaver 2016).

The proposed primary mechanism of pancreas expansion *in vivo* involves the extension of the proliferative tip domain, followed by lateral appearance of side branches (Villasenor et al. 2010). Another study, in *ex vivo* pancreatic explants, has suggested that 76% of bifurcations during ductal branching occur via lateral branching, while 13% appear as a result of terminal bifurcation (Puri & Hebrok 2007). The relative proportions of branching modes might be dependent on time in development and could coexist or be exclusive for specific timepoints. Figure 5 presents the two modes of branching.

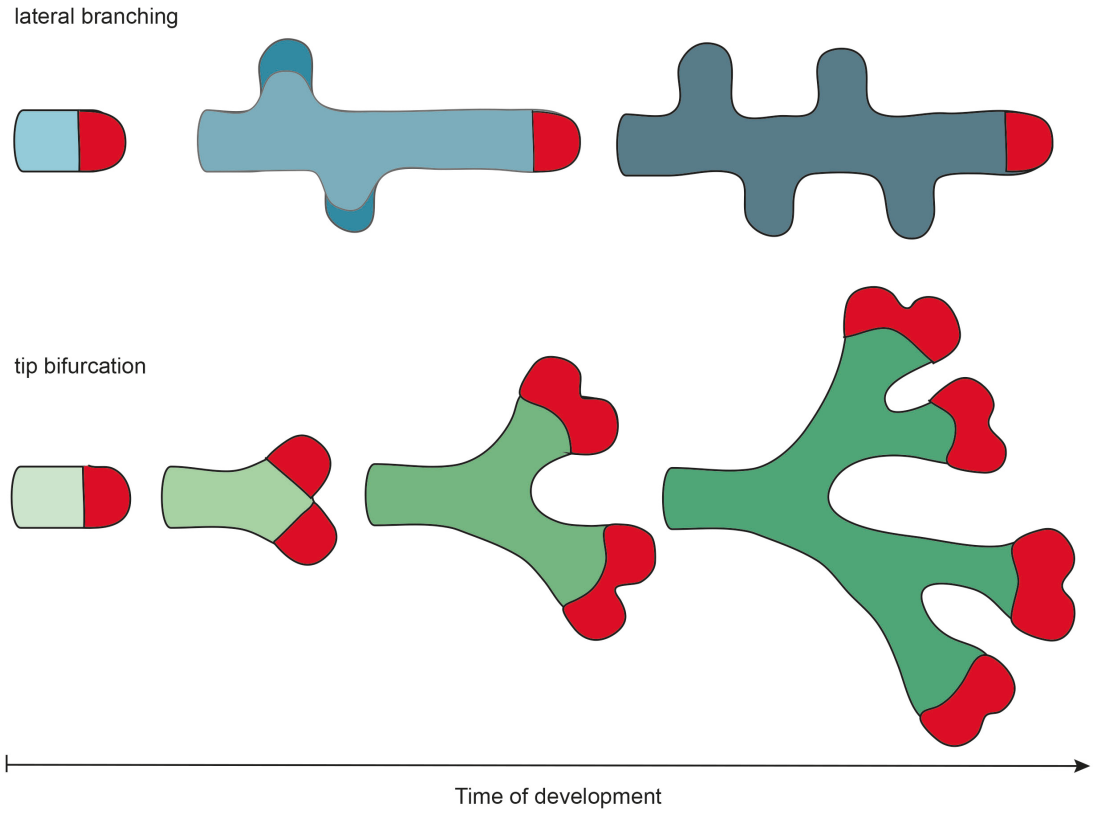

Figure 5. *Modes of branching morphogenesis (adapted from Iber & Menshykau, 2013). Lateral branching is based on extension of the leading branch by proliferation of tip region (in red) and side branches emerging subsequently (top panel). Tip bifurcation driven branching is driven by proliferation and simultaneous bifurcation of leading branch(es), which continues over generations of branches (bottom panel).*

Despite the increasing understanding of how various signalling pathways affect the formation of branches and the cellular mechanism of pancreatic branching itself, the field calls for a model of a cellular mechanism guiding the process of branching morphogenesis including the coordinated development and expansion of all pancreatic compartments, i.e. ductal, acinar and islet. Such a model should explain the simultaneous specification of tissue into ducts and enzyme secreting cells at the tips of the branches.

1.5.5 Mechanism of islet formation

The molecular pathways controlling the differentiation of progenitors into endocrine precursors and mature islet cells have been studied intensively, due to keen interest in differentiation of hormone expressing and glucose responsive islet β-cells *in vitro* for potential treatment of diabetes (D'Amour et al. 2006; Pagliuca & Melton 2013; Pagliuca et al. 2014). However, the cellular and mechanical mechanisms controlling islet formation and growth are unclear. Islet neogenesis follows a set of steps including transient expression of *Ngn3*, delamination of endocrine precursors from ductal epithelium into surrounding stromal tissue, and migration and coalescence into endocrine clusters, which later mature into islets (Gouzi et al. 2011). In the following sections, I will outline the cellular and mechanical models of these processes according to the current literature.

1.5.6 Islet delamination control

Islets are formed from cells delaminating from ductal epithelium. It is not clear how the tubular network of ducts supports efficient endocrine specification and how cells become mature hormone producers. It is likely that the apico-basal polarity of ducts might play a role in correct delamination of endocrine precursors, which is essential for the cells to migrate and receive differentiation-stimulating signals (Villasenor et al. 2010). The process of delamination itself may be crucial for ensuring efficient islet mass production. Cells detaching and migrating away from the ductal epithelium may prevent over-crowding within ductal structures and enable the generation of new waves of endocrine progenitors from the ductal epithelium (Johansson et al. 2007).

The process of delamination itself, i.e. the mechanism, which enables the cells to detach, change their shape into ovoid (Miller et al. 2009) and migrate through stroma, is not fully understood. Endocrine precursors are believed to be leaving the epithelium via either asymmetric cell division (ACD) or via epithelial to mesenchymal transition (EMT). However, it is not understood if these processes overlap, coexist independently, are mutually exclusive, or occur in sequence. ACD is related to the fact that cell fate determinants are distributed unevenly between daughter cells (reviewed in Knoblich 2008) and may result in one of the cells taking a “drop-like” phenotype (Miller et al. 2009). Evidence for components of EMT still need to be provided, however, there is an increasing number of studies which suggest this is the process taking place extensively during endocrine delamination.

A factor mediating delamination, migration and the switching on of EMT programme is Ngn3, also a master regulator of endocrine differentiation (Rukstalis & Habener 2007; Miyatsuka et al. 2011). The function of Ngn3 seems to be regulated in a dosage-dependent manner. Indeed, sustained *Ngn3* expression is necessary to induce delamination from the epithelium and endocrine differentiation in the chick. On the other hand, transient *Ngn3* overexpression is able to induce differentiation into glucagon expressing endocrine cells, however, these cells rarely delaminate from the epithelium. This shows that Ngn3 can induce a differentiation program without inducing the epithelium delamination program. Indeed, in the chick embryo, Ngn3 controls delamination and endocrine differentiation independently (Gouzi et al. 2011), but to the best of my knowledge this has not been shown in the mouse.

The mechanism via which Ngn3 promotes islet delamination has been investigated by studying the expression of markers associated with migration. In particular, the research has focused on the analysis of co-expression between Ngn3 and markers of EMT, as EMT promotes cell shape changes and migration. EMT is commonly associated with increased Snail2 (associated with increased migration; as in del Barrio & Nieto 2002; Belgiovine et al. 2016; Henderson et al. 2015) and decreased E-cadherin levels (associated with decreased adhesion to surrounding cells). In mouse and chick embryos the cells at the periphery of the ductal epithelium lose

apical polarity, strongly decrease E-cadherin, break-down basal lamina and cluster into islets of Langerhans (Gouzi et al. 2011). Decrease in the expression of E-cadherin is sufficient to promote delamination from the epithelium (Gouzi et al. 2011). Indeed ectopic Ngn3 expression triggers E-cadherin expression decrease and EMT marker expression (Gouzi et al. 2011), which suggest a role of Ngn3 in driving the EMT-like delamination of endocrine precursors in addition to their specification. Furthermore, 80% of cells expressing high levels of Ngn3 co-express Snail2 (Rukstalis & Habener 2007), which suggests that the EMT programme may be switched early on, at the beginning of endocrine commitment. Finally, Gouzi et al. show that Ngn3 directly controls Snail2 protein post-transcriptionally to repress E-cadherin (Gouzi et al. 2011). Hence, it appears that Ngn3 is essential for endocrine delamination induction.

Another factor, which may play a key role in regulating this process, is cdc42. The role of cdc42 in ensuring correct tubulogenesis by regulating the polarity of cells (Kesavan et al. 2009) has been discussed in Section 1.5.2. However cdc42 also appears important for correct endocrine lineage differentiation (Kesavan et al. 2014). Given the role of cdc42 in tubulogenesis, it is likely that by affecting ductal tree formation, the endocrine differentiation from ductal-delaminating cells is also influenced. Furthermore, cdc42 may play a role in regulating the adhesive properties of Ngn3 precursors. Indeed, fewer Ngn3+ cells were found in *cdc42* knockout mice as compared to wild type, and fewer and smaller clusters of insulin and glucagon expressing cells were observed at E15.5 (Kesavan et al. 2009).

At the same time, overexpression of constitutively active Cd42 impaired islet delamination and endocrine differentiation (Kesavan et al. 2014). Cdc42 has been suggested to work via impairing cell-cell junction disassembly. Therefore, while in the initial stages, this junction establishment is important for apico-basal polarity and correct duct establishment (tubulogenesis), as a consequence resulting in correct islet differentiation, later on it could regulate cellular adhesion and hence control islet delamination and specification. However, from the study, it is not clear if decreased hormone production is a consequence of impaired delamination (Kesavan et al. 2014). Cdc42

regulates β-cell differentiation by acting via N-WASP signalling. Constitutively active *cdc42* mice express higher levels of N-WASP and genetic ablation of *N-WASP* in β-cells expressing constitutively active cdc42 partially restores both delamination and B cell differentiation (Kesavan et al. 2014). Overall, it appears that cdc42 may influence endocrine cell specification by regulating ductal tubulogenesis as well as adhesive properties of delaminating precursors. The right dose of cdc42 expression appears therefore essential for correct islet development.

Rac1 is another factor, which may play a role in regulating endocrine delamination from the ducts. Blocking Rac1 in β-cells impairs β-cell migration. As a consequence the islet clusters remain in much closer contact with the ductal epithelium (Greiner et al. 2009), possibly due to blocked Rac1 being unable to reduce E-cadherin levels.

Lastly, EGFR signalling has been shown to play a role in the formation of islets. Even though the *EGFR*-/- mice die within 1 week after birth, the pancreas appeared macroscopically normal. The islets, however, displayed an abnormal 'streak-like' phenotype with association with the ducts unlike the normal spherical shape. The proliferation of β-cells was also reduced (Miettinen et al. 2000).

1.5.7 Generation of correct islet mass

In addition to understanding the process of endocrine precursor delamination and migration, it is important to understand how islets acquire their specific size, shape and structure. What makes islets adopt an ovoid shape (Miller et al. 2009), how many endocrine precursors coalesce together to form an islet, how the composition of islets with particular distribution of constituent hormone-producing cells is achieved, and how the optimal pancreatic mass is achieved? This will be outlined in the current and following sub-sections.

An important role in the regulation of the total islet mass is played by the Ngn3 transcription factors, as both deficiency and excess of Ngn3 cause abnormal endocrine development. In *Ngn3* null mice, the development of endocrine cells is impaired (Wang et al. 2007). Only a few glucagon-producing cells

persist, but these may arise due to activity of Mist1 (Wang et al. 2008). Similarly, the over-expression of *Ngn3* results in a decreased endocrine cell mass (Apelqvist et al. 1999). Over-expression causes pre-mature differentiation of progenitor cells into the endocrine lineage at a cost of the pool of progenitor cells, which results in an overall decreased mass of endocrine tissue (Apelqvist et al. 1999).

The cellular mechanism that leads to correct islet mass production is partially understood. 80% of islet cell mass at birth is due to endocrine-progenitor proliferation and subsequent differentiation, while the remaining 20% arises from endocrine cell duplications (Bouwens & Rooman 2005). After birth, new endocrine cells stop arising. It might either be due to loss of competency or the lack of instructive signals. Indeed, the injury models suggest the latter, as in such extreme conditions it might be possible to activate Ngn3 (Kopp et al. 2011). After birth, self-duplication becomes the predominant mechanism of increasing and maintenance of islet cell mass to accommodate for the growth of the body and organ itself (Dor et al. 2004; reviewed in Pan & Wright 2011)

1.5.8 Islet size control

The regulation of islet size is not well understood. Both in embryos and in neonates, the endocrine cells proliferate contiguously, forming branched cord-like structures (Miller et al. 2009). Aggregation of cell clusters, i.e. fusion, is another probably coexistent mechanism of islet formation in the embryonic pancreas, considering the polyclonal origin of islets (Deltour et al. 1991; Ma et al. 2010). At postnatal day 1, the largest islets are 1000 times larger in terms of area than the smallest islets (Jo et al. 2011). Such variability may arise both from heterogeneous proliferative potential of islet cells and from islet fusion events (Jo et al. 2011).

In the postnatal stages, islet fission of large interconnected islet-like structures is taking place, presumably at the α -cell spanning regions (Miller et al. 2009), generating islets of different sizes. It has been suggested that α-cells cause constriction of islets resulting in the formation of the core and mantle structure (Cabrera et al. 2006; Brissova et al. 2005). However, a more recent study has contradicted the hypothesis of mantle formation (Kharouta et al. 2009). The

most active phase of islet fission is at 3 weeks after birth (Jo et al. 2011). However, it needs to be noted that there is a very large increase in islet number between P18 and P21 and fission does not contribute significantly to the islet number increase at this period. In small islets, only 30-50% of existing small islets are a result of fission, while the remaining ones results from normal growth from single β-cells (Miller et al. 2009; Jo et al. 2011). The latter might reflect the division of progenitor cells or neogenesis from the ducts. Islet cell neogenesis seems an unlikely process, as most lineage tracing studies so far have revealed that no *de novo* islet cell production takes place after birth (Solar et al. 2009; Shih et al. 2012; Zhou et al. 2007; Furuyama et al. 2011; Kopinke et al. 2011; Kopp et al. 2011)

Islet fusion is probably insignificant at postnatal stages, because: a) the number of islets initially increases and then becomes constant in adult tissue, b) islets become more circular with time, c) the number of segments in “mutli-joined” islets decreases over time (Jo et al. 2011). The abundance of fission events and lack of fusions explains the drastic morphological difference between the cord-like branching islet structures in embryos and neonates and the spherical islets in the adult.

Overall, postnatal stages are the phase of major islet number and size increases. It has been shown that 80% of total β-cell mass in adult mice results from postnatal islet formation and growth (Jo et al. 2011). The process of islet formation is complete by 4 weeks, with little or no islet formation afterwards and a low β-cell proliferation potential in the adult regardless of islet size (Jo et al. 2011).

Interestingly, the size of islets seems to be conserved between species including human and mice, while the number of islets generally increases with the size of a species. This suggests a certain intrinsically regulated limit to islet size. Little is known about the mechanism regulating islet size (Jo et al. 2011; Jo et al. 2007; Kilimnik et al. 2012; Jo et al. 2012), but it is expected that there is an optimal size of an islet as a functional unit (Henderson 1969). For example, it has been shown by Jo et al. that coupled β-cells secrete insulin more effectively than the single β-cells, and they can generate bursting

action potentials, in contrast to single β-cells that produce spiking action potentials (Jo et al. 2005).

Focusing on the variability of islet sizes within an individual organism, there is a significant extent of variation following exponential dynamics, with size ranging from small clusters of less than 10 cells to large islets containing several thousand endocrine cells (Jo et al. 2011; Jo et al. 2012). It has been suggested that the variability of islet sizes may arise from stochastic proliferation of cells, or that islet fusion and fission may account for this variability (Jo et al. 2011; Jo et al. 2012; Jo et al. 2007; Seymour et al. 2004). Islets of various sizes are distributed throughout the whole pancreas – through head, body and tail (Jo et al. 2011). Furthermore, islet distribution does not depend on gender of mice (Jo et al. 2011).

1.5.9 Islet structure control

The delaminated Ngn3+ cells are unipotent precursors (Desgraz & Herrera 2009), but as a population they can differentiate into α, β, δ, PP and ε cells. It is not well understood what controls the proportions of different islet cells, but it may be partly dependent on timing. Johansson and colleagues induced *Ngn3* expression at different times (Johansson et al. 2007). They found that endocrine progenitors go though phases of different “competence states”, in which certain endocrine cell subtypes are more likely to form (Fig. 6). For example, activation of Ngn3 during the first 48 hours of pancreatic development (E8.5-E10.5) results in exclusive production of glucagon-secreting α -cells. This is followed by a second competency window, in which insulin and pancreatic polypeptide cells arise. Finally, after E14.5, somatostatin-producing cells appear and α-cell formation ceases (see Fig. 6). These competency windows seem to be due to cell-autonomous rather than extrinsic factors from surrounding mesenchyme, because epithelium-mesenchyme co-culture from different stages of development does not alter the outcome of different competency stages (Johansson et al. 2007). Notch signalling could be involved in the regulation of endocrine cell proportions in a dosage or signal duration fashion (Ninov et al. 2012; Li et al. 2012; Li et al. 2015).

Furthermore, islets are known to be of an ovoid shape (Miller et al. 2009) and composed of the so called α-cell 'core', and β-cell surrounding peripheral 'mantle' (Cabrera et al. 2006; Brissova et al. 2005). However, a more recent study has contradicted the hypothesis of mantle formation in mice (Kharouta et al. 2009).

Interestingly, several factors involved in the possible regulation of islet composition have been identified. One of them is HNF6, expressed in islet cells until E18.5 *in vivo* (Gannon et al. 2000). It appears that downregulation of *HNF6* after E18.5 in developing pancreata is essential for correct structure formation (Gannon et al. 2000). Gannon et al. have shown that persistent expression of HNF6 in islet cells causes disrupted islet architecture and loss of β-cell function. In their experiment, the transgenic mice were diabetic, and islets were composed of hyperplastic islets, which remained in contact with the ducts. The numbers of α, β, Δ and PP cells was significantly increased, and abnormal intermingling of endocrine cells with β-cells was observed. Furthermore, β-cells displayed a profound dysfunction, evident by the lack of insulin response to elevated glucose levels and severely reduced Glut-2 (glucose transporter) expression (Gannon et al. 2000).

CTGF, connective tissue growth factor, is another molecule expressed during the pancreatic development – at high levels in the ductal epithelial cells and the pancreas-associated vasculature, as well as at low levels in the developing insulin+ cells, but it is downregulated in the β-cells after birth (Crawford et al. 2009). CTGF is required for the establishment of normal islet endocrine cell ratio and architecture, as *CTGF* null embryos result in a highly elevated number of α-cells, paralleled by a significant decrease in the β-cell count. The islets also show a dramatic decrease in β-cell proliferation during late gestation (Crawford et al. 2009). The molecular mechanism of CTGF action is unknown, however, it is believed to be a secreted protein known to modulate several growth factor signalling pathways including TGF-β, BMP and Wnt (Crawford et al. 2009).

Finally, Nkx2.2, which is normally required for correct endocrine differentiation, has been shown to affect islet structure and composition.

Nkx2.2 repression results in an impaired maintenance of β-cell function and as a consequence disrupted islet architecture (Doyle & Sussel 2007).

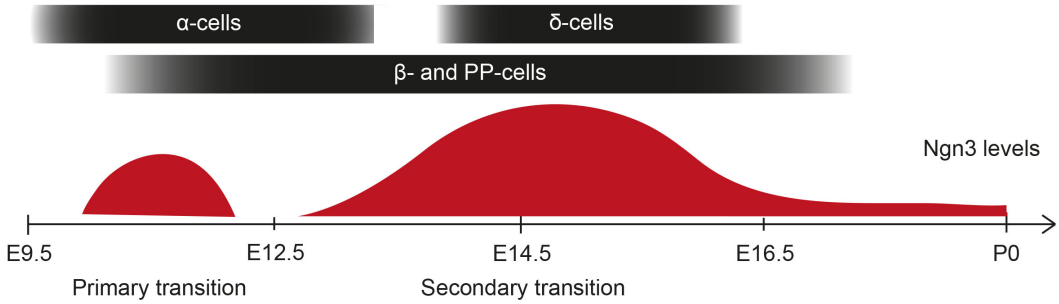

Figure 6. *Ngn3 is expressed in two waves during pancreatic development (adapted from Johansson et al. 2007). The first wave starts at E9.5 and lasts until the onset of secondary transition at E12.5 and results in the formation of early α-cells. The second wave begins soon after secondary transition, during which the cells are capable of differentiation into β and PP cells, followed by δ-cells.*

1.5.10 Control of pancreas size

The understanding of pancreatic size control is limited and it is not clear which factors regulate pancreatic size. The formation of branches appears to be an important mechanism of controlling the pancreas size, as mice with mutations of genes affecting branching morphogenesis resulted in reduced branch-tree size and decreased size as a consequence (Bhushan et al. 2001; Kesavan et al. 2009; Villasenor et al. 2010; Miettinen et al. 2000, see Section 1.5.2).

The major contribution to the understanding of this question comes from a study by Stanger et al. (Stanger et al. 2007). When early progenitor cells were deleted until E12.5, pancreas growth was vastly diminished to 6% of the wild type pancreas size. Hence, the initial pool of progenitors determines the final pancreas size. This suggests that the initial pool of progenitors might contain cells which are already highly committed and which therefore cannot compensate ablation by enhanced proliferation, as is the case in the liver (Stanger et al. 2007). This is in contrast to previous studies, which suggest relatively high extent of multipotency, and by extension stem cell-like character, in the pancreas for these stages (Solar et al. 2009; Shih et al. 2012; Zhou et al. 2007; Furuyama et al. 2011; Kopinke et al. 2011; Kopp et al. 2011). It is also plausible, however, that the cells perform ‘cell-counting’, meaning that they can only carry out a certain number of divisions, as observed in other systems (Bernitz et al. 2016). Therefore, the low proliferation of cells might not be related to their potency state. Alternatively, the effect of ablation of cells at specific developmental stages on pancreas growth could be related to morphological processes taking place. It has been suggested that plexus formation and remodelling, which takes place between E9.5 and E12.5 (Pan & Wright 2011), could be responsible for determining the final pancreas size. Ablation of cells during that time would result in an incorrect/decreased size of plexus, setting an incorrect framework for pancreas formation.

1.5.11 Role of blood vessels in pancreas morphogenesis

Similarly to the mesenchyme, the role of which was outlined in previous sections, blood vessels, which associate with the growing pancreatic bud, also play a very important function in influencing pancreas morphogenesis.

At E8.5, the dorsal pre-pancreatic region comes in contact with vascular endothelium, which is absolutely necessary for the establishment of the pancreatic domain. Aorta-less *Xenopus laevis* embryos fail to express pancreatic genes, while the co-culture of mouse dorsal pre-pancreatic endoderm with dorsal aortae induces Pdx1 and insulin expression in cells (Lammert et al. 2001). The mechanism of action may be via VEGF, which is secreted by vascular endothelium. Mis-expression experiment of *VEGF-A* under *Pdx1* promoter causes islet hyperplasia and ectopic number of insulin-positive cells (Lammert et al. 2001). Knockout *VEGFR2* mice fail to activate Ptf1a expression in dorsal pancreatic bud (Yoshitomi & Zaret 2004). The maintenance of Pdx1 expression requires interaction with aortic endothelium even though it is not initially required for the induction of the gene (Yoshitomi & Zaret 2004). It has also been suggested that aortic signals may be conveyed via promotion of survival of dorsal mesenchyme, which produces Fgf10 and maintains Ptf1a expression and progenitor pool expansion (Jacquemin et al. 2006), hence not affecting pancreas specification directly. The nature of influence of the aorta on pancreas development requires further investigation.

Later on, during branching morphogenesis the endothelial cells become localised to the central/trunk regions (Lindsay et al. 2006; Magenheim et al. 2011; Pierreux et al. 2010), and remain distant from the tip region where the acinar cells differentiate. It appears that amongst the factors expressed by endothelial cells, non-nutritional signal, VEGF-A is a key player affecting pancreas morphogenesis (Magenheim et al. 2011; Pierreux et al. 2010). *In vivo* ablation of *VEGF-A* results in reduced endothelial differentiation and excessive acinar differentiation (Magenheim et al. 2011; Pierreux et al. 2010). Forced *VEGF-A* expression-induced hypervascularisation enhances expression of trunk marker Hes1 and loss of tip markers Cpa and amylase

(Magenheim et al. 2011; Pierreux et al. 2010). *VEGF* ablation in explants favours acinar formation and causes hyperbranching (Magenheim et al. 2011; Pierreux et al. 2010). Lastly, VEGF-A signalling is also required but not sufficient for endocrine differentiation (Magenheim et al. 2011). Overall, it appears that VEGF-A controls pancreas morphogenesis physically and by means of molecular signalling restricting branching and differentiation of acinar and endocrine lineages.

1.5.12 Unanswered questions of pancreas morphogenesis

Despite an increasing understanding of pancreas morphogenesis and how signalling might affect some of the morphogenic processes, certain important questions remain unanswered.

First, it is not understood what roles are played by plexus remodelling and tip branching in establishing the mature ductal branch patterns and in determining the final pancreas size. Our understanding of the two processes is currently limited. How plexus remodelling takes place requires further investigation. In the future, research should focus on mapping the plexus dynamics, in order to determine whether any conserved patterns of remodelling can be identified or whether the process is stochastic. It is also not clear how plexus remodelling is linked to tip-trunk domain generation. Some reviews suggested that plexus remodelling could exert pressure in the core parts of the pancreas hence pushing outwards the protrusions of the epithelium (Pan & Wright 2011). However, no evidence for this has been provided, and therefore this should be addressed in the future studies. Furthermore, it is not clear what the mode of tip branching is, as most studies have been carried out on early tip domain (until E14.5), without focusing on later stages of branching morphogenesis (Zhou et al. 2007). Others were conducted in *ex vivo* explant systems and therefore require validation in *in vivo* settings (Puri & Hebrok 2007; Villasenor et al. 2010; Dahl-Jensen et al. 2016; Petzold et al. 2013)

Secondly, the regulation of ductal branching requires further mechanical understanding. Even though the factors regulating proliferation and branching have been examined (Bhushan et al. 2001; Kesavan et al. 2009; Villasenor et

al. 2010; Miettinen et al. 2000), it is not clear how the structure of individual ductal subtrees is regulated and how individual branches are initiated and terminated. It should be the focus of future studies to identify the cellular mechanism of this process as well as the inhibitory molecules locally affecting the branches. The candidate factors could involve inhibitors of pathways playing a role in branch structure regulation (Villasenor et al. 2010; Miettinen et al. 2000; Petzold et al. 2013). Furthermore, the role of ECM and mesenchyme and their secreted molecules should be the focus of future investigations, in order to identify the inhibitors (Li et al. 2004; Bhushan et al. 2001; Ahnfelt-Rønne et al. 2010).

Thirdly, much focus in the field of pancreatic biology has been devoted towards the molecular and spatial characterisation of possible multipotent cells (Zhou et al. 2007; Kopp et al. 2011; Solar et al. 2009; Kopinke et al. 2011; Rovira et al. 2010), due to their potential use in the β-cell differentiation for diabetes replacement therapies. A previous study has indicated the tip domain as the host of multipotent cells (Zhou et al. 2007), which requires further verification using clonal-level lineage tracing . It is not clear what molecular or physical cues could have an effect on this restriction, and whether the restriction within the niche would be random or related to position and hence subject to exposure from different physical and biochemical cues. This area requires further investigation.

Finally, the field is currently lacking a refined theory, which would explain the 3-dimentional development of all pancreatic lineages. Despite an increasing understanding of molecular pathways driving the specification of distinct lineages, the coordination of these with morphological changes taking place is not clear.

1.6 Aims of the Thesis

In my thesis I aim to study cell specification and morphogenesis of the developing pancreas, based on lineage tracing of random populations of pancreatic progenitors traced from *R26* ubiquitous promoter induced at low, statistically-defined frequency, exploiting the *R26*-CreERT2; *R26*-Confetti system. Previous studies have been based on lineage tracing at non-clonal induction levels, with quantification of clones arising from possibly more than one labelled progenitors (Kopinke et al., 2011; Kopp et al., 2011; Shih et al., 2012; Solar et al., 2009; Zhou et al., 2007), hence affecting the readout of potency outcomes. The lineages were traced from specific pancreatic promoters, hence providing useful information about the potency of small pancreatic populations, but failing to provide the information about the general potency of the whole tissue. I therefore set out to optimise the *R26*-CreERT2; *R26*-Confetti system to ensure clonality within statistical confidence, and to enable the 3-dimentional clonal data acquisition involving the information about the constituent cell types.

I then sought to understand the potency of cells in primary and secondary transition, and whether there was any relationship between clone sizes and their potency. Next, I aimed to study the morphological processes, with a focus on ductal branching morphogenesis, using the EdU proliferation kinetics assay, lineage tracing from the *R26*, as well as *Sox9* promoter. I aimed at identifying the mechanism driving pancreatic growth and the coordinated development of 3 pancreatic lineages in order to understand how the pancreas reaches its final size and composition. I also wanted to examine if there was any relationship between morphological and specification events.

Furthermore, I aimed at optimising the single cell sorting and sequencing technique in order to determine cellular heterogeneity and decipher the relationship between the main pancreatic lineages, which would serve as a molecular mechanism shedding light on the functional lineage tracing analysis.

Lastly, I aimed at studying islet morphogenesis using the R26-CreERT2; R26-Confetti system in order to gain understanding about how the islet size

regulated, what is the mode of islet cell proliferation during islet formation, how many endocrine precursors contribute to islet formation, and whether the proliferative capacity of individual endocrine precursors regulates islet size.

Chapter 2

Materials and methods

2.1 Studying pancreatic development *in vivo*

2.1.1 Breeding and Tamoxifen treatment of transgenic animals

For lineage tracing experiments, mice expressing an inducible version of cre recombinase ERT2 under a direction of a promoter (*Rosa26 or Sox9*) were crossed with transgenic reporter mice expressing the Confetti 'Brainbow 2.1" cassette (Livet et al. 2007; Ventura et al. 2007).

Pregnant females at various stages of their pregnancy were injected intraperitoneally with 10mg/mL Tamoxifen in corn oil after careful optimisation to induce the cells at a clonal frequency. The doses and stages of injection are provided in the Table 1. The tissues form the pups were collected at E14.5, E18.5, P14 and P28.

Mouse genotype	**Stage of injection**	**Dose of Tamoxifen**
Rosa26-ERT2; Confetti (Brainbow 2.1)	E9.5	0.020 mg/g
	E12.5	0.025 mg/g
	E15.5	0.015 mg/g
	E18.5	0.010 mg/g
***Sox9*-ERT2; Confetti (Brainbow 2.1)**	E12.5	0.020 mg/g

Table 1. *Tamoxifen dose for injection of transgenic mice at different developmental stages.*

2.1.2 EdU (5-ethynyl-2'-deoxyuridine) injection for EdU proliferation assay

To study the proliferation kinetics of developing pancreas, the pregnant females were injected with 20ug/g of weight at various stages of pregnancy. Pancreata from embryos or pups were collected and fixed in 4% PFA at 4°C as described below.

2.1.3 Tissue fixation

The dissected tissues were fixed in 4% PFA at 4°C – lengths of fixation were dependent on stage of pancreatic tissue, and are provided in the Table 2.

Tissue developmental stage	Fixation length
Until E16.5	45 minutes
E16.5-E18.5	4 hours
P0 and older	Overnight

Table 2. *Length of fixation of the pancreas in 4% PFA depending on the developmental stage of the tissue.*

Subsequently the tissues underwent three PBS washes – each half an hour and 1 hour long for pancreata aged below E16.5 and pancreata above E16.5, respectively.

2.1.4 Tissue preparation and cryostat sectioning

Pancreata aged E16.5 or younger were placed in a well with 500µl of 20% sucrose in PBS for half an hour. Older pancreata were placed in a tube with 5ml of 30% sucrose in PBS for approximately 2-4 hours until the pancreas moved to the bottom of the tube. Tissues from E16.5 embryos or younger were washed in PBS 3 times for half an hour. Older tissues were washed 3 times in PBS for 1 hour. Subsequently the samples were placed in OCT and stirred around to remove the excess PBS covering the tissue. Finally, the pancreata were placed in OCT in an embedding form, which was then placed on dry ice to freeze. The frozen blocks were either sectioned immediately with the Leica cryostat or stored at -80°C beforehand.

Thin sections were cut at 10µm, while thick sections amounted to 80 or 100µm. After the thick sections were placed on slides, they were left to dry for 5-10 minutes. After sectioning the slides were either moved to the freezer or immunostained.

2.1.5 Staining of thin cryostat sections

This method was used initially in the optimisation of visualisation of 3D clonal data together with visualisation of pancreatic compartment markers, in order to be used for serial reconstructions of thin sections. If the cryostat sections were stored in the freezer previously, then the slides were thawed at room temperature for about 5 minutes. The slides were rehydrated 3 times in PBS for 5 minutes. The slides were then immersed in 0.01% Triton-100X in PBS for 5 minutes. Next, the slides were briefly dried and the tissue sections on the slide were then surrounded with a hydrophobic barrier pen and left until the barrier dried. The non-specific binding between the primary antibodies and the tissue was blocked by incubating in 2% donkey serum, 0.01% Triton-100X in PBS for 45 minutes in a humid chamber. Subsequently, the primary antibodies diluted in 2% donkey serum, 0.01% Triton-100X in PBS were applied overnight at 4°C. The list of primary antibodies used for staining of thin sections is presented in Table 3. The slides were then washed in PBS 3 times for 15 minutes. The sections were next incubated with secondary antibody and DAPI diluted in 2% donkey serum, 0.01% Triton-100X in PBS for 2 hours at room temperature in humid chamber in the dark. The slides were washed in 0.01% Triton-100X in PBS once for 5 minutes, and 3 times in PBS for 15 minutes. The slides were then dried briefly and mounted with an anti-fading Calbiochem mounting medium from Sigma-Aldrich. The coverslip was placed on the slide covered with mountant avoiding the bubble formation.

2.1.6 Staining of thick cryostat sections

This method was used for obtaining 3D clonal data together with visualisation of tissue compartments. The slides taken from the freezer were left to thaw for 5 minutes at room temperature. The slides were washed with PBS two times for 5 minutes, and then 3 times for 5 minutes with 0.5% Triton-100X in PBS. Next, the slides were briefly dried and a circle around the tissue was drawn

with a barrier pen. Permeabilisation buffer composed of 0.5% Triton-100X, 4% DMSO, 2% donkey serum in PBS was applied onto tissue encircled by the barrier pen and incubated in humid chamber overnight at 4°C. Next the tissue sections were incubated in primary antibodies diluted in 2% donkey serum, 1%DMSO, 0.5% Triton-100X in PBS for 3 days at 4°C. The list of primary antibodies used for staining of thick sections is presented in Table 3. The samples were subsequently thoroughly washed by rinsing 3 times in 0.2% Triton-100X in PBS, washing for 30 minutes in 0.2% Triton-100X in PBS and then for 1 hour. The sections were next incubated in secondary antibody (1:800) and DAPI in 0.5% Triton X-100, 1% DMSO, 2% DS in PBS for 3 days. Next, the samples were washed thoroughly in 0.2% Triton-100X in PBS by rinsing three times in 0.2% Triton-100X in PBS, washing for 15 minutes in 0.2% Triton-100X in PBS, and washing in PBS twice for 2 hours.

2.1.7 Mounting of immunostained thick sections

Special method for mounting thick cryostat sections was necessary, due to opaque nature of pancreatic tissue. The sections were left to dry briefly. Next, a 200µm spacer from SunjiLab was placed on the slide to surround a tissue section. Subsequently, RapiClear 1.52 mountant medium from SunjiLab of refractive index 1.52 was applied to sections to match the tissue refractive index. A coverslip was then placed on the slide covered with mountant and spacer.

2.1.8 Staining of whole-mount pancreata

Whole-mount immunostaining was used to visualise clones and pancreatic compartments, where the tissue clearance methods were sufficient for the thickness of the whole organ. All staining steps were performed in wells of a 4-well plate from NUNC for tissues from animals younger than P7, and 5ml tubes for older pancreata, shaking on a shaker. Whole-mount pancreata were permeabilised and blocked in 0.5% Triton-100X, 4% DMSO, 2% donkey serum in PBS overnight at 4°C. Next, the pancreata were incubated in primary antibodies diluted in 2% donkey serum, 1%DMSO, 0.5% Triton-100X in PBS for 3 days at 4°C. The list of primary antibodies used for staining of whole-mount samples is presented in Table 3. The samples were

subsequently thoroughly washed by rinsing 3 times in 0.2% Triton-100X in PBS, washing for 30 minutes in 0.2% Triton-100X in PBS and then for 1 hour. The sections were then incubated in secondary antibody (1:800) and DAPI in 0.5% Triton X-100, 1% DMSO, 2% DS in PBS for 3 days. Next, the samples were washed thoroughly in 0.2% Triton-100X in PBS by rinsing three times in 0.2% Triton-100X in PBS, washing for 15 minutes in 0.2% Triton-100X in PBS, and washing in PBS twice for 2 hours.

2.1.9 Mounting of whole-mount pancreata

Whole-mount pancreata required mounting of tissue with clearance method, as this would enable imaging of the sample through the whole thickness without significant loss of information. Whole-mount pancreata were placed on MatTek plates and dried briefly with Kimwipes tissue from KimTech. The pancreas was then incubated in RapiClear 1.52 (amount covering the tissue) overnight. The next day fresh RapiClear 1.52 was applied onto tissue, before imaging.

Antibody	Species	Company	Dilution	Use
Anti-CK19 (Troma III)	Rat	Hybridoma bank	1:270	Thick and thin sections, Whole-mount
Anti-Chromogranin A	Rabbit polyclonal	Abcam (ab15160)	1:190	Thick and thin sections, Whole-mount
Anti-Amylase	Goat polyclonal	Santa Cruz Biotechnology (sc-12821)	1:250	Thick and thin sections, Whole-mount
Anti-Nr5a2	Goat polyclonal	Abcam (ab18293)	1:250	Thick and thin sections, Whole-mount
Anti-*Sox9*	Rabbit polyclonal	Millipore (AB5535)	1:250	Thick and thin sections, Whole-mount
Anti-GFP	Rabbit polyclonal	Life Technologies (A11122)	1:500	Thick and thin sections
Anti-Insulin	Guinea pig polyclonal	Abcam (ab7842)	1:200	Thick and thin sections, Whole-mount
Anti-Glucagon	Mouse monoclonal	Abcam (ab10988)	1:200	Thick and thin sections, Whole-mount
Anti-Somatostatin	Rabbit polyclonal	DAKO (A0566)	1:200	Thick and thin sections, Whole-mount
Anti-Polypeptide P	Goat polyclonal	Abcam (ab77192)	1:200	Thick and thin sections, Whole-mount

Table 3. *List of antibodies tested for immunostaining of thin and thick cryostat sections, and whole-mount samples.*

2.1.10 EdU ClickiT reaction staining of whole-mount pancreata for EdU proliferation assay

EdU incorporation into S-phase active cells had to be visualised upon collection of EdU injected samples. Whole-mount pancreata or thick cryosections were incubated in 0.5% Triton-100X, 4% DMSO, 2% donkey serum in PBS at 4°C overnight in wells of 4-well plates from NUNC or on slides in a humid chamber respectively. The next day the samples were incubated in ClickiT reaction cocktail as outlined and in the order of Table 4. for 4 hours at room temperature protected from the light.

Component	Preparation	Volume per 500µl total
Click-iT EdU reaction buffer (Component D)	Prepare at 1X by diluting in deionised water	440µl
$CuSO_4$(Component E)	None	10µl
Alexa Fluor azide (Component B)	None	1.2µl
Click-iT® EdU buffer additive (Component F)	Prepared at 1X by diluting in deionised water	50µl

Table 4. *EdU ClickiT reaction cocktail components.*

Subsequently the reaction cocktail was removed and samples were washed in 2% donkey serum in PBS 3 times for 15 minutes and then the thick section or whole-mount staining and mounting protocol was followed.

2.1.11 Imaging with Leica SP5

Confocal microscopy was used for imaging thin and thick sections or whole-mount embryonic and neonatal pancreas. The settings for different fluorophores imaged are presented in Table 5.

Fluorophore	Laser	Detector	Wavelength detection range [nm]
DAPI	UV	PMT1	430-471
CFP	458nm	hyD2	467-502
GFP/ 488 Alexa Fluor	476nm	hyD2	495-521
YFP	514nm	hyD2	527-559
RFP/ 555 Alexa Fluor	561nm	hyD4	572-614
647 Alexa Fluor	633nm	PMT5	645-711

Table 5. *Multichannel imaging settings on confocal Leica SP5 microscope.*

Z stack imaging and tissue tiling were performed, where necessary, in order to visualise whole clones.

2.1.12 Image analysis with Volocity software

Volocity software was used to record parameters from imaged tissue sections such as volumes of objects, the 3D (x,y,z) coordinates of centres of objects, as well as boundary points. By setting intensity thresholds manually for every image, to account for the variability of the intensity in clone visualisation and marker immunostaining, the differently coloured clusters were identified and the required parameters computed by the software. In addition to this, information about the cluster constituent cell types was collected by looking at co-localisation of clusters with pancreatic markers in the Z-layer mode of Volocity.

2.1.13 Image processing with Imaris 8.1.2

To obtain 3D images from Z-stacks from an image captured by the Leica SP5 microscope, Imaris software was used. The software was also used to create 3D objects, such as ductal reconstructions, by setting intensity threshold and smoothness parameters.

2.1.14 3D reconstruction with Unwarp J in Image J software

Unwarp J is a plugin developed for Image J that enables 3D reconstruction of images by matching them together by unwarping a source image so that it is deformed/warped to resemble a target image. The plugin was used with

interactive landmarks to provide guidance to the registration procedure. Thick section images containing multiple Z-stacks were first 3D projected into a flat image and then the matching point pairs were applied at the landmark regions of the source and target image (usually boundary of tissue or characteristic clones spanning multiple sections). The image warping was then performed by the software, using vector-spline regularization term to constrain the deformation to be physically realistic. The warping algorithm was saved and applied to all Z-stack images of the target image. All the Z-stacks of source and target images were subsequently merged together in Image J, and 3D reconstruction created in Imaris 8.1.2.

2.1.15 Preparation of pancreatic buds for FACS sorting for single cell RNA-sequencing (scRNA-Seq) analysis

In order to look at gene expressions of single pancreatic cells, I carried out fluorsecence activated cell sorting (FACS) followed by single cell RNA sequencing. Pancreatic buds were dissected from embryos at either E13.25 or E15.25. In addition to the samples for FACS sorting and subsequent single-cell sequencing, pancreatic buds or stomach tissue for FACS negative controls were collected. Single buds and control tissues were dissociated in 200µl TrypLE-5X from Thermo Fisher Scientific in sterile Eppendorf tubes for 20 minutes at 37°C in a heat block and re-suspended gently with a pipette every 5 minutes. Subsequently the dissociated pancreatic buds in TrypLE-5X were quenched in 250µl of 2% FCS in PBS (FACS buffer) and spun for 5 minutes at 400rcf in a swing bucket centrifuge. The supernatant was then removed leaving about 20µl of liquid to avoid the aspiration of cells. Next the cells were washed with 250µl of FACS buffer, centrifuged at 400rcf in the swing bucket centrifuge and the supernatant aspirated. The samples for single cell sequencing, the single stained controls (Tie2-positive or CD45-positive), the triple/ quadruple-stained controls (Tie2-positive, CD45-positive, DAPI positive) were incubated in 1:100 diluted 25µl FcyR (anti-mouse CD16/32 clone: 93) from eBioscience in FACS buffer for 10 minutes on ice. In the meantime 500µl of FACS buffer was added to DAPI-positive and non-stained control tubes. Following the incubation in FcyR solution, the cells were incubated in single (Tie2 or CD45) or double antibody solutions (Tie2 and

CD45) at 1:200 in FACS buffer for 30 minutes on ice. Antibody details are outlined in the Table 6. Subsequently the immunostained samples with 500µl FACS buffer were washed and spun. Next DAPI solution was placed in tubes at 1:5000 dilution, where appropriate. The contents of all Eppendorf tubes were moved to labeled polypropylene Falcon FACS tubes and stored on ice.

Antibody against	Fluorophore	Manufacturer	Concentration
Tie-2	APC	Biolegend	1:200
CD45	FITZ	Biolegend	1:200

Table 6. *Antibodies used for FACS sorting of pancreatic bud cells.*

2.1.16 Single cell lysis for scRNA-Seq

The scRNA-Seq protocol was adapted from Smartseq2 (Picelli et al. 2014). All experiments up to (but excluding) the cDNA amplification step were performed under a UV-sterilised hood with laminar flow, with all the surfaces free of RNase and DNA.

Initially 96-well plates for single cell collection and lysis were prepared. One µl of RNase inhibitor to 19 µl of 0.2 % (vol/vol) Triton X-100 solution, and 2.3 µl of the solution was aliquoted per well. Single cells were then sorted into wells of the 96-well plate by FACs. The gates were set to sort for DAPI-, CD31-, Tie2- cells of embryonic pancreatic buds. The plates were sealed with an adhesive lid and spun down the plate at 700 g for 1 minute. The plates were stored at -80°C before the sequencing for up to 6 months.

2.1.17 Reverse transcription for scRNA-Seq

The annealing mixture was prepared as in Table 7. and 2µl of annealing mix per well used. The 96-well plate was then centrifuged at 700g for 1 minute. Subsequently the samples were incubated at 72°C for 3 minutes and immediately placed on ice afterwards. The plates were then centrifuged at 700g for 1 minute.

Component	Amount
ERCC 20x	10µl
Oligo-dT 100µM	10µl
dNTP 10mM	100µl
dH_20	80µl
TOTAL	200µl

Table 7. *Annealing mix components.*

The reverse transcription mix was then prepared as in Table 8. and 5.6µl of reverse transcription mix added per well. The 96-well plate was then centrifuged at 700g for 1 minute.

Component	Volume per well	Volume per 96-well plate
Superscript II RT (200U/µl)	0.5 µl	50 µl
RNase inhibitor (20 U/µl)	0.25 µl	25 µl
5X superscript II first strand buffer	2 µl	200 µl
100 mM DTT	0.5 µl	50 µl
5 M Betaine	2 µl	200 µl
1 M $MgCl_2$	0.06 µl	6 µl
TSO (100 µM)	0.1 µl	10 µl
dH_2O	0.29 µl	29 µl
TOTAL	5.7 µl	570 µl

Table 8. *Reverse transcription mix components.*

The 96-well plates were then placed in the PCR machine and the programme as in Table 9. used.

Cycle	Temperature	Time	Purpose
1	42	90 min	RT and template switching
10	50	2 min	Unfolding of RNA secondary structures
10	42	2 min	Completion/continuation of RT and template switching
1	70	15 min	Enzyme inactivation
-	4	Hold	Safe storage

Table 9. *SMART-RT PCR machine programme.*

2.1.18 PCR preamplification for scRNA-Seq

The PCR mix was prepared as in Table 10. and 15µl added per well of a 96-well plate. The 96-well plate was then centrifuged at 700g for 1 minute.

Component	Volume per well	Volume per 96-well plate
KAPA HiFi Hotstart ReadyMix (2x)	12.5 µl	1250 µl
IS PCR primer (10 µM)	0.25 µl	25 µl
dH_2O	2.25 µl	225 µl
TOTAL	15 µl	1500 µl

Table 10. *PCR mix components for PCR preamplification step.*

The PCR programme was run for the samples according for the settings outlined in Table 11.

Cycles	Temperature (°C)	Time	Purpose
1	98	3 min	Denature DNA
21	98	20 sec	Denature DNA
	67	15 sec	Anneal DNA
	72	6 min	Extend DNA
1	72	5 min	Extend DNA
-	4	hold	-

Table 11. *SMART-PCR settings.*

2.1.19 PCR purification for scRNA-Seq

Ampure XP beads were equilibrated to room temperature for 15 minutes, then vortexed for several seconds. 25µl of Ampure XP beads were added to each sample (1:1 ratio) and mixed by pipetting until the solution appeared homogenous. The solutions were transferred to a 96-well plate with a compatible magnet stand. The mixture was incubated for 8 minutes at room temperature to allow the DNA to bind to the beads. The 96-well plate was placed on the magnetic stand for 5 mins or until the solution was clear and the beads had been collected at one corner of the well. The liquid was then carefully removed without disturbing the beads. The beads were washed with 200 µl of 80 % ethanol (vol/vol) for 30 seconds, and then the ethanol removed. This step was repeated and any trace of ethanol was removed and the beads left to dry completely at room temperature for 5 minutes. Subsequently, 20µl of EB from Qiagen was added and mixed 10 times to re-suspend the beads. The plate was first incubated in EB away from the magnet for 2 minutes, and then for 2 minutes on the magnet or until the solution appeared clear and beads have accumulated in a corner of the well. Finally, the supernatant was collected without disturbing the beads and transfer to a fresh tube.

2.1.20 Library preparation for scRNA-Seq

Tagmentation, which involves transposon cleaving and tagging of double-stranded DNA with a universal overhang, was carried out using the Illumina Nextera XT DNA sample preparation kit. The protocol was based on the Tagmentation protocol from Fluidigm. First, the NT Buffer was brought to room temperature, and vortexed if precipitate was visible. The Tagment DNA Buffer was warmed to room temperature. The other reagents from the Illumina Nextera XT DNA sample preparation kit were thawed and mixed by gently inverting the tubes 3–5 times, followed by a brief spin in a microcentrifuge. The Pre-mix was created in a 1.5 ml PCR tube, according to the Table 12. 3.75 µl of the pre-mix was added to each well of a library preparation 96-well plate, and 1.25µl of the sample from the sample plate was moved to the library preparation plate. The plate was then sealed and centrifuged at 2,000 rpm for 1 minute to remove bubbles.

Reagent	**Volume per sample (µl)**	**Volume per 96 well plate (with 25% overage)**
Tagmentation DNA buffer	2.5	300
Amplification Tagment Mix	1.25	150
Sample	1.25	
Total	5.0	

Table 12. *Pre-mix for library preparation.*

The library preparation plate was then placed in the thermal cycler according to the table 13.

Temperature (°C)	**Time**
55	10 minutes
10	Hold

Table 13. *Thermal cycler protocol.*

Subsequently 1.25µl of NT buffer per sample were placed in each well to neutralise the samples. The plate was then sealed and centrifuged at 2000 rpm for 1 minute. Next, 3.75µl of Nextera PCR Master Mix (NPM) was added to each well of the library preparation plate. 1.25µl of Index Primer (1-12)

were pipetted to the corresponding well of each row of the library preparation plate, as presented in Table 14.

	N701	**N702**	**N703**	**N704**	**N705**	**N706**	**N707**	**N708**	**N709**	**N710**	**N711**	**N712**
S501	S501/ N701	S501/ N702	S501/ N703	S501/ N704	S501/ N705	S501/ N706	S501/ N707	S501/ N708	S501/ N709	S501/ N710	S501/ N711	S501/ N712
S502	S502/ N701	S502/ N702	S502/ N703	S502/ N704	S502/ N705	S502/ N706	S502/ N707	S502/ N708	S502/ N709	S502/ N710	S502/ N711	S502/ N712
S503	S503/ N701	S503/ N702	S503/ N703	S503/ N704	S503/ N705	S503/ N706	S503/ N707	S503/ N708	S503/ N709	S503/ N710	S503/ N711	S503/ N712
S504	S504/ N701	S504/ N702	S504/ N703	S504/ N704	S504/ N705	S504/ N706	S504/ N707	S504/ N708	S504/ N709	S504/ N710	S504/ N711	S504/ N712
S505	S505/ N701	S505/ N702	S505/ N703	S505/ N704	S505/ N705	S505/ N706	S505/ N707	S505/ N708	S505/ N709	S505/ N710	S505/ N711	S505/ N712
S506	S506/ N701	S506/ N702	S506/ N703	S506/ N704	S506/ N705	S506/ N706	S506/ N707	S506/ N708	S506/ N709	S506/ N710	S506/ N711	S506/ N712
S507	S507/ N701	S507/ N702	S507/ N703	S507/ N704	S507/ N705	S507/ N706	S507/ N707	S507/ N708	S507/ N709	S507/ N710	S507/ N711	S507/ N712
S508	S508/ N701	S508/ N702	S508/ N703	S508/ N704	S508/ N705	S508/ N706	S508/ N707	S508/ N708	S508/ N709	S508/ N710	S508/ N711	S508/ N712

Table 14. *Indexing of single cell RNA-sequencing samples.*

The plate was then sealed with adhesive film and centrifuged at 2,000 rpm for 1 minute. Next, the plate was placed onto a thermal cycler and PCR amplification performed according to protocol in Table 15.

Temperature (°C)	**Time**	**Cycles**
72	3 minutes	1
95	30 seconds	1
95	10 seconds	12
55	30 seconds	
72	60 seconds	
72	5 minutes	1
10	hold	-

Table 15. *PCR amplification protocol.*

The amplified products were stored at -20 °C.

2.1.21 Library pooling and clean-up for scRNA-Seq

Agencourt AMPure XP beads were warmed up to room temperature and vortexed. Library pool was created by pipetting the appropriate volume from each sample and the corresponding AMPure bead volume. For 96 samples, 1µl volume of each sample was taken to reach 96µl total volume, with 87µl AMPupe bead volume (90% of total pool volume). The two were mixed well by pipetting up and down 5 times and left to incubate at room temperature for 5 minutes. The tube was then placed on a magnetic stand for 2 minutes, and the supernatant carefully removed without disturbing the beads. Next, 1ml of freshly prepared 80% ethanol was added and incubated for 30 seconds on the magnetic stand. Then the ethanol was removed. This ethanol wash step was repeated, and the beads were allowed to air dry on bench for 10-15 minutes. For the elution of 96 samples, 50µl of elution buffer were used. The tube was then vortexed and incubated for 2 minutes at room temperature. Then the tube was placed on a magnetic stand for 2 minutes. The entire volume of supernatant was transferred to another PCR tube. Finally, the library size distribution was checked on an Agilent high-sensitivity DNA chip. The quantification of pooled library was carried out using KAPA library quantification kit.

2.2 Studying pancreatic development with *ex vivo* explant system

2.2.1 Ex vivo explants in collagen culture

2.2.1.1 Culture

Ex vivo explant system was optimised in an attempt to use it for live imaging and the study of clonal development. Pancreatic buds were dissected at E12.5 or E13.5. Plates with fibroblasts in *ex vivo* culture medium were prepared, in order to provide the explant with growth signals, as outlined in Table 16. Filter membranes with a drop of collagen in the middle were placed floating in the medium. Dorsal pancreatic bud was inserted into the collagen and then the whole filter was moved down to stick to the bottom of the plate. The explants were left to grow for 2, 4 and 7 days with the medium being changed every 2 days. At each end-point the buds were removed gently from collagen, fixed for 45 minutes in 4% PFA at 4°C and then washed 3 times in PBS for 15 minutes each wash.

Component	Concentration	Manufacturer
GMEM	550 ml	Life Technologies
Penicillin/Streptomycin	100x	Life Technologies
Sodium pyruvate	100x	Life Technologies
Non-essential amino acids	100x	Life Technologies
Glutamine	100x	Life Technologies
Fetal Bovine Serum	100ml	Life Technologies
b-mercaptoethanol	100x	Life Technologies

Table 16. *Ex vivo pancreatic bud culture medium.*

2.2.1.2 Vibratome sectioning

For visualisation of clones from *ex vivo* cultured pancreatic buds, thick section Vibratome sectioning was used. Following fixation in 4% PFA as described above, the tissue was immersed in liquid 3% low melting point agarose (40℃) and left to cool down. The solid agarose with pancreatic buds was cut with a vibrating microtome (Leica VT100S, velocity: 0.9mm/s, amplitude: 0.65mm) into semi-thick sections (150µm). Sections were embedded in Vectashield (Vector Laboratories) on microscope slides.

2.2.1.3 Staining of vibratome sections

The vibratome sections were permeabilised in 0.5% Triton-100X, 2% donkey serum, 4%DMSO in PBS overninght at 4°C in wells of 4-well plates from NUNC.

The primary antibody dilution was made up in 0.5% Triton-100X, 2% donkey serum, 1%DMSO in PBS. The incubation in primary antibody solution was carried out for 2-3 days at 4℃. The samples were subsequently thoroughly washed by rinsing 3 times in 0.2% Triton-100X in PBS, washing for 30 minutes in 0.2% Triton-100X in PBS and then for 1 hour. The sections were then incubated in secondary fluorescently-tagged antibody (1:800; secondary antibodies were from Life Technologies) and DAPI in 0.5% Triton-100X, 1% DMSO, 2% DS in PBS for 2-3 days. Next, the samples were washed thoroughly in 0.2% Triton-100X in PBS by rinsing three times in 0.2% Triton-100X in PBS, washing for 15 minutes in 0.2% Triton-100X in PBS, and washing in PBS twice for 2 hours. The sections were finally mounted on slides with mountant from Calbiochem and coverslips. The summary of primary antibodies used is presented in the Table 17.

Antibody against	Manufacturer	Antibody species	Dilution
Pdx1	Abcam (Ab47267)	Rabbit polyclonal	1:200
Insulin	Abcam (ab7842)	Guinea pig polyclonal	1:200
GFP	Life technologies; A11122	Rabbit polyclonal	1:500

Table 17. *Primary antibodies – summary of manufacturer and dilution used in immunostaining of Vibratome sections of ex vivo explants.*

2.2.2 Ex vivo culture on fibronectin

2.2.2.1 Culture

Another *ex vivo* system was optimised to improve upon the limitations of the previous system. The *ex vivo* growth on fibronectin system is based on a previous publication (Petzold & Spagnoli 2012), and has been shown to be effective at achieving branching morphogenesis and is a suitable system for live imaging. Amongst the substrates tested, the authors found that fibronectin gave best result when it comes to observation of branching morphogenesis.

35-mm Petri dish with 20-mm diameter glass microwell bottom from MatTek Corporation were used – 1 dish per 1 pancreatic explant. One day before the dissection and isolation of the pancreatic buds, the bottom of the wells was coated with fibronectin (50ug/ml in 1X-PBS) with a minimum volume of 150µl and left at 4°C overnight. On the day of dissection, the fibronectin was aspirated, the well was rinsed with PBS and 150µm of *Ex vivo* pancreatic bud medium (see Table 16.) added and placed in the incubator at 37°C.

The dissected pancreatic bud was transferred into MatTek dish with a glass Pasteur pipette. To ensure spreading during culture, the mesynchyme surrounding the explant was slightly ripped with a fine needle. Then the dishes were gently placed in a tissue culture incubator (37°C, 5% CO2) for a few hours to enable the attachment of explants to the glass bottom. Once attached, the dish was filled with 1.5-2ml of the culture medium, pre-warmed at 37°C. The culture medium was changed every 2 days.

2.2.2.2 Whole-mount immunostaining of pancreatic buds grown *ex vivo* on fibronectin

Whole-mount immunostaining was carried out on pancreatic explants grown on fibronectin in order to preserve the spreading pattern achieved during *ex vivo* culture (see above) and to enable imaging in the MatTek plates. The culture medium was aspirated and the explant was washed once with PBS. The explants were fixed with 2ml 4% PFA on ice for 20 minutes. The plate was gently swirled from time to time. The 4% PFA solution was removed and the explant washed 3 times with 2 ml of PBS for 10 min each at room

temperature. Then the samples were placed in 2ml of blocking solution of 0.1% Triton-100X, 3% donkey serum in PBS for 30 min at room temperature. The primary antibody was diluted in blocking solution and about 150µl of the solution added to the microwell to cover the whole explant, and left overnight at 4°C. Information about primary antibodies used is presented in Table 18. In order to prevent evaporation, the MatTek plates were placed in a humid chamber. The next day the antibody was removed, and the samples washed in 1X PBS, 3 times for 30 minutes. The secondary antibody was diluted in blocking solution, using Alexa Fluor dye secondary antibodies diluted 1:750. DAPI was added to the solution for nuclear staining. About 150µl of the dilution was added to microwells and left to incubate at RT for 2 hours in the dark, in a humid chamber to avoid evaporation. Finally, the samples were washed 3 times with 2ml of 0.1% Tween-20 in PBS for 30 minutes each at room temperature and then once in PBS to remove Tween-20. The samples were mounted in Calbiochem mountant.

Antibody against	Manufacturer	Antibody species	Dilution
Insulin	Abcam (ab7842)	Guinea pig polyclonal	1:200
GFP	Life technologies (A11122)	Rabbit polyclonal	1:500
CK19	Abcam (ab52625)	Rabbit monoclonal	1:200
Glucagon	Abcam (ab10988)	Mouse monoclonal	1:200
Amylase	Santa Cruz Biotechnology (sc-12821)	Goat polyclonal	1:200

Table 18. *Primary antibodies – summary of manufacturer and dilution used in immun*ostaining of pancreatic explants grown according to Petzold & Spagnoli *2012.*

2.2.3 Tamoxifen treatment *ex vivo*

For *ex vivo* Tamoxifen induction of *ex vivo* culture system of Rosa26-CreERT2; Rosa26-Confetti pancreatic buds 10nM OH-Tamoxifen was provided in the medium for 18 hours and then replaced with OH-Tamoxifen-free medium.

2.3 Statistical methods

2.3.1 Statistical analysis of clonality of lineage tracing induction

The assessment of clonality of induction of *R26*-CreT2; *R26*-Confetti system was necessary in order to assure the correct assessment of potency of tissue.

First, spatial x,y and z coordinates of individual clones, as well as their relative volume in terms of acinar, ductal and islet compartments (for the E9.5 to P14, E12.5 to P14 and E12.5 to P28 tracings) were manually assessed. This information was collected for all tracings considered.

Statistical analysis of clonality of data was performed in collaboration with Dr Edouard Hannezo from the University of Cambridge. It involved computing the probabilities of distances between clones of the same and different colour and comparing their distributions. An assumption was set that all clones were independently induced, meaning that the probability of finding clones of the same colour should be independent of distance, i.e. *P(r)* constant, which we set as our null-hypothesis.

Next, a non-parametric bootstrapping method was used to build confidence intervals on the prediction from the null hypothesis. We thus calculated for each individual pancreas the probability for a clone to have one of the four confetti colours, and randomly re-assign colours of clones according to this average property. This procedure was performed 1000 times, and calculated in each case the rescaled probability P(r). Finally, we calculated a 95% confidence interval at each distance r from this resampled probability distribution, in order to assess how much experimental deviations of P(r) from a constant value can be due to random statistical variations. We plotted in Fig 16 these confidence intervals for each individual mouse induced at E12.5 and traced until P14, together with the experimental measurements of P(r). Exponential probabilities, although showing statistical variations, were consistently included within the 95% confidence interval from the null-hypothesis. Where statistically significant excess of clones of the same colour at short distances was observed (mouse 1, Fig. 16), this was then corrected statistically for this bias by grouping all clones of the same colour within a

given radius, in order to return to the probability value expected from clonal induction.

The details of clonality tests and demonstration of potency outcomes are presented in Chapter 3.4.3.

Finally, for the E15.5 to P14 and E18.5 to P14 induction lineage tracings, only the potency was assessed, via the same methods as described in Chapter 3.4.3. In order to ensure clonality, given that the density of labelled clones was higher, I only used the rare colours in the quantifications.

2.3.2 Comparison of distributions

Cumulative distributions of rescaled clone and ductal subtree sizes were used in this thesis to present and compare clonal and ductal subtree size variability. Cumulative distribution presents a function of variable X being smaller or equal to a certain value.

Mann-Whitney statistical test was used to assess the match of any two distributions. Mann-Whitney test is based on a null hypothesis, which assumes that all the observations of both groups are independent of each other, or in other words it is equally likely that a randomly selected value from one sample will be less than or greater than a randomly selected value from a second sample. Two distributions are independent if $P<0.05$. The comparison of clone and subtree size distributions, as well as distributions of potency outcome between amylase-control and initial potency experiment resulted in $P>0.5$, indicative of a close match of distributions under study.

Quantile-quantile plots were also computed to compare the various distributions. In order to provide an additional goodness of fit metric, we computed the coefficient of determination R^2 of the quantile-quantile plots to the predicted curves of $f(x)=x$ if the distributions were perfectly identical. We found $R^2=0.87$ for the E18 subtree distribution versus the P14 acinar distribution, $R^2=0.83$ for the E18 subtree distribution versus the P14 ductal distribution and $R^2=0.99$ for the P14 acinar distribution versus the P14 ductal distribution. Moreover, we found $R^2=0.89$ (respectively $R^2=0.93$) when comparing the P14 acinar (respectively ductal) distribution versus the

theoretical subtree size distribution (derived for mammary gland branching morphogenesis; Chapters 4.6 and 4.7). These are indicative of close correspondence between the shape of these various distributions.

2.3.3 Model of branching morphogenesis

Computational modelling was carried out to infer the dynamics of growth of pancreatic compartments. The model of stochastic bifurcation and termination of ductal branches was developed in collaboration with Dr Edouard Hannezo from the University of Cambridge, making use of a model previously shown to predict the network heterogeneity of the mouse mammary gland epithelium (Scheele et al. 2017). The model is based on a paradigm, whereby equipotent "active" terminal end-buds choose stochastically between ductal bifurcation and termination (inactivation), where cells irreversibly stop contributing to branching morphogenesis.

In the case of purely ductal end-driven morphogenesis, the history of branching decisions can be "read off" from the topology of the ductal tree network. By averaging across branches of the same generation, *n*, defined as the number of branch points separating a given branch from the primordial central ducts from which branching morphogenesis proceeds, estimates can be made of the evolving bifurcation/termination probabilities. The generation number can be uniquely defined as both mammary and pancreatic ductal trees are simple graphs, i.e. we do not observe any loops or reconnections between two independent subtrees starting from the main trunk.

Moreover, in common with the mammary gland, the reconstruction and modelling of pancreatic ductal trees is simplified by the fact that morphogenesis proceeds in a largely two-dimensional setting (See Chapter 4.8), with subtrees not growing below or above one another, and ductal cross-overs occurring rarely. This offers a simple heuristic explanation for how environmental signals can provide a feedback mechanism to arrest ductal bifurcation, viz. ductal termination. A generic feature of this type of dynamics is that the probabilities of ductal branching versus termination converge towards balance (as steric constraints require each branching event to be compensated, on average, by a ductal termination event; Scheele et al. 2017)

Thus, when averaging ductal branching versus termination decisions at a given generation, *n,* the problem reduces to a Galton-Watson process in a spatially varying environment. An active ductal terminus A_n, at generation *n*, can either divide symmetrically to give rise to two active offspring termini $A_n \rightarrow 2A_{n+1}$, with probability *1-q(n),* or stop contributing to ductal morphogenesis (i.e. terminate), $A_n \rightarrow \varnothing$, with probability *q(n)*. In the case of mammary gland pubertal morphogenesis, the probability *q(n)* quickly converged, within a few generations, towards balance with q(n)=½, indicative of near compensation between ductal branching and termination. This results in subtree size distributions, expressed in terms of the number of total branches in a given subtree, which are characteristically broad with an exponential tail, fitting quantitatively with the experimental data. This means that most subtrees stochastically stop contributing to branching morphogenesis, while an ever-diminishing surviving population ends up giving rise to nearly all of the peripheral regions. Interestingly, as discussed in the main text, this is very much the phenomenology that we see in the branching pattern of whole-mount pancreas (Fig. 27). Accordingly, we find a broad subtree size distribution which matches well with both the distribution of clone sizes (acinar and ductal) and its mammary gland counterpart. This argues for a common mechanism of branching morphogenesis resulting, at least in part, from ductal bifurcation and termination.

Thus, we made use of the measured branching probabilities *q(n)* obtained for the mouse mammary gland to obtain a prediction of the total subtree size (which is defined as $\sum_{\mathbf{n}} A_n$) distribution, through a numerical integration of the associated Galton-Watson “birth-death” process. We also simulated in Figure 33 typical outputs of such tree topologies, using the Galton-Watson model described above for $q=1/2$, independent of *n.*

Again, as described previously (Scheele et al. 2017), we assume that ducts consist of *N* equipotent multipotent precursors, which are randomly allocated to one the two offspring ducts upon bifurcation, such that each new duct received *N/2* self-renewing precursors. One should note that relaxing this equal repartition assumption does not give rise to qualitatively different

behaviour to the one we describe here. Each cell then divides to replenish the pool, to give rise again to *N* precursors per tip. Interestingly, even in the absence of any active competition between cells, this is expected to drive monoclonal conversion of lineage-labelled ducts. This is because, upon bifurcation, a clone will be randomly segregated, and thus enriched in one of the tips, and depleted in another. In the limit of randomly allocated cells, i.e. cell mixing, which is relevant here (as we do not see cohesive streams of clones before monoclonal conversion), monoclonal conversion is expected to occur slowly, as clone sizes increase linearly with the number of tip bifurcations undergone.

Therefore, for *N=30* precursors per tip, one never observes monoclonal conversion over the time-scales relevant for pancreatic morphogenesis (Fig. 33). This is in stark contrast to the experimental data, which is characterized by very rapid monoclonal conversion of ducts (Fig. 33), on the scale of just a few generations. Therefore, this heavily constrains the number of tip precursors that are located in each individual ductal terminus. Simulations of as few as *N=4* precursors per ductal terminus yield a reasonable speed of monoclonal conversion.

One should note that cell competition during ductal bifurcation would speed up the process, but not yield qualitatively different results, as average clones sizes would still increase only linearly with generation number. Interestingly, such a behaviour of monoclonal conversion of entire ductal subtrees of the pancreas, seen both from ductal-containing clones and acinar-containing clones validates *a posteriori* such a ductal end-splitting mechanism of morphogenesis.

2.3.4 Single cell sequencing methods

Pooled libraries were sequenced using the Illumina HiSeq 4000 system (single-end 50 bp reads). Reads were aligned using G-SNAP (Wu & Nacu 2010) and the mapped reads were assigned to Ensembl genes (release 81) (Flicek et al. 2014) by HTSeq (Anders et al. 2015). Raw data has been uploaded to National Center for Biotechnology Information GEO (accession number GSE89798).

The single cell sequencing analysis was carried out in collaboration with Dr Steffen Rulands from the University of Cambridge. To identify poor quality cells, three metrics were used: (1) the proportion of aligned reads, (2) the number of endogenous reads and (3) the number of features with more than 1 read. We filtered for cells with (1) more than 20% aligned reads, (2) more than 200,000 endogenous reads and (3) more than 5000 detected features. We only considered genes that were detected in at least 2 cells, with a variance greater than 0.001.

Out of the 672 cells that were captured in the experiment, 516 (77%) were used for downstream analysis. Reads were normalized using the deconvolution method as implemented in the scran package (A & K 2016).

We then performed dimensionality reduction using PCA, resulting in two distinct groups of cells. Using the epithelial marker *Epcam* we identified one of these clusters as pancreatic cells (303 cells). Focusing on the pancreatic cells alone, we performed t-SNE (Krijthe 2015) followed by k-means clustering from R's statistics package on the 500 most variable genes and identified the cellular identity of cells in the three clusters using known markers for acinar, ductal and islet cells.

To identify co-varying genes, we computed Spearman's ρ for a list of genes which, according to literature, are associated with pancreatic development, and used $2 - \rho$ as a dissimilarity index for hierarchical clustering.

Using the destiny package (Angerer et al. 2016), we employed a diffusion map (parameters: sigma=95, k=302) and used the DPT function to arrange cells in pseudo time. Three distinct branches were identified and, based on the expression of proliferation markers (such as Mki67) and various specification and differentiation markers (such as *Cpa1* or *Neurog3*), we identified the branch containing sample "SLX-11256.N701_S506" as the one "earliest" in its developmental stage and used this cell as a starting point to calculate the diffusion pseudo time.

2.4 Statistical reporting

In Fig. 8, representative images were selected based on analysis of *n=4* mice for each *2, 4* and *7* days of *ex vivo* culture. In Fig. 9, representative images were selected based on analysis of *n=4* mice for E13.5 and E14.5 collection timepoint.

In Fig. 10, representative images were selected based on analysis of sections from *n=4* mice for E18.5 collection timepoint and *n=3* mice for the P14 collection timepoint. In Fig. 11, representative images were selected based on analysis of sections from *n=3, 3, 2* and *2* mice for E9.5, E12.5, E15.5 and E18.5 induction timepoint, respectively. In Fig. 13, representative images were selected based on analysis of sections from *n=3* mice.

In Fig. 15, 16, 17, 20, 21, 24, 25, 27, 28, 29 and 30, 254 clones induced at E12.5 and traced until P14 were scored from *n=3* mice. Error bars represent mean and SD or SEM (outlined in Figure legends). In Fig. 16, 18, 20, 22, 32 representative images were selected based on analysis of 254 clones induced at E12.5 and traced until P14 were scored from *n=3* mice.

In Fig. 16, 17, 20, 41, 25, 27, clones induced at E9.5 and traced until P14 were scored from *n=2* mice.

In Fig. 17, and 25, 84 clones induced at E12.5 and traced until P28 were scored from *n=2* mice. Error bars represent mean and SD.

In Fig. 19, EdU+ cells were analysed for *n=3 (*E13.5) *n=2(E15.5)* and *n=9* mice (18.5).

In Fig. 23 and 24, 26 clones induced at E12.5 and traced until P14 were scored from *n=2* mice for the amylase immunostaining control.

In Fig. 26, 27, subtree sizes were measured for *n=3* mice and *n=43* independent subtrees. Error bars represent mean and SD.

In Fig. 28, pancreas mass was measured for *n=3* mice (E18), *n=5* mice (P7), *n=11* mice (P14) and *n=4* mice (P28). Error bars represent mean and SEM. In Fig. 28, pancreas length, width and height were measured for *n=3* mice

(E13.5), *n=3* mice (P14) and *n=3* mice (P28). Error bars represent mean and SEM. In Fig. 28, the percentage of DBA+ cells was calculated from sections from *n=5* pancreata.

In Fig. 33, 78 clones induced at E15.5 and traced until P14 were scored from *n=2* mice. In Fig. 33, 70 clones induced at E18.5 and traced until P14 were scored from *n=2* mice.

For Fig. 36, 37, 38, 39, 40, and Table 21 and 22, 516 single cells were isolated from *n=7* mice for the single-cell RNA sequencing (*n=5* for E13.25 and *n=2* for E15.25).

In Fig. 41-44, 26 islet clones from *n=2* mice were quantified for E9.5 induction, and 68 islet clones from *n=3* mice for E12.5 induction.

Chapter 3

Results: Clonal analysis

3.1 Introduction

This chapter is the first of the four Results chapters. In this chapter, I present outcomes of the optimisation of lineage tracing to study the development of pancreas, together with the assessment of the levels of induction in *R26*-CreT2; *R26*-Confetti mice, and general characterisation of clone types observed with lineage tracing of E12.5-induced cells.

The chapter aims at answering the following research questions:

- What is the best system and conditions to study pancreatic development with *R26*-CreT2; *R26*-Confetti lineage tracing?
- How do I ensure that clonal levels of induction are achieved?
- What is the potency of pancreas in primary and secondary transitions?
- Is there variability between clone sizes and is it related to potency?

The chapter starts by presenting the principles behind confetti lineage tracing, and the optimisation of the method. This is followed by an outline of the quantification of clone and tissue landmarks, and explanation of the conducted clonality assessment, essential for ensuring the accuracy of potency analysis. I then discuss the potency of tissue at the onset of primary and secondary transition.

3.2 Optimisation of the system for studying cell fate decisions in development with Confetti reporter system

3.2.1 Confetti reporter line

Genetic lineage tracing has been used to study the effects of some genes on pancreatic development. These have helped the understanding of lineage relationship in the pancreas. However all the studies to date have been performed at high density of labelling (Zhou et al. 2007; Solar et al. 2009; Kopinke et al. 2011; Schaffer et al. 2010; Kopp et al. 2011; Pan et al. 2013). Clonal density of induction, i.e. clones arising from a single cell, are required for accurate analysis of lineage potencies.

In order to achieve statistically defined clonal density level of induction, Confetti reporter mice (*R-26*-Confetti) were used in this thesis. R26-Confetti is a multicolour Cre-reporter that was first used for lineage tracing by Snippert et al. in their study of intestinal homeostasis (Snippert et al. 2010). They integrated the construct consisting of a strong CAGG promoter, a LoxP-flanked Neo^R - which serves as a transcriptional roadblock, and the Brainbow-2.1 cassette (Livet el al., 2007), into Rosa26 locus. After Cre-recombination the roadblock is removed and the Brainbow 2.1 cassette is recombined to produce one of the 4 fluorescent proteins in random (see Fig. 7).

With the aid of multicolour reporter – confetti – driven by a ubiquitous promoter *R26* (*R26*-RCreT2; *R26*-Confetti), random, non-lineage specific cells in the pancreas can be labelled at different frequency (in a Tamoxifen concentration-dependent manner) and at different developmental stages. The labelling of cells in different colours enables the statistical assessment of clusters of the same colour as to whether they belong to one or several clones (see later), based on the comparison of probabilities of finding clones of the same colour versus different colour at a certain distance. Furthermore, the use of such a multicolour system enables the discrimination between the clonal progeny of neighbouring progenitor cells within the same niche.

In this project, I aimed to study the potency of cells in primary and secondary transition of pancreatic development and examine the dynamics of pancreatic ductal, acinar and islet compartments in the secondary transition.

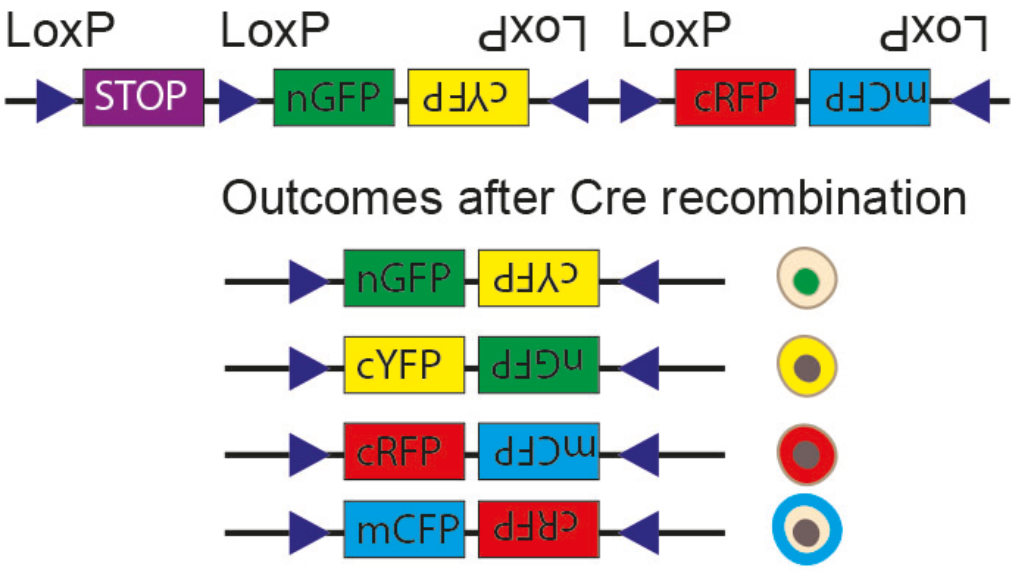

Figure 7. *The basis of the stochastic multicolour Cre-Reporter R26-Confetti cassette reporter (Livet et al. 2007) and fluorescent protein expression (nuclear GFP – nGFP, cytoplasmic YFP – cYFP, cRFP, and membrane CFP – mCFP). Brainbow2.1 encoding 4 fluorescent proteins was inserted into Rosa26 locus. Upstream of the cassette, a strong CAGG promoter, a loxP site, and a neomycin resistance roadblock were placed. Upon Cre-activation, the neomycin roadblock is removed while the brainbow2.1 cassette recombines stochastically to generate one of the four fluorescent protein sequences. GFP is nuclear, CFP is membrane-bound, while the remaining 2 are cytoplasmic.*

3.2.2 Cre induction *ex vivo* and *in vivo*

I aimed at optimising the protocol for the induction of cells in *R26*-RCreT2; *R26*-Confetti embryonic pancreas, in order to study the potency of cells and morphogenic processes during development. Hence, I prioritised the optimisation of *ex vivo* and *in vivo* methods described below, in order to obtain clonal levels of *R26*-Confetti-reporter induction, as well as to achieve systems recapitulating normal development and tissue morphogenesis.

Ex vivo

Initially, I aimed at using an *ex vivo* pancreatic development system to induce and live-trace the induced cells, in order to take record of cell proliferation and migration in real time. Furthermore, this method would enable the avoidance of complications related to *in vivo* injection of pregnant females. Specifically, embryo abortion and inability to reach full term of pregnant females have been reported, as Tamoxifen interacts with oestrogen receptor (Grese et al. 1997). Therefore, I set out to test the range of concentrations of OH-Tamoxifen to achieve clonal level of induction.

R26-Confetti mice were mated with *R26*-CreERT2 mice. Pancreatic buds were dissected from embryos at E13.5, as I planned to exploit this system to look at the events of secondary transition. In the first *ex vivo* protocol tested, the explants were embedded in a drop of collagen that was placed on a filter membrane. The membrane, in turn, was floating in a medium for *ex vivo* culture (see methods) similar to the liquid-air phase method previously described (Duville et al. 2007). Collagen was used to replicate the stimuli that the buds may receive from ECM during development *in vivo*.

Different concentrations of OH-Tamoxifen were tested and the 10nM OH-Tamoxifen was eventually applied for 18 hours as an optimal concentration for the induction of cells. The explants were maintained in the medium for 2, 4, and 7 days, subsequently fixed and sectioned with Vibratome and co-stained against insulin. The result of Tamoxifen induction and co-staining against the endocrine marker is presented in Figure 8.

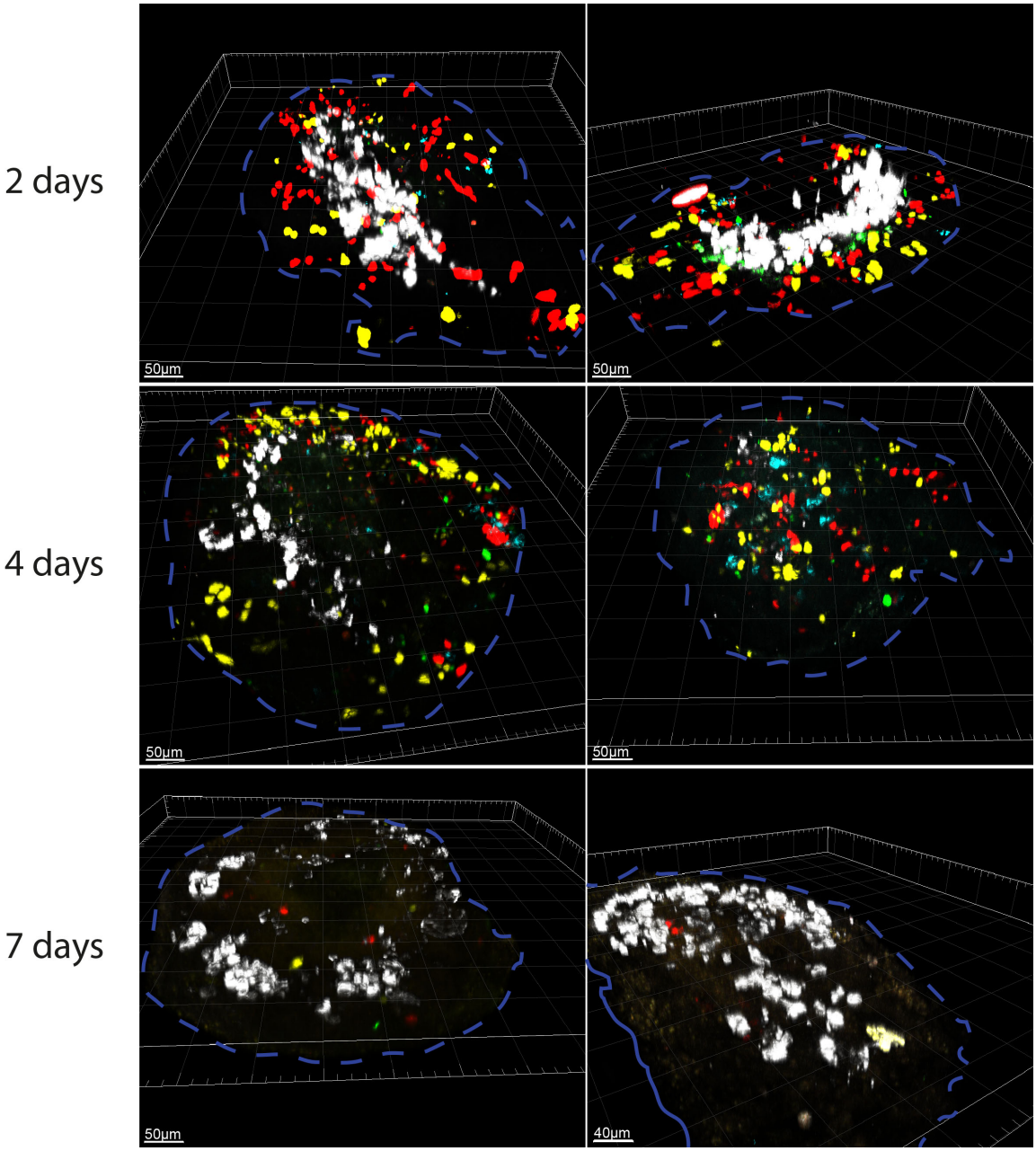

Figure 8. *Confetti pancreatic bud growth ex vivo in collagen, on filter membranes, in pancreatic bud medium. Recombination was induced with 10nM OH-Tamoxifen for 18 hours and the buds were fixed after 2, 4 and 7 days of ex vivo growth. Cyan, green, yellow, and red are confetti colours. Insulin is grey. Periphery of the tissue is marked with navy blue dashed line based on tissue autofluorescence visualised in Imaris software. Representative images were selected based on analysis of n=4 embryos from 3 litters for each 2,4, and 7 days of ex vivo culture.*

Figure 8 reveals that at subsequent *ex vivo* chase timepoints, the number of confetti+ cells decreases, suggesting that the cells are dying in this *ex vivo* growth system. Furthermore, the cells seem to be induced preferentially at the periphery of the bud, which suggests that Tamoxifen in unable to penetrate into deeper layers of the tissue due to collagen encapsulating the pancreatic bud. Finally, the *ex vivo* grown pancreatic bud displays a round, restricted shape as compared to that of the *in vivo* developing pancreata, which could be due to collagen limiting the growth of the bud by exerting pressure.

Altogether, it appears that the *ex vivo* growth of pancreatic buds in collagen has significant disadvantages, such as an impaired growth and survival of cells. I therefore decided to undertake an alternative protocol for the culture of embryonic pancreatic explants. The new method involves growing the buds on laminin-coated MatTek plates in a pancreatic growth medium according to a protocol developed previously (Petzold and Spagnoli 2012). This system has been suggested to reliably recapitulate the branching morphogenesis process with the evidence for development of the major pancreatic lineages (Petzold and Spagnoli 2012). This system is also optimal for live imaging, as MatTek plates contain imaging coverslip at the bottom of the dish.

I therefore first aimed to characterise the development and growth of pancreatic buds using this system. Pancreatic buds were dissected at E13.5 (for studying secondary transition phase of pancreatic development), and the same concentration (10nM) and duration of OH-Tamoxifen treatment (18 hours) as in the previous method was applied. I found that, in contrast to the collagen embedding method, the development of pancreatic explant was not space-constrained.

However, I encountered an antibody immunostaining problem when staining the explants against various pancreatic compartments (data not shown). Finding optimal conditions for immunostaining, which would enable long enough exposure to antibodies for good penetration without detaching the explants from the surface of the culture MatTek plate turned out to be unfeasible. In the future, the optimisation of staining and clearance protocols should resolve this problem.

In vivo

The two *ex vivo* protocols were optimised and tested in order to potentially apply them for live imaging analysis. *Ex vivo* OH-Tamoxifen system has the advantage of avoiding the adverse effects of Tamoxifen injection into pregnant females. However, *ex vivo* pancreatic development did not recapitulate the *in vivo* development to a satisfying degree. I therefore turned to *in vivo* system optimisation. I sought to determine if feasible concentrations of Tamoxifen could be used for injection of pregnant females without adverse effects related to pregnancy. I also aimed at using the samples obtained from *in vivo* tracing for assessment of the two *ex vivo* methods described above, as they would serve as a reference point. Furthermore, were this experimental set-up successful, then I would be able to look at the potency of cells and morphogenic events of primary transition in addition to secondary transition events. Studying the primary transition phase would be impossible with an *ex vivo* approach, as technically, I would be unable to dissect pancreata at embryonic stages below E12.0 due to its small size.

I first optimised the dose for Tamoxifen injection of pregnant females at E12.5, as studying the cell fate and morphogenesis of secondary transition was our primary focus. Additionally, studying the structure and clonal morphology of *in vivo* obtained pancreata would enable the comparison with and validation of the two *ex vivo* systems outlined above.

The optimised dose of Tamoxifen for injection at E12.5, which provided clonal density labelling in embryonic pancreas, amounted to 0.025ug/g weight of pregnant mouse. Embryos were collected at different developmental stages – E13.5, E14.5 to assess whether suitable induction frequencies were obtained; and E18.5, P14, P28 to obtain information about the morphological changes within the tissue and clonal structure. The samples were then fixed in 4% PFA and imaged whole-mount (E13.5, E14.5 and E18.5) or in thick sections (P14) with confocal Leica SP5 microscope (representative images shown in Fig. 9, 10). Optimisation of sectioning and immunostaining methods is outlined in the

next section. None of the embryos were aborted, and the pancreata were of normal size and macroscopic phenotype.

The observation of clones traced between E12.5-E13.5 and E12.5-E14.5 revealed that the clonal levels of induction were achieved, as sparse clones consisting mainly of single cells were detected (Fig. 9). The fluorescent proteins were induced evenly throughout the pancreatic bud, showing an advantage over the *ex vivo* in collagen protocol, whereby labelled cells were located at the peripheral parts of the pancreas. Furthermore, the construct was non-leaky, i.e. no confetti fluorescent proteins were detected in the negative control samples without Tamoxifen injection (Fig. 9). Lastly, there was an increase in the number of fluorescent proteins between E13.5 and E14.5, suggesting that recombination is not complete by E13.5, consistent with a previous report suggesting that Cre recombination can take between 12 and 36 hours (Danielian et al. 1998).

The clones collected at the end of secondary transition, at E18.5, and at P14, show cohesive morphological structures spanning over 100 µm or more (Fig. 10). The structure of clones is more complex as compared to the clones obtained with *ex vivo* system (Fig. 8, 10). This suggests that the *ex vivo* system might not recapitulate pancreatic development *in vivo*. The apparent significant advantage of the *in vivo* method is that all divisions, migration events and other processes occur in embryos *in utero* and therefore cannot be a consequence of artificial conditions.

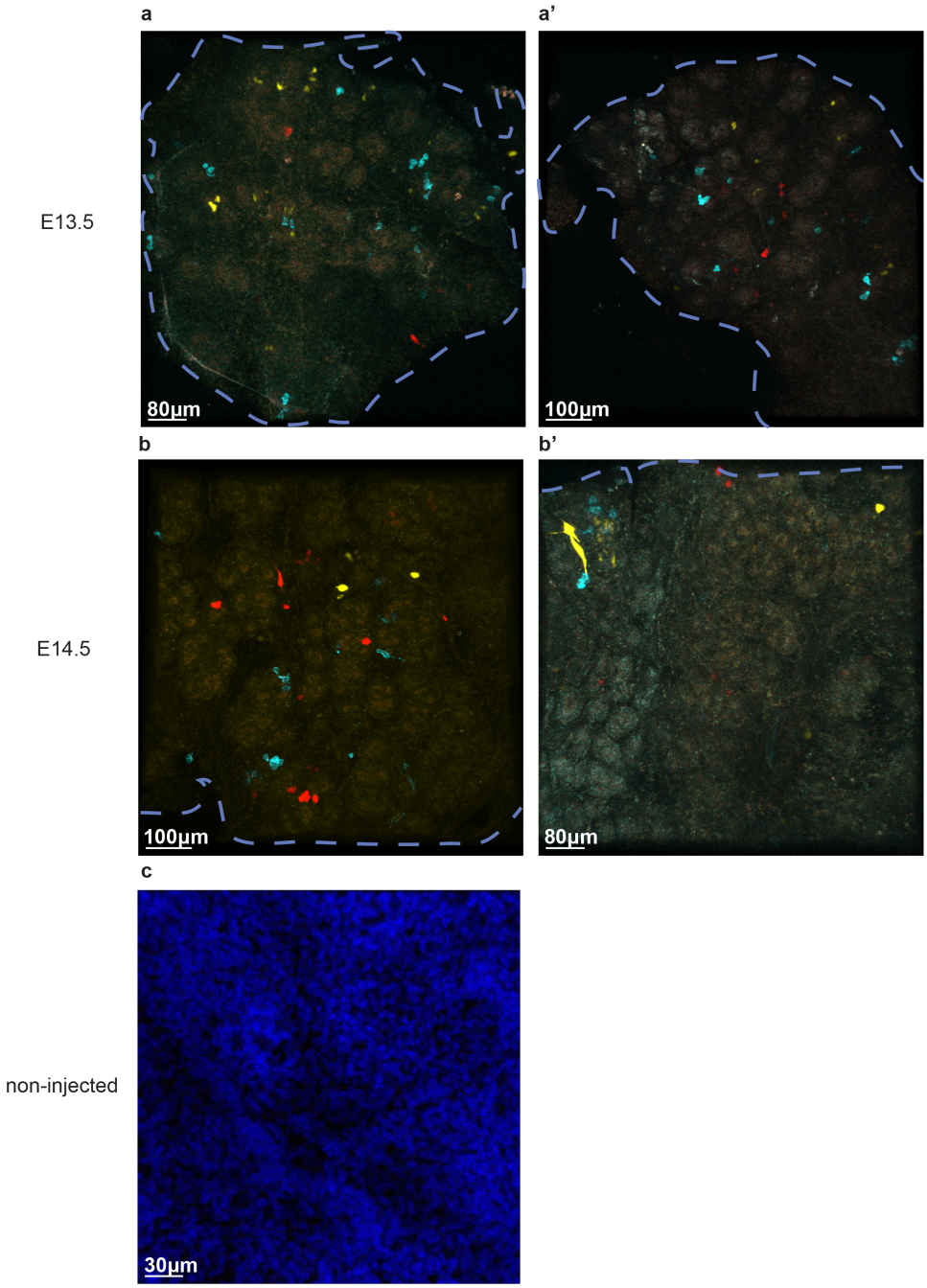

Figure 9. *Confetti pancreatic bud induction with 0.025ug/g mouse Tamoxifen injection in R26-CreT2; R26-Confetti mice. The injection was performed on E12.5 and the samples were collected at (a, a') E13.5 and (b, b') E14.5 to verify that the clonal levels of induction were achieved. For each timepoint 2 independent pancreata are presented (c) Non-injected samples showed no confetti-colours, revealing that the construct is non-leaky. Confetti colours are cyan, green, yellow, and red. Boundaries of tissue based on autofluorescence are in blue. Representative images were selected based on analysis of n=4 embryos from 2 litters for E13.5 and E14.5 collection timepoint.*

Finally, given the successful experiment of E12.5 induction of pancreata *in utero*, I decided to optimise the injection protocol for the lineage tracing of cells at other developmental timepoints. I was interested in E9.5 induction to study the events and potency of cells in primary transition phase. Additionally, I looked at E15.5 and E18.5 timepoints of induction in order to study branching morphogenesis and potency of cells at later stages of the secondary transition. The optimised doses for all Tamoxifen injection timepoints, together with representative images of samples induced at those timepoints and collected at P14 are presented in Figure 11.

From the representative images of samples induced at different developmental timepoints and collected at P14, it is clear that clonal levels of induction were obtained with E9.5 and E12.5 Tamoxifen injections. For E15.5 and E18.5, the induction levels were higher than for the other timepoints, despite testing a series of lowering doses aimed at achieving the clonal levels of induction. However, I have observed that not all confetti fluorescent proteins are expressed to an equal extent (see Section 3.3.3 for more details), with some of the labels, such as green and cyan being almost five times less abundant than the common red and yellow labels (see Section 3.3.3). I therefore decided to focus on the green and cyan clones when further analysing the E15.5 and E18.5 induction timepoints.

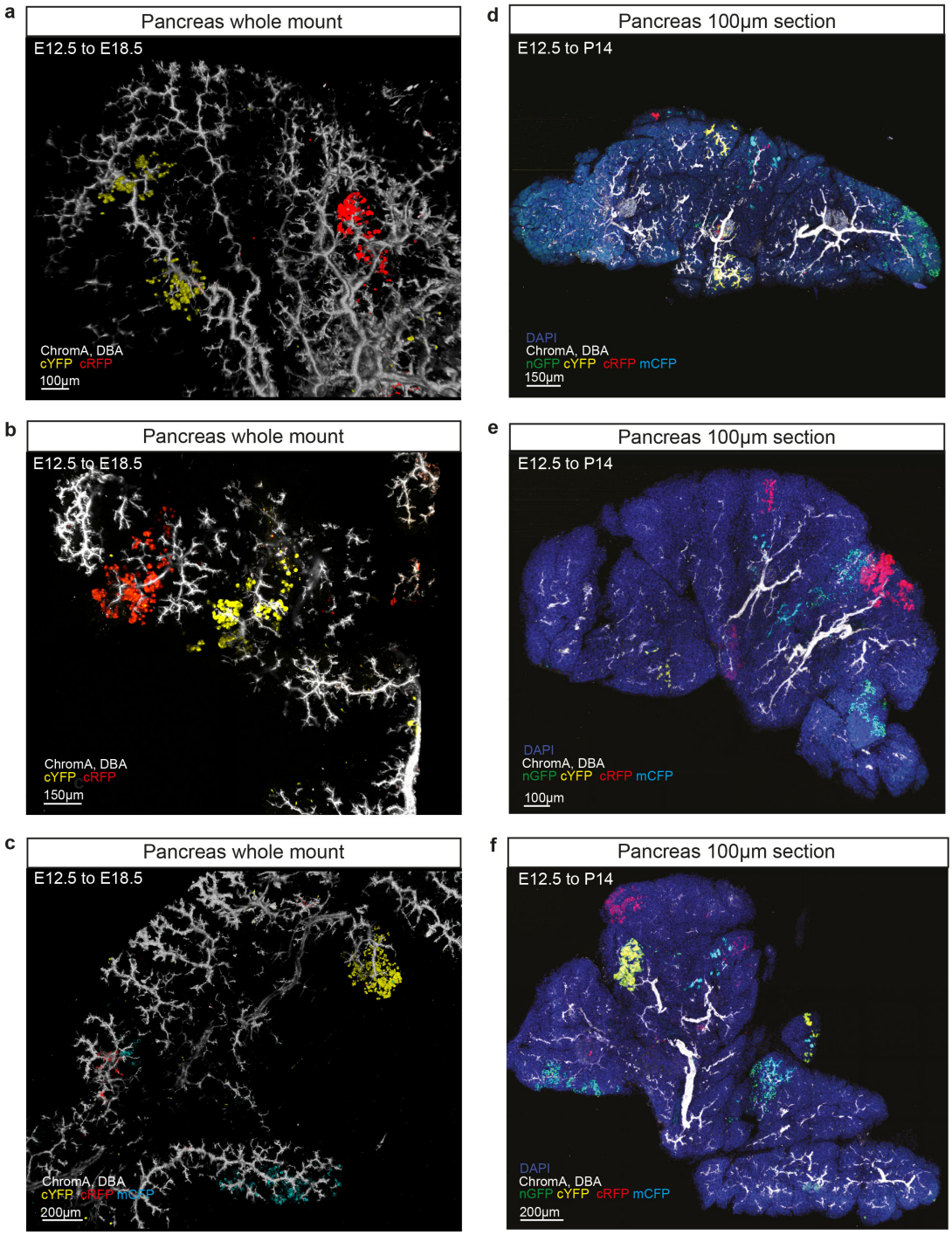
a
Pancreas whole mount
E12.5 to E18.5
ChromA, DBA
cYFP cRFP
100µm
d
Pancreas 100µm section
E12.5 to P14
DAPI
ChromA, DBA
nGFP cYFP cRFP mCFP
150µm
b
Pancreas whole mount
E12.5 to E18.5
ChromA, DBA
cYFP cRFP
150µm
e
Pancreas 100µm section
E12.5 to P14
DAPI
ChromA, DBA
nGFP cYFP cRFP mCFP
100µm
c
Pancreas whole mount
E12.5 to E18.5
ChromA, DBA
cYFP cRFP mCFP
200µm
f
Pancreas 100µm section
E12.5 to P14
DAPI
ChromA, DBA
nGFP cYFP cRFP mCFP
200µm

Figure 10. *Clones from E12.5 induction lineage tracing with collection timepoints at (a-c) E18.5 and (d-f) P14. The clones were very cohesive, with a significant amount of variation between clone sizes, ranging from just a few cells as the RFP clone in (d) to large clones (a-f). DBA marks ducts in white for (a-f). Chromogranin A marks ducts in white for (d-f). Nuclei are stained with DAPI in blue (d-f). Representative images were selected based on analysis of sections from n=4 mice from 3 litters for E18.5 and n=3 mice from 3 litters for the P14 collection timepoint.*

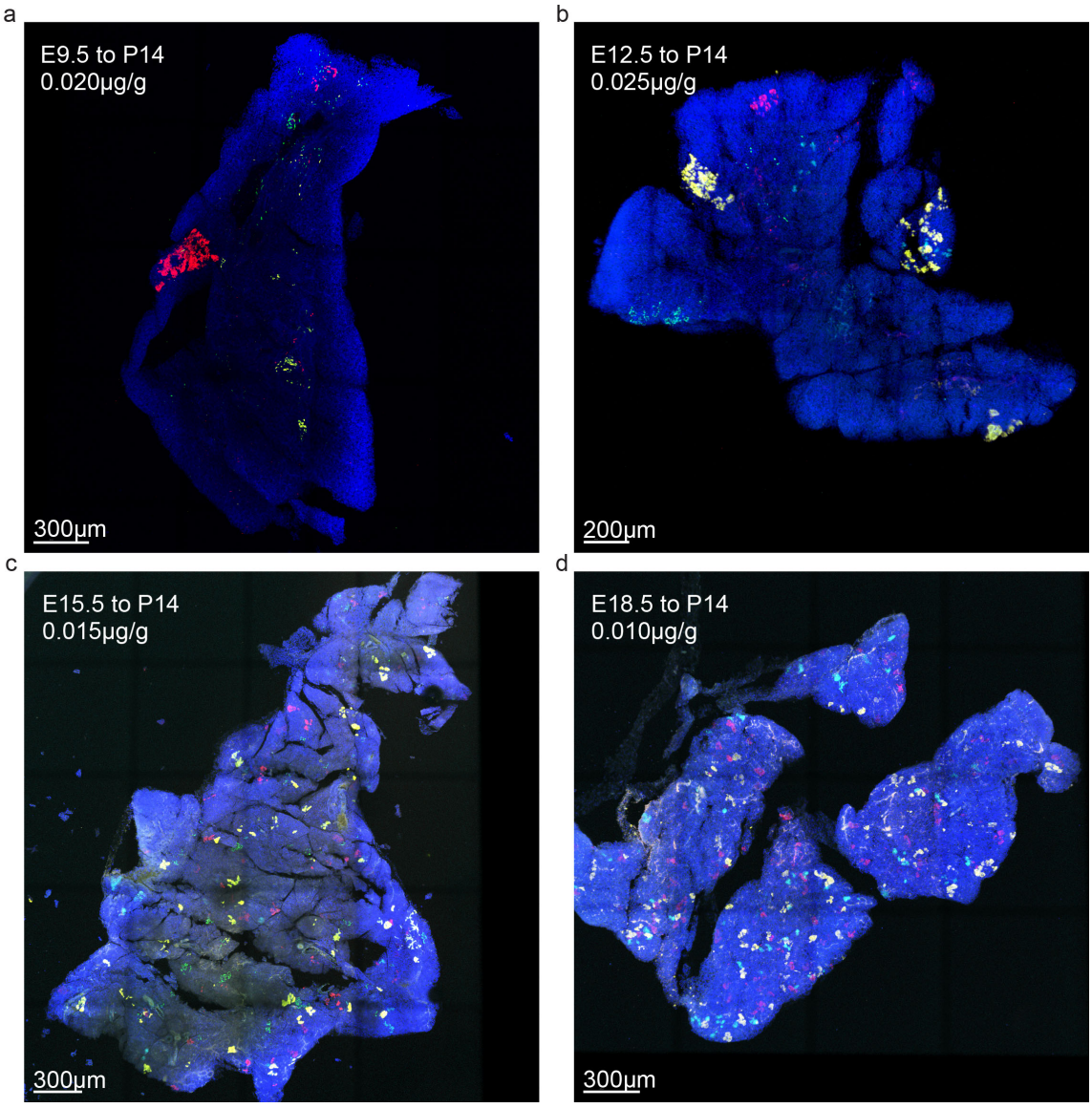

Figure 11. *P14 samples induced at various timepoints. Dosage of Tamoxifen injection written in the top left corner for (a) E9.5, (b) 12.5, (c) E15.5, and (d) E18.5. Induction was clonal for (a) E9.5 and (b) E12.5 timepoints of injection. Higher levels of induction were obtained for E15.5 and E18.5 injection timepoints, and therefore only rare confetti colours – green and cyan – were used for the analysis of clones. Representative images were obtained based on analysis of sections from n=3, 3, 2 and 2 mice (3, 3, 2 and 2 litters) for E9.5, E12.5, E15.5 and E18.5 induction timepoint, respectively.*

3.2.3 Summary of *ex vivo* and *in vivo* optimisation

In summary, the three methods described above reveal distinct advantages and disadvantages, and can therefore be used for distinct purposes. The advantage of the two *ex vivo* approaches is that cellular dynamics can be traced in real time. The first *ex vivo* in collagen growth system, however, turns out unsuitable, because the OH-Tamoxifen is able to induce the cells only at the periphery and the cells start to die after four days of culture. The second *ex vivo* method of culturing cells on MatTek plates adapted from Petzold and Spagnoli, 2012 appears more feasible in terms of the morphology of the explants. Differentiation into all three major pancreatic lineages has been reported previously (Petzold and Spagnoli, 2012). This method would require further verification of how well the pancreatic development is recapitulated in this system. Furthermore, this method would require immunostaining optimisation in order to achieve sufficient penetration of the antibody without detachment of the explants.

Hence, in summary, the *ex vivo* explant system on MatTek plates (Petzold and Spagnoli, 2012) would enable the study of secondary transition events and potency upon further confirmation of the model. However, the system would not be applicable for use of studying the primary transition processes, due to my inability to dissect embryos earlier than E12.0.

Finally, the *in vivo* induction by Tamoxifen injection of pregnant females is ideal for pulse and chase experiments, but live lineage tracing is not possible in embryos. However, this method provides information about cellular events in normal physiological development. From the initial snapshot of samples traced from E12.5 to P14 and E9.5 to P14, it is clear that clones were cohesive and their evolution could be easily inferred, based on relatively limited migration of cells and small distances between individual clusters (see schematic in Fig. 12). Therefore, despite the infeasibility of live lineage tracing *in vivo*, this system appears to be an optimal choice for the study of pancreatic development at various developmental stages.

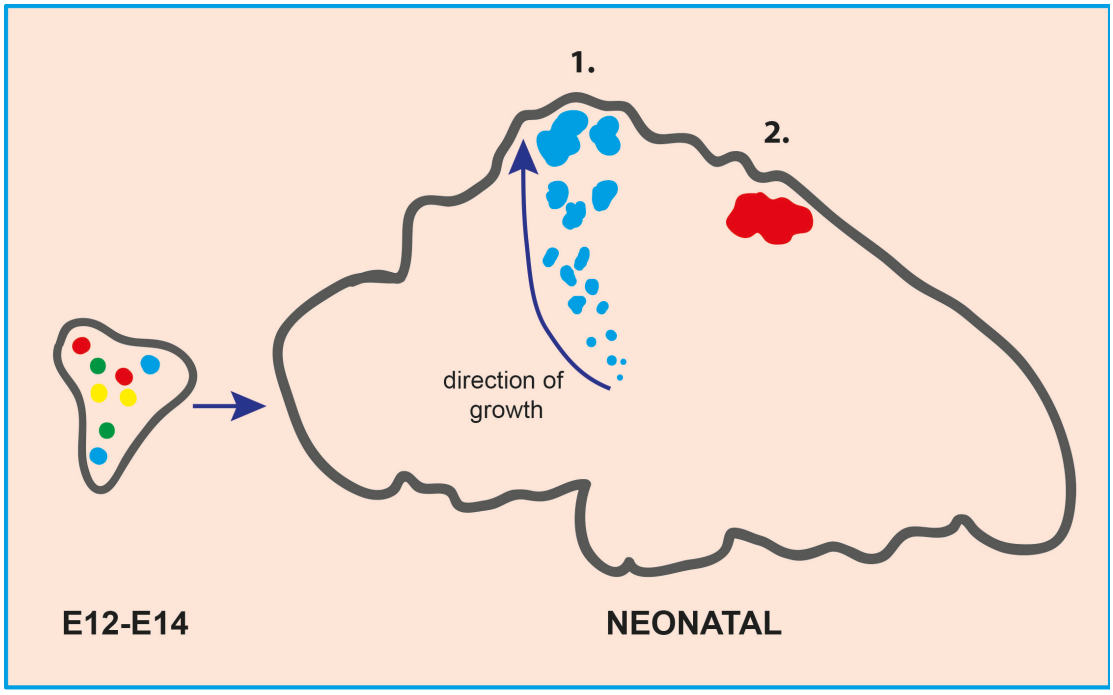

Figure 12. *Evolution of clones during development. The clones were cohesive, with distances between fragments being usually smaller than 30µm, occasionally reaching 50µm. This enables the study of the evolution of clones over time, i.e. their migration and proliferation of constituent cells. mCFP label in the schematic depicts a clone, which has migrated over distance in the direction of tissue growth, leaving the trace of smaller clusters behind, and larger clusters at the leading edge due to more time for proliferation.*

3.2.4 Optimisation of 3D clonal data acquisition

In this study, I aimed to look at dynamics of different pancreatic compartments during secondary transition and maturation, as well as the potency of cells both in the primary and secondary transition. For that purpose, acquiring 3-dimensional (3D) clonal information was necessary, as migration of cells in development is significant. Hence, a protocol of sectioning and immunostaining required optimisation (see Methods).

Previous studies of development and potency of pancreas have involved the analysis of serial thin sections (Zhou et al. 2007; Solar et al. 2009; Kopp et al. 2011; Kopinke et al. 2011; Pan et al. 2013). I therefore attempted to use this method to analyse our samples. However, even though the potency of confetti+ clusters could be easily determined, the assignment of clusters into clones turned out to be problematic, as typically clones spanned multiple sections. Furthermore, with the use of thin sections it would be nearly impossible to infer the 3D shape and morphology of clones. Hence, I attempted to carry out 3D reconstruction of serial sections. Multiple softwares were tried, and eventually Image J with a plugin, UnwarpJ, was used (see Methods, Section 2.1.14). However, the process of reconstruction from multiple 7µm sections was very time consuming. Therefore, I attempted to optimise other sectioning methods, which were not previously commonly used in the lineage tracing studies of pancreatic development.

Consequently, I next attempted to obtain thick vibratome sections, 200-300µm (as in Fig. 8, see methods). This method proved very useful for small pancreatic buds and collagen *ex vivo* explants. However, for neonatal and adult tissue this method turned out to be unfeasible, as the sections tended to separate into smaller parts due to lobular structure of pancreas at these stages. This would prevent the accurate acquisition of whole 3D clonal structures. Similarly, I tested the tissue chopper from Leica, and a similar issue of section disintegration was encountered.

I then tested the use of whole-mount tissue for immunostaining (see Methods). This method was very useful for embryonic pancreas as it could depict whole clones and their position with respect to the tissue outline.

However, the method proved to be unsuccessful for immunostaining of whole-mount neonatal pancreas, as the antibody penetrance was problematic.

Therefore, the methods tested, such as vibratome sections and whole-mount used for immunostaining, turned out to be very suitable for the analysis of embryonic tissue, but were inadequate for neonatal pancreas. Hence, as a solution for obtaining 3D clonal reconstructions in neonatal samples, I set out to test thick cryostat sectioning of 100µm, followed by subsequent immunostaining. This method proved to be effective, as the thick sections adhered well to slides maintaining the lobular structure of pancreas in the correct arrangement. Immunostaining optimisation was successful.

Altogether, all the methods were very useful and can be applied to serve different purposes (See Table 19). For my project, I decided to use whole-mount immunostaining for the analysis of embryonic pancreata, and thick cryosection immunostaining for neonatal tissue analysis.

Sectioning method	Advantages	Disadvantages
Thin frozen sections	Good antibody penetrance, used in previous studies (Zhou et al. 2007; Solar et al. 2009; Kopp et al. 2011; Kopinke et al. 2011; Pan et al. 2013)	Difficult to infer constituent cell types in the whole clone and to infer morphological features
Vibratome sections (200-300µm)	Good for embryonic pancreata	Structure not preserved in neonatal and adult pancreata, as lobules disintegrate
Tissue chopper from Leica	Good for embryonic pancreata	Structure not preserved in neonatal and adult pancreata, as lobules disintegrate
Whole-mount	Good for embryonic pancreata, as whole clones and their position with respect to tissue outline preserved	Not suitable for neonatal and adult pancreas due to antibody penetrance and imaging issues
Thick cryostat sections (up to 100µm)	Good for both embryonic, neonatal and adult pancreata. Enables the preservation of lobular structure of neonatal and adult tissue.	Whole embryo clonal data cannot be obtained directly

Table 19. *Advantages and disadvantages of the tested sectioning methods.*

3.2.5 Optimisation of immunostaining

Since I was interested in studying the potency of clones and their contribution to the dynamics of different pancreatic compartments, a set of markers needed to be used simultaneously, such as the islet marker (anti-Chromogranin A antibody), ductal marker (dolichos biflorus agglutinin, DBA), and acinar marker (anti-amylase antibody). However, I was limited by the number fluorophores that could be used without bleedthrough between the imaging channels with the use of Leica SP5 confocal microscope. Five imaging channels on the confocal microscope were already used by imaging of the confetti cassette and nuclear stain DAPI, so only one channel for staining of the tissue for pancreatic compartments was left. It is important to emphasise the importance of the use of a multicolour confetti reporter for verifying the clonality of induction, i.e. verifying with statistical confidence that an assigned clone is not a merge of multiple clones. This is not possible with single colour reporter mice, unless extremely low induction levels paralleled by an unfeasible number of embryos are used.

Therefore, I looked for markers which could be assigned to the one remaining imaging channel. Fortunately, since the islets and ducts displayed distinct morphologies (see Figure 13), so I was able to stain ducts and islets in one channel after careful optimisation of the Chromogranin A antibody and DBA concentrations, which would enable simultaneous detection of their intensities of staining for the two compartments.

The amylase antibody could not be used in parallel, as then nearly the whole volume of pancreas would be stained in one channel and the distinct compartments could not be identified. However, in a set of control stainings, I verified that nearly all non-ductal and non-islet parts of the dissected pancreata were acinar (see Figure 13), and I decided to use this as an approximation of cell type, given the large number of clones I was planning to quantify (over 200 clones, see Section 3.3.2).

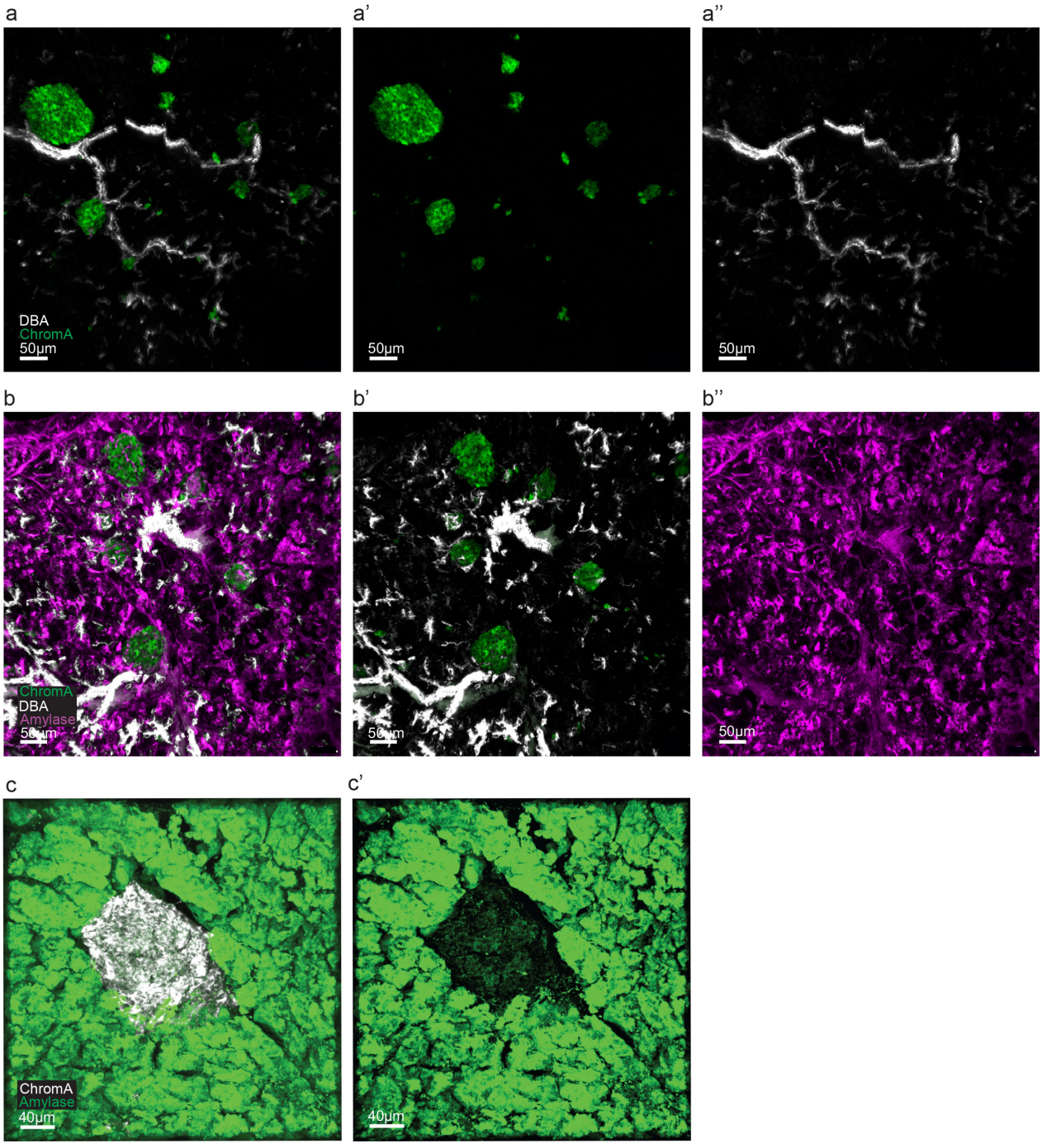
a
a'
a''
DBA
ChromA
50µm
50µm
50µm
b
b'
b''
ChromA
DBA
Amylase
50µm
50µm
50µm
c
c'
ChromA
Amylase
40µm
40µm

Figure 13. *Verification of staining markers. (a) Combination of two markers for islet Chromogranin A (green) and ductal DBA (white) shows that the two compartments display clear morphological differences and therefore can be stained in one channel for potency analysis of confetti+ cells. Since hallmark morphological differences distinguish ductal and islet compartments, in the clonal lineage study, these features can be imaged using the same channel. This allows us to reserve other channels for DAPI staining and to discriminate all of the fluorescent reporters used in the confetti tracing. (b) Combination of all three markers with islet Chromogranin A (green), ductal DBA (white) and acinar amylase (pink) shows that all the markers are exclusive and the majority of DBA- Chromogranin A- tissue is amylase+. (c) Combination of two markers for islet Chromogranin A (white) and acinar amylase (green) shows complete exclusion of two markers. Representative images were selected based on analysis of sections from n=3 mice.*

3.3 Clonal analysis: E9.5 and E12.5 induction

3.3.1 Collection timepoints

In the first part of the analysis, I wanted to focus on samples induced at the onset of primary and secondary transition, i.e. E9.5 and E12.5 respectively. This would enable the comparison of potencies and morphological behaviours between the two phases. Therefore, the experimental protocol involved an intraperitoneal injection of pregnant females at E9.5 or E12.5 of their pregnancy. The samples were collected at E18.5 (before birth), P14 and P28 (Fig. 14). This would allow enough time for the structure of clones to develop, in order for us to be able to conclude morphological patterns in the developing tissue, as well as acquire an accurate estimate of potency of clones, as the mature markers of pancreas development would be expressed by these stages.

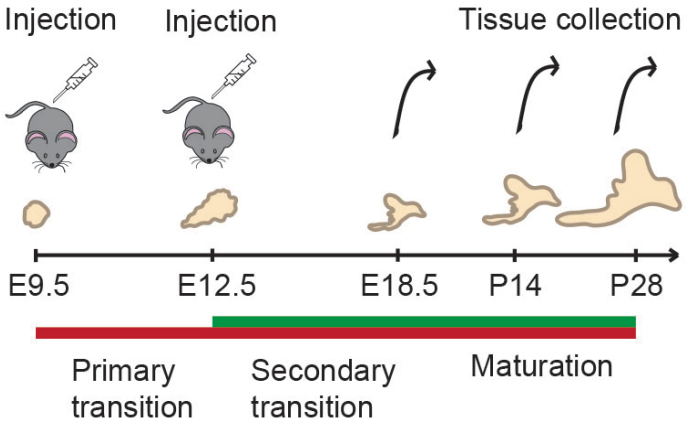

Figure 14. *Outline of experiment for R26-RCreT2; R26-Confetti lineage tracing. Injections were carried out at either E9.5 or E12.5 and collection timepoints were at E18.5 embryos and P14 and P28 neonates.*

3.3.2 Quantification of clonal data

In order to gain a better understanding of clone size distributions, the position of clones with respect to tissue landmarks, as well as their potency, I aimed at assessing clonal features by quantifying a comprehensive set of parameters. These are outlined in the Table 20, and include clone volume, coordinates of the centre of clusters within clones, constituent cell types, and others. The potencies of clones were subsequently inferred – tripotent clones contained all three major cell lineages (acinar, ductal, and islet), bipotent clones contained any two of the three lineages, while unipotent clones contained only one lineage. These were quantified for 244 clones from 3 mice for E12.5 to P14 tracing, 50 clones from 2 mice for E9.5 to P14 tracing, and 84 clones from 2 mice for E12.5 to P28 tracing. These were later used for the downstream quantitative analysis.

Parameter	Explanation
Clone ID	Each clone is given a unique number to group all clusters belonging to one clone together.
Clone volume	Clone volume is used as a measure of clone size, as it is proportional to cell number.
Clone surface area	Clone surface area together with clone volume provides a measure of clone complexity.
Centroid X, Y, Z	Coordinates of the centre of a confetti cluster. Helps determine whether multiple confetti clusters arise from one or several clones.
Bounds X, Y, Z	The dimensions of a smallest possible cuboid to include a given cluster, provides an indication of the complexity of clone structure.
Shape Factor	Between 0 and 1. The greater the value, the more round the cluster is.
Longest Axis	Gives information about the extent of migration of a given clone/cluster.
Cluster shape comments	Descriptive category, used to provide any additional information.
Cell composition	Used broadly to describe the constituent cell types and hence infer the potency of clones. These include acinar only, acinar majority, ductal only, ductal majority, islet only, islet majority, tripotent clones, mixed (with equal contribution of 2 compartments).
Total number of islets	Total number of islets in a given section studied.
Number of confetti-labelled islets	Number of islets containing a confetti+ cell(s) in a given section.
Labelled islet ID	All labelled islets are assigned a unique number so that the appearance of several confetti colours (indicative of polyclonality) can be reported.
Labelled islet volume	This enables the assessment of islet clone size in proportion to the size of islet compartment it occupies. As a consequence, the relative contribution of a given clone to islet growth can be assessed.
Islet Centroid X,Y, Z	Helps determine the processes of possible islet fission, where multiple islets are labelled in the same colour.
Surface Area	Together with the volume, provides a measure of shape of the islet.
Any other comments about the clone behaviour	Provides any other information about clonal morphology and composition, which may be important for analysis.

Table 20. *Parameters quantified in the analysis of lineage tracing data with E9.5 and E12.5 induction.*

3.3.3 Analysis of clonality of data

I aimed to study the potency of cells during pancreas development, and therefore I set out to analyse individual clones, ensuring all clones were derived from single cells rather than the merging of multiple cells. In developmental contexts, where proliferation and migration are vast, it is particularly important to ensure that the induction levels of reporter construct are clonal, i.e. all clones derive from a single cell.

There has been a large number of lineage tracing studies performed in the past, suggesting abundant tripotency until E14.5 or later. In particular, lineage tracing studies based on *Cpa1* expression in tip cells and *Hnf1β* expression in trunk cells suggest that both domains retain tripotent precursors until at least E13.5 (Solar et al. 2009; Zhou et al. 2007). Indeed, tracing studies of Sox9 expressing cells suggest that tripotent cells may persist even after birth (Kopp et al. 2011; Furuyama et al. 2011). However, these studies were based on non-clonal induction levels, meaning that the apparent tripotency could result from the merging of several populations of lineage-restricted cells. Hence, I sought to readdress the question of potency with the methodological advancement of using clonal-level lineage tracing, and therefore I prioritised ensuring the clonality of our lineage-traced samples.

Initially, the clusters of labelled cells and their progeny were identified as belonging to one clone based on threshold distances separating the clusters. Two clusters would be categorised as a single clone unless the distance between them was exceeding the threshold (Fig. 15a).

I then wanted to verify this heuristic clonal assignation to confirm that the clonal grouping was correct. In order to assess this, I turned to statistical analysis. This was carried out in collaboration with Dr Edouard Hannezo from the University of Cambridge. We challenged the clonality of our manual reconstructions in several ways.

We first took advantage of the fact that we label cells in four different colours (CFP, RFP, GFP and YFP) and computed the probability of finding two clones of the same colour at a certain distance for all clonal pairs in a given pancreas

analysed given the distribution of distances between clones of different colours. We reasoned that, if we had under-estimated clonal fragmentation in our heuristic reconstructions, i.e. clusters coming from separate clones were grouped as one clone, then there should be an excess of clones of the same colour at small distances in heuristic grouping as compared to the calculated probability. In the converse case, there should be an insufficiency of clones of the same colour at small distances. In an ideal clonal assay, all clones should have been independently induced, so that the probability of finding clones of the same colour should be independent of distance, i.e. *P(r)* constant.

In order to statistically assess such clonality, we needed to statistically determine what the null-hypothesis would give, i.e. “our assay is clonal”. In order to rescale the probability of finding two clones of the same colour at a given distance, and in order not to be influenced by the complex shape and convolution of the pancreas, we computed the probability of finding two clones of any colour at a given distance and used this to rescale the probability of finding two clones of the same colour. In the clonality hypothesis, clones are independent, so the resulting rescaled probability should be independent of distance. Next, we used a non-parametric bootstrapping method to build confidence intervals on the prediction from the null-hypothesis. We thus calculated for each individual pancreas the probability for a clone to have one of the four confetti colours, and randomly re-assigned colours of clones according to this average property. We performed this procedure 1000 times, and calculated in each case the rescaled probability *P(r).* Finally, we calculated a 95% confidence interval at each distance *r* from this resampled probability distribution, in order to assess how much experimental deviations of *P(r)* from a constant value can be due to random statistical variations. We plotted these confidence intervals for each individual mouse induced at E12.5 and traced until P14 in Figure 15b, together with the experimental measurements of *P(r).* Interestingly, we found that the experimental probabilities, although showing statistical variations, were consistently included within the 95% confidence interval from the null-hypothesis. However, in some mice (such as mouse 1) we observed a statistically significant excess of clones of the same colour at short distances. We thus

corrected statistically for this bias by grouping all clones of the same colour within a given radius, in order to obtain the probability value expected from clonal induction (values shown by black dashed lines in Figure 15b).

To further test the clonality of the data, we performed two independent controls. First, we noticed that one of the mice was stochastically induced at a dose twice as low as its two other counterparts (Fig. 15c). We therefore segregated the potency data (see Section 3.4 for details) for each individual mouse in order to check whether the labelling dose influenced our results. For instance, one could have assumed that tripotency observed in the data resulted from unwanted merger of independent clones. However, interestingly, we found that the potency outcome was faithfully reproduced for each individual mouse (Fig 15d), lending additional credence to our results.

Second, we also noticed that the four confetti colours were represented in very different proportions (Fig. 15e), we grouped all three mice for this statistical assay). In particular, there were more than 5 times as many RFP clones than CFP clones, with GFP and YFP clones sitting at an intermediate probability. We therefore segregated the potency data for each individual colour, and found both that the degree of unipotency was independent of the colour examined (Fig. 15f), and that in general, the ratio of unipotency, bipotency and tripotency were consistent in all colours examined (Fig. 15f). This again strongly argues in favour of the clonality of the data, given that CFP cells consisted of less than 0.3% of all pancreatic cells, making the merger events very unlikely.

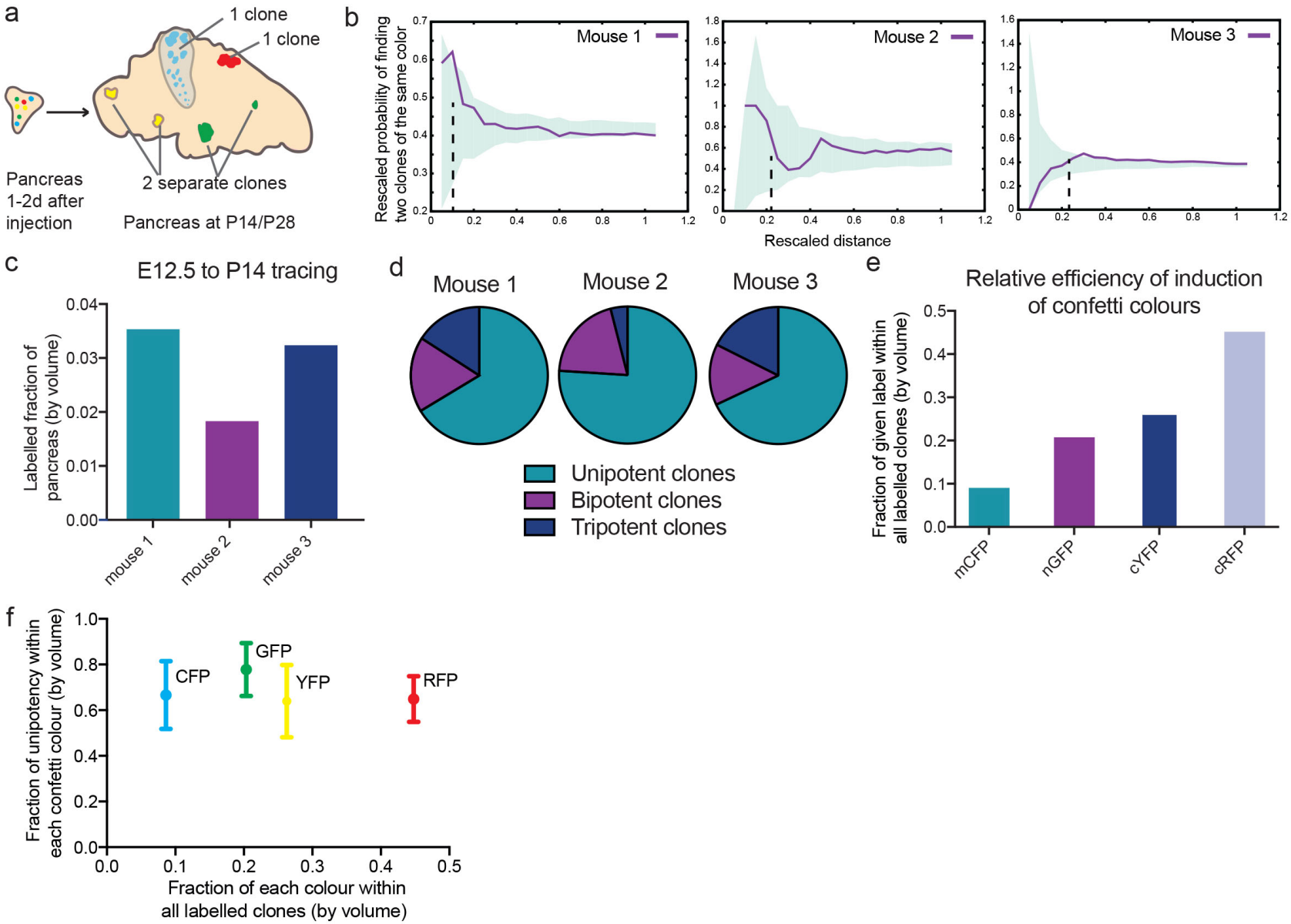
a
1 clone
1 clone
Pancreas
1-2d after
injection
2 separate clones
Pancreas at P14/P28
b
Rescaled probability of finding two clones of the same color
Mouse 1
Mouse 2
Mouse 3
Rescaled distance
c
E12.5 to P14 tracing
Labelled fraction of pancreas (by volume)
mouse 1
mouse 2
mouse 3
d
Mouse 1
Mouse 2
Mouse 3
Unipotent clones
Bipotent clones
Tripotent clones
e
Relative efficiency of induction of confetti colours
Fraction of given label within all labelled clones (by volume)
mCFP
nGFP
cYFP
cRFP
f
Fraction of unipotency within each confetti colour (by volume)
CFP
GFP
YFP
RFP
Fraction of each colour within all labelled clones (by volume)

Figure 15. *Clonality assessment. (a) Schematic indicating methods of clonal assignment based on cohesiveness and distances between constituent labelled cell clusters (see Section 3.4.3, Statistical Methods in Section 2.3). (b) Rescaled probability (purple thick line) of finding another clone of the same colour as a function of rescaled distance from a given clone, for all three R26-Confetti mice induced at E12.5 and traced until P14 (left, centre and right panels). For each mouse, the clone-clone distance was rescaled by the average distance in three-dimensions between two clones randomly chosen across sections of a given pancreas. The probability of finding a clone of the same colour at a given distance was rescaled by the probability of finding two clones of any colour at the same distance. The shaded lines represent the 95% confidence interval of rescaled probability under the assumption that the data was clonal. The dashed black line shows the distance used for fragment grouping to define a clone. (c) Fraction of fluorescently labelled cells at E12.5 in the P14 pancreas of different mice. (d) Global potency of P14 clones induced at E12.5, segregated for each individual mouse, showing that the potency of each is consistent with the ensemble average (see Fig. 17a), and independent of the frequency of induction shown in (c). (e) Colour balance of confetti clones induced at E12.5 and traced until P14, grouping all three pancreases. Cyan is the least represented colour while Red is the most represented. (f) Global potency of P14 clones induced at E12.5, segregated for each individual confetti colour. 254 clones from 3 mice from 3 litters were scored. Figure generated in collaboration with Dr. Edouard Hannezo, using data that I collected.*

3.4 Clonal lineage tracing with E9.5 and E12.5 induction provides evidence for early and progressive lineage restriction

Pancreatic samples were thick cryostat sectioned and immunostained for the compartment markers such as ductal DBA and islet Chromogranin A. The clones, which were at the intersection of several thick sections were then serially reconstructed, in order to obtain correct clonal parameters, such as clone volume, cellular composition and location with respect to tissue landmarks (see Section 3.3.2).

The analysis of E9.5 and E12.5 lineage traced samples revealed that clones remained remarkably cohesive in both ductal and acinar compartments. This was revealed in the E18, P14 and P28 collected timepoints, as individual clusters belonging to a clone were not separated by large distances (usually less than 200 µm) (Fig. 16 a-h). However, the E9.5-traced clones were slightly more spread out than the E12.5-traced clones. This indicates that, despite large-scale cell rearrangements, the dispersion of proximate cells during the development, particularly during secondary transition, is limited.

Clones were observed over a wide range of sizes, with some containing thousands of cells spanning large areas of tissue, while others contained only a few cells (Fig. 16 d,e). I therefore quantified the size of all clones and could see that the distribution was indeed very broad (Fig. 16i). This raises the question of what is the underlying tissue growth principle, giving rise to such a wide variation in proliferation capacity of cells. I hypothesised that the large variability in clone sizes could result from the variable potency of clones.

I therefore turned to the analysis of potency. In order to assess this, I quantified 248 clones from 3 mice for E12.5 to P14 tracing, and 50 clones from 2 mice for E9 to P14 tracing. Each clone was labelled specifically with respect to its potency (as well as the other parameters, as in Chapter 3.3.2) based on the mature pancreas markers expressed. Hence, based on cell composition, I identified uni-, bi- and tripotent clones with only one, two or three acinar compartments present within a clone respectively. Amongst the

clones, I identified different permutations across all three lineages (Fig. 17a-d).

Strikingly, examining the composition of clones traced from E12.5 to P14 and P28, I found that the majority were unipotent (Fig. 17a,c-d). This implies that the lineage potential of most precursors has already become restricted by E12.5, contrasting with previous findings (Zhou et al. 2007; Solar et al. 2009; Kopp et al. 2011; Furuyama et al. 2011). Indeed, these results suggest that reports of extensive tripotency as late as E12.5-E14.5 may be an artefact of high density labelling, tracing the evolution of lineages instead of individual cells.

I was then interested in comparing these results with the potency of cells at the beginning of primary transition, E9.5, as according to literature the precursors at this stage should be entirely tripotent (Shih et al. 2013). Examination of the clonal composition from E9.5 to P14 tracing (Fig. 17a,b) performed under the same conditions revealed that the majority of clones remain bi- or tripotent (64%), as expected from the lack of tip-trunk segregation at this early stage (Pan and Wright 2011). Yet, even at this timepoint, around 25% of induced cells generated unipotent clones, indicating that lineage restriction begins unexpectedly early in development.

Hence, altogether the potency outcome was very surprising and revealed that very early and rapid lineage restriction is taking place during pancreas development, with most of cell specification being complete by the end of primary transition. From secondary transition onwards only rare tripotent progenitors are present in the tissue.

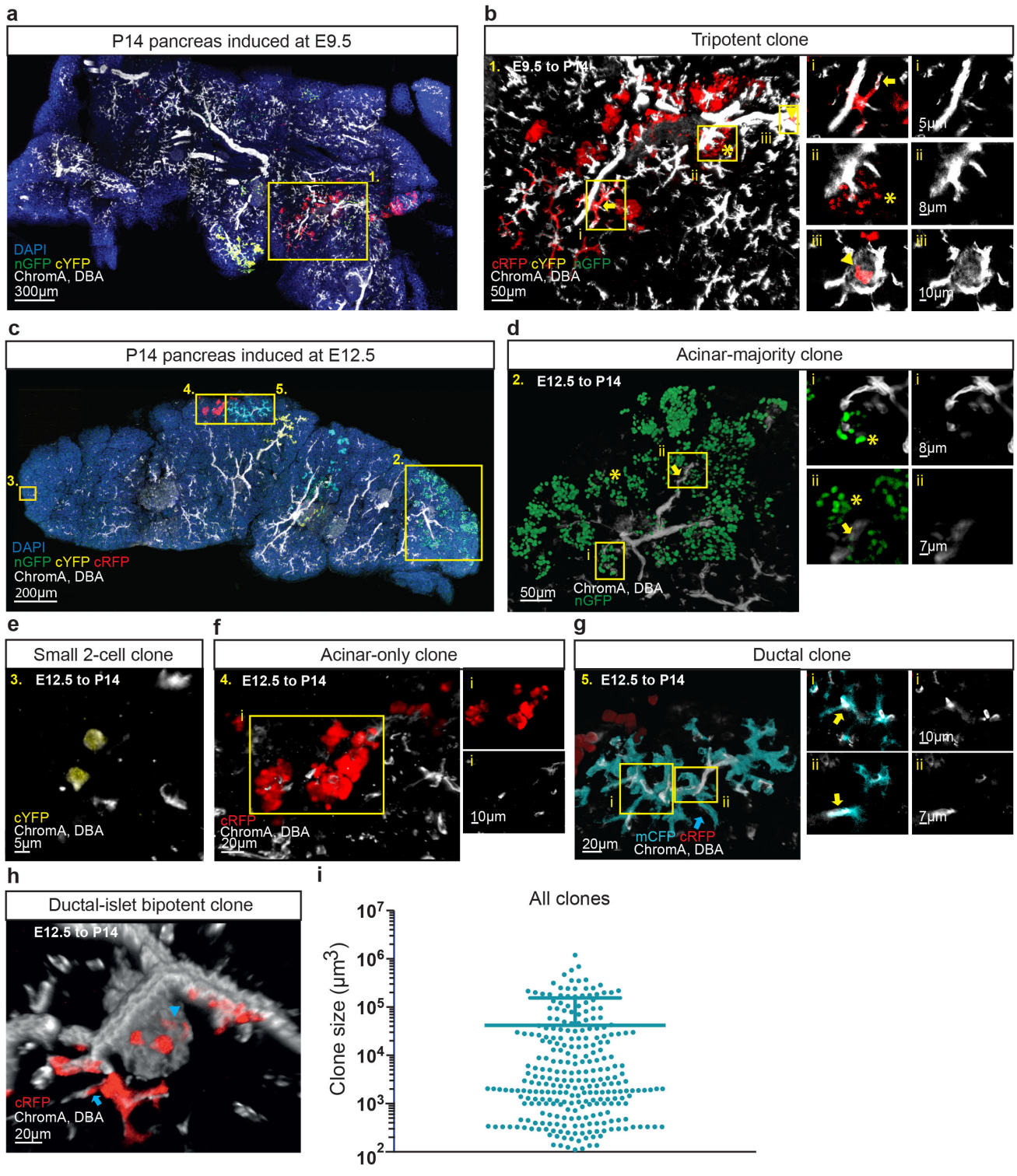
a
P14 pancreas induced at E9.5
DAPI
nGFP cYFP
ChromA, DBA
300µm
b
Tripotent clone
1. E9.5 to P14
cRFP cYFP nGFP
ChromA, DBA
50µm
5µm
8µm
10µm
c
P14 pancreas induced at E12.5
DAPI
nGFP cYFP cRFP
ChromA, DBA
200µm
d
Acinar-majority clone
2. E12.5 to P14
50µm
ChromA, DBA
nGFP
8µm
7µm
e
Small 2-cell clone
3. E12.5 to P14
cYFP
ChromA, DBA
5µm
f
Acinar-only clone
4. E12.5 to P14
cRFP
ChromA, DBA
20µm
10µm
g
Ductal clone
5. E12.5 to P14
20µm
mCFP cRFP
ChromA, DBA
10µm
7µm
h
Ductal-islet bipotent clone
E12.5 to P14
cRFP
ChromA, DBA
20µm
i
All clones
Clone size (µm3)
10^7
10^6
10^5
10^4
10^3
10^2

Figure 16. *Quantitative lineage tracing reveals evidence of early lineage commitment of heterogeneous pancreatic precursors. (a) Thick 100µm section of P14 pancreas induced at E9.5. (b) Zoom on tripotent clone from (a) containing islet, acinar and ductal components (indicated by arrowhead, asterisk and arrow, respectively) with zoom on single Z-sections demonstrating the contribution of clones to different pancreatic compartments. (c) Thick 100µm section of P14 pancreas induced at E12.5 reveals heterogeneous clonal outcomes of various potencies. (d) Acinar majority clone from (c) (acinar compartment indicated with asterisk) surrounding a network of ducts with rare labelled ductal cells (indicated by arrow) and shown in zoom on single Z-section. (e) Small clone from (c) containing a few cells (f). Representative unipotent acinar-only clone from (c) surrounding unlabelled ducts (indicated by arrow). The lack of overlap between clone and ducts is indicated in single Z-section images on the right (g) Ductal-only clone from (c), containing monoclonal ducts (indicated by arrow) and ductal overlap show on single Z-sections on the right. (h) bipotent clone from (c) in red (cRFP) (islet and ductal compartments indicated by arrowhead and arrow, respectively) (i) Complete size distribution for all clones induced from E12.5 to P14.Bars indicate mean and S.D. Nuclei are stained with DAPI (blue), islets immunostained using Chromogranin A antibody (white) and ducts stained with DBA (white). I counted 41 clones from n=2 mice (2 litters) for the E9.5 to P14 tracing, 254 clones from n=3 mice (3 litters) for the E12.5 to P14 tracing.*

Observing such wide distribution of clone sizes and all potencies of clones (uni-, bi-, and tripotent) with both induction timepoints, I wondered whether heterogeneity of progenitor potency could explain the wide variability of clone sizes, with multipotent progenitors giving rise to large clones and unipotent progenitors generating small clones. As outlined in the previous section 3.3.2, both potency and clone sizes were recorded simultaneously; hence the correlation between the two parameters could be examined. Although multipotent clones were, on average, slightly larger than unipotent clones, each category still contained clones spanning three orders of magnitude in size (Fig. 17e) suggesting that the observed heterogeneity does not derive from the labelling of progenitors with different specification potentials.

a

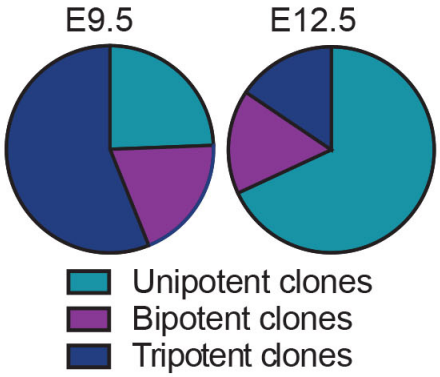

b E9.5 to P14

Clone type	Frequency (%)
Unipotent acinar	22.0
Unipotent ductal	0.0
Unipotent islet	2.4
Bipotent acinar-ductal	14.6
Bipotent acinar-islet	4.9
Bipotent ductal-islet	0.0
Tripotent	56.1

c E12.5 to P14

Clone type	Frequency (%)
Unipotent acinar	59.9
Unipotent ductal	3.1
Unipotent islet	5.1
Bipotent acinar-ductal	10.5
Bipotent acinar-islet	4.7
Bipotent ductal-islet	1.2
Tripotent	15.6

d E12.5 to P28

Clone type	Frequency (%)
Unipotent acinar	69.8
Unipotent ductal	1.2
Unipotent islet	1.2
Bipotent acinar-ductal	24.4
Bipotent acinar-islet	0.0
Bipotent ductal-islet	0.0
Tripotent	3.5

e

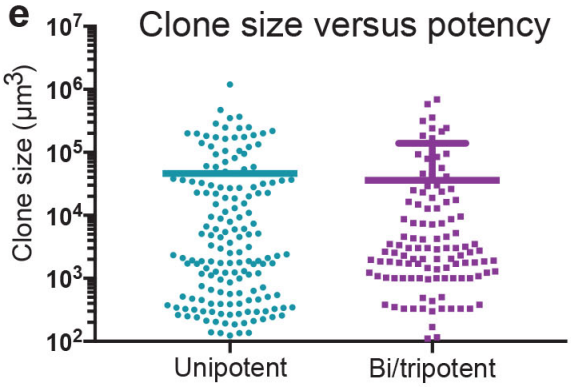

Figure 17. *Rapid cell fate restriction in the developing pancreas. (a) Global potency of clones induced at E9.5 and E12.5, indicating a shift towards unipotency. (b-d) Table of all clone types traced from (b) E9.5 to P14, (c) E12.5 to P14, and (d) E12.5 to P28. (e) Complete size distribution for all clones induced from E12.5 to P14 segregating unipotent and multipotent clones. Mean and SD presented. I counted 41 clones from n=2 mice (2 litters) for the E9.5 to P14 tracing, 254 clones from n=3 mice (3 litters) for the E12.5 to P14 tracing, 84 clones from n=2 mice (2 litters) for the E12 to P28 tracing.*

3.5 Discussion

In this chapter, I applied the technique of multicolour-reporter lineage tracing from a ubiquitous *R26* promoter, in order to study the potency of pancreatic cells in primary and secondary transition, ensuring clonal density of induction. This was a novel approach in studying pancreas development, as previous studies have mainly focused on tracing of specific lineages of cells, and were based on non-clonal induction levels (Zhou et al. 2007; Solar et al. 2009; Kopp et al. 2011; Kopinke et al. 2011; Pan et al. 2013).

In this chapter, I first aimed to optimise conditions for studying pancreas development, to ensure that lineage tracing data recapitulate physiological development.

Next, I aimed to optimise the methods for obtaining 3D clonal data arising during pancreatic development. This is a major advancement compared to previous studies whereby thin sections were analysed (Zhou et al. 2007; Solar et al. 2009; Kopp et al. 2011; Kopinke et al. 2011; Pan et al. 2013). In developmental contexts, the migration of cells may be vast and therefore correct assignment of clones is essential for the potency outcome.

Furthermore, I also optimised the dose of Tamoxifen for *in vivo* injections to ensure clonal levels of induction of the confetti construct, followed by statistical analysis to carefully assess the clonality. My *R26*-CreT2; *R26*-Confetti lineage tracing enabled us to discover early and rapid lineage restriction, taking place already in the primary transition. This is in contrast to previous literature (Kopp et al. 2011; Furuyama et al. 2011, Zhou et al. 2007, Solar et al. 2009). The difference may be due to the fact that in the previous studies the apparent tripotency could arise from the merging of independent lineage restricted precursors. Furthermore, the mentioned studies did not attempt to look at individual clones, but rather quantified the total percentage of islet, ductal and acinar lineage labelling within thin sections, which were not serially re-constructed.

In comparison, I observed that at E9.5 the tissue showed much higher extent of tripotency. However, already at this early stage, a quarter of cells were

unipotent. This further emphasises that lineage restriction may be taking place much earlier than previously reported, when cells are thought to be morphologically and functionally identical (reviewed in Benitez et al. 2012; Shih et al. 2013; Pan & Wright 2011). One previous study confirms my finding, whereby the expression of genes associated with specific lineage maturation were shown to be upregulated in certain cells already at this stage (Chiang and Melton 2003).

Altogether, the results summarised above have answered the questions and aims set out at the beginning of the chapter regarding the optimisation of conditions for the study of pancreatic development with *R26*-CreT2; *R26*-Confetti lineage tracing, ensuring the clonal levels of induction of the tracing data, gaining the understanding of the variability of clone sizes and its nature, as well as assessing the potency of pancreas in primary and secondary transition. In summary, this chapter reveals a rapid lineage restriction taking place already in primary transition of pancreatic development.

Chapter 4

Results: Branching morphogenesis

4.1 Introduction

This chapter follows after the first chapter of findings based on the genetic lineage tracing with *R26*-CreT2; *R26*-Confetti combined with statistical analysis, showing early lineage restriction starting already in primary transition of development.

In this chapter I present analysis of morphology and other clonal parameters from *R26*-CreT2; *R26*-Confetti lineage tracing, combined with the analysis of tissue macroscopic parameters and tissue kinetics. This is all combined with computational modelling of the quantified data, undertaken in collaboration with Dr Edouard Hannezo and Prof. Benjamin Simons.

This chapter aims at answering our main research questions:

- How is pancreas morphogenesis coordinated with lineage specification?
- What drives the growth of the pancreatic tissue?
- How does the pancreas reach its final structure and internal composition?

The chapter starts by studying the morphology of clones and focusing on their dynamics to infer developmental patterns. I then propose ductal branching morphogenesis as a process responsible for the coordinated growth of the mentioned lineages. Next, I present a set of controls showing the validity of

the potency and morphological findings, including an additional lineage tracing study from the *Sox9* promoter and an immunostaining experiment. Next, I present the macroscopic parameters of developing pancreas to infer dynamics of pancreatic growth. Finally, I focus on determining the underlying mechanism driving the process of branching morphogenesis, identified as the process driving parallel development of all pancreatic lineages.

Altogether, the findings of this chapter enable us to present a model explaining the morphogenesis of pancreas with a novel explanation of the coordination of organ growth with the simultaneous development of acinar, ductal and islet lineages.

4.2 Pancreas growth is tip driven based on E12.5 induction lineage tracing and EdU proliferation assay

The findings of the previous chapter showed rapid cell fate restriction within developing pancreas, combined with a very wide proliferative heterogeneity, evident from the clone size distribution, and independent of the potency of individual clones. Therefore, to understand the source of clone size heterogeneity and to gain an insight into dynamics and large-scale patterning of tissue during the secondary transition, I decided to examine the location and spatial organization of clones.

Pancreas morphogenesis has been a subject of several studies (Zhou et al. 2007; Pan et al. 2013; Bankaitis et al. 2015; Shih et al. 2016), however the 3D cellular mechanism coordinating pancreas growth and simultaneous development of acinar, ductal and islet lineages are not well understood.

As outlined in the introduction, the role of central plexus in driving the pancreas growth is not clear, and has been a subject of discussion (Bankaitis et al. 2015; Pan and Wright 2011). I therefore first considered whether the specification of pancreas relies on an early phase of expansion that precedes plexus remodelling, or whether the bulk of expansion takes place through a later phase of ductal branching, once the plexus is formed. I reasoned that if clonal expansion occurs mainly before plexus remodelling, clones would become fragmented and dispersed across adjacent ductal subtrees. However, if, on the other hand, ductal expansion is derived from the activity of precursors localized to side-branches of the plexus, clones induced at E12.5 would track segments of individual ductal subtrees (see Fig. 18a for schematic).

Notably, I found that the vast majority of ducts that contained labelled cells (ca. 80%) were characterized by a high degree of monoclonality (Fig. 18b), meaning that stretches of ducts over subsequent branching (bifurcation) points were uniformly labelled with confetti+ cells. Furthermore, these clonally labelled ducts were restricted to the same subtree, generally extending to the periphery of the ductal network (Fig. 18b). This suggests that the growth of

ductal lineage could be tip-driven, and occurring after ductal plexus has been formed.

Remarkably, I also found that the majority (ca. 90%) of acinar cell-containing clones, including unipotent (acinar-only) clones, were closely associated with single ductal subtrees across multiple generations of consecutive branching events (Fig. 18c), indicating a tight correlation between branching morphogenesis and the expansion of the acinar compartment, as well as a similar mechanism guiding the development and expansion of the two lineages. I was determined to find the mechanism, which guides the parallel dynamics of the two lineages.

Altogether, the fact that the two types of clones follow the ductal branches over multiple generations suggests that, during the secondary transition, pancreas development follows a coordinated process of ductal-end driven branching morphogenesis rather than plexus remodelling, guided by precursors at the termini of ducts that self-renew through serial rounds of branching and give rise to cells that form the trailing ducts and the acinar cells that associate with the ends of terminated ducts.

Furthermore, from rare and stochastic local high-level induction sections, I could occasionally observe ductal branching (Fig. 18b) and branch-associated acinar clones (Fig. 18c) occurring within one subtreee (Fig. 18d), lending further support to this hypothesis. This is however a qualitative observation, and it needs to be shown in a quantitative manner whether real correlation between the dynamics of ductal and acinar compartment exists (see Section 4.6).

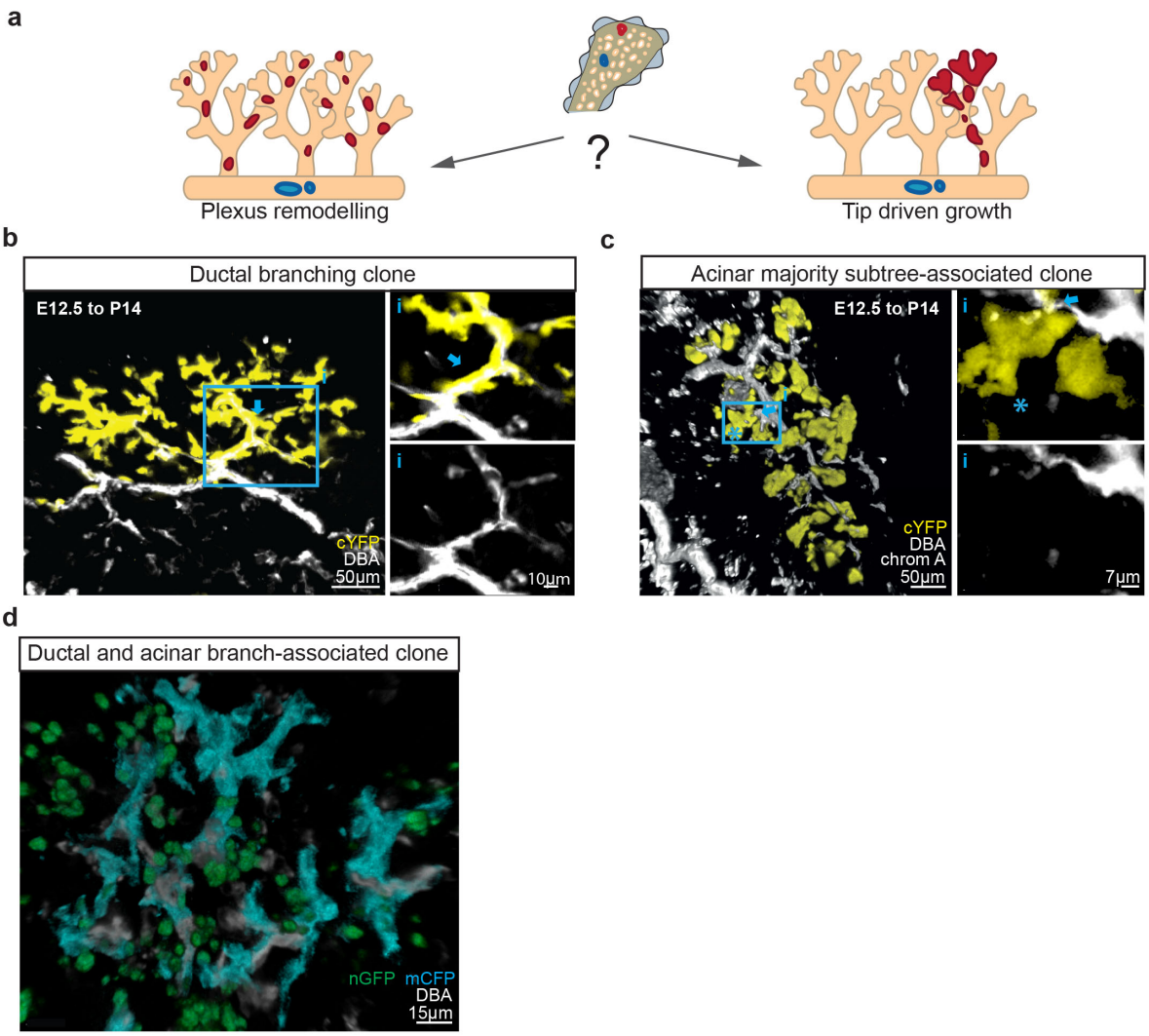
a
Plexus remodelling
?
Tip driven growth
b
Ductal branching clone
E12.5 to P14
cYFP
DBA
50µm
i
i
10µm
c
Acinar majority subtree-associated clone
E12.5 to P14
cYFP
DBA
chrom A
50µm
i
i
7µm
d
Ductal and acinar branch-associated clone
nGFP mCFP
DBA
15µm

Figure 18. *Morphology and potency of clones reveal evidence for ductal end-driven branching morphogenesis. (a) Schematic depicting the different types of clones that would be expected to arise as a result of pancreatic growth being driven either by plexus remodelling or ductal end-driven morphogenesis. (b) Ductal branching clone monoclonally labelling the distal parts of ducts (arrow) with zoomed in single Z section on the right showing the overlap of DBA with cYFP. (c) Ductal terminus-associated acinar clone with acinar cells (asterisk) closely surrounding ducts stained with DBA (white), with zoomed in single Z section on the right showing very small overlap of DBA with cYFP (arrow). (d) Rare local high induction levels that were recorded occasionally show ductal branching clone as in (b), and ductal terminus-associated acinar clone as in (c) occupying the same branch, suggesting a common mechanism driving the morphogenesis of the two lineages. Representative clones based on analysis of 254 clones from n-3 mice (3 litters) are shown.*

Since both the ductal branching clones and ductal terminus-associated acinar clones were nearly monoclonally labelling the ductal and acinar compartment respectively at the peripheral region of pancreas, I hypothesised that the growth of the organ could be tip-driven, i.e. the acinar and ductal cells at the periphery proliferate and push the outwards expansion of the growing pancreatic bud. In order to verify the hypothesis I turned to EdU proliferation assay, which labels cells with an active S phase of the cell cycle. I hypothesised that if the mode of pancreas growth is tip driven, then I should detect enrichment of EdU+ cells in the peripheral regions of the pancreas. Hence, with the short-term EdU incorporation (2h chase) experiment and whole-mount imaging at E13.5, E15.5 and E18.5, I studied the kinetics of growth in development of pancreas (Fig. 19a).

I first looked at the general proliferation within whole pancreatic buds. The EdU+ cells were distributed densely around the entire pancreatic volume by bulk observation. This could suggest that the cells were proliferating evenly throughout the pancreas, without any enhancement of proliferation at the peripheral/tip regions (Fig. 19b-f), contradicting the tip-driven growth hypothesis, suggested in Fig. 18.

However, since I observed ductal branching clones and branch-associated acinar clones located at peripheral tissue areas (Fig. 18), I hypothesised that pancreatic growth could be ductal-end driven. I therefore sought to look at the proliferation of ducts specifically, expecting higher extent of proliferative heterogeneity, with Edu+ cells being enriched at the ductal-ends. Furthermore, given the fact that the acinar compartment takes up about 90% of the adult mouse pancreas (Benitez et al. 2012), it is not surprising that the acinar cells show a generally high proliferation without a clear heterogeneity.

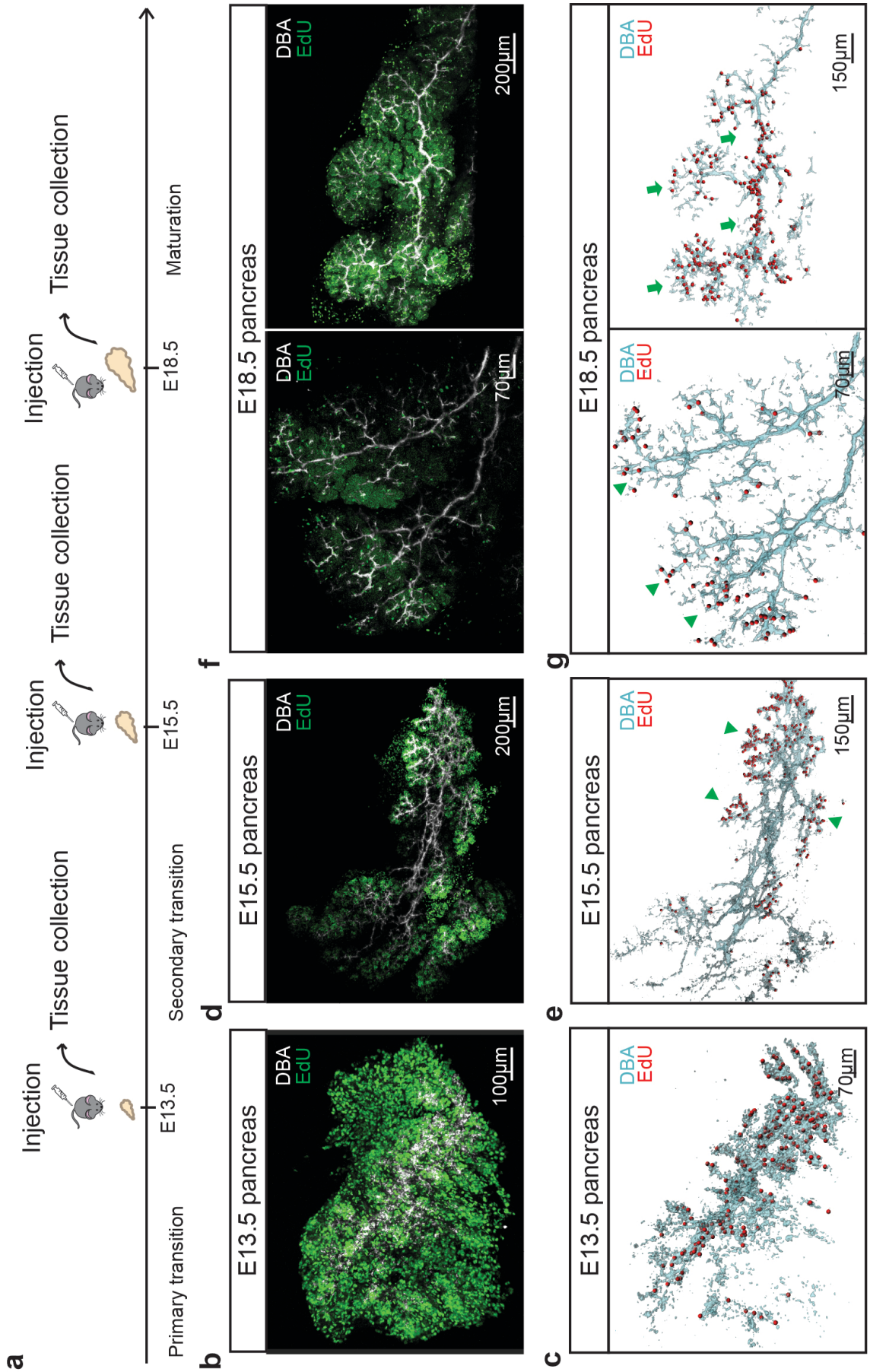
a
Injection
Tissue collection
Injection
Tissue collection
Injection
Tissue collection
Primary transition
E13.5
Secondary transition
E15.5
E18.5
Maturation
b
E13.5 pancreas
DBA
EdU
100µm
c
E13.5 pancreas
DBA
EdU
70µm
d
E15.5 pancreas
DBA
EdU
200µm
e
E15.5 pancreas
DBA
EdU
150µm
f
E18.5 pancreas
DBA
EdU
70µm
200µm
g
E18.5 pancreas
DBA
EdU
70µm
150µm

Figure 19. *Examining proliferative heterogeneity in the developing pancreas. (a) Schedule of EdU incorporation experiments. (b-g) Short term (2h) EdU-incorporation shows proliferative activity of ductal and acinar cells. Top panels: whole-mount pancreatic ducts (stained for DBA, white) and EdU (green); bottom panels: ductal surface reconstruction (blue) with ductal EdU+ cells marked in red. At E13.5 (b,c), proliferation is evenly distributed throughout the ducts (n=3 mice, 3 litters) whereas, at E15.5 (d,e), proliferation occurs predominantly at the periphery of the pancreas in the tip regions of ducts (n=2 mice, 2 litters). At E18.5 (f,g), proliferation patterns become heterogeneous with some regions displaying ductal end-enrichment (n=4 mice, 3 litters, arrowheads, left), while others proliferate more homogeneously (n=5 mice, arrows, right).*

Therefore, I decided to focus on the proliferation in the ducts, and perform a threshold based 3D outline of ductal structures using Imaris software and the visualisation protocol of all EdU+ cells within the ducts converted into regular spheres for data presentation purposes (Fig. 19c,e,g, see Methods Chapter 2.1.13), in order to analyse ductal and Edu+ colocalisation. Consequently, focusing on the proliferation within the ducts, I found a uniform pattern of proliferation at E13.5 (Fig. 19b,c). It is likely that by this stage the tissue is still morphologically and proliferatively homogenous, as the separation of tip-trunk domains has just started to take place. However, at E15.5, ductal proliferation (and, to a lesser degree, acinar proliferation) was greater in peripheral regions of ductal subtrees, with a particular enrichment of activity at the ends of ducts (Fig. 19d,e, arrowheads), consistent with ductal-end driven growth. Short-term EdU incorporation at E18.5 showed a more heterogeneous pattern, with some parts of the pancreas characterized by enhanced proliferation at ductal termini (Fig. 19f,g, arrowheads), while other regions displayed more uniform proliferation throughout the ductal network (Fig. 19f,g, arrows). Together, these results are consistent with the early stages of branching morphogenesis being fuelled by self-renewing precursors positioned at ductal termini, while, at later stages, growth is dominated by local expansion of ducts, as well as acini and islets.

4.3 Precursors at ductal-ends are a mixture of committed and multipotent precursors based on E12.5 induction lineage tracing

Given the hypothesis of ductal-end driven growth, I was interested in finding out the cellular composition of the proliferative ductal-ends. I therefore considered several alternative possibilities of clone types arising as a consequence of different progenitor cell types at ductal ends. Hence, concentrating on the E12.5 induction, I reasoned that if branching morphogenesis is driven by multipotent progenitors, clones tracking whole subtrees should contain a mixture of acinar, ductal, as well as islet cells (Fig. 20a). If, on the other hand, branching morphogenesis is driven by fate-restricted progenitors, clones tracking whole subtrees should be of either purely acinar or ductal type (Fig. 20b,c). I therefore wanted to verify these three options with the clonal data.

I looked at the potency and morphology of clones induced at E12.5. First, I carried out analysis of the potency of clones grouped with respect to pancreatic compartment contained within a clone, i.e. the distribution of potencies of acinar, ductal and islet compartment containing clones. I found that some 70% of acinar-containing clones induced at E12.5 were unipotent (representative clone in Fig. 20d), lending support to the second hypothesis of fate-restricted progenitors driving branching morphogenesis. For comparison, at E9.5, when the pancreatic anlage emerges, the percentage of unipotency was much lower and amounted to ~60% (Fig. 20d). The fact that these unipotent acinar clones induced at E12.5 often spanned multiple rounds of consecutive branching of the same ductal subtree suggests that acinar cells arise from acinar-committed precursors that localize at the terminus of growing ducts and undergo renewal during ductal bifurcation (Fig. 18c, 16d).

By contrast, the vast majority of ductal cell-containing clones traced from E12.5 were found to be multipotent (Fig. 20e). These included tripotent clones (Fig. 20f), bipotent ductal-acinar clones with typically sparsely labelled ductal cells (representative image in Fig. 18c), as well as bipotent ductal-islet clones (representative image in Fig 20g). The tripotent and ductal-islet bipotent clones commonly contained islet precursors delaminating from the trailing

ducts left behind the proliferative ductal-ends. The multipotency extent within the ductal compartment was even higher for E9.5 induction (Fig. 20e).

Altogether these findings suggest that growing ductal termini carry both rare multipotent progenitors and fate-restricted acinar and ductal progenitors, which act cooperatively to drive pancreatic growth. This is in contrast to the previous literature suggesting multipotent tip domain driving pancreas morphogenesis (Zhou et al. 2007)

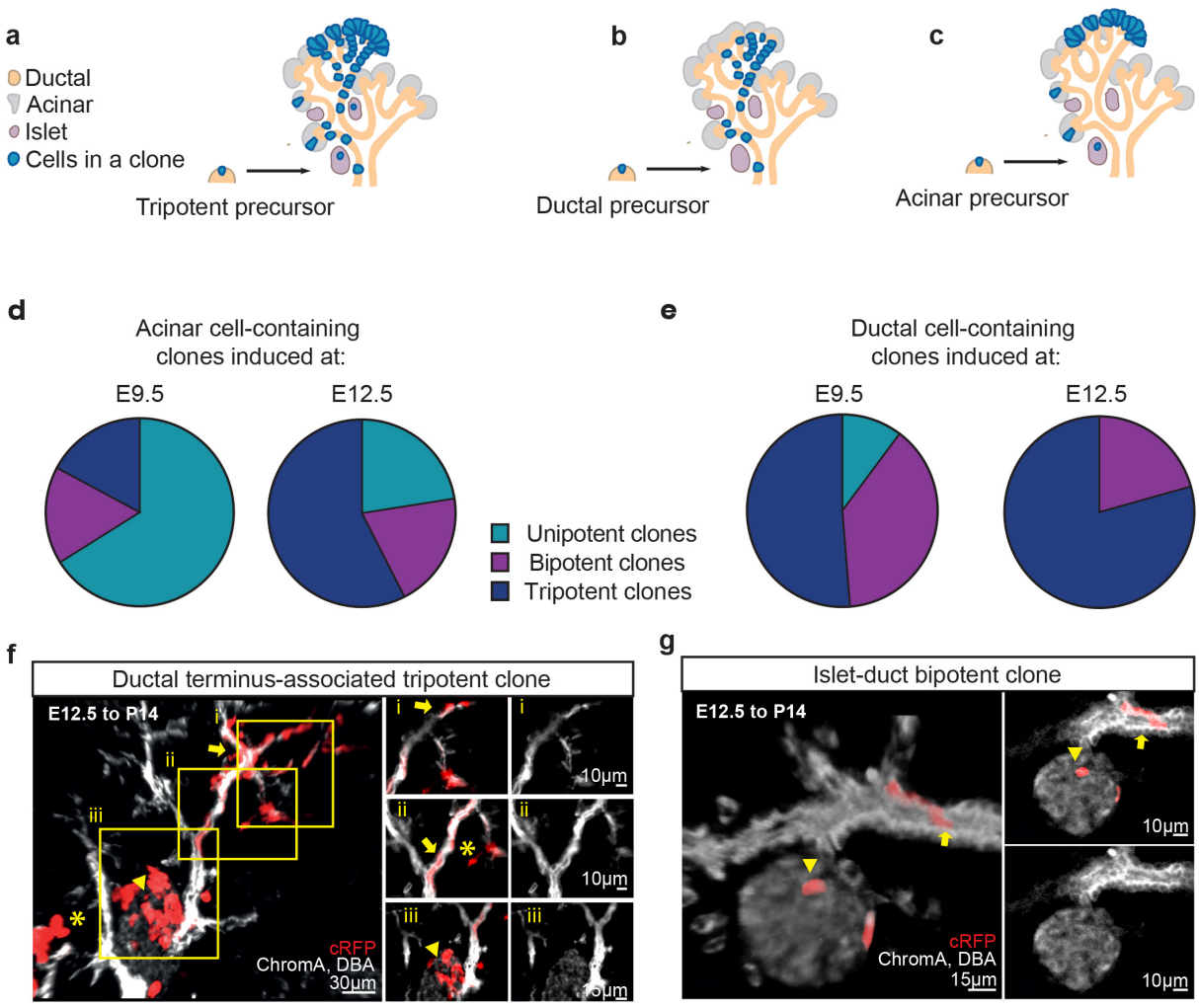

Figure 20. *Ductal ends are composed of a mixture of rare tripotent and commited acinar and ductal precursors. (a-c) Schematics demonstrating the distinct clone morphologies arising from the labeling of differents type of ductal-end precursors with (a) depicting a tripotent clone, (b) a unipotent ductal clone, and (c) a unipotent acinar clone. Potency of (d) acinar cell- and (e) ductal cell-containing clones induced at E9.5 and E12.5. I counted 41 clones from n=2 mice (2 litters) for the E9.5 to P14 tracing, 254 clones from n=3 mice (3 litters) for the E12.5 to P14 tracing. Ductal cells remain bi- and tripotent, whereas acinar precursor clones become increasingly lineage-committed. Ductal-terminus associated tripotent (f) and bipotent (g) clone. Islet, ductal and acinar compartments indicated by arrowhead, arrow and asterisk, respectively.*

I previously found no relationship between the potency of clones and the clone size when analysing all clones (see Section 3.4, Fig.17e). However, I was interested if there was any relationship between the potency and clone size within the individual compartments, and whether fate-restriction of pancreatic precursors was accompanied by a decreased propensity to undergo self-renewal. Strikingly, I found that the difference between the average size of unipotent acinar clones and that of bi-/tripotent clones containing acinar cells was not statistically significant (Fig. 21a). The same feature was observed for clones containing ductal cells (Fig. 21b), showing that ductal and acinar unipotent precursors retained full growth potential even after fate-restriction has taken place. These results indicate that the majority of self-renewing acinar-committed precursors are specified early in development (during the tip-trunk segregation) and are replenished by the multipotent ductal precursors only rarely during the later stages of development.

In summary, the potency and spatial localisation of clones shown in this section are suggestive of a cellular hierarchy in which, during the secondary transition, minority populations of multipotent and fate-restricted self-renewing precursors, localized at the growing ductal termini, coordinate the process of branching morphogenesis, giving rise to ductal progenitors that expand the maturing ducts, acini that arise at the ductal ends, as well as delaminating islet precursors (Fig. 21c).

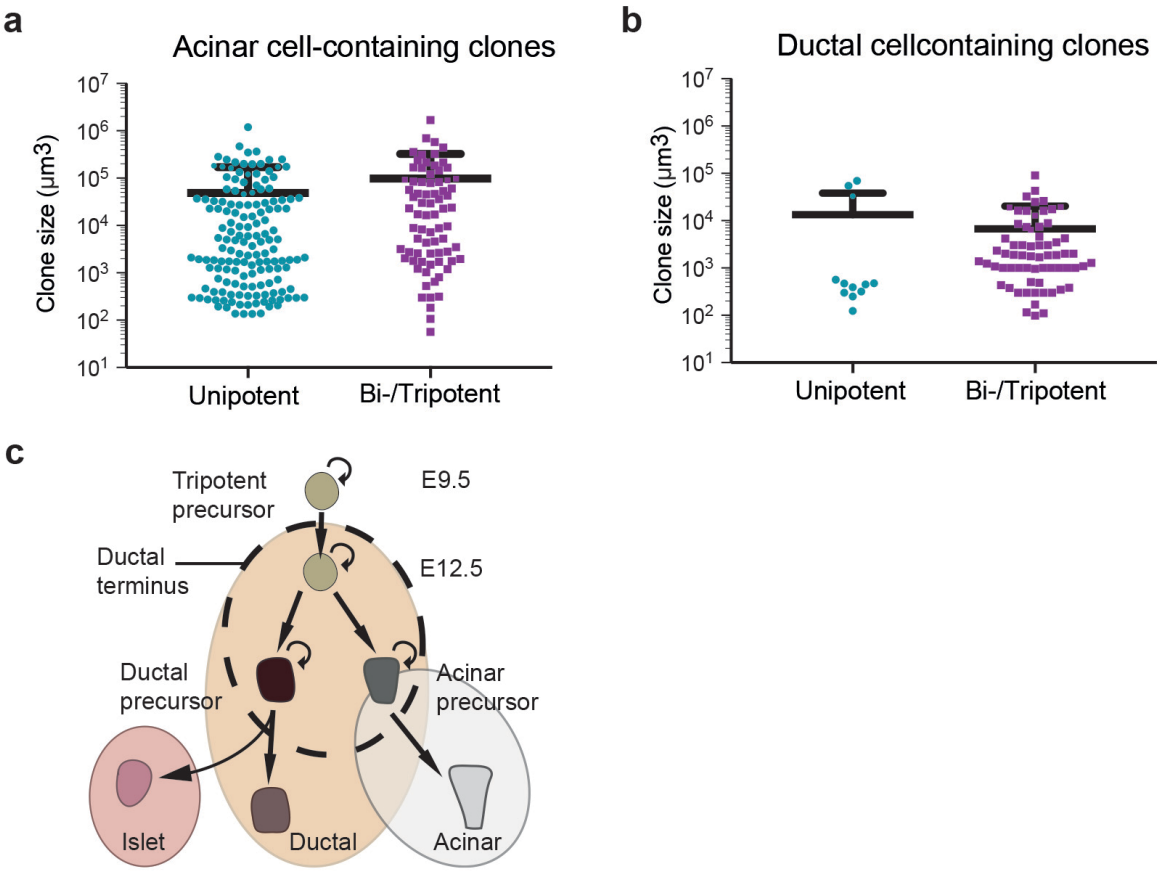

Figure 21. *Inferring hierarchy of progenitors in the pancreas. Comparison of subclone sizes in the (a) acinar and (b) ductal compartment for unipotent vs. bi-/tripotent clones, showing no statistically significant differences. Bars indicate mean and S.D. I counted 254 clones from n=3 mice (3 litters). (c) Hierarchy of multipotent precursors and their lineage-restricted progeny inferred from the lineage tracing data.*

4.4 *Sox9*-CreERT lineage tracing confirms previous findings of ductal-end driven pancreas morphogenesis

To consolidate the findings from Section 4.2 and 4.3, I turned to a targeted lineage tracing strategy using a *Sox9*-CreERT2 mouse model (Kopp et al. 2011), to exclude the possibility of the results reported in the previous sections arising from some artefacts related to the *R26* promoter tracing and to exclude the possibility of tracing of non-pancreatic lineage cells such as stroma or mesenchyme.

Examination of clones induced at E12.5 revealed a morphology and potency similar to that found using the ROSA26 model (Fig. 22a,b). I observed both the monoclonally-labelling ductal clones spanning ducts over multiple ductal branchings, as well as the branch-associated unipotent or acinar majority clones. These are indicative of the ductal-end driven morphogenesis described in the sections before (Section 4.2, 4.3). Although Sox9 expression has been associated with tripotency (Kopp et al. 2011; Furuyama et al. 2011), my findings suggest that, by E12.5, the majority of individual *Sox9*+ cells are already fate-restricted to either the acinar or the ductal/islet lineage. This discrepancy may arise from the non-clonal levels of induction in the previous studies (Kopp et al. 2011; Furuyama et al. 2011), with apparent tripotent clones arising from a possible merging of lineage-committed cells.

In summary, *Sox9*-CreT2 lineage tracing at E12.5 confirms the previous findings of extensive tissue fate restriction by the end of primary transition and supports the model of ductal-end driven growth and the coordinated formation of the three main pancreatic lineages.

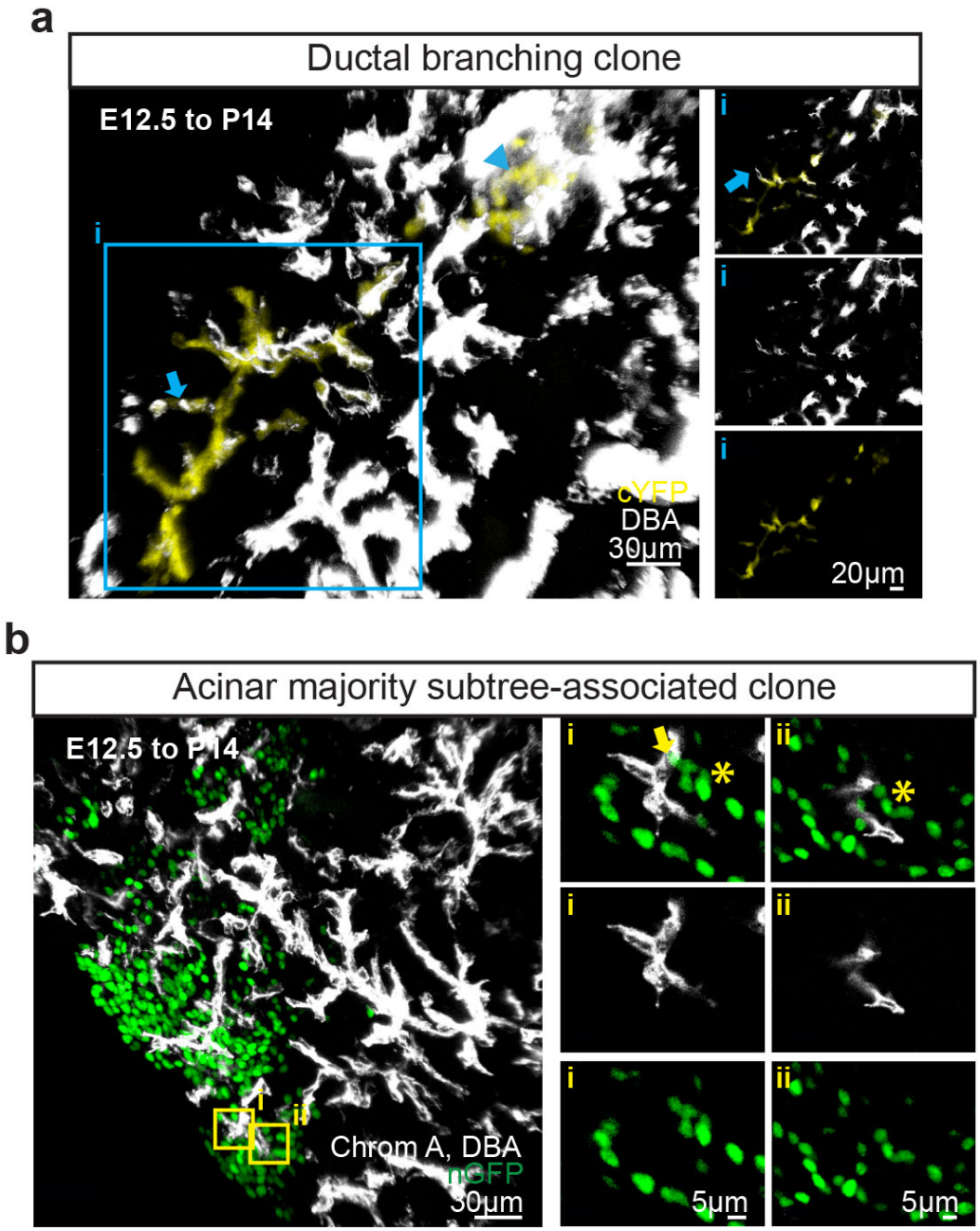

Figure 22. *Sox9 lineage tracing control. (a-b) Sox9-CreERT2; R26-Confetti lineage tracing recapitulates the basic morphology and cell type composition of clones in Fig. 18b,c with both (a) branched ductal clones and (b) acinar subtree-associated clones present in abundance, supporting the hypothesis that self-renewing ductal and acinar precursors at ductal termini drive pancreatic growth. Ductal and acinar compartments indicated by arrow and asterisk, respectively. Representative images from analysis of 50 clones from n=3 mice are shown.*

4.5 Early lineage restriction and potency distribution is confirmed by amylase co-immunostaining

As outlined before, the use of the multicolour reporter system was essential for obtaining clonal levels of induction with a use of a feasible number of embryos in order to provide an accurate assessment of clonal potency. However, with the use of multicolour confetti cassette, I was left with only one channel for imaging, when visualising the samples, which was used for the simultaneous islet and ductal staining. As a consequence, I was not able to stain for the acinar marker in the lineage traced samples. However, I carried out an immunostaining control, which revealed that the vast majority of dissected pancreatic sections that were not DBA+ Chromogranin A+ were amylase+ (see Section 3.2.5 and Fig. 13). I therefore used an assumption that all non-Chromogranin A+ non-DBA+ cells were acinar, given the control immunostaining and the large number of quantified clones (244 for E12.5 to P14 lineage tracing, 50 for E9.5 to P14 tracing). Nevertheless, as the correct cell fate assignation was very critical for this study, I decided to re-stain the samples with amylase in another channel, controlling for the undesirable bleed-through effect.

As before, I could observe that the vast majority of the tissue, which was not ductal and non-islet was acinar (Fig. 23), and the major clone types based on potency and morphology as in Figure 18 and Figure 16d-h with only DBA and Chromogranin A immunostaining, were confirmed (Fig. 23). I therefore sought to quantify the clones obtained with the amylase co-immunostaining control in order to compare the distributions of potencies with that of DBA and Chromogranin A immunostaining quantification.

I quantified the potency of 26 clones from 2 mice from the amylase co-immunostaining control samples, and compared the result with the distribution of clone potency in the initial DBA, Chromogranin A-immunostaining quantification. Crucially, I found that the potency distribution of the requantified clones was very similar to the ones I had reported before in Chapter 3.4 (no statistically significant difference, Fig. 24).

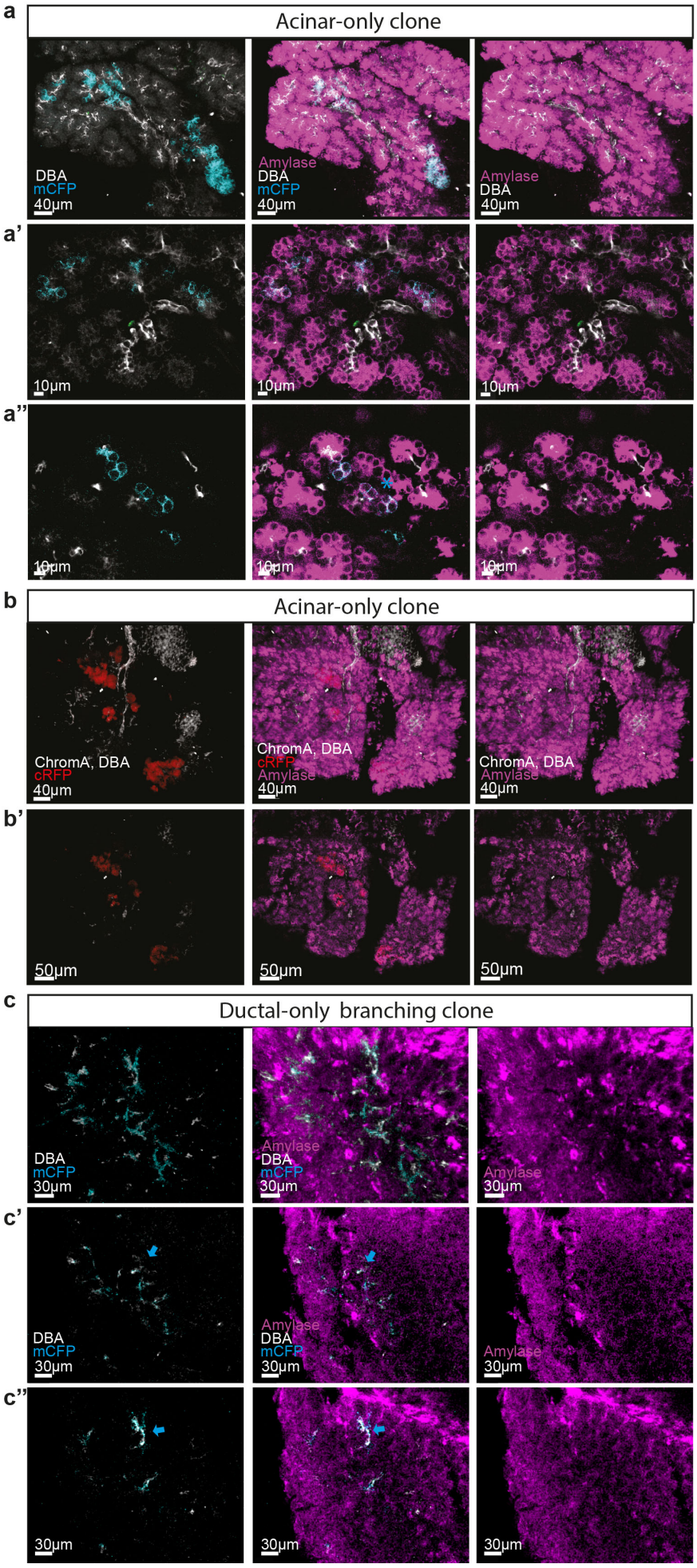
a
Acinar-only clone
DBA
mCFP
40µm
Amylase
DBA
mCFP
40µm
Amylase
DBA
40µm
a'
10µm
10µm
10µm
a''
10µm
10µm
10µm
b
Acinar-only clone
ChromA, DBA
cRFP
40µm
ChromA, DBA
cRFP
Amylase
40µm
ChromA, DBA
Amylase
40µm
b'
50µm
50µm
50µm
c
Ductal-only branching clone
DBA
mCFP
30µm
Amylase
DBA
mCFP
30µm
Amylase
30µm
c'
DBA
mCFP
30µm
Amylase
DBA
mCFP
30µm
Amylase
30µm
c''
30µm
30µm
30µm

a

E12.5 induction - amylase control

Clone type	Frequency (%)
Unipotent acinar	57.7
Unipotent ductal	15.4
Unipotent islet	3.8
Bipotent acinar-ductal	19.2
Bipotent acinar-islet	0.0
Bipotent ductal-islet	0.0
Tripotent	3.8

b

E12.5 induction

Clone type	Frequency (%)
Unipotent acinar	59.9
Unipotent ductal	3.1
Unipotent islet	5.1
Bipotent acinar-ductal	10.5
Bipotent acinar-islet	4.7
Bipotent ductal-islet	1.2
Tripotent	15.6

c

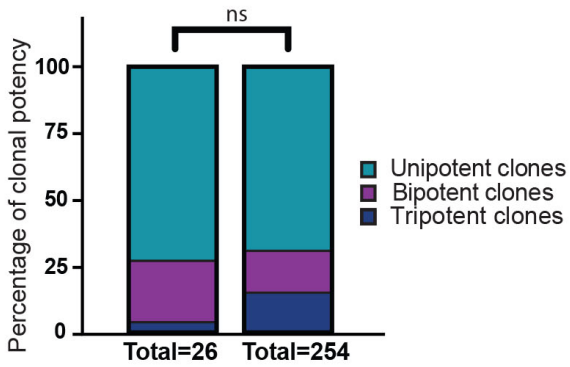

Figure 23. *Comparison of potency outcome between original DBA and Chromogranin A immunostaining clonal analysis and amylase co-immunostaining control. Frequency of different clone types by cell composition for (a) E12.5 induction with 26 clones (n= 2mice, 2 litters) requantified with additional amylase co-immunostaining in additional to DBA and Chromogranin A, and (b) E12.5 induction with 254 clones quantified (n= 3 mice, 3 litters, same dataset as Fig. 17). (c) Comparison of global potency between both quantification methods showed no statistically significant difference.*

Figure 24. *Additional verification of clone types with amylase immunostaining. Branch-associated (a) mCFP and (b) cRFP clone, and (c) branching ductal clone co-stained with amylase (pink), islet and duct (white) shown as 3D projection and (a', a'', b',c', c'') as individual z-sections. The vast majority of tissue that was non-ductal and non-islet was acinar. mCFP and cRFP in a and b colocalised with amylase+ cells. mCFP in c colocalised with DBA. Representative images from the analysis of 26 clones from n= 2mice (2 litters) are presented*

4.6 Establishing the link between acinar and ductal dynamics based on clonal quantification

As outlined before, qualitatively I observed collaborative behaviour between the ductal and acinar compartment. I identified two conserved groups of clones by morphology and cell composition: the acinar clones tracking ducts over generations of branches, and nearly monoclonally labelled ducts over multiple bifurcations (see Fig. 18b-d, 22a-b). However, I wanted to test and confirm the hypothesis of this collaborative behaviour by performing statistical analysis.

In order to verify this, I looked at clone size distributions. Clone sizes were quantified (see Section 3.3.2). The variability of clone sizes within the ductal and acinar lineage was very broad for both compartments, although the acinar clones were on average significantly larger (Fig. 21a-b). This is consistent with the literature, whereby acinar cells make up 90% of the mature organ (Benitez et al. 2012), as this would imply that the acinar precursors need to proliferate more during development. As explained above, there was no correlation between clone size and potency size for all clones grouped together (Fig. 16i).

I therefore aimed to determine the mechanism responsible for generating such broad clonal size distributions, and to compare the structure of acinar and ductal clonal distributions. This analysis was carried out in collaboration with Dr Edouard Hannezo and Prof. Benjamin Simons. In order to compare the two clone size distributions, we rescaled the clone sizes within each lineage, by dividing all clones sizes by the average clone size within each compartment. This enables the comparison of variability between compartments. We then plotted these rescaled clone sizes on a cumulative distribution curve, which is a probability function of a variable X (rescaled clone size) being of a given value or smaller (multiple of average size and smaller). This enables the comparison of the structure of heterogeneity of clone sizes, and hence the proliferation of cells, between distributions of different ranges of sizes.

Comparison of ductal and acinar cell-containing clones showed that the size distributions of the respective clone compartments, rescaled by the average size, was strikingly similar both between lineages at P14 (Fig. 25a-b, P=0.68, Mann-Whitney test). That is, while their average sizes differ by more than an order of magnitude (E12.5 to P14 tracing), the chance of finding a clone larger than some multiple of average remains the same for both the acinar and ductal lineage, revealing similar dynamics of the two compartments.

Observing the matching pattern of clonal behaviour I wanted to find out whether the dynamics of proliferation were consistent for the clones traced between E12.5 and P14 and the clones traced between E12.5 and P28. Indeed the cumulative distributions of the two were highly matched. (Fig. 25c, P=0.63 for acinar lineage and P=0.95 for ductal lineage, Mann-Whitney tests; Statistical Methods in Chapter 2.3).

Furthermore, I wanted to find out if the dynamics of the proliferation within the lineages was the same in primary and secondary transition. Indeed, I could see that the cumulative distributions of acinar and ductal lineage were matching for E9.5 traced clones (E9.5 to P14) (Fig. 25d-e), showing that the growth of two compartments is also coordinated in primary transition. Additionally, analysing the distributions for the same lineages (acinar or ductal) between the two induction timepoints (E9.5 and E12.5), a match could be observed, suggesting that the same mechanism is driving morphogenesis in primary and secondary transition (Fig. 25f-g).

Altogether, this suggests that the gross heterogeneity in clone sizes may share a common origin in the collective fate decisions of self-renewing progenitors during branching morphogenesis.

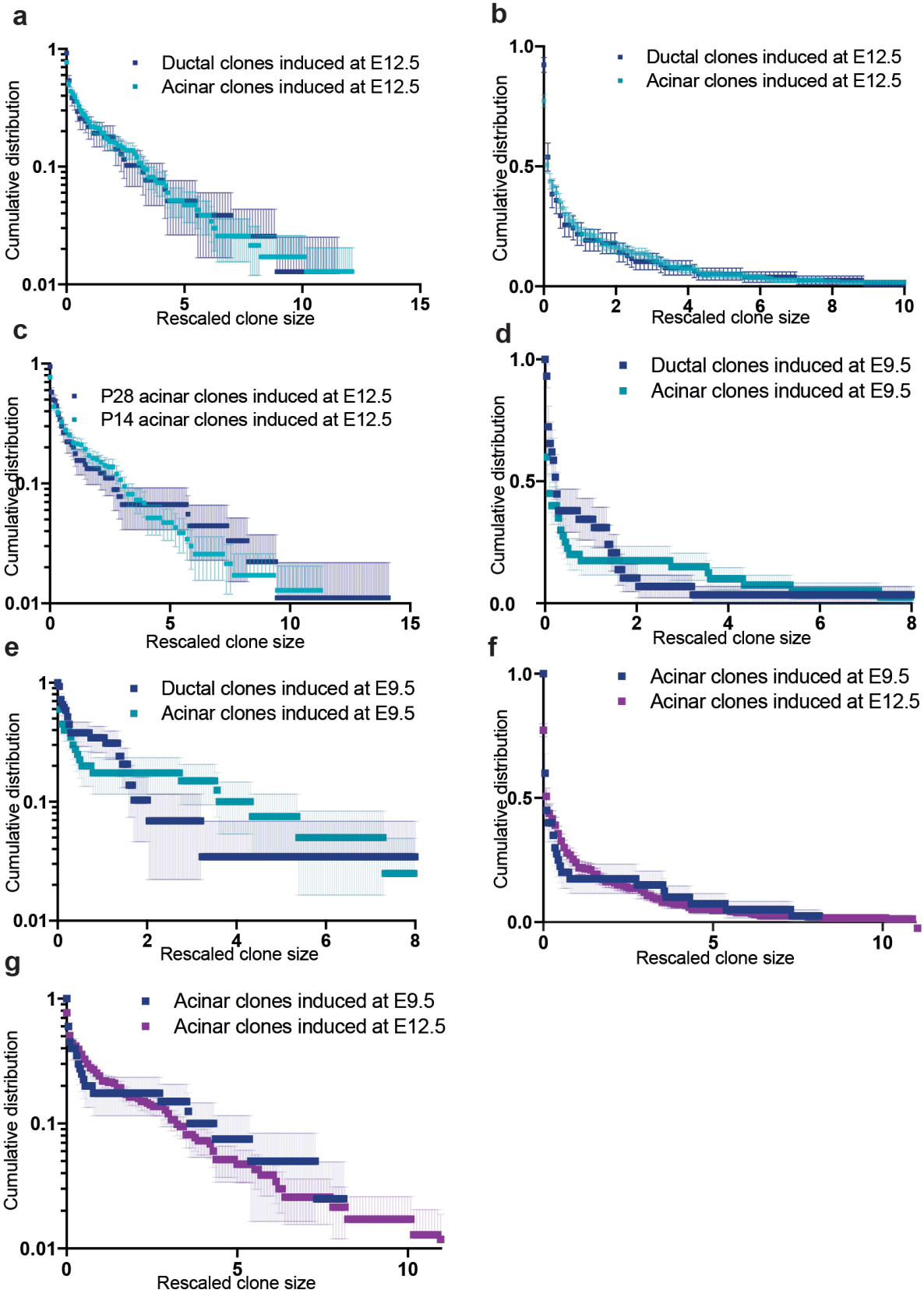
a
Ductal clones induced at E12.5
Acinar clones induced at E12.5
Cumulative distribution
Rescaled clone size
b
Ductal clones induced at E12.5
Acinar clones induced at E12.5
Cumulative distribution
Rescaled clone size
c
P28 acinar clones induced at E12.5
P14 acinar clones induced at E12.5
Cumulative distribution
Rescaled clone size
d
Ductal clones induced at E9.5
Acinar clones induced at E9.5
Cumulative distribution
Rescaled clone size
e
Ductal clones induced at E9.5
Acinar clones induced at E9.5
Cumulative distribution
Rescaled clone size
f
Acinar clones induced at E9.5
Acinar clones induced at E12.5
Cumulative distribution
Rescaled clone size
g
Acinar clones induced at E9.5
Acinar clones induced at E12.5
Cumulative distribution
Rescaled clone size

Figure 25. *Comparison of distributions of clone sizes from E9.5 and E12.5 induction timepoints. Sizes in each distribution (x-axis) were rescaled by their respective ensemble averages. (a-b) Cumulative size distribution of ductal and acinar compartments in clones induced at E12.5 plotted on (a) logarithmic and (b) linear y axis. (c) Cumulative size distribution (plotted on logarithmic y axis of rescaled P14 and P28 collected acinar clone sizes induced both at E12.5. (d-e) Cumulative size distribution of ductal and acinar clones induced at E9.5 plotted on (d) log and (e) linear y axis. (f-g) Cumulative size distribution of acinar clones induced at E9.5 and E12.5 plotted on (f) log and (g) linear y axis. I counted 41 clones from n=2 mice (2 litters) for the E9.5 to P14 tracing, 254 clones from n=3 mice (3 litters) for the E12.5 to P14 tracing, 84 clones from n=2 mice (2 litters) for the E12 to P28 tracing.*

4.7 Ductal branching morphogenesis provides a common mechanism for development of acinar and ductal lineages

I was interested in identifying the origin of the consistent progenitor heterogeneity in the acinar and ductal compartment. As there was no correlation between the potency and clone size, I wondered whether the broad and heterogeneous distribution of clone sizes could arise from the stochastic decision of progenitor proliferation versus proliferation termination. Such behaviour of clones has been described previously (Klein and Simons 2011), and is associated with exponential curve for cumulative distribution, as in the birth-death events. However, the cumulative distributions observed for ductal and acinar lineages contained larger tails of the distribution, inconsistent with this hypothesis.

Since I observed a matching clonal behaviour and morphology of acinar and ductal clones being associated with the ductal network, I hypothesised that the progenitors within the ducts could give rise to the specific clone size distributions. This would provide a mechanism of coordinated tissue growth in development. To challenge this hypothesis, I assessed the emergence and degree of gross heterogeneity of the growing ductal network itself by carrying out ductal whole-mount immunostaining of pancreata at different stages of development. In line with previous reports (Puri and Hebrok 2007; Kesavan et al. 2009; Villasenor et al. 2010; Bankaitis et al. 2015; Shih et al. 2016), the analysis of whole-mount tissue at E13.5 and E15.5 revealed a transition from a plexus structure to central primordial ducts from which multiple smaller ducts start to branch (Fig. 26a,b). By E18.5, whole-pancreas ductal reconstructions revealed a strikingly complex and intricate ductal network, reflecting multiple (>10) rounds of serial branching events tracking back to the primordial duct (Fig. 26c,d), consistent with a phase of branching morphogenesis. Notably, focusing on measurements made from whole-mounts at E18.5, I found that some ductal subtrees remain small, localized to the centre of the pancreas, and comprise only a limited number of branch segments (Fig. 26d). By contrast, other subtrees expanded radially, reaching

out to the periphery of the organ and colonizing a large volume of tissue (Fig. 26d).

To find out the extent of ductal subtree heterogeneity, I quantified the raw distribution of subtree sizes (Fig. 26e,f), defined as the total number of branches (i.e. segments between two bifurcation points) within each subtree emanating from the primordial ducts (indicated with dashed line in Fig. 26a-c). How the ductal network was individually reconstructed for each subtree and how subtreees were distinguished is presented in schematic in Figure 26e. Strikingly, when compared to the clonal data, I found that the rescaled cumulative subtree size distribution (as described in Section 4.6) matched closely with that of the rescaled clone size distributions of both the ductal and acinar compartments (Fig. 27a-c), suggesting that clone size heterogeneity might indeed derive from the heterogeneity of the branching process. I verified this finding further by plotting the ductal subtree distributions with clone distributions from different lineages and induction timepoints revealing consistently matching dynamics (Fig. 27d-e).

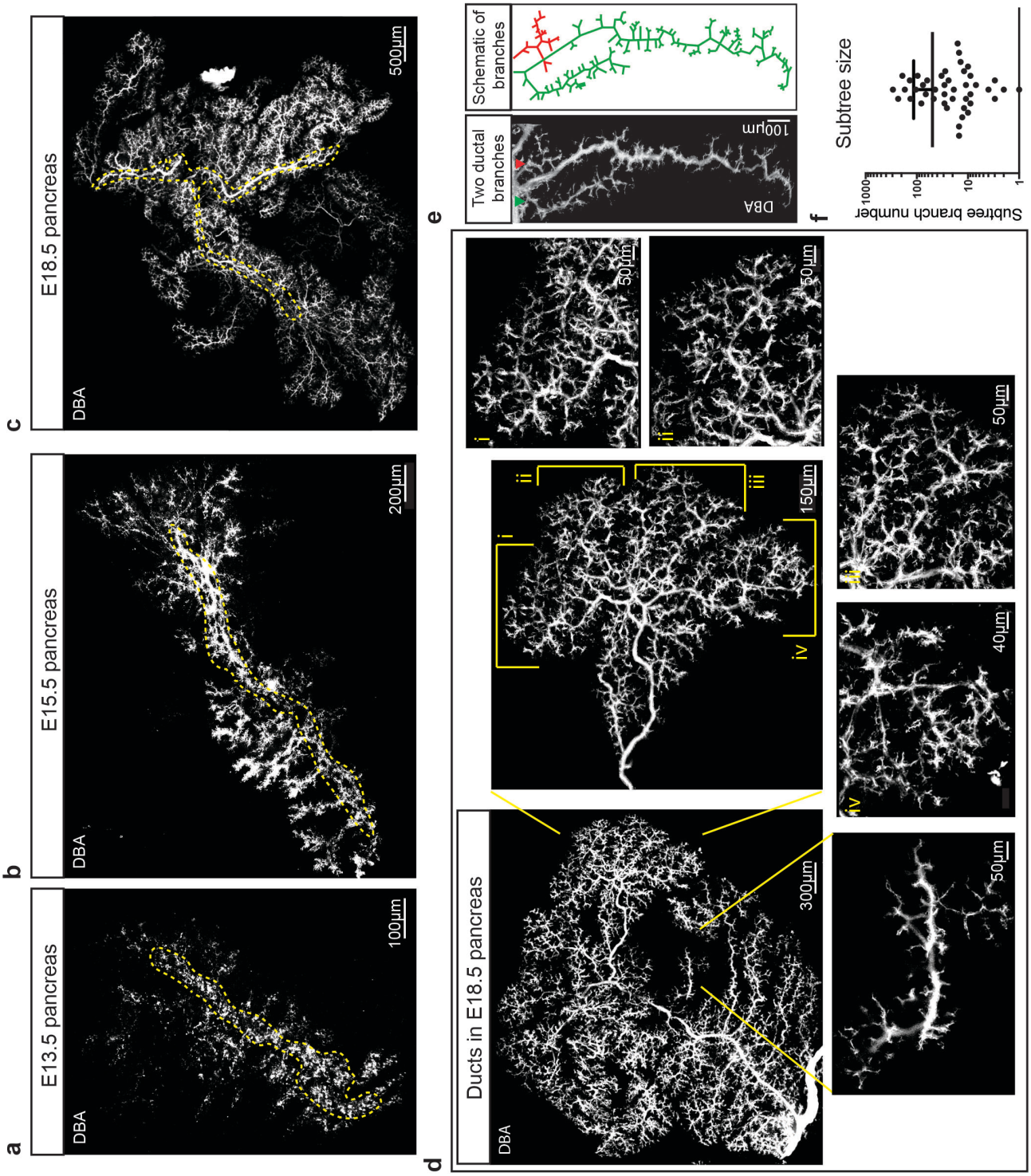
a
E13.5 pancreas
DBA
100µm
b
E15.5 pancreas
DBA
200µm
c
E18.5 pancreas
DBA
500µm
d
Ducts in E18.5 pancreas
DBA
300µm
i
50µm
ii
50µm
i
ii
iii
iv
150µm
iii
50µm
iv
40µm
v
50µm
e
Two ductal branches
DBA
100µm
Schematic of branches
f
Subtree size
Subtree branch number
1000
100
10
1

Figure 26. *Ductal network development in vivo. (a-c) Evolution of pancreatic ductal network stained in whole-mount with Dolichos biflorus agglutinin (DBA) at (a) E13.5, (b) E15.5 and (c) E18.5. Central plexus indicated in outline by dashed blue lines. (d) Branching structure of an E18.5 pancreas (ducts stained by DBA, white), with insets i-iv highlighting the heterogeneity of branch and subtree sizes. (e) Zoomed-in image of two pancreatic subtrees of E18.5 pancreas (left) and sketch of the two branches used in subtree size quantification (right), demonstrating the heterogeneity of branching morphogenesis. (f) Subtree sizes (scored by number of branches arising from a large central duct) determined from E18.5 pancreas. Subtree sizes were measured for n=3 mice and n=43 independent subtrees. Bars indicate mean and S.D.*

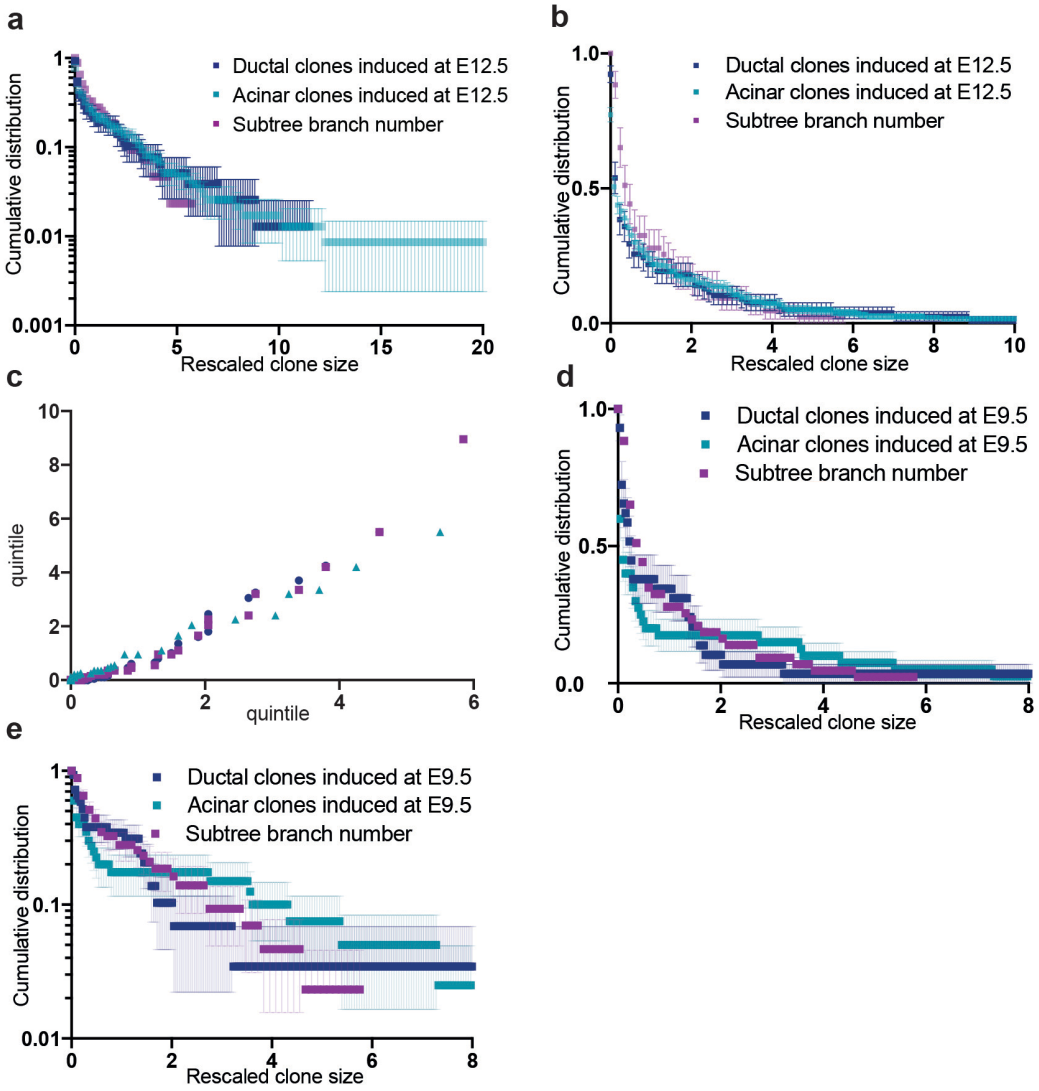
a
Ductal clones induced at E12.5
Acinar clones induced at E12.5
Subtree branch number
Cumulative distribution
Rescaled clone size
b
Ductal clones induced at E12.5
Acinar clones induced at E12.5
Subtree branch number
Cumulative distribution
Rescaled clone size
c
quintile
quintile
d
Ductal clones induced at E9.5
Acinar clones induced at E9.5
Subtree branch number
Cumulative distribution
Rescaled clone size
e
Ductal clones induced at E9.5
Acinar clones induced at E9.5
Subtree branch number
Cumulative distribution
Rescaled clone size

Figure 27. *Comparison of subtree size and clone size distributions at E9.5 and E12.5. Sizes in each distribution (x-axis) were rescaled by their respective ensemble averages. (a-b) Cumulative size distribution of ductal and acinar compartments in clones induced at E12.5 together with subtree size distribution (number of branches) determined from E18.5 pancreas plotted on logarithmic (a) and linear (b) y axis. (c) Quintile-quintile plot comparing cumulative size distribution of P14 ductal compartment clones (induced at E12.5) versus P14 acinar compartment clones (induced at E12.5) in cyan; P14 ductal compartment clones (induced at E12.5) versus pancreas subtree size (at E18.5) in pink; P14 acinar compartment clones (induced at E12.5) versus pancreas subtree size (at E18.5) in dark blue. (d,e) Cumulative size distribution of ductal and acinar compartments in clones induced at E9.5 overlaid with the cumulative subtree size distribution (number of branches) determined from E18.5 pancreas plotted on linear (d) and log (e) y axis. I counted 41 clones from n=2 mice (2 litters) for the E9.5 to P14 tracing, 254 clones from n=3 mice (3 litters) for the E12.5 to P14 tracing. . Subtree sizes were measured for n=3 mice and n=43 independent subtrees. Bars indicate mean and S.D.*

4.8 Macroscopic quantification of pancreatic growth

Based on the clonal data, I inferred that pancreas growth was driven by branching morphogenesis of ductal-ends. I was therefore interested in how the process of tissue morphogenesis related to macroscopic changes in pancreas structure, such as mass, dimensions and relative tissue composition.

I therefore first measured the mass of the pancreas for different stages including E18.5, P7, P14 and P28, for N= 3, 5, 11, and 4 mice respectively. Similarly to previous reports, the curve of growth displayed an exponential curve (Stanger et al. 2007) consistent with even proliferation of cells throughout development and maturation phase (Fig. 28a).

Furthermore, from whole-mount dissected pancreata I observed that the organ appeared to expand more in the width and primarily length, but significantly less in the height dimension (Fig. 28b). Therefore, I attempted to quantify these parameters. Indeed between E13.5 and P14 the pancreas grew ~6 times in width, ~10 in length and only ~3 in height. For the growth between E13.5 and P28, these ratios amounted to ~11, ~10, ~5, respectively. Therefore the growth of pancreas appears to take place primarily in 2D.

Furthermore, since I analysed distributions of ductal and acinar clone sizes, as described in the previous sections (Sections 4.6, 4.7), I was therefore interested in what was the composition of the tissue with respect to these compartments. This would reveal whether the proliferation of cells within the clones from the given compartments is proportional to the kinetics of the total compartment expansion.

I first looked at the ductal compartment, as I was able to reliably quantify the percentage of ductal area out of total pancreatic area (N= 3 mice). Ducts constituted 10% of the whole pancreas, as analysed from multiple thick sections taken from different levels of pancreas (Fig. 28c). This value is consistent with previous literature (Benitez et al. 2012).

The second major clone type was acinar. Quantification of the fraction of acinar cells in the whole pancreas was impossible due to variable penetration

of the amylase antibody through the thickness of sections under study. I therefore decided to compare the increase in acinar average clone size between E12.5 and P14, as well as between E12.5 and P28, with the increase in total pancreas volume (roughly calculated from the measurement of parameters in Fig. 28b). Assuming that the acinar compartment amounts to as much as 90% of the pancreatic tissue as previously reported (Benitez et al. 2012), I reasoned that the increase in acinar clone volume should be comparable to the increase in pancreas volume. Indeed, this turned out to be the case, hence verifying the representativeness of the confetti labelling (Fig. 28d).

Altogether, these results indicate that globally pancreatic growth happens by even proliferation of cells, which contributes primarily to the increase of pancreas in width and length. Therefore, it could be assumed that pancreatic development is happening primarily in 2D.

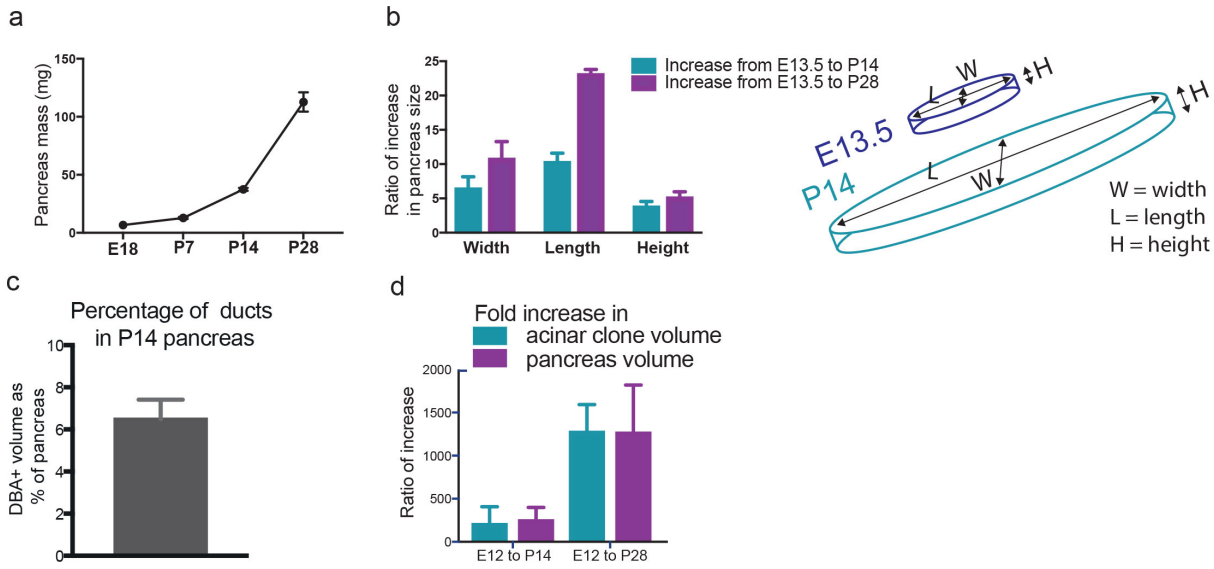

Figure 28. *Growth characteristics of the murine pancreas including (a) changes in pancreatic mass between E18.5 and P28; (b) fold-change in pancreas width, length and height from E13.5 to P14 and P28, as defined in the schematic inset. Bars indicate mean and S.E.M. (c) Percentage of pancreas that belongs to the ductal compartment at P14. (d) Fold increase in the size of the pancreas as a whole and in the acinar compartment-containing of clones between E13.5 and P14, and E13.5 and P28 indicating that clones are representative of the tissue. Bars indicate mean and S.E.M. Pancreas mass was measured for n=3 mice (E18), n=5 mice (P7), n=11 mice (P14) and n=4 mice (P28). Pancreas length, width and height were measured for n=3 mice (E13.5), n=3 mice (P14) and n=3 mice (P28). The percentage of DBA+ cells was calculated from sections from n=5 pancreata.*

4.9 Mechanism underlying branching morphogenesis based on a modelling scheme

Based on the previous findings of ductal branching morphogenesis driving the coordinated development of pancreatic lineages, we then sought to develop a minimal modelling scheme in collaboration with Dr Edouard Hanezzo and Prof. Benjamin Simons. We aimed to capture the dynamics of the ductal branching process and thereby challenge quantitatively the interpretation of the clonal data. To construct the model, we first noted that heterogeneity in clone sizes did not correlate with the potency of individual progenitors (see Section 3.4). However, we also noted that pancreas development is largely two-dimensional (Fig. 28b in Section 4.8). Furthermore, we noted that ductal branches show few intersections (see Section 4.7, Fig. 26a-d). We therefore questioned whether heterogeneity in clone/subtree size could arise from external influences on the collective dynamics of equipotent branching ductal termini. In particular, noting that small subtrees were often terminated while "shadowed" by surrounding larger expanded subtrees (Fig. 26d), we considered whether competition of equipotent ductal termini for space could recapitulate such growth heterogeneity.

We thus proposed a model of branching morphogenesis in which "active" ductal termini at the growing pancreas periphery would be free to branch and elongate, while branching of termini "imprisoned" by neighbouring ducts in more central regions would become arrested (Dahl-Jensen et al. 2016). In this model, ductal termini "choose" between branching into two active ductal termini, thus expanding clone size, or differentiation arresting further ductal growth. Such dynamics gives rise intrinsically to "branched" clones, which are heterogeneous in size, with an ever-diminishing minority of ductal termini remaining active.

The model's predicted subtree size distribution was compared to the experimental distribution of acinar and ductal clone sizes. The results showed excellent agreement (Fig. 29a, see Statictical Methods in Chapter 2.3 for details of the model). This shows that the heterogeneity of pancreas subtree (as well as clone) sizes can be explained quantitatively by a simple paradigm

in which all ductal termini have *a priori* the same growth potential, but their activity is checked by growth-arresting extrinsic signals (Fig. 29a,b), which could arise from neighbouring ducts. Within each ductal terminus, pools of self-renewing ductal precursors fuel ductal elongation and bifurcation, while differentiated acinar cells arise at the ends of terminated ducts.

Interestingly, the theory distribution presented in Figure 29 is based on theoretical concepts developed previously in the mammary gland epithelium and kidney (Scheele et al. 2017). However given its close match with the pancreas compartment dynamics, this is a very likely mechanism of pancreatic tissue growth. Furthermore, this points to a conserved mechanism of branching morphogenesis within different organs.

I therefore plotted the mammary gland rescaled clone size distribution against different combinations of acinar and ductal compartment clones induced at different timepoints and subtree sizes at E18.5, to verify if indeed the two organs follow the same pattern of proliferation dynamics (Fig. 30). Again, there was a striking match in the structure of these distributions, suggesting that indeed a process of stochastic bifurcation and branch termination may be driving pancreas morphogenesis.

I therefore decided to look at the network, which would develop in the pancreas based on the assumptions of the stochastic bifurcation and termination model. The simulation was run by Dr Edouard Hannezo and resulted in the ductal network presented in Fig. 31, which resembles the pancreas ductal network at E18.5 (see Fig. 26).

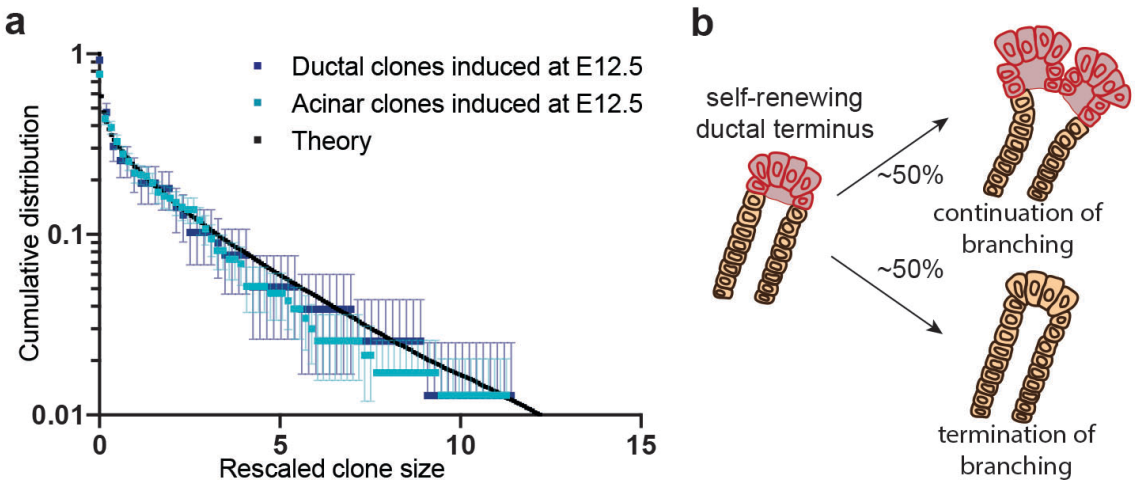

Figure 29. *Acinar and ductal distribution overlaid with the theory plot distribution show a good match. Theoretical subtree size distribution (a) based on a model of equipotent ductal termini, sketched in (b), choosing with near-balanced probabilities between symmetric branching into two ductal termini, or ductal termination, where branching becomes arrested and cells differentiate. (For details of the model, see Statistical Methods in Chapter 2.3). Acinar and ductal distribution are obtained from the quantification of 254 clones from n=3 mice (3 litters) for the E12.5 to P14 tracing.*

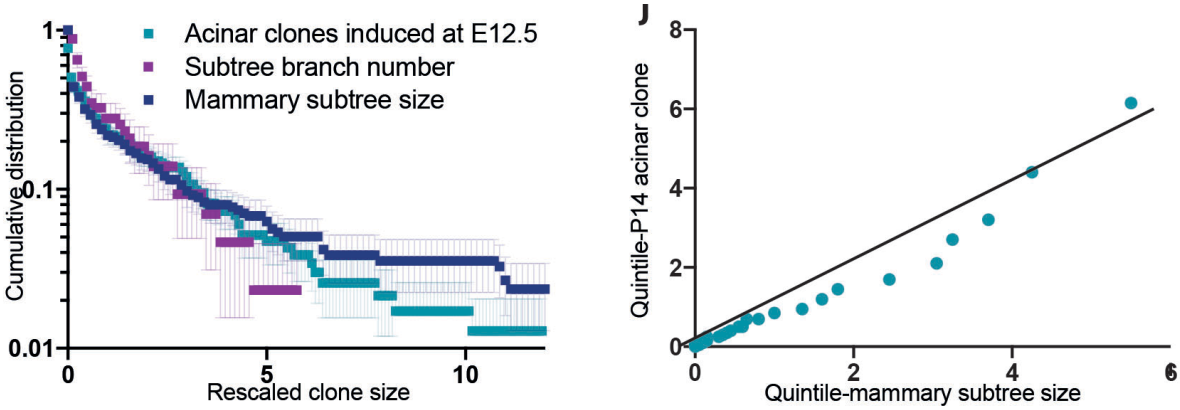

Figure 30. *Comparison of subtree size distribution, clone size distribution and mammary gland subtree distribution. Sizes in each distribution (x-axis) were rescaled by their respective ensemble averages. (a) Cumulative size distribution (plotted on logarithmic y axis) of acinar compartments in clones induced at E12.5, pancreatic subtree size and mammary gland epithelium subtree size (Scheele et al. 2017), showing similar growth dynamics between developing pancreas and mammary gland. (b) Quintile-quintile plot comparing the cumulative size distribution of P14 acinar compartment clones (induced at E12.5) versus mammary subtree size (Scheele et al. 2017). Acinar clone distribution was obtained from the analysis of 254 clones from 3 mice for the E12.5 to P14 lineage tracing. Subtree sizes were measured for n=3 mice and n=43 independent subtrees.*

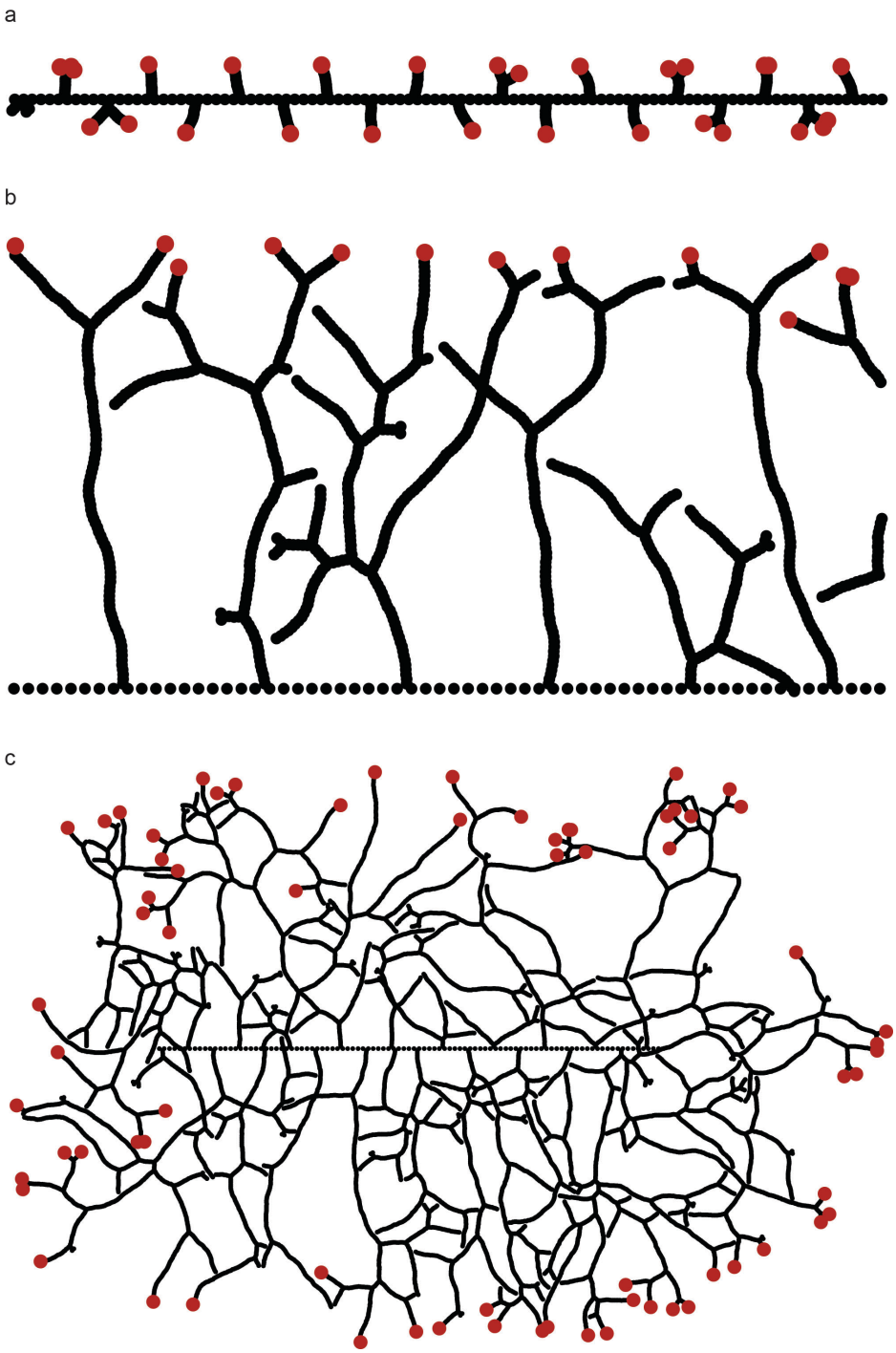

Figure 31. *Ductal network generated from simulations of stochastic proliferation and termination of ductal ends. The model assumes 2D network development and termination of branching upon encounter with another branch. (a) Main duct with arising side branches are presented for the initial stages of pancreatic development (b) ductal network on one side of the main duct after a few generations of branching (c) network developed after multiple generations of branching.*

In summary, it appears that pancreas morphogenesis is driven by proliferative ductal ends carrying fate restricted and multipotent progenitors, which stochastically decide to bifurcate or terminate a branch, as the clonal size distributions match the model theory distribution. The encounter of another ductal-end may induce signals causing the local termination of a branch. However, the question of what may be the source of signals affecting the local termination of branches is still outstanding. These could arise from mesenchyme and stroma, or from the signalling molecules released by the neighbouring termini. This should be the subject of future studies.

4.10 Multiplicity of ductal-end niche progenitors

Based on the insights presented in the previous section (Section 4.9), which suggest that pancreas morphogenesis is driven by proliferative ductal-ends which stochastically decide to bifurcate or terminate, in collaboration with Dr Edouard Hannezo and Prof. Benjamin Simons, we turned to consider the number of self-renewing precursors within a given ductal terminus, which would be responsible for driving the branching morphogenesis. Since the ends of ducts appear roughly constant in size throughout development, and are frequently cleft-shaped (Bankaitis et al. 2015), we proposed that ductal bifurcation segregates precursors approximately equally, after which they undergo a round of symmetric duplication to recover their original density.

Using the inferred branching principles, we then simulated clonal dynamics based on random segregation of labelled cells based on a previously developed model (Scheele et al. 2017). Chance segregation and expansion of clonally-labelled precursors during ductal bifurcation allows the fraction of lineage-labelled cells in newly formed ducts to “drift” in size, leading to a gradual process of “monoclonal conversion” in which, with increasing branch generation along the network, ducts eventually become either fully labelled in a single confetti colour or completely unlabelled (Fig. 32a). Importantly, the rate of monoclonal conversion scales in inverse proportion to the number of self-renewing ductal precursors contained in each terminus, because of the relative proportion of a labelled cell out of all ductal-end progenitors (Fig. 32b-d).

Inspection of the experimental data showed that labelled subtrees are initially mosaic (both in the acinar and ductal compartment), but undergo rapid monoclonal conversion along the ductal network so that, in many cases, more distal ends become entirely comprised of confetti+ cells characterized by a single colour (Fig. 32e). Importantly, comparing the rate of monoclonal conversion in representative ductal-containing clones (Fig. 32e) with the rates from theoretical trees generated for different number of precursors (Fig. 32b-d), it appears that only as a few as 4-6 self-renewing precursors are located at the ductal-ends (Fig. 32b-e and Statistical Methods in Chapter 2.3). This is in contrast to the mammary gland epithelium, whereby there is a large number of “stem cells” hosted in each tip (Scheele et al. 2017).

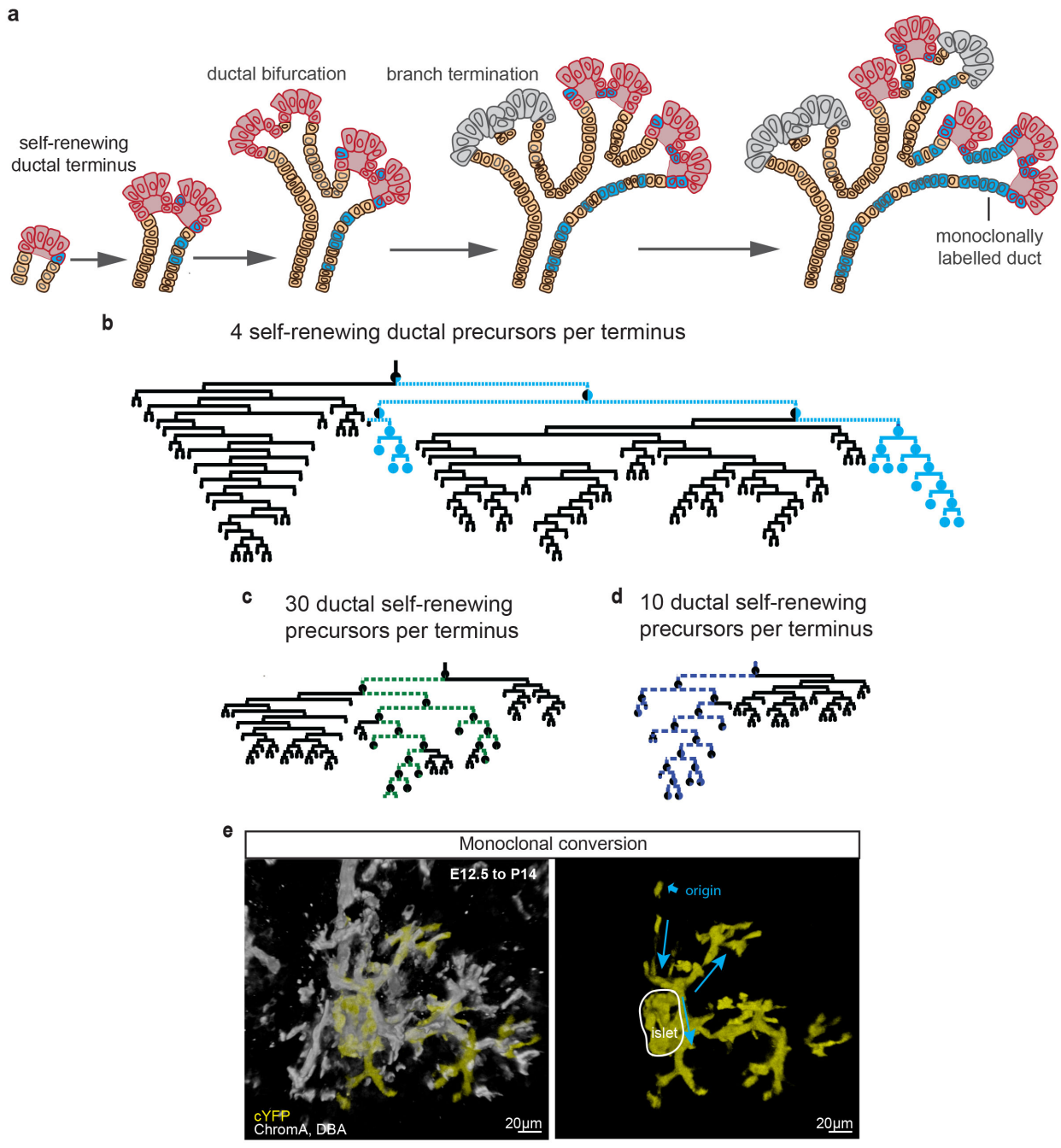
a
self-renewing
ductal terminus
ductal bifurcation
branch termination
monoclonally
labelled duct
b
4 self-renewing ductal precursors per terminus
c
30 ductal self-renewing
precursors per terminus
d
10 ductal self-renewing
precursors per terminus
e
Monoclonal conversion
E12.5 to P14
origin
islet
cYFP
ChromA, DBA
20µm
20µm

Figure 32. *Branching morphogenesis in the ductal termini is driven by a small number of self-renewing progenitors. (a) Schematic depicting the process of monoclonal conversion. (b-d) Simulation of a theoretical subtree containing (b) 4, (c) 30, (d) 10 self-renewing ductal precursors per ductal terminus with one initially-labelled precursor cell (for details, see Methods Theory). (e) Representative ductal clone showing monoclonal conversion; the direction of ductal growth is indicated with an arrow. Comparison with simulations (b-d) suggests that growing ductal termini are composed of as few as 4 self-renewing ductal precursors. Representative image in (e) was obtained from the analysis of 254 clones from 3 mice for the E12.5 to P14 lineage tracing.*

4.11 Branching morphogenesis is very rapid in pancreas development inferred from E15.5 and E18.5 induction lineage tracing

Since I could observe dynamic branching morphogenesis based on the morphology of clones induced with E12.5 lineage tracing, I was interested in finding out until which stages of development the morphogenesis persists. I therefore carried out an additional experiment, whereby mice were injected with Tamoxifen at E15.5 and E18.5 (Fig. 33a). The dose was optimised, and amounted to 0.015 and 0.010 mg of Tamoxifen per g of pregnant female at E15.5 and E18.5 respectively. The induction levels were higher than for the E9.5 and E12.5 induction experiments. Hence, in order to assure clonality, as in the previous experiments, I decided to focus the analysis on the rare cyan+ and green+ clones (Fig. 33b,c, see Section 3.3.3).

At E15.5, I observed smaller clones that still tracked subtrees over several rounds of branching. These clones were either unipotent ductal (Fig. 33d,e), acinar (Fig. 33d,f), or rarely bipotent ductal-acinar or islet-ductal (Fig. 33d,g,h). At E18.5, all clones were compact (Fig. 33i,j), with minimal, but non-zero (ductal-acinar) bipotency (Fig 33d,k), and no longer spanned multiple branches, consistent with branching morphogenesis being replaced by a process of growth via local dilation of an existing tree structure. Altogether, these results reveal that branching morphogenesis is far less active at later stages of development, meaning that most rapid branching morphogenesis is presumably taking place over the few days between E12.5 and E15.5.

Furthermore, the quantification of potency reveals that the tissue is vastly restricted at these stages. Analysis of 78 clones from 2 mice for E15.5 and 61 clones from 2 mice for E18.5 showed extensive unipotency, with no tripotent clones detected beyond E15.5 (presented in Fig 33b-k).

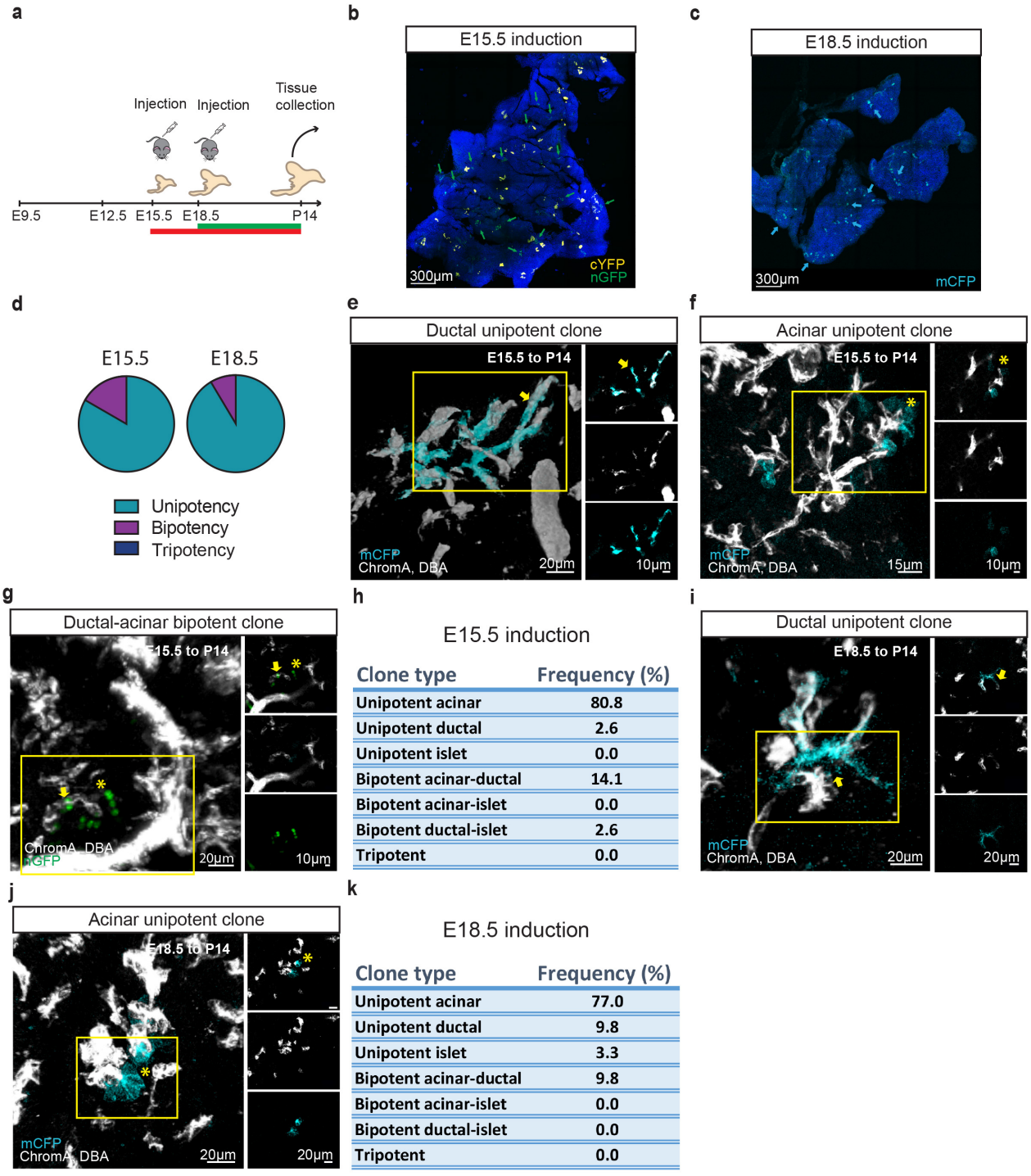

Clone type	Frequency (%)
Unipotent acinar	80.8
Unipotent ductal	2.6
Unipotent islet	0.0
Bipotent acinar-ductal	14.1
Bipotent acinar-islet	0.0
Bipotent ductal-islet	2.6
Tripotent	0.0

Clone type	Frequency (%)
Unipotent acinar	77.0
Unipotent ductal	9.8
Unipotent islet	3.3
Bipotent acinar-ductal	9.8
Bipotent acinar-islet	0.0
Bipotent ductal-islet	0.0
Tripotent	0.0

Figure 33. *Branching morphogenesis and lineage restriction is very rapid during development. (a) Outline of experiment with induction at E15.5 and E18.5. Section of (b) E15.5 and (c) E18.5 samples showing the induction levels of rare colour, (a) green and (b) cyan. Clones are indicated with arrows. (d) Clones induced at E15.5 and E18.5 were mainly unipotent. (e-g) P14 pancreas induced at E15.5 showing only a few rounds of branching events in (e) ductal and (f) acinar compartment. In addition to unipotent clones as in (e) and (f), bipotent ductal-acinar clones were also observed (g). (h) Permutations of all clone types and their relative frequency for E15.5 induction. (i-j) P14 pancreas induced at E18.5 revealing only a single bifurcation event within traced clones and unipotency in (i) ductal and (j) acinar compartment. (k) Permutations of all clone types and relative frequency for E18.5 induction timepoint. Ductal and acinar compartments indicated by arrow and asterisk, respectively. I counted 78 clones from n=2 mice for E15.5 to P14 tracing, and 61 clones for n=2 mice for E18.5 to P14 tracing.*

4.12 Discussion

In this chapter, I presented the results of the analysis of clone morphology, potency and dynamics based on lineage tracing with *R26*-CreT2; *R26*-Confetti, *Sox9*-CreT2; *R26*-Confetti at various developmental timepoints. This was combined with computational modelling of clonal data. Altogether, this led us to a model of branching morphogenesis, explaining the coordinated growth of the entire organ.

The first part of this chapter was concerned with studying the morphology of clones, which led to the hypothesis of ductal-end driven pancreatic growth. This was further confirmed by EdU proliferation assay, which showed enrichment of EdU+ cells at ductal ends as compared to the core parts of ducts at 15.5. Previous studies have suggested that proliferation at tips around E12.5 may be taking place (Zhou et al. 2007). Additionally, proliferative cells were shown to be enriched at ductal-ends of branches in an *ex vivo* system (Puri and Hebrok 2007; Dahl-Jensen et al. 2016), with a recent study contradicting these findings (Marty-Santos and Cleaver 2016). Altogether, it appears that the mode of pancreatic growth and branching morphogenesis of the ducts is not understood. Our study confirms the previous findings of enhanced proliferation of cells at peripheral regions of the pancreas. While the previous *in vivo* study (Zhou et al. 2007; Petzold and Spagnoli 2013) suggested proliferation in the tip domain of the early bud, I show that this peripheral proliferation is maintained at later stages at ductal ends of subsequent branches.

Next, I aimed to decipher the cellular composition of ductal-ends, based on the analysis of clones associated with pancreatic ductal subtrees. This led to the hypothesis that the proliferative ductal-ends contain both rare multipotent precursors and a majority of ductal and acinar-committed precursors. This finding provides a cellular mechanism of how morphogenesis of the three core pancreatic compartments is coordinated. However, our findings are in contrast to a previous study, claiming that pancreas morphogenesis is driven by a multipotent domain (Zhou et al. 2007). The discrepancy between our findings and the previously published study (Zhou et al. 2007) may arise from the

clonal versus non-clonal levels of induction, as well as the fact that the previous study looked at the Cpa1+ lineage rather than at random cells from the ductal-end/tip domain.

Subsequently, I presented results of control experiments involving *Sox9*-CreERT lineage tracing and amylase co-immunostaining, which demonstrated the validity of the clonal potency and morphology outcomes based on *R26*-CreERT2 tracing, thereby excluding the possibility of non-pancreatic contribution to clone interpretation. Interestingly, the outcome of *Sox9*-CreERT2 lineage tracing revealed a significant level of lineage restriction in contrast to previous studies suggesting the Sox9+ domain as the site of multipotent progenitors (Furuyama et al. 2011; Solar et al. 2009). This discrepancy between the results of this thesis and the published studies may also arise from the use of non-clonal levels of induction previously, which may alter the accuracy of potency assessment.

The next parts of this chapter were aimed at deciphering the mechanism involved in the coordinated ductal and acinar dynamics. I first looked at the development of the ductal network, observing extensive heterogeneity, which was then quantified. The rescaled subtree size, and the acinar and ductal clone size distributions revealed a high correlation, indicating that pancreas growth may indeed be driven by the ductal branching morphogenesis. Furthermore, the analysis of the distributions of the same lineages (acinar or ductal) between the two induction timepoints analysed (E9.5 and E12.5) showed that they follow the same dynamics, suggesting that the same mechanism is driving morphogenesis in the primary and secondary transition. This is a surprising finding, given the literature stressing the importance of plexus remodelling at the initial stages of pancreatic growth (Bankaitis et al. 2015; Pan and Wright 2011). Nevertheless, it is possible that, while plexus formation and remodelling are still active, already the first ductal ends/tips appear early on and are guiding the pancreatic expansion.

Furthermore, I aimed at providing a model explaining the coordination of acinar and ductal lineages resulting in the particular distributions of clone sizes, and hence accounting for the dynamics of the pancreas growth. The

assumptions and constraints for the model were set up based on previous clonal and ductal network observations described above, as well as the quantification of macroscopic tissue parameters. Therefore, in collaboration with Dr Edouard Hannezo and Prof. Bejamin Simons, we proposed a model of stochastic bifurcation and termination of ductal-ends containing proliferative cells at ductal-ends. We found that on average 4 ductal-end precursors at each ductal end drive the branching morphogenesis. To the best of my knowledge, this is the first model up to date, presenting a cellular mechanism for coordination of the morphogenesis of all three pancreatic lineages (Iber and Menshykau 2013).

Finally, from this study it appears that the process of branching morphogenesis is very rapid and seems to be most active between E12.5 and E15.5 and decreasing in intensity afterwards, with a maximum of two branching/bifurcations at E18.5 observed from lineage tracing data.

The results summarised above have therefore answered the questions set out at the beginning of the Chapter regarding the coordination of morphogenesis to drive simultaneous specification of the three pancreatic lineages, and the way in which pancreas size and composition are regulated.

In summary, this chapter proposes a mechanism of tissue growth, whereby in a largely committed tissue, a minority population of acinar-committed, ductal-committed, and rare multipotent progenitors at proliferative ductal-ends drive the coordinated morphogenesis of the tissue, as presented in the schematic in Figure 34.

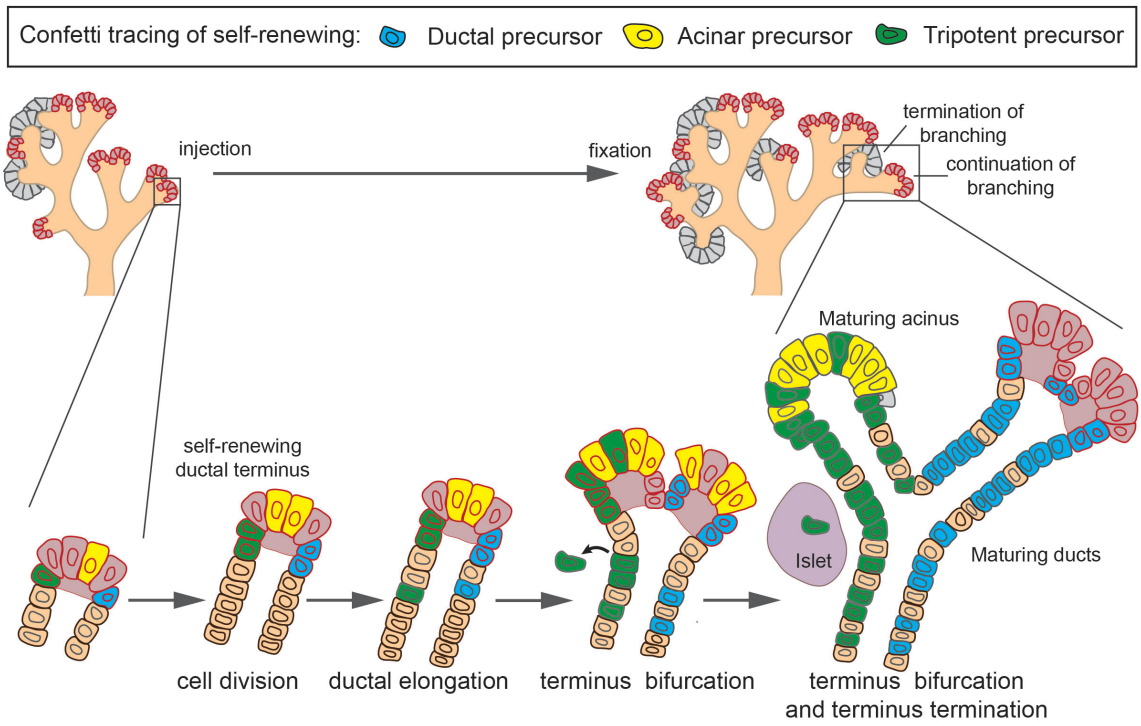

Figure 34. *Summary schematic depicting morphogenic events during the second phase of pancreatic development. Pancreas morphogenesis follows from a process of stochastic ductal bifurcation and termination driven by self-renewing fate-restricted ductal and acinar precursors, as well as rarer tripotent precursors, which become depleted after E15.5. The figure presents the potential evolution of a single labelled mCFP+ ductal precursor, cYFP+ acinar precursor and cRFP tripotent precursor.*

Chapter 5

Results: Single cell RNA sequencing analysis

5.1 Introduction

This chapter follows after the second chapter of findings, which showed early lineage restriction and ductal-end stochastic bifurcation and termination driving the coordinated morphogenesis of acinar, ductal and islet lineage in the pancreas.

This chapter aims at answering the following research questions, related to the functional lineage tracing-based findings of the previous chapter, with the use of single cell sequencing method:

- Is there molecular evidence of early tissue heterogeneity?
- Do single cell RNA sequencing results provide support for the findings of proliferative ductal-ends and more quiescent core parts of ducts?
- Is there a lineage hierarchy in developing pancreas, which would account for the observed localisation of tripotent progenitors together with acinar and ductal-committed precursors within the ductal-ends?
- What are the potential markers associated with the tripotent progenitors at ductal-ends?
- What are the potential markers associated with progressive differentiation of multipotent precursors?

In this chapter, I present the results of single-cell RNA sequencing with the follow up analysis, which includes principal component analysis (PCA) separation of pancreatic cells for downstream analysis in chapter 5.3, t-distributed stochastic neighbour embedding (t-SNE (Krijthe 2015)) clustering of cells with similar gene expression profiles and the study of the cluster gene heterogeneity, the analysis of gene heterogeneity between cells with heatmap plots in chapter 5.4, as well as diffusion pseudotime analysis of lineage relationship in chapters 5.5 and 5.6.

The chapter starts by an outline of the optimisation of the method for obtaining single cell RNA sequencing data. Next, I describe quality control and identification of pancreatic cells, which is followed by the downstream analysis. This includes the study of heterogeneity within the tissue based on the tSNE plot and heatmap analysis. Subsequently, I demonstrate the lineage relationship between acinar, ductal and islet cells using diffusion pseudotime. This analysis enabled me to identify genes, which may be expressed in the multipotent ductal-end niche cells.

Altogether, my findings support and share further insight into the findings of the functional lineage tracing analysis presented in the previous chapter.

5.2 Method optimisation for sorting of single cells

The results of the previous chapters revealed a mechanism of pancreatic development, whereby in a vastly cell-fate restricted tissue, proliferative ductal-end multipotent and fate-restricted progenitors guide the growth of the organ. I therefore looked for molecular justification for the observations and results of the functional lineage tracing analysis, i.e. whether I could confirm the early lineage commitment and ductal-end driven tissue growth with localised niche precursors. I turned to the single cell sequencing analysis to investigate the molecular basis of the observed functional heterogeneity of pancreatic precursors. I focused on E13.25 as a matching point for the lineage tracing analysis, due to Cre recombination taking between 12 and 36 hours post Tamoxifen administration (Danielian et al. 1998), as well as E15.25 to investigate whether and how the molecular signature of progenitors evolves during development.

First, the protocol for obtaining single cells for sequencing had to be optimised in order to ensure non-biased FACS sorting of single cells. I decided to avoid the immunostaining and sorting for the epithelial marker Epcam, commonly used to label cells of the early pancreatic bud (Trzpis et al. 2007), as there is evidence that it may be enriched in ductal and islet committed cells during the later stages of development (Schnell et al. 2013). Instead, I negatively sorted against endothelial CDC45 and blood Tie2 markers, to prevent contamination of these non-pancreatic lineages. After optimisation of the single cell isolation, I generated single cell sequencing libraries using the previously developed protocol (Picelli et al. 2014) in collaboration with the group of Prof. Berthold Gottgens from the University of Cambridge (Fig. 36).

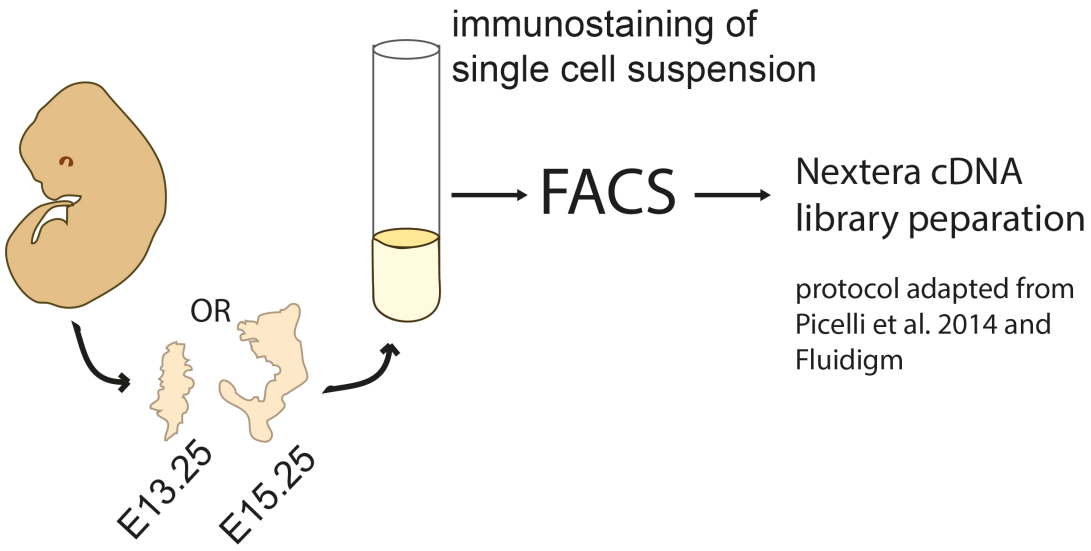

Figure 35. *Schematic of single cell sequencing experiment. Pancreata were dissected at either E13.25 or E15.25 and negatively sorted against CDC45 and Tie2 endothelial and blood markers, respectively. Subsequently the Nextera cDNA library preparation was performed according to Picelli et al. 2014 protocol.*

5.3 Quality analysis and identification of pancreatic cells

In collaboration with Dr Steffen Rulands from the University of Cambridge we performed the downstream bioinformatics analysis of sequence reads from the two experiment timepoints. To identify poor quality cells, three metrics were used: (1) the proportion of aligned reads, (2) the number of endogenous reads and (3) the number of features with more than 1 read. We filtered for cells with (1) more than 20% aligned reads, (2) more than 200,000 endogenous reads and (3) more than 5000 detected features. We only considered genes that were detected in at least 2 cells, with a variance greater than 0.001. Out of the 672 cells that underwent single cell RNA sequencing, 516 (77%) passed quality control measured and were used for downstream analysis. Reads were normalized using the deconvolution method as implemented in the scran package in R software (A and K 2016).

Combining data from E13.25 and E15.25 single cell sorted pancreata, we first performed dimensionality reduction by principal component analysis (PCA). This identified two distinct clusters of cells. Based on the complementary expression of *Epcam* and *Vimentin*, one of these clusters was identified as mesenchyme (*Epcam*- *Vimentin*+), while the remaining cluster was pancreatic (303 cells; *Epcam*+ *Vimentin*-). Figure 36 presents t-distributed stochastic neighbour embedding (tSNE) clustering of all cells, which groups cells of similar gene expression patterns together (Krijthe 2015, Van Der Maaten et al. 2008), highlighted for *Epcam* gene expression. Two subsets of *Epcam*+ and *Epcam*- cells can be distinguished in the tSNE plot, corresponding to pancreatic epithelial and non-epithelial lineages (Fig. 36).

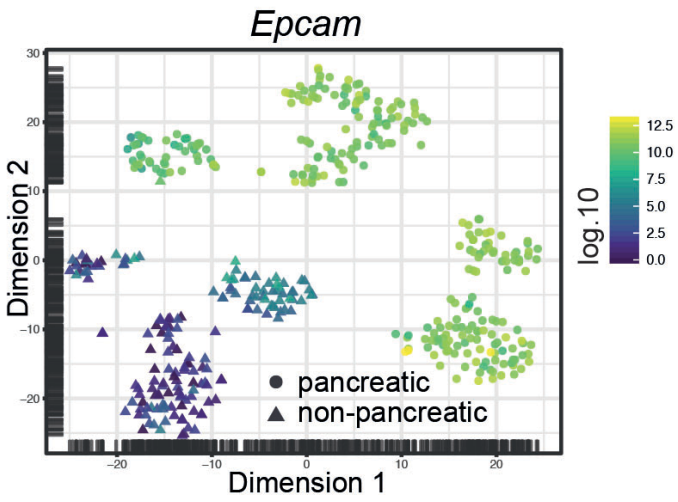

Figure 36. *tSNE plot highlighting Epcam expression with the Epcam+ cells (green), which were used for downstream analysis of pancreatic cells. Log10 normalised expression scale was applied. Single cells were isolated from n=7 embryos from 7 litters (n=5 embryos for E13.25 and n=2 embryos for E15.25).*

5.4 Gene expression heterogeneity analysis

Focusing on the pancreatic cells alone, we performed dimensionality reduction by t-SNE (Krijthe 2015) for E13.25 and E15.25 cells, followed by k-means clustering of 303 cells from R's statistics package on the 500 most variable genes and identified the cellular identity of cells in the three clusters using known markers for acinar, ductal and islet cells. This identified 4 distinct clusters of cells (Fig. 37a) corresponding to an early endocrine-committed cluster (based on *Neurog3* expression; Shih et al. 2013, Pan and Wright 2011) (Fig. 37b), an early (E13.25) and a late (E15.25) acinar cluster (*Ptf1a, Cpa1, Myc;* Shih et al. 2013, Pan and Wright 2011*)* (Fig. 37c-e), and a cluster expressing elevated trunk/ductal markers (*Sox9, Hes1, Nkx6-1;* Shih et al. 2013, Pan and Wright 2011) (Fig. 37f-h). The late acinar cluster contained the E15.25 cell gene reads, and showed enhanced levels of *Ptf1a, Cpa1* and *Myc* as compared to the early E13.25 cluster. This pattern of expression was consistent with the early lineage-commitment of pancreatic cells, as observed from the lineage tracing data.

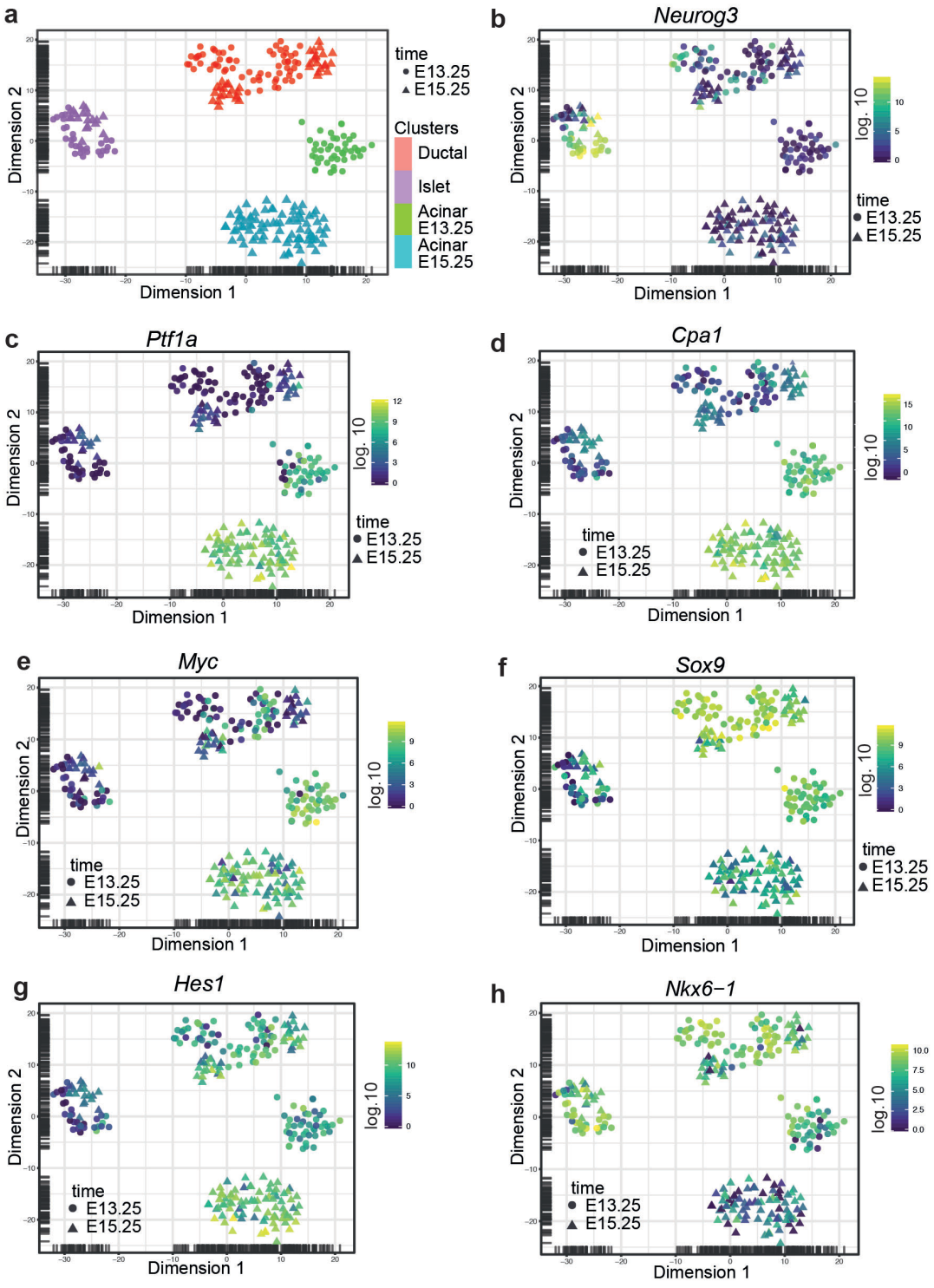
a
Dimension 2
Dimension 1
time
E13.25
E15.25
Clusters
Ductal
Islet
Acinar E13.25
Acinar E15.25
b
Neurog3
log.10
c
Ptf1a
d
Cpa1
e
Myc
f
Sox9
g
Hes1
h
Nkx6−1

Figure 37. *Single-cell RNA sequencing analysis suggests early fate restriction (a) t-SNE plot obtained from combining cells from pancreas obtained from n=5 embryos at E13.25 and n=2 embryos at E15.25 showing islet, early (E13.25) and late (E15.25) acinar and ductal clusters, as identified by the expression of marker genes in respectively (b) Neurog3; (c-e) Ptf1a, Cpa1 and Myc and (f-h) Sox9, Hes1 and Nkx6-1. Log10 normalised expression scale was applied. Single cells were isolated from n=7 embryos from 7 litters (n=5 embryos for E13.25 and n=2 embryos for E15.25).*

Notably, within each of the four clusters, pancreatic genes revealed a surprising degree of homogeneity, even between the two timepoints – E13.25 and E15.25 (Fig. 37). This homogeneity is further evident in a heat plot (Fig. 38), which presents all individual cells and the expression of genes I selected as important for pancreatic development. The uniformity of gene expression pattern between E13.25 and E15.25 is surprising, as the E13.25 timepoint corresponds to the beginning of secondary transition while E15.25 stage of development is characterised by more intense lineage maturation. The major difference between the two timepoints was evident in the two separate clusters of early and late acinar cells, whereby the E13.25 and E15.25 cells were clustered separately (Fig. 37).

However, the homogeneity of expression within clusters and its conservation across timepoints (Fig. 37-38) could suggest that the early tip-trunk polarity established at the beginning of secondary transition is conveyed in the branching morphogenesis. The exact cellular and molecular mechanism controlling this would call for future investigation. However, it is likely that the emerging tip regions at E12.5/E13.5 become the first branches. During branching morphogenesis, the ductal ends of these branches carry the tip-like cells, which are conveyed to future branching generations via rounds of bifurcation. The leading edge ductal-ends could therefore carry the ‘tip-like’ cells, while the trailing ducts would become more ‘trunk-like’ in character.

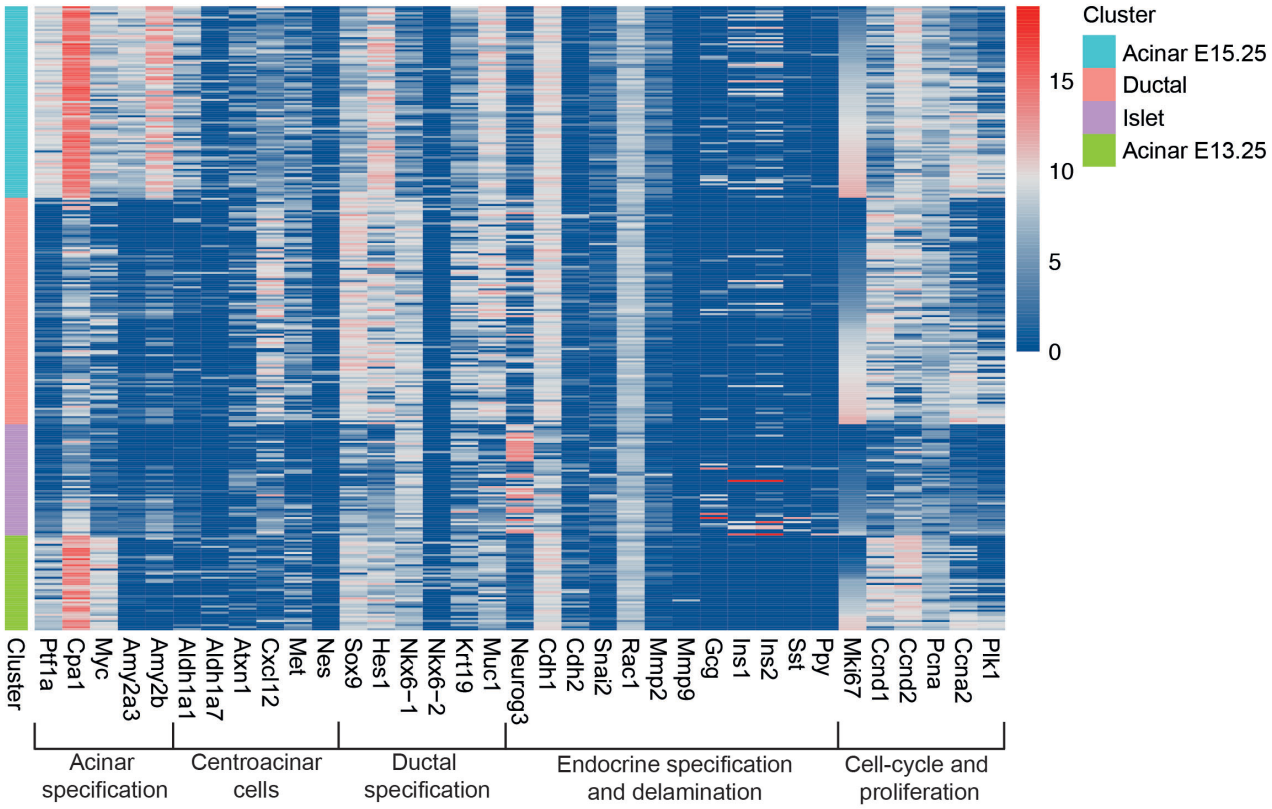

Figure 38. *Heatmap plot showing expression levels of pancreatic genes for individual cells reveal a high degree of uniformity within clusters and across timepoints, E13.25 and E15.25. Genes are grouped into clusters based on their presumed role in development. Log10 normalised expression scale was applied. Single cells were isolated from n=7 embryos from 7 litters (n=5 embryos for E13.25 and n=2 embryos for E15.25).*

The major variability was between the acinar clusters at E13.25 and E15.25, as the E15.25 cells expressed increased levels of *Ptf1a*, as well *Aldh1* and *Hes1 (*Fig. 38*)*. Ptf1a is a known acinar-associated marker (Pan and Wright 2011; Shih et al. 2013), hence its enhanced expression may be necessary for the maturation of acini at later stages. Hes1 is both an early progenitor marker and a trunk marker at later stages of development (Pan and Wright 2011; Shih et al. 2013). Aldh1 is a presumptive centroacinar marker (Rovira et al. 2010). The role of Hes1 and Aldh1 in the maturation of acinar lineage requires future investigation. Combining the finding of distinct molecular signatures of acinar clusters at E13.25 and E15.25 with the model of branching morphogenesis based on the lineage tracing study presented in chapter 4, it is possible that the later timepoint acinar gene expression corresponds to mature acinar cells at ductal-ends, which arise upon termination of a branch.

Islet precursors were distinguished based on the *Neurog3* expression (Fig. 37b). Within the clusters, I could observe some level of heterogeneity of islet maturation-related gene expression. Based on the heatmap plot, 2 and 4 out of 303 cells expressed *Ins1* and *Ins2* respectively, 3 out of 303 cells expressed *Gcg*, 1 out of 303 expressed *Sst*, and a general pattern of *Cdh2* downregulation was observed, consistently with the associated delaminating phenotype of islet precursors (Fig. 38). This early expression of islet maturation markers further emphasises the extent of specification within the tissue at these early stages, supporting the hypothesis of early lineage restriction.

The most significant variation in the gene expression was observed with pan-proliferation *Mki67* marker, as illustrated in the heatmap plot (Fig. 38) and tSNE plot highlighting *Mki67* gene expression (Fig. 39). Indeed, the tSNE ductal cluster (see Fig. 37a) is divided structurally (by its shape) into two sub-clusters. Importantly, these sub-clusters are characterised by segregated levels of *Mki67*, with low and high expression in the left and right sub-cluster respectively (Fig. 39). Importantly, this separation is not based on developmental age. This may be indicative of a separation between proliferatively-active ductal termini and less active trailing ducts as presented in the previous chapter 4.

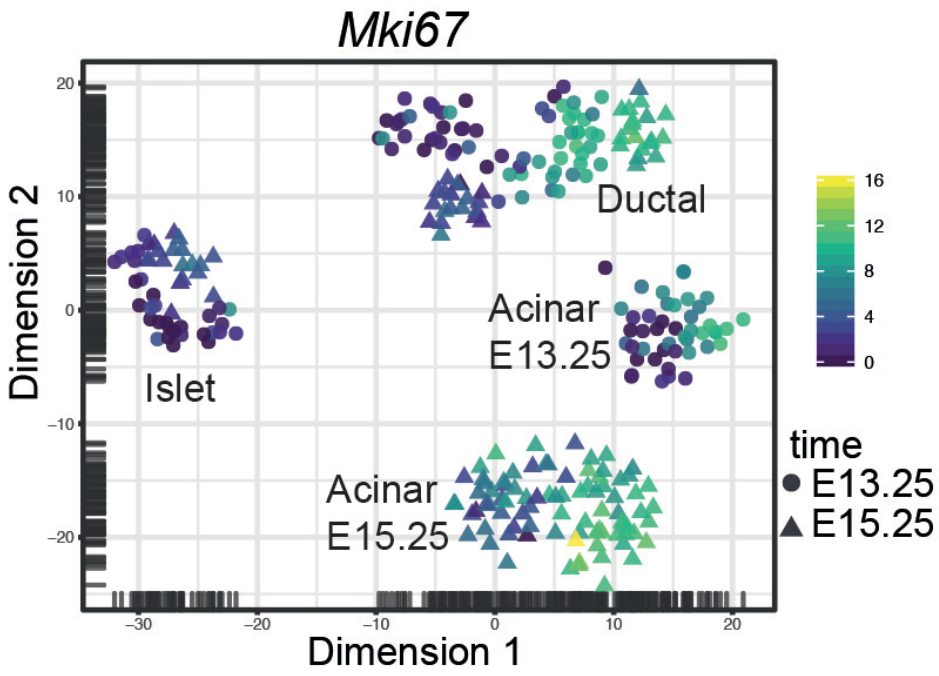

Figure 39. *tSNE plot showing bipolar expression of pan-proliferative marker Mki67 in the ductal cluster (top-centre). The left sub-cluster and right sub-cluster show high and low levels of Mki67 expression respectively, resembling the defined functional proliferative boundaries between ductal-ends and core ductal parts, as shown with in vivo lineage tracing (Chapter 4). Single cells were isolated from n=7 embryos from 7 litters (n=5 embryos for E13.25 and n=2 embryos for E15.25).*

Furthermore, additional *Mki67* expression variability could be observed in the acinar clusters at E13.25 and E15.25 (bottom right, middle right of Fig. 39). This is consistent with the model of branching morphogenesis driven by proliferative ductal-ends, proposed in the previous chapter (Chapter 4). The growing ductal ends would carry acinar and ductal proliferative progenitors, while the terminating ends would contain both acinar and ductal progenitors showing low proliferative capacity.

Interestingly, the other proliferation markers, such as *Ccna2, Pcna, Ccnd2 and Ccnd1 (data not shown)*, did not show a similar bipolar heterogeneity within the ductal and acinar clusters and appeared to be more randomly heterogeneous. This discrepancy between *Mki67* and the other factors, may arise from the fact that *Mki67* is a pan-proliferation marker, while the others are cell-cycle stage dependent and therefore show much variation.

Observing such clear *Mki67* segregation into two ductal tSNE subclusters of high and low expression, indicative of a possible ductal-end and core ductal domains, I was interested in finding correlations between *Mki67* and other gene markers. Such correlated factors would qualify as potential markers for the future lineage tracing analysis. This would enable the characterisation of the presumptive proliferative ductal-end niche carrying the progenitors driving pancreatic expansion. However, the analysis of correlations did not reveal any meaningful candidate genes. This may be a result of insufficient number of cells analysed in the experiment.

In summary, the analysis of tSNE plots supports the findings of lineage tracing analysis, whereby early lineage commitment was observed. At E13.25 and E15.25, I already identify clusters expressing markers of the mature pancreatic lineages. The observed uniformity of gene expression within clusters and timepoints might be associated with conserved set of rules guiding branching morphogenesis (see Chapter 4). The sequencing analysis gives further insight into the proliferative heterogeneity, lending support to the existence of highly proliferative ductal-end domain and the more quiescent core part of ducts.

5.5 Diffusion pseudotime analysis

To further dissect the lineage relationship between the acinar, ductal and islet cells at both E13.25 and E15.25, we employed diffusion pseudo-time (DPT) ordering of the single-cell RNA-seq data (Haghverdi et al. 2016). In collaboration with Dr. Steffen Rulands we used destiny package (Angerer et al. 2016), employed a diffusion map (parameters: sigma=95, k=302) and used the DPT function to arrange cells in pseudo time.

We found ductal cells standing at the apex of the lineage hierarchy (Fig. 40a), and diverging into acinar and islet sub-branch. This ordering of clusters was further confirmed by the appearance of cells in a timepoint-wise fashion, with ductal E13.25 cells followed by ductal E15.25 cells, followed by E13.25 acinar evolving into E15.25 acinar cells on one side branch, and islet E13.25 evolving into islet E15.25 cells in another branch. This supports the validity of the arrangement of the clusters, with the ductal cluster at the apex. This finding is consistent with the functional lineage tracing findings, whereby tripotent precursors can be found within the termini of growing ducts, indicating their ductal origin.

Consistent with the tracing data, we found *Sox9* expression present in both the ductal and acinar cluster, becoming progressively down-regulated in opposition to the up-regulation of the tip maker *Cpa1* ($P< 5.5\ 10^{-12}$ for both, Fig. 40b,c*)*. *Cpa1* has been reported to mark the multipotent domain in development (Zhou et al. 2007) and hence its up-regulation along the axis of the DPT plot is surprising. However, it is possible that in the previous study the apparent tripotency results from the non-clonal levels of induction and merging of independent lineage-restricted cells (Zhou et al. 2007).

The other marker, which was correlated with the direction of the diffusion pseudotime is *Aldh1* (Fig. 40d). Again, this is a surprising finding, as *Aldh1* has been considered to be a marker of multipotent centroacinar cells (Rovira et al. 2010), rather than being associated with differentiation. However, the mentioned study involved sorting of Aldh1+ cells and growing them as *ex vivo* explants followed by the study of pancreatic lineage specification. Therefore Aldh1+ cells may actually not be multipotent *in vivo*.

Finally, we were also interested in looking at *Mki67* gene, as it showed an interesting bipolar heterogeneity within the ductal tSNE cluster (Fig. 39). Interestingly, *Mki67*-high cells in the ductal cluster plotted on DPT segregate toward the acinar branch side, while the *Mki67*-low cells segregate towards the islet branch of the graph (Fig. 40e), consistent with ductal- and acinar-committed progenitors residing in the proliferative ductal terminus, while islet cells derive from less proliferative trailing ducts, left behind the growing ductal-ends.

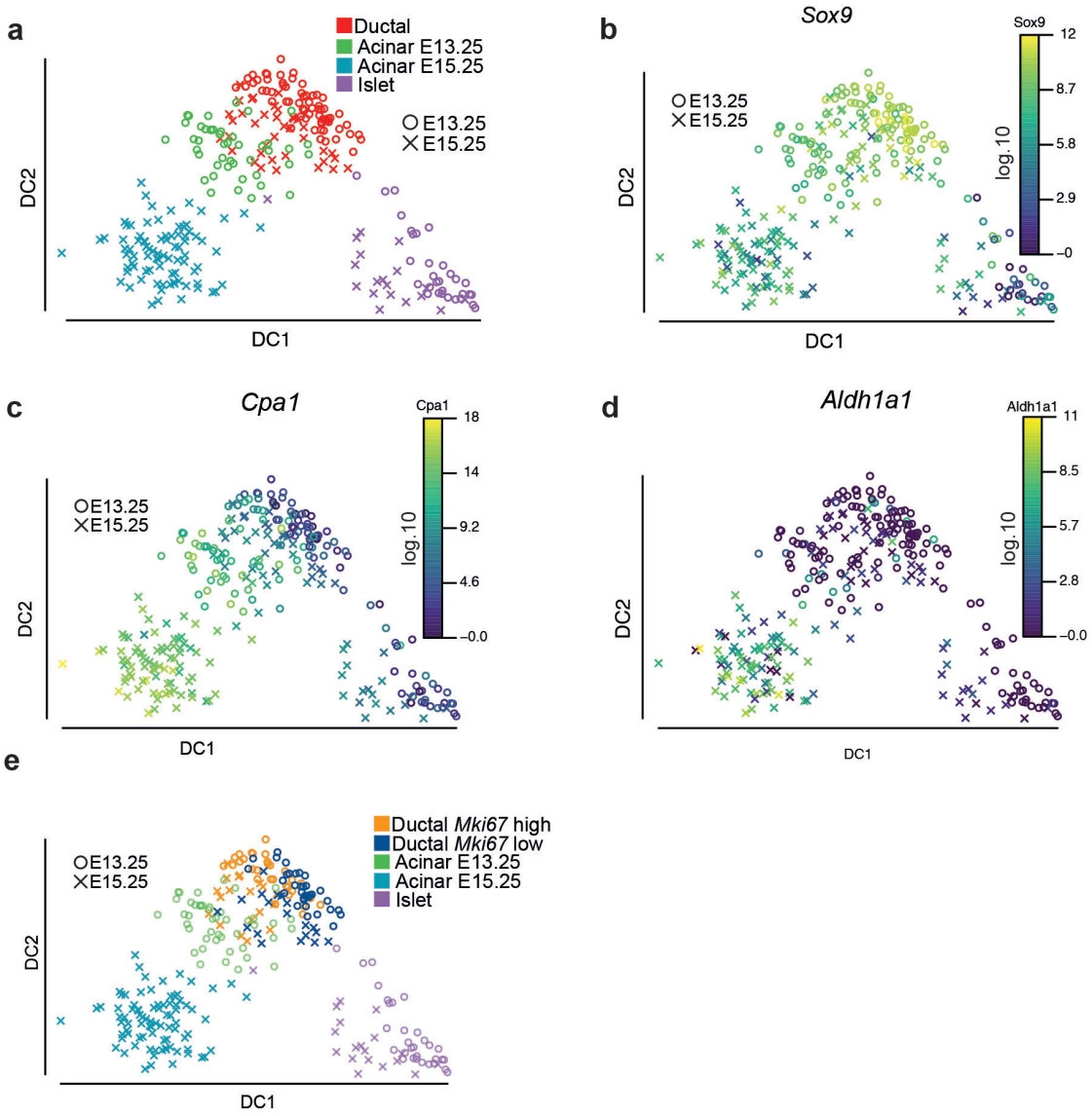

Figure 40. *Diffusion pseudotime reveals lineage hierarchy. (a) Diffusion pseudotime plot reveals evidence of lineage segregation with ductal cells at the apex of a hierarchy that branches separately into acinar and islet lineages. Diffusion pseudotime plots with both E13.25 (circles) and E15.25 (crosses) cells indicating that (b) Sox9 is anti-correlated ($P< 5.5\ 10^{-12}$) with DPT direction, i.e. expression is upregulated at the apex, while (c-d) Cpa1 and Aldh1 are correlated ($P< 5.5\ 10^{-12}$) with DPT direction, i.e. expression is upregulated in differentiating cells. (e) DPT plot for Mki67 showing Mki67 high cells segregating towards acinar branch and Mki67 low cells segregating towards islet branch, consistent with the lineage tracing data, which indicate that acinar and ductal cells retain full proliferative potential. Single cells were isolated from n=7 embryos from 7 litters (n=5 embryos for E13.25 and n=2 embryos for E15.25).*

In summary, the analysis of the diffusion pseudotime plots indicates a lineage hierarchy with ductal cells at the apex of the lineage hierarchy, consistently with the observation of ductal associated tripotent clones in lineage tracing analysis. I identified genes, which may be up-regulated in ductal-end associated progenitors among the known pancreas development associated genes. Among them, Sox9 is up-regulated in the multipotent precursors, while Cpa1 is up-regulated with the direction of lineage differentiation, inconsistently with previous literature (Zhou et al. 2007).

5.6 DPT Correlated genes

In the section above, I showed how the expression of three genes associated with pancreas development, namely *Sox9, Cpa1* and *Aldh1,* is related to the direction of the diffusion pseudotime. This improves the understanding of the genes, which may be expressed by multipotent progenitors at ductal-ends. Prompted by this initial analysis, I was interested in identifying novel genes, which could be associated with precursor multipotency. The analysis provided me with an extensive list of genes correlated and anti-correlated with the direction of the diffusion plot, i.e. genes associated with differentiation into lineages and multipotency, respectively (See Table 21 and 22).

Among the genes presented in Table 21 and 22, some were general regulatory and maintenance genes with an unknown role in the differentiation or maintenance of multipotency, such as *Map1b* coding for microtubule associated protein 1b, *Ubb* coding for ubiquitin B, *Rbfox* responsible for alternative splicing of pre-mRNA, *Mcm2* and *6* coding for minichromosome maintenance complexes essential for eukaryotic genome replication, *Acaa2* coding for acetyl CoA Acetyltransferase 2 and others. Other genes were identified previously as being expressed in pancreatic multipotent precursors such as *Onecut1* and *Sox9* (Shih et al. 2013), or as being associated with lineage commitment such as *Amy2a1,2,3,4,5, Pax6* and *Maf6* (Shih et al. 2013). There was also a significant group of genes of unknown function.

In order to narrow down the list of potential genes which could play a role in multipotency and lineage specification, I decided to take advantage of a recently published list of genes with conserved expression between pancreata

from different species (Tarifeño-Saldivia et al. 2017). I reasoned that these genes could play a key role in pancreatic development and function. I therefore decided to compare the list of genes correlated and anti-correlated with direction of diffusion plot with the list of genes from the mentioned study. Those genes are presented in the Table 21 and 22 as highlights. It turned out that the vast majority of the genes highlighted by the DPT plot analysis have shown conserved expression in pancreata from different species.

I decided to focus on the genes anti-correlated with the direction of DPT in order to better characterise the potential multipotent niche. Among the highlighted genes there were the known players in pancreatic development, such as ***Sox9*** and ***Onecut 1***. *Onecut 1* is expressed in the multipotent precursor cells of the early pancreatic bud (Shih et al. 2013), and Sox9 has been previously associated with tripotency at later developmental stages (Solar et al. 2009; Kopp et al. 2011). Therefore it can be speculated that both could be the potential markers of the multipotent niche.

Other interesting candidates were not previously extensively covered in the literature of pancreatic development, however their role in other contexts indicated a possible function in the establishment or maintenance of multipotency. For instance ***Lgr4***, a gene coming from the same family and possibly redundant to *Lgr5* (Tsai et al. 2016) was identified in the search. The association of *Lgr5* with the multipotency in the intestinal tissue (Sato et al. 2011) draws attention to the potential role of *Lrg5* in the regulation of multipotency during pancreatic development. This speculation could be studied in the future.

Another candidate gene included ***Fgfr2.*** The Fgf receptor is commonly expressed by cells in response to Fgf signalling. This would imply the proximity of the potential multipotent cells to a source of Fgf signalling, such as the mesenchyme surrounding the pancreas. (Bhushan et al. 2001). This is consistent with the possible location of the stem cell niche at ductal-ends (Chapter 4), which are typically located at peripheral parts of the tissue. Therefore the expression of Fgfr2 at ductal-ends should be investigated.

Furthermore, ***PTN*** is another interesting factor, as it has been shown to delay the maturation of the mammary gland (Rosenfield et al. 2012). Its role in pancreas development could thus also be studied.

Several other genes have been previously described to be implicated in the pancreatic tumorigenesis, such as ***Ajuba***, ***Lamc2*** and ***Yap1*** (Gruber et al. 2016; Morvaridi et al. 2015; Kosanam et al. 2013; Chen et al. 2016). Cancer is commonly associated with abnormal proliferation of cells and stem cells are believed to be the cells of origin of multiple tumours (reviewed in Beck & Blanpain 2013). Therefore, there is a possibility that these genes could be involved in regulating the multipotency and proliferative capacity of cells.

A surprising candidate gene identified in the list of DPT anti-correlated genes was ***Notch2*** and ***3***. Notch signalling seems to inhibit the differentiation of early pancreatic progenitor cells, while at later stages it drives their specification into ductal lineage (Kopinke et al. 2011). Hence its role in pancreas development seems ambiguous and context dependent, possibly relying on the dosage of the expression levels (Kopinke et al. 2011), as well as the spatiotemporal dynamics. Its role in the maintenance of multipotency at later stages of pancreatic development should be investigated.

Rbms3 is another interesting candidate as it binds to the 3'UTR of *Ptf1a* mRNA enhancing its expression (Lu et al. 2012). Ptf1a has been shown to drive acinar specification, however it is also expressed in early pancreatic bud progenitors (Shih et al. 2013). Similarly to Notch, it's role may be context dependent and its possible role in regulating multipotency during later pancreatic development could be studied in the future. The expression pattern of both Rbms3 and Notch 2 and 3 could be investigated in order to find out whether there is any preferential localisation of these factors at ductal-ends.

In summary, I have speculated a list of factors, which may be up-regulated in ductal-end associated precursor cells. It should be the focus of future studies to select some of these markers based on literature search and carry out immunostaining of E12.5-induced lineage-traced samples. This would enable the investigation of the potential co-expression of these factors with the tripotent clones and the potential ductal-end proliferative niche, observed with

the lineage tracing analysis (Chapter 4). This would help to characterise the niche environment driving pancreatic expansion during development.

Ndrg1	1700086L19Rik	Fam183b	Nbea	Kdm7a	Rab27a	Ap3s1-ps2
Rab3d	Tpst2	Hid1	Slc36a1	Mast3	Selenok	Cyp4b1
Rimbp2	Lhx1	Amy1	Atp8b1	Ldlr	Tecpr1	Spint2
Neurod1	Rundc3a	Mfap4	Try10	Tmem206	Arl4a	Ctsf
Cpe	Ids	Nol4	Dst	Deptor	Scn4b	Aqp8
Mical2	Kif1b	Dusp5	Gm43861	Lhfpl2	Kcnc3	1700023F06Rik
Vwa5b2	Elavl4	Dll3	Srl	Dusp10	Insm1	Bend7
Ptprn2	Syt7	Slc7a14	Ankrd12	Scfd1	Dpysl5	Ivd
Pclo	Chga	Gm5409	Amy2a5	Tspan5	Ppp1r37	Clip3
Ell2	Rapgef4	Ubb	Npdc1	Tekt2	Pla2g2f	Lmx1b
Map1b	Tubb3	Stxbp1	Pde1c	Nova2	Ap3b2	3110043O21Rik
Atp2a3	Syt13	Grin2c	Amy2a4	Smim14	Vil1	Gm10334
Btg2	Ttll7	Rbfox3	Abhd15	Ttc28	Ubald1	Gm17149
Malat1	Hepacam2	Glud1	1810041L15Rik	Cmtm4	Nod1	Tbc1d9
Cacna2d1	Kcnh6	Scgn	Rogdi	Pomt2	Ffar2	Rcan3
Gnao1	Runx1t1	Rfx6	Hagh	Kcnma1	Kif1a	Ralgds
Tmsb4x	Pcsk1n	Pdia2	Tmem185a	Usp16	Gabarapl2	Btg3
St18	Syp	NA	Mafb	Cd164l2	Rnase1	Gjd2
Baiap3	Scg3	Ap3s1	Pax4	St8sia3	Stxbp5l	Gng12
Fbxl16	Igfbpl1	Gpr142	Casz1	Tmbim1	Cnih2	Pcyt1b
Stat3	Pcsk1	Serpini1	Slc35d3	Map3k15	Myo6	Hipk3
Lhx1os	Gatsl2	Esyt1	Tmem163	Try4	Mxd1	Ptger3
Plcxd3	Cacna1a	C130021I20Rik	Mlxipl	Cyhr1	Dusp8	Clcn3
Cck	Sh2d5	Lrp11	Jund	Sdcbp	Sphkap	Adam23
Myt1	Lmna	Cnnm2	Basp1	Sytl5	Cela3b	Ncoa1
Chgb	Synpr	Dnajb1	Cmip	Gbf1	Mfng	Tmod2
Slc38a5	Gipr	Celsr3	Cela3a	Aqp12	Flnc	Isg20
Gdap1l1	Cryba2	Edem3	Pnmal2	Zdbf2	Mospd3	Map1a
1110008P14Rik	Ret	Arx	Sct	Pim2	Pkib	Sh2b3
Mtcl1	Abcb9	Pycr2	Olfm1	Rab7	C1galt1	Sec61b
Prnp	Madd	Atp6v0b	Kcnk16	Prss1	Ass1	Dnajb11
Hpca	Pak3	Ttyh2	Draxin	Cacna1h	Ndel1	Apba1
Disp2	Gnas	Pou3f4	Pdk2	Prss3	Try5	Cnot6l
Dbpht2	Zbtb7a	Dner	Gnptg	Fxyd3	Selenom	Gm5424
Pnmal1	Ncam1	Serping1	Rn18s-rs5	Gabbr2	Rap1gap2	Grina
Fndc3a	Gck	Fev	Gfpt1	Tfe3	Acadsb	Fa2h
Cadps	Sh3glb1	Actg1	Tmed8	Rgag4	Ddit3	Entpd3
Miat	Gfra3	Gng4	Zcchc18	Slc34a2	Oaz1	Qdpr
Celf3	Aacs	Amy2a2	Zfp174	Rgs16	Tmem57	Eif1
Pax6	Ppp2r5b	Gabarap	Bnip3	Mapk8ip2	Cela2a	Egr1
Ap1s2	Nhlh1	Trp53inp2	Amy2a3	Cbfa2t3	Tbc1d16	
Sel1l	Fam126a	Riiad1	Col4a3bp	Hmgn3	Ero1lb	

Sox9	Mest	Tcf7l2	S100a10
Wfdc2	Gpm6b	Cadm1	Rfc3
1700011H14Rik	Sestd1	Cgn	Cd24a
Slc38a4	Chrna4	Mcm3	Bex1
Vim	Clmn	Gm8292	Dtymk
Notch2	Igsf3	Gm14230	Fscn1
Gja1	Nme4	Peg12	Lamc2
Wnt7b	Greb1	Zfp36l1	Lgr4
Gm16551	Pxdn	Mex3a	Hunk
Habp2	Schip1	Hadh	Gm2693
Dusp9	Fam234b	Fmo2	Mir99ahg
Nrep	Acot1	Prdx6	Car14
Igfbp4	Apoc1	Gm7665	Ezr
Adamts1	Mcm6	Fjx1	Yap1
Rbp1	Wfdc15b	Ephb4	Bcap29
Mxra7	Tinagl1	2610035D17Rik	Gm6419
Ccnd1	Hyal2	Jag1	Col27a1
Gsta3	Hmga2	Tmem55a	Parp1
Cdh3	Cdc42ep1	Frem2	Ptgfrn
Rest	Efna4	Myl12b	Dbi
Serpinf1	Gm11223	Arl4c	Gm28710
Igfbp5	Hmgb3	Epb41l1	Mdfi
Onecut1	Prss23	P4ha3	Pltp
Sept9	Bmp7	Svbp	Bzw2
Mgst1	Capg	Serpina1b	Tmem171
Ptn	Igf2	Arhgef19	Tkt
Vill	Bicc1	Hhex	Acaa2
Smtnl2	Ddah1	Col18a1	Slc39a10
S100a16	Slc2a2	Msl3	Gm38078
Capn6	Pde5a	Tubb5	Rfc2
Notch3	Trip10	Rbms3	Eno1
Fgfr2	Tmem29	Ajuba	Itgb5
2500004C02Rik	Adgrg6	Stmn1	Pik3ap1
Rgma	Fras1	Smoc1	Gm5514
5730416F02Rik	Rara	Cmtm8	Cyp39a1
Fzd2	Sdc4		

Table 21. All genes correlated (P< 5.5 10^{-12}) with the direction of the diffusion plot. These indicate genes associated with differentiation into pancreatic lineages, including potential novel candidates. Genes of conserved expression in pancreata of different species are highlighted in red.

Table 22. All genes anti-correlated (P< 5.5 10^{-12}) with the direction of the diffusion plot. These present potential novel candidates for the multipotent domain in developing pancreas. Genes of conserved expression in pancreata of different species are highlighted in blue.

5.7 Discussion

Single-cell RNA sequencing has proved essential in providing molecular confirmation of the functional lineage tracing study results presented in chapters 3 and 4. Firstly, I confirmed the findings of the early lineage commitment due to cluster analysis with tSNE plots. This finding is generally contradictory to the previous pancreatic literature (Kopp et al. 2011; Kopinke et al. 2011; Solar et al. 2009; Furuyama et al. 2011; Zhou et al. 2007), whereby the extent of multipotency should be vast, especially at early stages such as E13.25. However, one previous study, based on microarray gene expression analysis suggested early commitment of cells, with evidence of endocrine gene expression already at E9.5 (Chiang and Melton 2003).

Next, I established lineage hierarchy, based on diffusion pseudotime – a method used to decipher branches in lineage relationships (Haghverdi et al. 2016). This revealed the ductal lineage cells at the apex of the hierarchy, giving rise to acinar and islet lineages. This is again consistent with the lineage tracing data presented in the previous chapter, whereby tripotent clones are associated with ductal-ends.

Furthermore, the study of genes correlated and anti-correlated with the direction of the diffusion pseudotime has revealed a list of genes, which may be expressed in the multipotent precursor cells. These factors could be the focus of future studies related to characterisation of ductal-end niche and the associated tripotent clones.

Lastly, the gene expression pattern revealed by the t-SNE and heatmap analysis show great uniformity of gene expression within clusters and between the timepoints studied. This conservation of gene expression patterns suggests that, in contrast to previous studies placing emphasis on temporal progression of tip-trunk segregation into ductal morphogenesis (Shih et al. 2013), branching dynamics may be obeying a simple and conserved set of rules throughout the secondary phase of development. This could mean that the tip-trunk fate polarity established early on is conveyed via distal ductal-ends during consecutive branching processes.

In summary, the single cell RNA sequencing study presented in this chapter has shed light on the underlying molecular programmes that orchestrate pancreatic development. The results generate novel insights into the understanding of pancreatic cellular heterogeneity and lineage relationship.

Chapter 6

Results: Islet morphogenesis

6.1 Introduction

This chapter is the last of the four Results series. Here, I present the outcomes of the ubiquitous *R26*-CreERT2 lineage tracing and quantification (See Chapter 3), with the focus on islet dynamics. The analysis is combined with computational modelling. This enables the study of the cellular mechanism of islet formation.

Islets of Langerhans are essential for correct blood glucose level regulation, and their abnormal development leads to diabetes mellitus (Edlund et al. 2001). While previous studies have mainly focused on specification pathways leading to β-cell differentiation (D'Amour et al. 2006; Pagliuca & Melton 2013; Pagliuca et al. 2014), the understanding of islet morphogenesis is limited. Previous research has shown that islets are polyclonal in origin (Deltour et al. 1991), and originate from the delamination of endocrine precursors from maturing ducts (Solar et al. 2009). Based on lineage tracing studies using a constitutive promoter, these lineage-restricted unipotent precursors were thought to undergo very few rounds of division after populating an islet (Desgraz and Herrera 2009). Moreover, it has been noted the islet size is highly variable in mouse as well as in human (Jo et al. 2012; Kilimnik et al. 2012). However, the origin of islet size heterogeneity, as well as the kinetics and number of islet precursors, are still largely unresolved. In this study, for the first time, I have carried out lineage tracing from the ubiquitous *R26*

promoter to focus on the dynamic contribution of cells - their proliferation and migration - to islet development.

In particular, this chapter aims at answering the following research questions regarding the cellular mechanism and dynamics of islet formation:

- How is islet size regulated?
- How many precursors contribute to islet formation?
- Is proliferative capacity of individual endocrine precursors regulating islet size?
- What is the mode of islet cell proliferation during islet formation?

The chapter starts with a description of islet compartment-containing clones – their potency and morphology. Next, I discuss the polyclonality of islets – a previously reported finding (Deltour et al. 1991). I then study the cellular mechanism of endocrine precursor delamination. Subsequently, I decipher the number of endocrine precursors, which merge together to form a functional islet. Lastly, I investigate the proliferative dynamics of precursor cells within islets after the early endocrine aggregates have been formed.

Altogether, this chapter reveals cellular mechanisms of different steps of islet formation, which have not been previously studied extensively, from early endocrine progenitor delamination, through coalesce of endocrine precursors, to local islet cell proliferation. The understanding of islet morphogenesis is essential, especially in the fast developing era of tissue engineering and regenerative medicine.

6.2 Islet clones – potency and morphology

The aim of this section was to characterise the potency and morphology of islet clones. Therefore, I was first interested in characterising the relationship between islet cells and other lineages. I wanted to find out whether there is any hierarchy between the pancreatic lineages (ductal, acinar and islet) and whether any common ancestors between the islet and other cell types can be identified. Furthermore, I sought to understand whether islets arise mainly from multipotent or committed precursors. I therefore first carried out the analysis of the E12.5 to P14 tracing study (see Chapter 3 – 4) and examined clones containing an islet component (as assessed by Chromogranin A staining), which consist of around one fifth of the total clone fraction (Fig. 17, Section 3.5). Parameters analysed included islet clone size, potency of islet-containing clone, islet size, centre coordinates of an islet, total number of islets in a given section, and the fraction of confetti+ labelled islets out of all islets in a given section (see Section 3.4.2 for quantification details).

Interestingly, the inspection of fixed samples at P14 collection timepoint (induced at E12.5) showed that the vast majority of islets contained no confetti+ cells. Amongst those islets that contained the confetti+ cells, the majority (>70%) only showed one confetti colour. This observation confirms the clonality of the assay (Fig. 41a). Of those clones that contained lineage labelled islet cells, the majority were found to be tripotent at both E9.5 (85%) and E12 (60%), although at E12.5 I could find small numbers of bipotent (21%) and unipotent (19%) islet-containing clones (Fig. 41b-e). The majority of the bipotent clones contained the ductal compartment (Fig. 41c,d). This observation is consistent with previous reports indicating that islet cells derive from progenitors delaminating from the ducts (Solar et al. 2009).

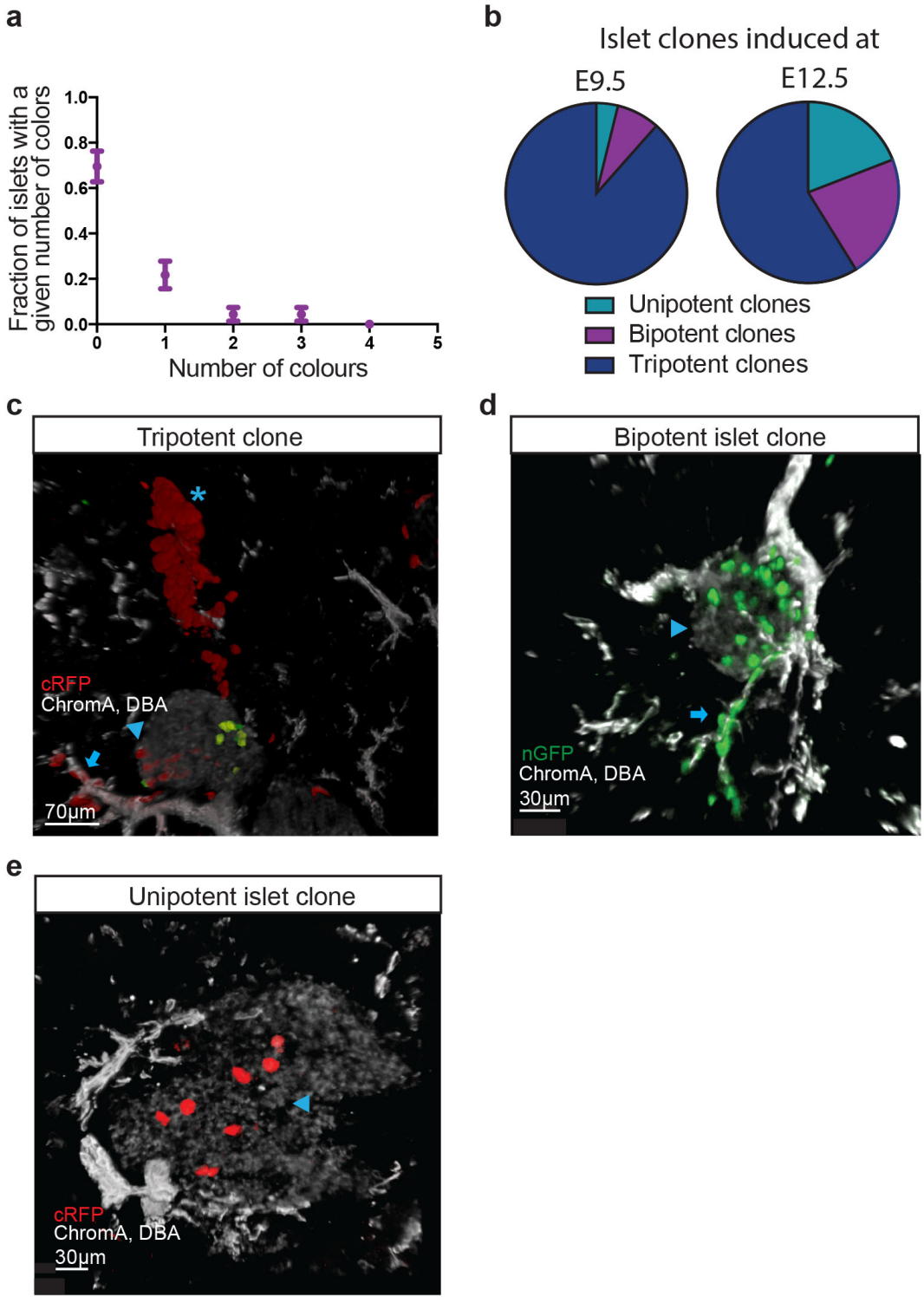
a
Fraction of islets with a given number of colors
1.0
0.8
0.6
0.4
0.2
0.0
0
1
2
3
4
5
Number of colours
b
Islet clones induced at
E9.5
E12.5
Unipotent clones
Bipotent clones
Tripotent clones
c
Tripotent clone
cRFP
ChromA, DBA
70µm
d
Bipotent islet clone
nGFP
ChromA, DBA
30µm
e
Unipotent islet clone
cRFP
ChromA, DBA
30µm

Figure 41. *Potency of islet containing clones. (a) Fraction of islets with a given number of confetti colour labelling. Most islets contain only a single label, confirming the clonality of the lineage tracing data. (b) Potency of islet cell-containing clones induced at E12.5 and E9.5 (c) Tripotent clone (d) Bipotent islet clone. (e) Unipotent islet clone. Islet, ductal and acinar compartment indicated with arrowhead, arrow and asterisk, respectively. 26 islet clones from n=2 mice (2 litters) were quantified for E9.5 induction, and 68 islet clones from n=3 mice (3 litters) for E12.5 induction.*

6.3 Polyclonality of islets

I aimed to study the clonality of islets, in order to determine whether islets arise from the merging of multiple endocrine precursors, or whether single endocrine cells contribute to islet formation. Therefore, I analysed the labelling of islets with confetti clones. Occasionally, I observed more than one confetti colour localised within an islet, suggesting polyclonal origin of islets. Furthermore, islet-containing clones occupied only 3.7% of the total islet volume on average, further supporting the finding of polyclonality (Fig. 41c-e). This result supports the previous reports (Deltour et al. 1991).

6.4 Initiation of islet formation

The next aim was to understand how the process of islet formation is initiated. The observed polyclonality of individual islets suggests that they must emerge from the coalescence of multiple precursors (Fig. 41c-e), (Deltour et al. 1991; Jo et al. 2012).

Since islets arise from delamination of Ngn3+ cells from the ducts, I wanted to determine the extent to which the delamination events affect islet size. Therefore I investigated whether the size of the endocrine component of islet-containing bipotent and tripotent clones correlated with the size of the ductal counterpart. I reasoned that if an islet results from the collective delamination of many ductal precursors with limited proliferation, then size of islet and ductal component of a clone ought to be correlated. Alternatively, if the islet compartment of a clone originates from the rare delamination of a ductal precursor, followed by subsequent proliferation, then islet and ductal clone size should be uncorrelated. From the data, I found only a weak correlation (R^2=*0.012*), supporting the latter hypothesis of islets arising from rare delamination of cells from the ducts (Fig. 42).

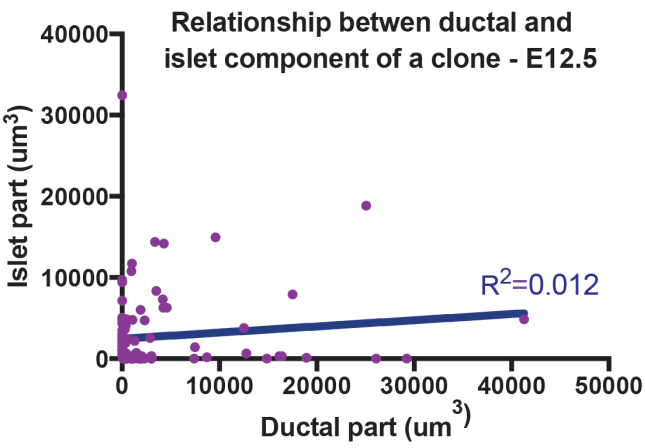

Figure 42. *Relationship between the size of ductal part and islet part of an islet clone. No correlation was seen between the two compartments. This supports hypothesis of rare delamination of endocrine precursors, followed by subsequent proliferation. 26 islet clones from n=2 mice (2 litters) were quantified for E9.5 induction, and 68 islet clones from n=3 mice (3 litters) for E12.5 induction.*

6.5 Multiplicity of endocrine progenitors

As mentioned before, I found that islets were never monoclonal in my analysis. Instead, islet-containing clones occupied just 3.7% of the total islet volume on average, with substantial variations across islets (Fig 41c-e, 43a). Figure 43a shows an example of such clone variability, revealing a smaller cRFP and a large cYFP clone. Thus, I wanted to find out if there was any relationship between the size of clones and the respective islets, in order to determine if islet size was regulated by the proliferative capacity of the constituent endocrine progenitors. I also aimed to infer the average number of precursors that would contribute to islet formation.

Since the tracing data were clonal, this enabled me to estimate the average number of independent precursors required to build an islet, which is obtained simply as the inverse of 3.7% (the average fraction of clone in an islet), i.e. I estimated that islets are founded by some *N=27 +- 6* independent precursors.

This is consistent with the observed high degree of islet polyclonality. Importantly, although there were very large variations (>30 fold) in islet volume, I could not find any statistically significant correlation between the volume of an islet and the size of the clone it contained (R^2=*0.001* for E12.5 induction*,* R^2*=0.074* for E9.5 induction*,* Figure 43b,c). This shows that variability in islet volume is not caused by local variations in the proliferative capacity of constituent cells, but must therefore originate from variations in the number of progenitors coalescing to form it.

This could either be due to local chemotactic cues acting on individual islet precursors, or to the subsequent merger/fragmentation of islets. The effect of fission and fusion events on the regulation of islet sizes is not understood, and it is possible that they are of different significance at different phases of islet formation (Jo et al. 2011). Of note, I observed that a small fraction of clones spanned multiple islets (8/55 for E12.5 to P14 traced samples), and these displayed a characteristic “dumbbell” shape described previously (Seymour et al. 2007). This indicates that fusion or fission could play a role at these stages of development. The relative significance of the two processes in the period between E12.5 and P14 should be investigated in the future.

To further strengthen my conclusions about the number of precursors contributing to islet development, I performed a parallel analysis based on the E9.5 tracing. Indeed, as islet formation occurs well after E12.5, I do not expect the results above to be different from that obtained with the E9.5 induction data. Interestingly, I found a very similar degree of islet polyclonality, with a clonal fraction consistent with some *N=25 +- 8* independent precursors creating an islet. This result confirms the robustness of the analysis and the *R26*-Cre; *R26*-Confetti system for studying islet morphogenesis.

In summary, lineage tracing from the ubiquitous *R26* promoter shows that islet size is not determined by the proliferative capacity of individual endocrine precursors, but by the merging of multipotent precursors. I find that on average around 26 precursors contribute to islet growth.

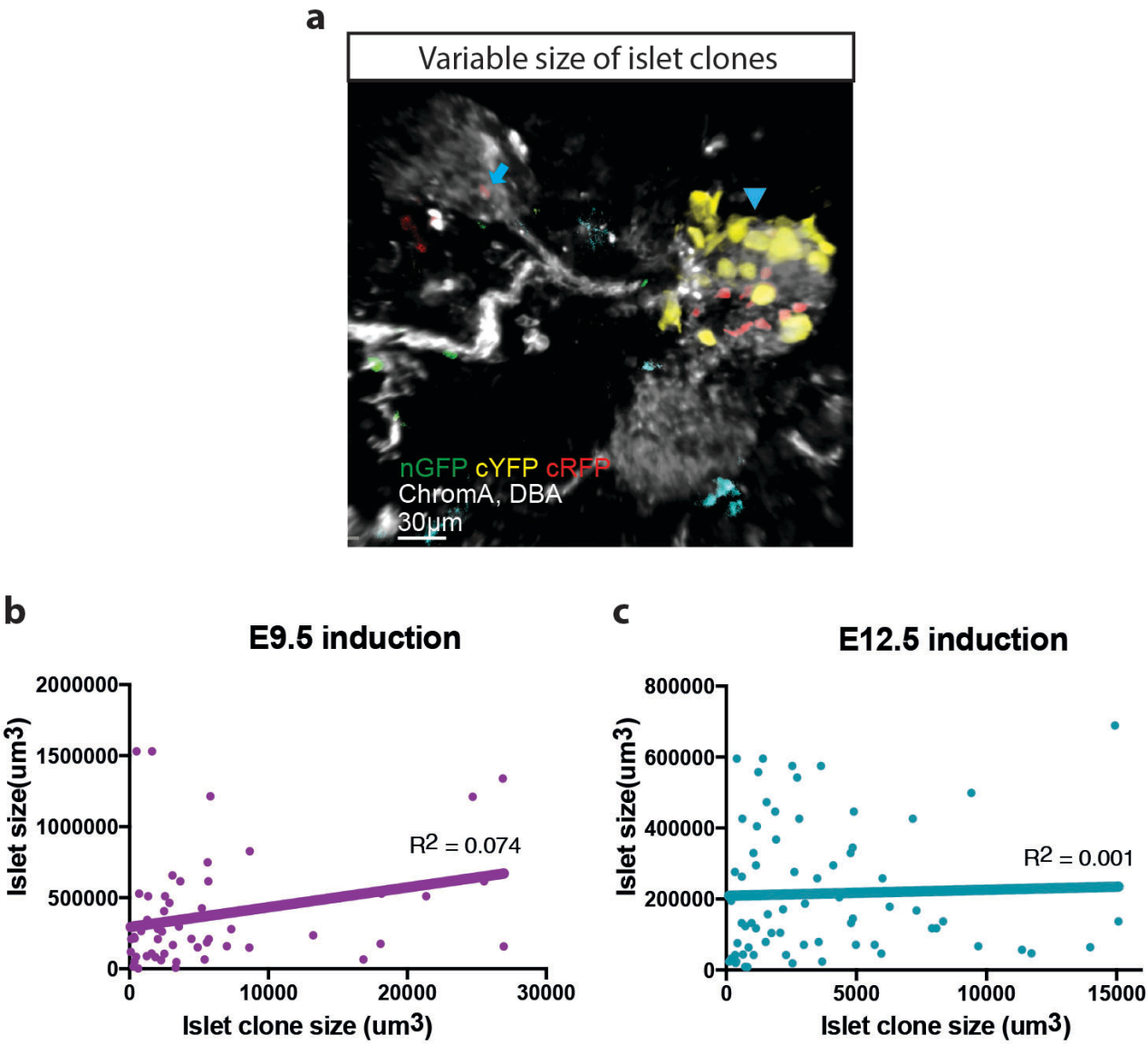

Figure 43. *Islet size is not determined by the proliferative capacity of endocrine progenitors. (a) Islet clones occupy different fractions of islet volume – red (cRFP) clone occupies a small fraction (arrow), while the yellow (cYFP) clone occupies most of the islet (arrowhead). (b-c) Islet clone size versus corresponding islet size in which a given clone is localised (volumes in µm^3). For E9.5 and E12.5 induction, the data show no correlation. 26 islet clones from n=2 mice (2 litters) were quantified for E9.5 induction, and 68 islet clones from n=3 mice (3 litters) for E12.5 induction.*

6.6 Mode of proliferation of islet precursors

Having gained insight into the cellular mechanism of endocrine delamination and aggregation into clusters, I was interested in understanding the dynamics of endocrine precursor proliferation within the maturing islets. In order to find out about the number and mode of cellular divisions, I studied the structure of islet compartment containing clones and in particular the size of the islet component. I found that the islet compartment size distribution from the E12.5 tracing data is broad and well-fitted by a single exponential. This observation, by analogy with multiple other systems (Klein and Simons 2011), indicates that islet precursors do not have a fixed and well-defined proliferative potential, but rather they undergo a pattern of stochastic growth, where islet progenitors choose stochastically between symmetric division into two islet progenitors and entry into quiescence. The E9.5 data fit an exponential curve but to a lesser degree than the E12.5 data (Fig. 44). This could be due to multiple independent delamination events from large ductal clones, which are more likely to arise in early development.

Altogether, our data indicate, that following the merging of endocrine precursors, the cells proliferate stochastically. Whether this could contribute to the variability in islet size described previously (Jo et al. 2011; Jo et al. 2007; Jo et al. 2012) is not clear. Others have previously suggested that stochastic proliferation is an unlikely mechanism driving islet size variability and it is more likely to arise from islet fission (Jo et al. 2011). My data, and in particular the lack of correlation between the islet clone and islet sizes (described above, Section 6.5), seems to confirm this hypothesis. This requires further investigation.

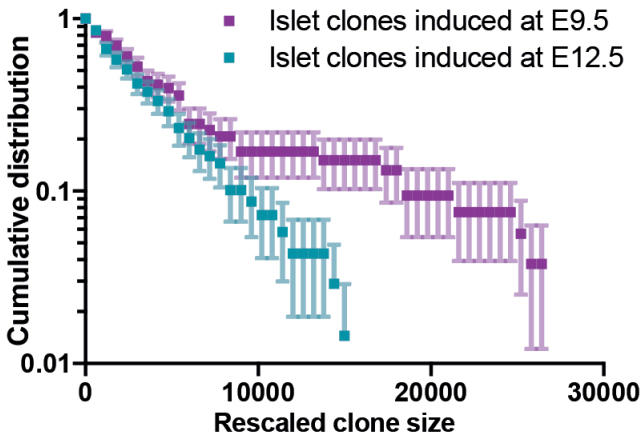

Figure 44. *Islet clone size distributions for E9.5 (pink) and E12.5 (blue) induction timepoints showing an exponential size dependence indicative of stochastic fate choices during proliferative expansion. Bars indicate mean and SD. 26 islet clones from n=2 mice (2 litters) were quantified for E9.5 induction, and 68 islet clones from n=3 mice (3 litters) for E12.5 induction.*

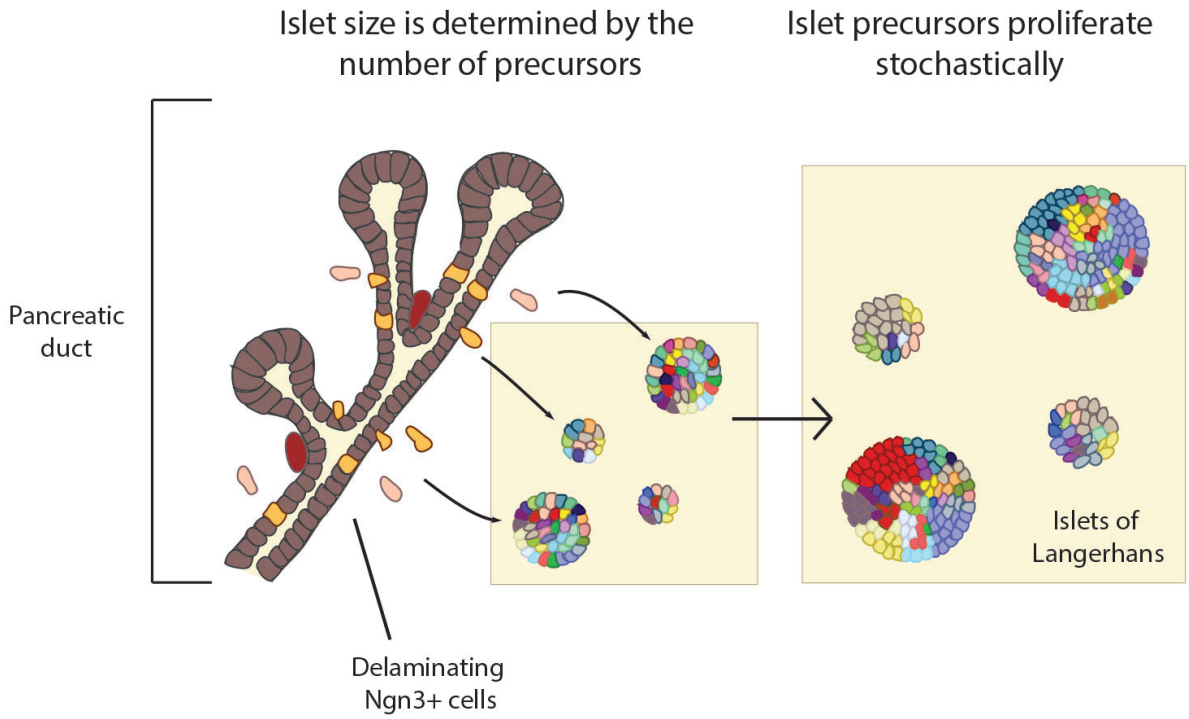

Figure 45. *Model of the formation of islets of Langerhans. The size of islets is determined by the number of precursors merging in an islet, which then proliferate stochastically upon populating an islet.*

6.7 Discussion

Previous studies have focused on the analysis of distribution of pancreatic islets to infer their mode of islet growth. These have shown that islets follow an exponential distribution (Jo et al. 2011), which has been explained by islet fission (Jo et al. 2011; Seymour et al. 2004), and local aggregation of islet cells (Herrera et al. 1991; Bouwens and De Blay 1996). In this study, for the first time, I have carried out lineage tracing from the ubiquitous *R26* promoter to focus on the dynamic contribution of cells - their proliferation and migration - to islet development.

My results suggest that islet size is regulated by the merging of precursors (Section 6.3, Fig. 41c-e), confirming previous report of polyclonality (Deltour et al. 1991), and follows from rare delamination from the ducts. On average, there are 20-30 lineage-restricted precursors that delaminate from ducts and aggregate into clusters of widely varying sizes. Islet cells then undergo a phase of independent stochastic expansion, randomly deciding between proliferation and quiescence/differentiation within islets (Fig. 45). This contradicts a previous study, which has suggested that islet cells proliferate homogenously (Brennand et al. 2007). However, the analysis was performed on β-cells exclusively with the MADM (mosaic analysis with double markers) system (Brennand et al. 2007), hence it may not be representative of all the islet lineages. In my analysis, I observed a wide range of clone sizes at the collection timepoint, including large clones of about 45 cells. This contrasts with the previous lineage tracing study, which revealed small clone sizes when traced using non-inducible Cre system, *Ngn3*-Cre (Desgraz and Herrera 2009). The apparent discrepancy between the two studies may arise from the fact that high levels of Ngn3 promoter activity may have been required to activate the MADM reporter construct leading to the tracing of already highly committed endocrine precursors (Desgraz and Herrera 2009).

Altogether, my results reveal a novel and comprehensive model of islet morphogenesis, which was possible due to multicolour non-biased lineage tracing in the pancreas, combined with quantitative analysis. This is in contrast to previous studies, which focused on the anatomy of islet sizes (Jo

et al. 2007; Jo et al. 2011; Jo et al. 2012). The improved understanding of islet morphogenesis is of great importance for regenerative medicine, in the treatment of diabetes, especially in the fast developing era of tissue engineering.

Chapter 7

Discussion

7.1 Contribution to the field

The findings of my PhD project reveal that pancreas growth is controlled and driven by proliferative ductal-end cells, which stochastically balance bifurcation and branch termination, while carrying multipotent as well as ductal and acinar-committed precursors. This provides insight into how the specification and growth of the three pancreatic lineages, i.e. ductal, acinar and islet, may be coordinated. No model that explains the cellular mechanism of parallel pancreatic compartment morphogenesis exists in the relevant literature, despite there being keen interest in understanding the control mechanisms regulating tissue size and composition (Stanger et al. 2007; Iber & Menshykau 2013; Shih et al. 2013; Pan & Wright 2011).

The research of this project also suggests that the tissue is vastly lineage restricted at early stages of development, with rapid cell fate commitment of cells taking place already in primary transition phase of pancreatic development, in contrast to previous reports claiming multipotency at these stages (Zhou et al. 2007; Solar et al. 2009; Kopp et al. 2011; Furuyama et al. 2011).

Furthermore, I elucidate a cellular mechanism of islet morphogenesis, whereby single ductal cells delaminate from ducts and coalesce together to form islets and, subsequently, proliferate stochastically. I also find that islet size is independent of the proliferative capacity of endocrine precursors.

Importantly, this study brings methodological advancements to the field of pancreatic development. Firstly, it is the first clonal lineage tracing study with the multicolour confetti-reporter system that has been performed in the pancreas. To reliably infer the fate potential of pancreatic precursors, it is essential to recover clonal information in a situation in which there is potential for large-scale cellular migration leading to clonal fragmentation. Until now, this problem has prevented the acquisition of clonal information, thereby significantly limiting our ability to understand the behaviour of *individual* cells during pancreatic development. Hence, the clonal study presented here is important for the correct interpretation of potency results and morphological behaviours.

In addition, I carry out an unbiased lineage tracing with *R26*-CreT2 promoter, which enables one to look at random populations of pancreatic cells and therefore infer the dynamics of all lineages. This has been supported by tracing from a pancreas-specific *Sox9* promoter, serving as a control for the ubiquitous lineage tracing and a comparison with the current literature, which focuses primarily on *Sox9* lineage tracing (Kopp et al. 2011; Furuyama et al. 2011).

I also carry out clearing protocols and reconstructions of images, which enables the visualisation of whole clones in 3D. This is very important for the interpretation of potency in the context of development, where cell migration is very active, as well as for the analysis of morphological processes such as branching morphogenesis of organs. This approach of 3D clonal analysis has not been applied previously in pancreas development studies; mainly thin serial sections have been analysed (Kopp et al. 2011; Furuyama et al. 2011).

Moreover, this study is the first extensively quantitative study of pancreas development *in vivo* up to date, and contains advanced computational modelling enabling the analysis of tissue dynamics.

Lastly, my PhD research involves a comprehensive combination of techniques such as whole-mount immunostaining of clonal lineage traced samples combined with proliferation assay and single cell sequencing. None of these approaches have been applied before, neither alone nor in combination, in the

context of pancreatic development, and therefore give rise to novel findings. The specific contributions of my research and the novel insight to the field are outlined in the sections below.

7.1.1 Cell fate restriction

Previous lineage tracing studies have been very useful in establishing the relationship between the cellular lineages in the developing pancreas. In particular, the fate of Pdx1+ early pancreatic progenitors, Ngn3+ endocrine precursors, Cpa1+ acinar precursors and Sox9 ductal precursors has been previously determined (Gu et al. 2002; Kawaguchi et al. 2002; Furuyama et al. 2011; Kopp et al. 2011). Furthermore, the method has been used to study the potency of cells at different developmental stages. In particular, tracing of Cpa1+ tip cells have shown tripotency until E14.5 (Zhou et al. 2007), similarly to the Hnf1B+ traced cells (Solar et al. 2009). Sox9+ cells, on the other hand, have been reported to be tripotent until E18.5 with rare tripotency persisting even within few weeks after birth (Kopp et al. 2011; Furuyama et al. 2011). Hence the Sox9+ compartment has long been believed to be the potential host site of multipotent progenitors, despite the failed attempts to find *de novo* islet precursor neogenesis from Sox9+ precursors in the adult pancreas (Kopp et al. 2011; Furuyama et al. 2011). However, the mentioned studies have been performed at non-clonal levels of induction and with a use of biased promoters. Therefore, I aimed to re-evaluate the question of pancreas potency and lineage relationship by studying the potency of individually labelled random pancreatic cells.

The results of *R26*-CreT2 lineage tracing suggest that the embryonic pancreas undergoes a rapid shift towards unipotency in the primary transition phase of development, and by E12.5 the majority of cells are unipotent. This contrasts with to the literature outlined above (Kopp et al. 2011; Furuyama et al. 2011, Zhou et al. 2007, Solar et al. 2009). The difference may be due to the fact that in the previous studies the apparent tripotency could arise from the merging of independent lineage restricted precursors. Furthermore, the aforementioned studies did not attempt to look at individual clones, but rather

quantified the total percentage of islet, ductal and acinar lineage labelling within thin sections, which were not serially re-constructed.

In comparison, I observed that at E9.5 the tissue showed a much higher extent of tripotency than at E12.5. However, already at this early stage, a quarter of cells were unipotent. This further emphasises that lineage restriction may be taking place much earlier than previously reported, when cells are thought to be morphologically and functionally identical (reviewed in Benitez et al. 2012; Shih et al. 2013; Pan & Wright 2011). One previous study confirms this finding, whereby genes associated with specific lineage maturation were shown to be enriched in certain cells already at this stage (Chiang & Melton 2003).

In order to further verify my hypothesis, I performed a single cell sequencing analysis. Ensuring non-biased investigation of pancreatic cells without enrichment for any early-committed lineages, I observed signs of early heterogeneity, with markers of acinar, ductal and endocrine lineage detected in individual cells. Hence, the functional results of lineage tracing were confirmed with the analysis of gene expression, in line with the previous microarray analysis (Chiang & Melton 2003)

7.1.2 Mode of pancreatic growth

The cellular mechanism of pancreas morphogenesis has been the focus of numerous studies. Enhanced proliferation of cells in the tip area at E12.5 has been observed (Zhou et al. 2007; Dahl-Jensen et al. 2016; Petzold et al. 2013). The proposed mechanism of pancreas expansion involves the extension of the proliferative tip domain, followed by lateral appearance of side branches (Villasenor et al. 2010). However, in this study the focus lies on the early tip domain rather than ductal ends at the tips of branches. Another study, in *ex vivo* pancreatic explants, has suggested that 76% of bifurcations during ductal branching occur via lateral branching, while 13% appear as a result of terminal bifurcation (Puri & Hebrok 2007). Another *ex vivo* explant study has confirmed enhanced tip proliferation (Dahl-Jensen et al. 2016), but contradicting evidence has been provided recently (Marty-

Santos & Cleaver 2016). Altogether, it appears that the mode of pancreatic growth and branching morphogenesis of the ducts is poorly understood.

My study confirms the previous findings of enhanced proliferation of cells at peripheral regions of the pancreas. While the previous *in vivo* study (Zhou et al. 2007; Petzold et al. 2013) suggested proliferation in the tip domain, I show that this peripheral proliferation is maintained at later stages at ductal ends of subsequent branches. I also propose that the mechanism of tissue growth is based on this ductal-end driven proliferation and bifurcation rather than ductal end extension followed by lateral branching, in contrast to previous suggestions (Villasenor et al. 2010; Puri & Hebrok 2007). Indeed, I observe conversion of single labelled confetti+ cells within ducts into monoclonal labelling of ducts at the peripheral regions of the tissue, which is only possible in the case of proliferation, bifurcation and extension of ductal ends. If the alternative, i.e. the lateral branching, were the case, then I would observe labelling of “main” and side branches without a gradual conversion from single cell labelling to covering the whole area of ducts in confetti+ colour. As this is not the case, therefore the unbiased lineage tracing suggests that branching morphogenesis is tip-bifurcation driven.

Why is there a discrepancy between this study and the previous reports (Villasenor et al. 2010; Puri & Hebrok 2007)? Villasenor and colleagues have looked at anatomical snapshots of the ducts in development and based on geometry they concluded the mode of ductal branching. However, the symmetrical appearance of branches at an approximately right angle from the “leading” branch is not sufficient evidence for lateral branching. More dynamic evidence, such as live imaging, would be required, however, this is technologically implausible to carry out in the embryos. The few live imaging studies that have been conducted for pancreas development (Puri & Hebrok 2007; Dahl-Jensen et al. 2016) were carried out in tissue explants, and therefore do not reliably recapitulate the *in vivo* conditions. Hence, my study, which presents snapshots of *in vivo* traced cells may be used as a proxy to live imaging. Indeed, approaches based on static pulse-chase assays can also give indirect insight into the dynamics of cell fate decisions by studying the evolution of timepoint snapshots, as emphasized by quantitative studies,

particularly in adult tissues (Snippert et al. 2010; Mascré et al. 2012; Visvader & Clevers 2016; Roy et al 2014), as well as in developmental contexts such as mammary gland (Scheele et al. 2017).

Another question, which has been related to the mode of pancreas growth, pertains to the contribution of central plexus remodelling in determining pancreatic size. It has been suggested that plexus remodelling by means of physical pressure may lead to the origin of first protrusions, i.e. tips, at the onset of secondary transition (Pan & Wright 2011). This suggests that plexus remodelling could play an important role in determining the final pancreas size. Indeed, deletion of pancreatic cells between E9.5 and E12.5, when plexus remodelling is taking place (Pan & Wright 2011), results in a significantly decreased adult pancreas size, while ablation of cells at later stages results in a more compensated tissue growth (Stanger et al. 2007). However, the reduced tissue growth as a result of cell deletion at E9.5-E12.5 might be the outcome of depletion of early progenitors, rather than the plexus remodelling itself. Furthermore, the role of plexus remodelling at later stages of development is not understood (Bankaitis et al. 2015).

My study has shown that the primary mechanism of tissue growth in secondary transition arises due to ductal-end driven proliferation of progenitors rather than plexus remodelling. I hypothesised that if plexus remodelling were vastly contributing to tissue growth, then I would observe disconnected clusters of labelled ducts during lineage tracing. However, I observed stretches of monoclonally labelled ducts indicating ductal-end driven growth being the main contributor to branching morphogenesis. Even though it has been suggested that plexus remodelling might persist beyond E12.5 until E15.5 (Bankaitis et al. 2015), it might be a “background” process of remodelling and nucleation of ducts rather than expansion. However, my findings do not contradict the suggestions of the role of pancreas remodelling on pancreas growth in primary transition, between E9.5 and E12.5 (Pan & Wright 2011).

7.1.3 Multipotent and restricted progenitors at ductal ends

It has been previously reported that tip cells may host multipotent, proliferative Cpa+ cells until E14.5 *in vivo* (Zhou et al. 2007). In *ex vivo* explant settings proliferative cells have been shown to exist at the ductal ends of branches (Puri & Hebrok 2007), however, this has not been demonstrated *in vivo*. One study has suggested that multipotent tip domains may be guiding pancreatic growth (Zhou et al. 2007).

Using clonal density ubiquitous promoter lineage tracing, I observed ductal-end proliferative cells *in vivo*, complementing the findings of the previous *ex vivo* study (Puri & Hebrok 2007). I showed that ductal ends carry acinar and ductal-committed precursors together with rare tripotent precursors, in contrast to the multipotent domain previously suggested (Zhou et al. 2007). By E15.5 the tripotent cells are completely depleted. The discrepancy between my own and the published study (Zhou et al. 2007) may arise from the clonal versus non-clonal levels of induction, as well as the fact that previous study looked at the Cpa1+ lineage rather than random cells within the ductal-end/tip domain.

The findings of this thesis offer an explanation as to how all the pancreatic lineages can develop in concert, whereby in a vastly lineage restricted tissue the early-committed precursors, together with some rare tripotent cells, are being carried together at ductal-ends. The ductal-ends bifurcate or terminate in a near-balanced stochastic process, resulting in a range of subtrees of variable size (different branch number), and the corresponding labelling of ductal and acinar branch-associated clones shifting towards monoclonallity over subsequent branches. Where a given branch terminates, the acinar and ductal committed precursors differentiate into mature acinar and ductal cells, respectively, while the islet cells delaminate from the trailing ductal bipotent or tripotent precursors.

It is not clear how the creation of proliferative niche environment at the ductal-ends is related to the early generation of tip-trunk polarity around E12.5. My sequencing data, whereby the cells at E13.25 and E15.25 show uniform and similar gene expression between the two timepoints suggests that the tip-

trunk polarity established at the onset of secondary transition may indeed be conveyed via the growing ductal-ends. It is plausible that the initially established tip domain proliferates and pushes the outgrowths, leaving behind the cells, which terminate proliferation, while the proliferative cells are conveyed at ductal-end bifurcation points.

7.1.4 Branch number regulation

Pancreatic ductal structure shows some conserved as well as some non-stereotypical features. The primary ductal frame is conserved between individuals and gives the pancreas its specific shape and anatomical features such as head, heal and ridge (Villasenor et al. 2010). At the same time, there is a significant amount of variability within the number of branches of individual ductal subtrees diverging from the main duct (Dahl-Jensen et al. 2016). What factors could account for this variability in subtree size is not clear. It is plausible that the main conserved ductal framework is brought about by plexus remodelling, while the side branches of variable size arise due to ductal end/tip-driven growth.

Indeed, my lineage tracing experiment with the induction at E12.5 shows that the growth of side branches appears to be tip driven and that plexus remodelling does not seem to play a role in the growth of the pancreas during secondary transition. I propose a model of stochastic near balanced ductal end bifurcation versus termination as a cellular mechanism of branch size regulation. This model fits well for my data of the ductal subtree size cumulative distribution. Hence, this process could account for the huge variability in the subtree sizes between individual pancreata and explain the relative composition of pancreatic sub-compartments.

The mechanism of stochastic bifurcation and termination of ductal ends has been shown to play a role in other organs, such as the mammary gland (Scheele et al. 2017). Importantly, since branching morphogenesis is a process taking place in a number of glandular organs and serves to maximise the surface area over constraint volumes within organisms, it is plausible that it may follow some conserved features (Iber & Menshykau 2013). Therefore, the mechanism of tip driven growth and stochastic branch bifurcation versus

termination could be present in more organs. This could be the focus of future studies.

The simulations of the model involve the assumption of branching occurring in 2D, and random proliferation and bifurcation of ductal-ends until another ductal end is encountered. The resulting ductal network contains a ductal density equivalent to that resulting from stochastic near-50% probability of ductal bifurcation versus termination. However, based on the premises of the model, the actual nature of regulation of bifurcation and termination is not purely stochastic but results from proximity of other ductal ends, which may affect physical and biochemical local environment. The factors involved in this local 'neighbour' regulation should be investigated. Furthermore, the extent of randomness of the ductal end 'collisions' themselves is not understood. For instance, it is not clear whether there are some internal factors secreted in the pancreas or external factors produced by surrounding tissue, which could attract the growth of branches in a particular direction. These could involve a biochemical or mechanical pressure gradient. ECM and mesenchyme could serve this function by posing physical resistance to elongation of ductal-ends and by expressing molecules such as laminin-1 in ECM (Li et al. 2004); Fgf10, Bmp4 in mesenchyme (Bhushan et al. 2001). In sum, it is not clear if ductal-end 'collisions', and therefore the process of near balanced stochastic bifurcation and termination, is purely random. Elucidation of the factors affecting local ductal-end bifurcation versus termination, and, in particular, the physical and biochemical cues involved, should be carefully investigated in the future.

Focusing on biomolecular regulation, among the likely candidate molecules involved would be the inhibitors of signalling pathways shown to play a role in regulation of pancreatic branching in mouse models (Bhushan et al. 2001; Miettinen et al. 2000; Villasenor et al. 2010; Petzold et al. 2013). To start with, Fgf signalling provided by the mesenchyme is a key pathway thought to play an important role in branching morphogenesis. *Ex vivo* organoids fail to grow without Fgf10 (Bhushan et al. 2001), while sustaining it uniformly in the medium maintains the branching (Miralles et al. 1999). However, it is plausible that mesenchyme is necessary for pancreatic bud growth induction but not

branching per se (Dahl-Jensen et al. 2016). Indeed, SU5402 inhibition of Fgf signalling prevents organoid formation and expansion, but does not affect the expansion in the branching phase (Greggio et al. 2013). This is consistent with the fact that FGFR2IIIb inactivation leads to hypoplasia at E12.5 and the hypoplasia is maintained but does not worsen as development proceeds (Pulkkinen et al 2003). Therefore, it is not clear if inhibition of Fgf signalling could affect the variability of subtree branch size, and should be the focus of future studies.

Another target pathway could be BMP signalling, which is induced by mesenchyme. Its inhibition via either Noggin overexpression of expression of dominant-negative BMP receptor causes pancreatic hypoplasia in mice, combined with reduced branching and excessive endocrine differentiation (Ahnfelt-Rønne et al. 2010).

ECM has been also shown to play a significant role in regulating branching morphogenesis. In addition to its effect via ECM-integrin signalling regulating cell adhesion in the cap region of the pancreas, possibly enabling local protrusion of tips (Shih et al. 2016), it also secretes molecules such as Laminin-1. Blocking laminin-1 in pancreatic explant cultures, impaired branching and reduced the expression of acinar markers (Li et al. 2004).

EphB and EGF signalling pathways have also been shown to play a role in regulating branch number in pancreata. EphB3-null/EphB2-dominant negative mice develop hypobranched pancreas with less and shorter branches, and overall lower exocrine mass (Villasenor et al. 2010). Branching morphogenesis is also impaired in *EGFR* (-/-) mice (Miettinen et al. 2000). Therefore, the search for EphB and EGF inhibitors expressed in the epithelium might be an important focus for future studies, as it could explain localised inhibition of branching, and the resulting stochastic variability of subtree branch number within different regions of the pancreas.

Ephrin and EGF could act by affecting the Rho GTPase activity in the pancreas as in other organs it has been shown that Rho GTPases are regulated by Ephrin, EGF and ECM integrin signalling (Heasman & Ridley 2008; Huveneers & Danen 2009; Poliakov et al. 2004). GTPases are believed

to be important in tubulogenesis (Heasman & Ridley 2008). It has been reported that tubulogenesis of pancreas is prematurely arrested in the absence of RhoA GTPase inhibitor Stard13 (Petzold et al. 2013) and that it acts via regulation of cytoskeleton organisation and ERK signalling.

Another signalling molecule, which could control the ductal branch formation in the pancreas is the hepatocyte growth factor (HGF), as it controls branching of prostate through the Hedgehog pathway (Lim et al. 2014). Both the Hedgehog and HGF are expressed during pancreatic development; however, conditional inactivation of HGF receptor has not been associated with any defect in pancreas morphogenesis (Sonnenberg et al. 1993; Mellado-Gil et al. 2011). On the other hand, HGF mediated migration of progenitors has been observed and this process could contribute to correct morphogenesis in mouse pancreas, as shown in zebrafish (Anderson et al. 2013).

The other candidate pathways, which could be involved in local regulation of branch bifurcation and termination, include Wnt/β-catenin and Notch pathways (Murtaugh et al. 2003; Baumgartner et al. 2014) due to their short-range activity. Some Wnt inhibitors, such as SRFPs and DKK, are expressed in the pancreas, with usually higher levels in the early pancreatic bud (Gauger et al. 2012; Dahl-Jensen et al. 2016). Notch has been previously shown to promote pancreatic progenitor proliferation (Greggio et al. 2013; Ahnfelt-Ronne et al. 2012). Candidate inhibitor molecules, which could be involved in the regulation of local branch termination, could include Jag1, which has been found to be expressed and inhibit Notch signaling in the pancreas (Golson et al. 2009a; Golson et al. 2009b). Other inhibitors could include Fringes and Dlk1, as they are expressed in the pancreas and have been shown to inhibit Notch signaling in other organs. Importantly, Dlk1 has been shown to inhibit branching morphogenesis in the salivary gland by repressing Notch signaling (García-Gallastegui et al. 2014). Therefore, the study of Notch inhibitors should be the focus of future research concerning the control of branching morphogenesis (described in Dahl-Jensen et al. 2016).

7.1.5 Pancreatic size control

Understanding of the factors controlling the regulation of pancreatic size is currently very limited. This thesis shows that pancreatic growth is tip driven during the secondary transition, with ductal ends stochastically 'deciding' between bifurcation and branch termination, and that plexus remodelling does not play a significant role in pancreatic expansion at these stages. These findings do not oppose the suggestion of the role of plexus formation on establishing the correct pancreatic size (Pan & Wright 2011). Indeed, towards the end of plexus remodelling short protrusions emerge on the peripheral parts of plexus (Bankaitis et al. 2015), from which the tip driven growth is likely to originate. Incorrect or decreased size of plexus could set an incorrect framework for pancreas branch formation. Indeed, previous research has suggested that deletion of cells until E12.5, when the plexus is remodelled (Pan & Wright 2011; Bankaitis et al. 2015), results in a highly decreased pancreatic growth to only 6% of the wild type pancreas size (Stanger et al. 2007). Consistently, a higher extent of growth compensation was observed for progenitor depletion at later developmental stages (Stanger et al. 2007).

However, the study by Stanger et al. also implies that the initial pool of progenitors might contain cells which are already highly committed, and therefore cannot compensate the ablation by enhanced proliferation, as is the case in the liver (Stanger et al. 2007). This is consistent with the findings of my thesis, whereby early and rapid cell fate restriction has been observed.

7.1.6 Re-evaluating lineage hierarchy

A lineage hierarchy hypothesis has been established based on lineage tracing studies performed at a high density of induction (Gu et al. 2002; Kawaguchi et al. 2002; Furuyama et al. 2011; Kopp et al. 2011; Zhou et al. 2007; Solar et al. 2009). The current model involves multipotent progenitor cells separating their domain into tip and trunk, mediated by Nkx6.1-Ptf1a cross-repression (Schaffer et al. 2010). The tip domain then gives rise to acinar precursors, while the trunk domain gives rise to ductal-islet bipotent progenitors (Fig. 46, reviewed in Shih et al. 2013).

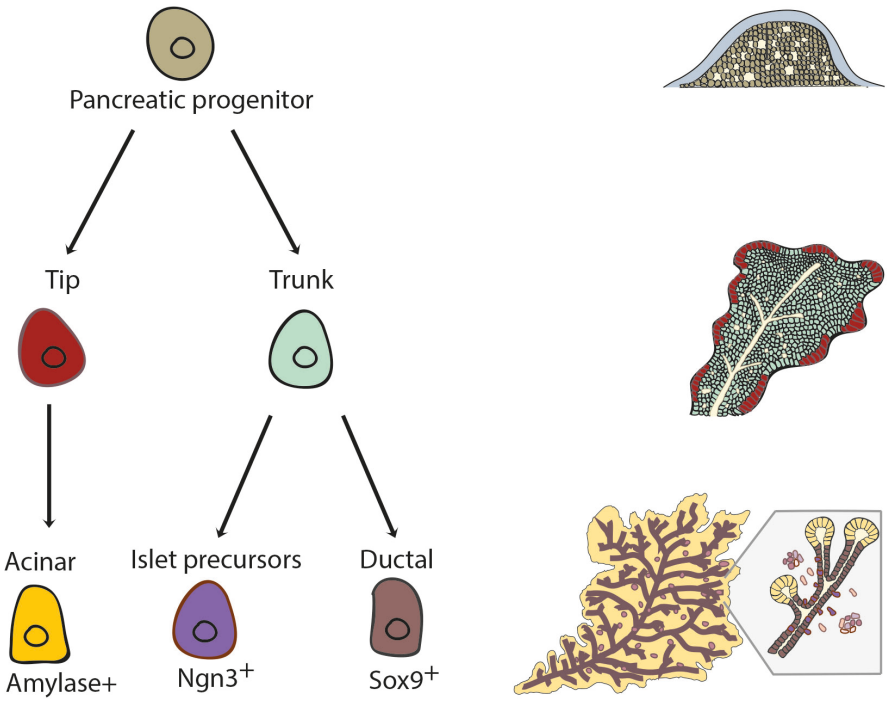

Figure 46. *Lineage hierarchy model based on previous lineage tracing studies (on the left; Gu et al. 2002; Kawaguchi et al. 2002; Furuyama et al. 2011; Kopp et al. 2011; Zhou et al. 2007; Solar et al. 2009) juxtaposed with a schematic of pancreatic morphological changes (on the right; see Fig. 2 in Chapter 1.1). Adapted from Shih et al. 2013.*

The non-biased ubiquitous promoter lineage tracing study of this thesis partially confirms this hierarchy. Importantly, however, the findings enrich the current understanding by showing that ductal-ends might be the proliferation-supportive niche environment for multipotent progenitors as well as cell fate-restricted progenitors. Single cell RNA sequencing results, and, in particular, the diffusion pseudotime plots (DPT), show that the Sox9+ ductal precursor cells are at the apex of the hierarchy, and separate into acinar and islet branches. Furthermore, the functional results of lineage tracing confirm this finding, as most of the tripotent clones are ductal-end associated, and, additionally, I observe an abundance of ductal-islet and ductal-acinar bipotent clones. This confirms that the ductal compartment might, indeed, be at apex of hierarchy. The lineage relationship inferred based on these findings is presented in Figure 47.

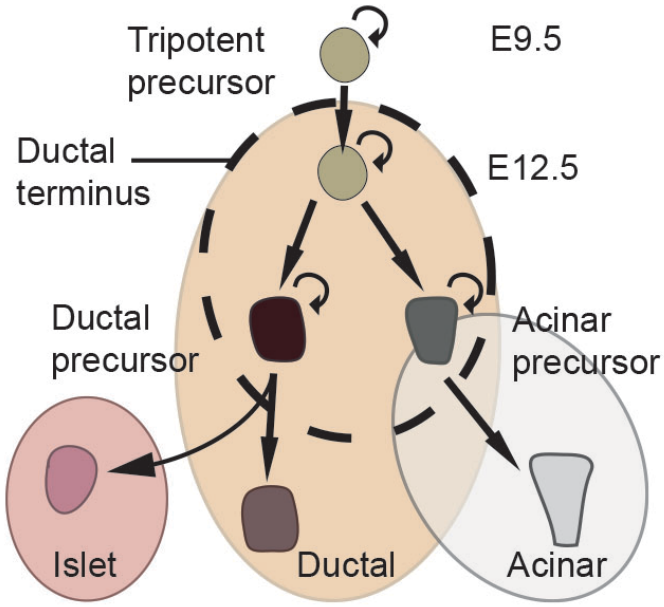

Figure 47. *Schematic of the lineage relationship based on ubiquitous R26-CreT2; R26-Confetti lineage tracing presented in Chapter 4 of this thesis.*

The analysis of diffusion pseudotime plots (DPT) of single cell RNA data has enabled me to identify genes associated with progenitor-like state as well as those correlated with progressive differentiation. The genes anti-correlated with the direction of DPT would be those expressed at high levels in the progenitor cells. On the other side, the genes correlated with the direction of DPT would be associated with differentiation of pancreatic lineages. Interestingly, I found that *Sox9* showed a very significant anti-correlation with the direction of DPT, supporting my hypothesis based on lineage tracing results of progenitor cells being localised at ductal-ends. This is also consistent with literature, whereby Sox9+ cells may be the source of multipotent cells until E14.5 or until birth (Furuyama et al. 2011; Kopp et al. 2011).

On the other hand, among the genes highly correlated with the direction of DPT was *Cpa*. This is a surprising finding, as previous studies suggest that “multipotent Cpa cells might be guiding pancreas morphogenesis” (Zhou et al. 2007).

In addition to looking at the genes known for their role in mouse pancreatic development, in collaboration with Dr. Steffen Rulands, we carried out an unbiased approach of searching for all genes, which show high anti-correlation with direction of DPT. In this way, I could identify potential novel markers of the multipotent pancreatic cells. The list of genes was numerous; however, in order to narrow it down to those which could actually perform a functional role in pancreas development, I compared it with a previously published list of genes with conserved expression between pancreata of different species (Tarifeño-Saldivia et al. 2017). Surprisingly, the majority of the genes identified in DPT correlation list also appeared in the list of Tarifeño-Saldivia et al. (Tarifeño-Saldivia et al. 2017). These genes are available in my thesis in Chapter 5.6 and could be used in the future to test various potential ductal-end niche markers.

Finally, I show that the relationship between the ductal and acinar lineage may be closer than previously suggested. Based on the previous hypothesis, the ductal lineage separates from the acinar lineage early on during the tip-

trunk domain separation (reviewed in Shih et al. 2013). However, the abundance of acinar-ductal bipotent clones at E12.5 observed with our analysis, and their persistence at later stages (E15.5 and E18.5) suggests that the separation of these two domains is not as sharp and symmetrical as previously suggested (Schaffer et al. 2010). This suggests that besides the canonical Ptf1a-Nkx6.1 cross-repression, other factors could be involved. In particular, it has been shown that *Prox1* deficient mice lack the second phase of endocrine production and the pancreata display enhanced acinar specification (Wang et al. 2005; Westmoreland et al. 2012). This could arise due to imbalanced tip-trunk separation. Therefore, Prox1 could have an impact on the separation of domains and play a role in determining the sharpness of the boundary, perhaps leaving a more plastic zone in between the tip and trunk domains.

7.1.7 Stem cell niche in developing pancreas

Previous studies have suggested that there may be a niche site of multipotent progenitors during pancreatic development, and it may perhaps persist after birth. Tip cells until E14. 5 have been shown to be multipotent (Zhou et al. 2007). On the other hand, some studies have implied that centroacinar cells, at the interface between ducts and acini, might be the host sites of multipotent progenitors even in the adult pancreas (Rovira et al. 2010). Furthermore, the *Sox9*+ lineage has also been associated with tripotency (Kopp et al. 2011; Furuyama et al. 2011).

The results of this thesis suggest that ductal-ends might serve as a proliferation-supportive niche for both the multipotent precursors as well as lineage restricted cells. The signals, which provide the proliferation-stimulating environment for the cells in the niche, should be examined in the future. The findings of this thesis serve as a comprehensive and integrative model explaining the previous, apparently contradictory, results (Zhou et al. 2007, Rovira et al. 2010, Kopp et al. 2011, Furuyama et al. 2011). At the early stages of development ductal-ends could coincide with the Cpa1+ tip domain (Zhou et al. 2007), later on the multipotent progenitors would appear at the interface of ductal and acinar compartment (centroacinar cells) (Rovira et al.

2010) and within the Sox9+ ductal-end domain (Kopp et al. 2011; Furuyama et al. 2011).

7.1.8 Islet morphogenesis

The control of islet growth and morphogenesis is not well understood. It has been shown that in embryos and in neonates the endocrine cells proliferate contiguously, forming branched cord-like structures (Miller et al. 2009). Aggregation of cell clusters, i.e. fusion, is another, probably coexistent, mechanism of islet formation in the embryonic pancreas, considering the polyclonal origin of islets and the significant variability in islet size (Deltour et al. 1991; Ma et al. 2010; Jo et al. 2011).

How islets of correct size are formed is not fully understood, and it is not clear whether the islet size is determined by the proliferative capacity of endocrine precursors. My study has shed light on the cellular mechanism of the islet formation. On average 26 precursors, which have delaminated from the ducts, migrate and coalesce together into endocrine clusters. However, islet size is independent of the proliferative capacity of the constituent endocrine progenitors. The endocrine precursors proliferate stochastically. Furthermore, islet fusion appears to be a rare event considering that multiple confetti colours appear rarely within the same islet. These findings provide a novel insight into the cellular dynamics of islet formation, which has been previously based on static analysis of islet size distributions (Jo et al. 2007; Kilimnik et al. 2009; Jo et al. 2012; Jo et al. 2011).

7.2 Limitations

Despite providing important advancements to the understanding of pancreatic development, there were certain limitations implicated in the current study. These were mainly related to technological limitations rather than experimental design. However, upon optimisation and improvement of the currently available technology, the following issues could be resolved.

7.2.1 Tissue markers

Firstly, I was limited in the number of tissue markers used to study the potency of cells due to the use of the multi-colour confetti-reporter system. Its importance, however, needs to be re-emphasised. To reliably infer the fate potential of pancreatic precursors, it is essential to recover clonal information in a situation in which there is potential for large-scale cellular migration leading to clonal fragmentation. This problem has prevented the acquisition of clonal information until now, significantly limiting our ability to understand the behaviour of individual cells during pancreatic development (Zhou et al. 2007; Solar et al. 2009; Kopp et al. 2011; Kopinke et al. 2011; Furuyama et al. 2011; Schaffer et al. 2010; Pan et al. 2013). It is only through the use of confetti labelling that I could achieve a statistically-defined level of confidence in the assignment of clones while still working with an acceptable number of embryos.

However, in using the confetti-labelling system, I was left with only one channel, which I used for imaging of both ducts and islets. Fortunately, since ducts and islets adopt a separate and distinct morphology, I could unambiguously infer the cell composition of clones (Fig. 13, Chapter 3.3.5). However, there was no channel left for imaging the acinar markers in the initial analysis, and I assumed that the acinar cells were the DBA-, Chromogranin A- cells from the dissected pancreata.

Importantly, I further confirmed the validity of this cell-type assignment by performing a set of control immunostainings using different channels for DBA, amylase and Chromogranin A to make sure that the ductal and endocrine compartments were indeed discernible (DBA and Chromogranin A; DBA,

amylase and Chromogranin A; Chromogranin A and amylase, Fig. 13). Indeed, the bulk of the tissue which was DBA- Chromogranin A- was indeed amylase+, hence given the number of clones quantified (244 for E12.5 to P14 tracing and 50 for E9.5 to P14 tracing), the assumption holds true.

The use of multiple staining markers in lineage traced samples has already been an issue in literature studying the potency of pancreas progenitors, as only 2 markers corresponding to 2 out of 3 pancreatic compartments (islet, ductal or acinar) were stained simultaneously, even when only one reporter colour was used for tracing (see, e.g., Zhou et al. 2007, Solar et al. 2009, Kopp et al. 2011, Kopinke et al. 2011, and Pan et al. 2013). Nevertheless, this issue should be optimised in the future by careful staining and improvement of imaging methods avoiding bleed-through between closely spaced imaging channels.

However, since correct potency assignment was vital for this study, I re-quantified the potency of a random subset of clones traced from E12.5 to P14 after co-staining for amylase, DBA and Chromogranin A (Fig. 23, Chapter 4.5), controlling for the risk of channels bleeding through and affecting the readout of other markers and clones. Crucially, I found that the potency distribution of the re-quantified clones was very similar to those initially reported (no statistically significant difference, see Fig. 24, Chapter 4.5).

Finally, I confirmed my conclusion about the morphology and potency of the *R26*-Cre;*R26*-Confetti clones through an additional *Sox9*-CreERT2 lineage tracing experiment from E12.5 to P14, demonstrating that clones are of pancreatic (and not extra-pancreatic) origin (Fig. 22, Chapter 4.4).

In summary, the simultaneous co-staining of multiple pancreatic markers has been a limitation of my study due to available technology. I managed to overcome it with a set of additional controls. Nevertheless, the current microscopy technology available does not allow me to image more than 3-4 pancreatic markers simultaneously. In the future, the field would benefit from looking at various markers of ductal cells and islet maturation markers, in order to gain additional insight into heterogeneity of cellular dynamics between different sub-compartments.

7.2.2 Region-specific single cell RNA sequencing

The single cell RNA sequencing experiments were very useful in shedding light on the molecular confirmation of early lineage commitment shown by the functional lineage tracing experiments, as well as the understanding of lineage relationship during development. However, in order to interpret the molecular mechanism guiding the branching behaviour and the potency of cells at ductal-ends specifically, laser capture would be an illuminating experiment to undertake, given the precision with which ductal regions could be studied. Unfortunately, there is currently no established method/protocol that would enable me to study the transcripts of single cells obtained from the laser-dissected area. Evidence from other organs (Scheele et al. 2017) suggests that cellular heterogeneity within ductal-ends may be vast, hence the sequencing of the bulk area without discrimination into individual could be uninformative. Therefore, the question of gene expression by single cells at ductal-ends should be re-addressed in the future, when appropriate methods and technology are available.

7.3 Future directions

Despite the advancements of the study, certain aspects following on from this research would benefit from further investigation, as they are key to understanding the development of the pancreas. These areas are outlined below.

7.3.1 Factors regulating local branch expansion

Firstly, my findings suggest that branching morphogenesis is guided by a near-balanced ductal bifurcation and termination, and that the distribution of subtree sizes matches a distribution of subtree branch number, where, on average, a newly arising branch has nearly 50% probability of termination. Despite the statistically stochastic nature of the process some factors could be involved in reregulating the proliferation versus termination decision of cells at ductal-ends and these potential extrinsic and intrinsic cues should be studied in the future, as explained below.

7.3.1.1 Biophysical factors

The pressure exerted by ECM and mesenchyme surrounding the pancreatic bud and its effect on the growth of individual subtrees within the tissue could be examined with microfluidics.

Additionally, the amount of ECM around various branches could be determined from imaging with second harmonics generation (Weigelin et al. 2016; Wu et al. 2015) in parallel to confetti reporter tracing and the use of tissue markers. This would enable one to gain an additional assessment marker, besides the ductal, acinar and islet stainings, without the sacrifice of any of the previously used imaging channels. In this way, one could infer whether there is any relationship between the amount of ECM surrounding the subtree and the subtree size itself. This would provide one with an understanding of how ECM regulates the local branch expansion.

7.3.1.2 Biochemical factors

The expression of inhibitors of major signalling pathways shown to regulate global branching patters *in vivo* (Miettinen et al. 2000; Villasenor et al. 2010;

Petzold et al. 2013; Bhushan et al. 2001; Ahnfelt-Rønne et al. 2010) within the pancreatic epithelium should be studied (as outlined in Chapter 7.1.4), including the effect of their deletion or local inhibition on individual branch size. This would allow one to identify pathways responsible for the local regulation of pancreas branching.

7.3.2 Ductal-end niche factors

My findings suggest that ductal-ends serve as a proliferation-supporting niche and a site for rare multipotent progenitors in a vastly lineage restricted tissue, until around E12.5. Understanding which factors are expressed by the ductal-end cells and the local environment cells would be key to elucidating the mechanism of branching morphogenesis and coordinated growth of acinar, ductal and islet lineages. There are several methodological approaches, with which the understanding of ductal-end niche factors could be improved, and these are outlined below.

7.3.2.1 Laser capture optimisation

Firstly, laser caption of specific ductal areas would enable the study of factors, which are enriched around ductal-ends as compared to the more central areas. However, up to date, no effective methods for single cell RNA sequencing of laser-captured cells have been developed. From the studies of ductal cells in branching morphogenesis in other organs it follows that the cellular heterogeneity plays a significant role (Scheele et al. 2017), calling for the study of individual cells within such processes. Therefore, optimising laser capture experiments whilst retaining cells at sufficient condition for single cell RNA sequencing could be the focus of future studies.

7.3.2.2 Testing genes identified from diffusion pseudotime correlations

The analysis of genes anti-correlated with the direction of the diffusion plot provided me with a list of potential novel candidate genes, which could be expressed in multipotent progenitors at ductal-ends. Subsequently, the list was narrowed down to the genes, which are expressed in pancreata of various species (Tarifeño-Saldivia et al. 2017), as these could be part of the core regulatory mechanisms in the development of the pancreas. It would be

key to verify some of these factors by co-immunostaining of the lineage traced tissue samples containing multipotent clones against those factors in order to find out if any of them are enriched at ductal-ends.

7.3.3 Potency analysis

I have studied the potency of single cell-derived clones and based on that I inferred a rapid cell fate restriction already in the primary phase of development. However, my analysis was restricted in the number of differentiation markers due to the use of multi-colour reporter cassette for lineage tracing (reasons for its use outlined in the previous section 7.2.1). If this technological limitation was overcome, then the understanding of the extent of tissue maturation and clone cellular heterogeneity could be enhanced by staining of multiple lineage-associated markers. The future analysis could include more extended analysis of islet maturation markers, such as the expression profile of various hormones. Furthermore, the analysis of ductal branching clones, indicative of tip-driven growth mode, would be enriched by simultaneous analysis of several ductal markers, such as DBA, CK19 and mucin. This would allow one to characterise the heterogeneity of the expanding ducts during intense tissue morphogenesis.

7.3.4 Ductal abnormality model

In this project, I have examined how branching morphogenesis controls pancreas growth in secondary transition and how it is essential for the coordination of the simultaneous development and expansion of three major pancreatic compartments. Given the crucial role of branching morphogenesis, it would be useful to turn to ductal abnormality models such as *EGFR*-/- and *EphB2/3* mutant mice (Miettinen et al. 2000; Villasenor et al. 2010) and study the effect of these mutations on the relative composition of pancreas and the branch structure – globally and locally. These models have been shown to result in the development of abnormal pancreas with abnormal development of the pancreatic lineages (Miettinen et al. 2000; Villasenor et al. 2010). However, whether this arises due to an effect on early bud emergence and proliferation, or whether indeed it has an impact on the branch formation itself is not clear. Therefore, these model systems would first need to be verified by

an *in vivo* time course analysis and comparison to wild type mice in order to point to the specific stages and processes which are affected in these mutant mouse lines.

7.4 Summary

Pancreas development involves a coordinated process in which an early phase of cell segregation and patterning is proceeded by a longer phase of lineage restriction, expansion, and extensive tissue remodelling. By combining quantitative clonal lineage tracing and whole-mount reconstruction with proliferation kinetics and single-cell transcriptional profiling, I define the functional basis of pancreas morphogenesis. My results show that the large-scale organization of tissue can be traced to the activity of self-renewing precursors that localize at the termini of growing ductal branches and act collectively to drive serial rounds of stochastic ductal bifurcation balanced by termination. During this process, multipotent precursors give rise to self-renewing acinar-committed precursors, which are conveyed with growing ducts, as well as fate-restricted ductal progenitors that expand the trailing ducts and give rise to delaminating endocrine cells. These endocrine precursors merge together, resulting in variable islet size, while their proliferation is stochastic and independent of islet size. Together, these findings define quantitatively how the functional behaviour and lineage progression of precursor pools serve to define the organization of pancreatic sub-compartments.

References

A, L., and K, B. (2016). scran: Methods for Single-Cell RNA-Seq Data Analysis. R package version 1.2.0.

Afelik, S., Chen, Y., and Pieler, T. (2006). Combined ectopic expression of Pdx1 and Ptf1a/p48 results in the stable conversion of posterior endoderm into endocrine and exocrine pancreatic tissue. Genes Dev. 20, 1441–1446.

Afelik, S., Qu, X., Hasrouni, E., Bukys, M.A., Deering, T., Nieuwoudt, S., Rogers, W., MacDonald, R.J., and Jensen, J. (2012). Notch-mediated patterning and cell fate allocation of pancreatic progenitor cells. Development 139, 1744–1753.

Ahnfelt-Rønne, J., Jorgensen, M.C., Klinck, R., Jensen, J.N., Fuchtbauer, E.-M., Deering, T., MacDonald, R.J., Wright, C.V.E., Madsen, O.D., and Serup, P. (2012). Ptf1a-mediated control of Dll1 reveals an alternative to the lateral inhibition mechanism. Development 139, 33–45.

Ahnfelt-Rønne, J., Ravassard, P., Pardanaud-Glavieux, C., Scharfmann, R., and Serup, P. (2010). Mesenchymal bone morphogenetic protein signaling is required for normal pancreas development. Diabetes 59, 1948–1956.

Anders, S., Pyl, P.T., and Huber, W. (2015). HTSeq-A Python framework to work with high-throughput sequencing data. Bioinformatics 31, 166–169.

Anderson, R.M., Delous, M., Bosch, J.A., Ye, L., Robertson, M.A., Hesselson, D., and Stainier, D.Y.R. (2013). Hepatocyte Growth Factor Signaling in Intrapancreatic Ductal Cells Drives Pancreatic Morphogenesis. PLoS Genet. 9, 1–10.

Andrew, D.J., and Ewald, A.J. (2010). Morphogenesis of epithelial tubes: Insights into tube formation, elongation and elaboration. Dev Biol 341, 34–55.

Angerer, P., Haghverdi, L., Büttner, M., Theis, F.J., Marr, C., and Buettner, F. (2016). Destiny: Diffusion maps for large-scale single-cell data in R. Bioinformatics 32, 1241–1243.

Apelqvist, A., Ahlgren, U., and Edlund, H. (1997). Sonic hedgehog directs specialised mesoderm differentiation in the intestine and pancreas. Curr. Biol. 7, 801–804.

Apelqvist, A., Li, H., Sommer, L., Beatus, P., Anderson, D.J., Honjo, T., Hrabe de Angelis, M., Lendahl, U., and Edlund, H. (1999). Notch signalling controls pancreatic cell differentiation. Nature 400, 877–881.

Duvillié B., Heinis M., Stetsyuk V. (2007). In vivo and in vitro techniques to study pancreas development and islet cell function. Endocr Dev. 12, 46–54.

Bankaitis, E.D., Bechard, M.E., and Wright, C.V.E. (2015). Feedback control of growth, differentiation, and morphogenesis of pancreatic endocrine progenitors in an epithelial plexus niche. Genes Dev. 29, 2203–2216.

del Barrio, M.G., and Nieto, M.A. (2002). Overexpression of Snail family members highlights their ability to promote chick neural crest formation. Development 129, 1583–1593.

Baumgartner, B.K., Cash, G., Hansen, H., Ostler, S., and Murtaugh, L.C. (2014). Distinct requirements for beta-catenin in pancreatic epithelial growth and patterning. Dev. Biol. 391, 89–98.

Beck, B. Blanpain, C. (2013). Unravelling cancer stem cell potential. Nat Rev Cancer 13, 727-38

Belgiovine, C., Chiesa, G., Chiodi, I., Frapolli, R., Bonezzi, K., Taraboletti, G., D'incalci, M., and Mondello, C. (2016). Snail levels control the migration mechanism of mesenchymal tumor cells. Oncol. Lett. 12, 767–771.

Benitez, C.M., Goodyer, W.R., and Kim, S.K. (2012). Deconstructing pancreas developmental biology. Cold Spring Harb. Perspect. Biol. 4.

Benod, C., Vinogradova, M. V., Jouravel, N., Kim, G.E., Fletterick, R.J., and Sablin, E.P. (2011). Nuclear receptor liver receptor homologue 1 (LRH-1) regulates pancreatic cancer cell growth and proliferation. Proc. Natl. Acad. Sci. 108, 16927–16931.

Bernitz, J.M., Kim, H.S., MacArthur, B., Sieburg, H., and Moore, K. (2016). Hematopoietic Stem Cells Count and Remember Self-Renewal Divisions. Cell 167, 1296–1309.

Beucher, A., Martín, M., Spenle, C., Collin, C., Gradwohl, G., and Poulet, M. (2012). Competence of failed endocrine progenitors to give rise to acinar but not ductal cells is restricted to early pancreas development. Dev. Biol. 361, 277–285.

Bhushan, A., Itoh, N., Kato, S., Thiery, J.P., Czernichow, P., Bellusci, S., and Scharfmann, R. (2001). Fgf10 is essential for maintaining the proliferative capacity of epithelial progenitor cells during early pancreatic organogenesis. Development 128, 5109–5117.

Bonal, C., Thorel, F., Ait-Lounis, A., Reith, W., Trumpp, A., and Herrera, P.L. (2009). Pancreatic Inactivation of c-Myc Decreases Acinar Mass and Transdifferentiates Acinar Cells Into Adipocytes in Mice. Gastroenterology 136.

Bort, R., Martinez-Barbera, J.P., Beddington, R.S.P., and Zaret, K.S. (2004). Hex homeobox gene-dependent tissue positioning is required for organogenesis of the ventral pancreas. Development 131, 797–806.

Botrugno, O.A., Fayard, E., Annicotte, J.S., Haby, C., Brennan, T., Wendling, O., Tanaka, T., Kodama, T., Thomas, W., Auwerx, J., et al. (2004). Synergy between LRH-1 and B-catenin Induces G1 cyclin-mediated cell proliferation. Mol. Cell 15, 499–509.

Bouwens, L., and De Blay, E. (1996). Islet morphogenesis and stem cell markers in rat pancreas. J Histochem Cytochem. 44, 947–951.

Bouwens, L., and Rooman, I. (2005). Regulation of pancreatic beta-cell mass. Physiol. Rev. 85, 1255–1270.

Brennand, K., Huangfu, D., and Melton, D. (2007). All β cells contribute equally to islet growth and maintenance. PLoS Biol. 5, 1520–1529.

Brissova, M., Fowler, M.J., Nicholson, W.E., Chu, A., Hirshberg, B., Harlan, D.M., and Powers, A.C. (2005). Assessment of Human Pancreatic Islet Architecture and Composition by Laser Scanning Confocal Microscopy. J. Histochem. Cytochem. 53, 1087–1097.

Burlison, J.S., Long, Q., Fujitani, Y., Wright, C.V.E., and Magnuson, M.A. (2008). Pdx-1 and Ptf1a concurrently determine fate specification of pancreatic multipotent progenitor cells. Dev. Biol. 316, 74–86.

Cabrera, O., Berman, D.M., Kenyon, N.S., Ricordi, C., Berggren, P.-O., and Caicedo, A. (2006). The unique cytoarchitecture of human pancreatic islets has implications for islet cell function. Proc. Natl. Acad. Sci. U. S. A. 103, 2334–2339.

Chen, X., Stauffer, S., Chen, Y., and Dong, J. (2016). Ajuba phosphorylation by CDK1 promotes cell proliferation and tumorigenesis. J. Biol. Chem. 291, 14761–14772.

Chiang, M.K., and Melton, D.A. (2003). Single-cell transcript analysis of pancreas development. Dev. Cell 4, 383–393.

Crawford, L.A., Guney, M.A., Oh, Y.A., DeYoung, R.A., Valenzuela, D.M., Murphy, A.J., Yancopoulos, G.D., Lyons, K.M., Brigstock, D.R., Economides, A., et al. (2009). Connective Tissue Growth Factor (CTGF) Inactivation Leads to Defects in Islet Cell Lineage Allocation and β-Cell Proliferation during Embryogenesis. Mol. Endocrinol. 23, 324–336.

D'Amour, K.A., Bang, A.G., Eliazer, S., Kelly, O.G., Agulnick, A.D., Smart, N.G., Moorman, M.A., Kroon, E., Carpenter, M.K., and Baetge, E.E. (2006). Production of pancreatic hormone-expressing endocrine cells from human embryonic stem cells. Nat. Biotechnol. 24, 1392–1401.

Dahl-Jensen, S.B., Figueiredo-Larsen, M., Grapin-Botton, A., and Sneppen, K. (2016). Short-range growth inhibitory signals from the epithelium can drive non-stereotypic branching in the pancreas. Phys. Biol. 13, 16007.

Danielian, P.S., Muccino, D., Rowitch, D.H., Michael, S.K., and McMahon, A.P. (1998). Modification of gene activity in mouse embryos in utero by a tamoxifen-inducible form of Cre recombinase. Curr. Biol. 8, 1323-S2.

Deltour, L., Leduque, P., Paldi, a, Ripoche, M. a, Dubois, P., and Jami, J. (1991). Polyclonal origin of pancreatic islets in aggregation mouse chimaeras. Development 112, 1115–1121.

Desai, B.M., Oliver-Krasinski, J., De Leon, D.D., Farzad, C., Hong, N., Leach, S.D., and Stoffers, D.A. (2007). Preexisting pancreatic acinar cells contribute to acinar cell, but not islet β cell, regeneration. J. Clin. Invest. 117, 971–977.

Desgraz, R., and Herrera, P.L. (2009). Pancreatic neurogenin 3-expressing cells are unipotent islet precursors. Development 136, 3567–3574.

Dichmann, D.S., Miller, C.P., Jensen, J., Heller, R.S., and Serup, P. (2003). Expression and misexpression of members of the FGF and TGFbeta families of growth factors in the developing mouse pancreas. Dev. Dyn. 226, 663–674.

Doetsch, F., Caillé, I., Lim, D.A., García-Verdugo, J.M., and Alvarez-Buylla, A. (1999). Subventricular Zone Astrocytes Are Neural Stem Cells in the Adult Mammalian Brain. Cell 97, 703–716.

Dontu, G., Abdallah, W.M., Foley, J.M., Jackson, K.W., Clarke, M.F., Kawamura, M.J., and Wicha, M.S. (2003). In vitro propagation and transcriptional profiling of human mammary stem / progenitor cells. Genes Dev. 17, 1253–1270.

Dor, Y., Brown, J., Martinez, O.I., and Melton, D. a (2004). Adult pancreatic beta-cells are formed by self-duplication rather than stem-cell differentiation. Nature 429, 41–46.

Dore, B.A., Grogan, W.M., Madge, G.E., and Webb, S.R. (1981). Biphasic development of the postnatal mouse pancreas. Biol Neonate. 40, 209–217.

Doyle, M.J., and Sussel, L. (2010). Nkx2.2 regulates beta-cell function in the mature islet. Diabetes 56, 1999–2007.

Edlund, H. (2001). Developmental biology of the pancreas. Diabetes 50, S5-7

Esni, F., Ghosh, B., Biankin, A. V, Lin, J.W., Albert, M.A., Yu, X., MacDonald, R.J., Civin, C.I., Real, F.X., Pack, M.A., et al. (2004). Notch inhibits Ptf1 function and acinar cell differentiation in developing mouse and zebrafish pancreas. Development 131, 4213–4224.

Flicek, P., Amode, M.R., Barrell, D., Beal, K., Billis, K., Brent, S., Carvalho-Silva, D., Clapham, P., Coates, G., Fitzgerald, S., et al. (2014). Ensembl 2014. Nucleic Acids Res. 42.

Fujikura, J., Hosoda, K., Iwakura, H., Tomita, T., Noguchi, M., Masuzaki, H., Tanigaki, K., Yabe, D., Honjo, T., and Nakao, K. (2006). Notch/Rbp-j signaling prevents premature endocrine and ductal cell differentiation in the pancreas. Cell Metab. 3, 59–65.

Fukuda, A., Kawaguchi, Y., Furuyama, K., Kodama, S., Horiguchi, M., Kuhara, T., Koizumi, M., Boyer, D.F., Fujimoto, K., Doi, R., et al. (2006). Ectopic pancreas formation in Hes1 -knockout mice reveals plasticity of endodermal progenitors of the gut, bile duct, and pancreas. J. Clin. Invest. 116, 1484–1493.

Fukuda, A., Kawaguchi, Y., Furuyama, K., Kodama, S., Horiguchi, M., Kuhara, T., Kawaguchi, M., Terao, M., Doi, R., and Wright, C.V.E. (2008). Reduction of Ptf1a Gene Dosage Causes Pancreatic Hypoplasia and Diabetes in Mice. Diabetes 57, 2421–2431.

Furuyama, K., Kawaguchi, Y., Akiyama, H., Horiguchi, M., Kodama, S., Kuhara, T., Hosokawa, S., Elbahrawy, A., Soeda, T., Koizumi, M., et al. (2011). Continuous cell supply from a Sox9-expressing progenitor zone in adult liver, exocrine pancreas and intestine. Nat. Genet. 43, 34–41.

Gannon, M., Ray, M.K., Van Zee, K., Rausa, F., Costa, R.H., and Wright, C. V (2000). Persistent expression of HNF6 in islet endocrine cells causes disrupted islet architecture and loss of beta cell function. Development 127, 2883–2895.

García-Gallastegui, P., Ibarretxe, G., Garcia-Ramírez, J.J., Baladrón, V., Aurrekoetxea, M., Nueda, M.L., Naranjo, A.I., Santaolalla, F., Sánchez-del Rey, A., Laborda, J., et al. (2014). DLK1 regulates branching morphogenesis and parasympathetic innervation of salivary glands through inhibition of NOTCH signalling. Biol. Cell 106, 237–253.

Gauger, K.J., Shimono, A., Crisi, G.M., and Schneider, S. (2012). Loss of sfrp1 promotes ductal branching in the murine mammary gland. BMC Dev. Biol. 12, 25.

Georgia, S., Soliz, R., Li, M., Zhang, P., and Bhushan, A. (2006). p57 and Hes1 coordinate cell cycle exit with self-renewal of pancreatic progenitors. Dev. Biol. 298, 22–31.

Golson, M.L., Le Lay, J., Gao, N., Brämswig, N., Loomes, K.M., Oakey, R., May, C.L., White, P., and Kaestner, K.H. (2009a). Jagged1 is a competitive inhibitor of Notch signaling in the embryonic pancreas. Mech. Dev. 126, 687–699.

Golson, M.L., Loomes, K.M., Oakey, R., and Kaestner, K.H. (2009b). Ductal Malformation and Pancreatitis in Mice Caused by Conditional Jag1 Deletion. Gastroenterology 136, 1761–1771.e1.

Gouzi, M., Kim, Y.H., Katsumoto, K., Johansson, K., and Grapin-Botton, A. (2011). Neurogenin3 initiates stepwise delamination of differentiating endocrine cells during pancreas development. Dev. Dyn. 240, 589–604.

Greenwood, A.L., Li, S., Jones, K., and Melton, D.A. (2007). Notch signaling reveals developmental plasticity of Pax4+ pancreatic endocrine progenitors and shunts them to a duct fate. Mech. Dev. 124, 97–107.

Greggio, C., De Franceschi, F., Figueiredo-Larsen, M., Gobaa, S., Ranga, A., Semb, H., Lutolf, M., and Grapin-Botton, A. (2013). Artificial three-dimensional niches deconstruct pancreas development in vitro. Development 140, 4452–4462.

Greiner, T.U., Kesavan, G., Ståhlberg, A., and Semb, H. (2009). Rac1 regulates pancreatic islet morphogenesis. BMC Dev. Biol. 9, 2.

Grese, T.A., Sluka, J.P., Bryant, H.U., Cullinan, G.J., Glasebrook, A.L., Jones, C.D., Matsumoto, K., Palkowitz, A.D., Sato, M., Termine, J.D., et al. (1997). Molecular determinants of tissue selectivity in estrogen receptor modulators. Proc. Natl. Acad. Sci. U. S. A. 94, 14105–14110.

Gruber, R., Panayiotou, R., Nye, E., Spencer-Dene, B., Stamp, G., and Behrens, A. (2016). YAP1 and TAZ Control Pancreatic Cancer Initiation in Mice by Direct Up-regulation of JAK–STAT3 Signaling. Gastroenterology 151, 526–539.

Gu, G., Dubauskaite, J., and Melton, D. a (2002). Direct evidence for the pancreatic lineage: NGN3+ cells are islet progenitors and are distinct from duct progenitors. Development 129, 2447–2457.

Haghverdi, L., Büttner, M., Wolf, F.A., Buettner, F., and Theis, F.J. (2016). Diffusion pseudotime robustly reconstructs lineage branching. Nat Methods. 13, 845-848.

Hald, J., Hjorth, J.P., German, M.S., Madsen, O.D., Serup, P., and Jensen, J. (2003). Activated Notch1 prevents differentiation of pancreatic acinar cells and attenuate endocrine development. Dev. Biol. 260, 426–437.

Hald, J., Sprinkel, A.E., Ray, M., Serup, P., Wright, C., and Madsen, O.D. (2008). Generation and Characterization of Ptf1a Antiserum and Localization of Ptf1a in Relation to Nkx6.1 and Pdx1 During the Earliest Stages of Mouse Pancreas Development. J. Histochem. Cytochem. 56, 587–595.

Hale, M.A., Kagami, H., Shi, L., Holland, A.M., Elsässer, H.P., Hammer, R.E., and MacDonald, R.J. (2005). The homeodomain protein PDX1 is required at mid-pancreatic development for the formation of the exocrine pancreas. Dev. Biol. 286, 225–237.

Haumaitre, C., Barbacci, E., Jenny, M., Ott, M.O., Gradwohl, G., and Cereghini, S. (2005). Lack of TCF2/vHNF1 in mice leads to pancreas agenesis. Proc. Natl. Acad. Sci. U. S. A. 102, 1490–1495.

Heasman, S.J., and Ridley, A.J. (2008). Mammalian Rho GTPases: new insights into their functions from in vivo studies. Nat. Rev. Mol. Cell Biol. 9, 690–701.

Hebrok, M., Kim, S.K., and Melton, D.A. (1998). Notochord repression of endodermal Sonic hedgehog permits pancreas development. Genes Dev. 12, 1705–1713.

Henderson, J.R. (1969). Why Are the Islets of Langerhans ? Lancet 294, 469–470.

Henderson, V., Smith, B., Burton, L.J., Randle, D., Morris, M., and Odero-Marah, V.A. (2015). Snail promotes cell migration through PI3K/AKT-dependent Rac1 activation as well as PI3K/AKT-independent pathways during prostate cancer progression. Cell Adhes. Migr. 9, 255–264.

Herrera, P.L. (2000). Adult insulin- and glucagon-producing cells differentiate from two independent cell lineages. Development 127, 2317–2322.

Herrera, P.L., Huarte, J., Sanvito, F., Meda, P., Orci, L., and Vassalli, J.D. (1991). Embryogenesis of the murine endocrine pancreas; early expression of pancreatic polypeptide gene. Development 113, 1257–1265.

Herrera, P.L., Nepote, V., and Delacour, A. (2002). Pancreatic Cell Lineage Analyses in Mice. Endocrine 19, 267–277.

Horn, S., Kobberup, S., Jørgensen, M.C., Kalisz, M., Klein, T., Kageyama, R., Gegg, M., Lickert, H., Lindner, J., Magnuson, M.A., et al. (2012). Mind bomb 1 is required for pancreatic β-cell formation. Proc. Natl. Acad. Sci. U. S. A. 109, 7356–7361.

Huveneers, S., and Danen, E.H.J. (2009). Adhesion signaling - crosstalk between integrins, Src and Rho. J. Cell Sci. 122, 1059–1069.

Iber, D., and Menshykau, D. (2013). The control of branching morphogenesis. Open Biol. 3, 130088.

Inada, A., Nienaber, C., Katsuta, H., Fujitani, Y., Levine, J., Morita, R., Sharma, A., and Bonner-Weir, S. (2008). Carbonic anhydrase II-positive pancreatic cells are progenitors for both endocrine and exocrine pancreas after birth. Proc. Natl. Acad. Sci. U. S. A. 105, 19915–19919.

Jacquemin, P., Yoshitomi, H., Kashima, Y., Rousseau, G.G., Lemaigre, F.P., and Zaret, K.S. (2006). An endothelial-mesenchymal relay pathway regulates early phases of pancreas development. Dev. Biol. 290, 189–199.

Jensen, J., Pedersen, E.E., Galante, P., Hald, J., Heller, R.S., Ishibashi, M., Kageyama, R., Guillemot, F., Serup, P., and Madsen, O.D. (2000). Control of endodermal endocrine development by Hes-1. Nat. Genet. 24, 36–44.

Jo, J., Kang, H., Choi, M.Y., and Koh, D.S. (2005). How noise and coupling induce bursting action potentials in pancreatic {beta}-cells. Biophys. J. 89, 1534–1542.

Jo, J., Choi, M.Y., and Koh, D.S. (2007). Size distribution of mouse Langerhans islets. Biophys. J. 93, 2655–2666.

Jo, J., Kilimnik, G., Kim, A., Guo, C., Periwal, V., and Hara, M. (2011). Formation of pancreatic islets involves coordinated expansion of small islets and fission of large interconnected islet-like structures. Biophys. J. 101, 565–574.

Jo, J., Hara, M., Ahlgren, U., Sorenson, R.L., and Periwal, V. (2012). Mathematical models of pancreatic islet size distributions. Islets 4, 10–19.

Johansson, K. a, Dursun, U., Jordan, N., Gu, G., Beermann, F., Gradwohl, G., and Grapin-Botton, A. (2007). Temporal control of neurogenin3 activity in pancreas progenitors reveals competence windows for the generation of different endocrine cell types. Dev. Cell 12, 457–465.

Jonckheere, N., Mayes, E., Shih, H.P., Li, B., Lioubinski, O., Dai, X., and Sander, M. (2008). Analysis of mPygo2 mutant mice suggests a requirement for mesenchymal Wnt signaling in pancreatic growth and differentiation. Dev. Biol. 318, 224–235.

Jones, E.A. V., le Noble, F., and Eichmann, A. (2006). What Determines Blood Vessel Structure? Genetic Prespecification vs. Hemodynamics. Physiology 21, 388–395.

Jung, J., Zheng, M., Goldfarb, M., and Zaret, K.S. (1999). Initiation of mammalian liver development from endoderm by fibroblast growth factors. Science 284, 1998–2003.

Kageyama, R., Ohtsuka, T., and Kobayashi, T. (2007). The Hes gene family: repressors and oscillators that orchestrate embryogenesis. Development 134, 1243–1251.

Kanai-Azuma, M., Kanai, Y., Gad, J.M., Tajima, Y., Taya, C., Kurohmaru, M., Sanai, Y., Yonekawa, H., Yazaki, K., Tam, P.P.L., et al. (2002). Depletion of definitive gut endoderm in Sox17-null mutant mice. Development 129, 2367–2379.

Kawaguchi, Y., Cooper, B., Gannon, M., Ray, M., MacDonald, R.J., and Wright, C.V.E. (2002). The role of the transcriptional regulator Ptf1a in converting intestinal to pancreatic progenitors. Nat. Genet. 32, 128–134.

Kesavan, G., Sand, F.W., Greiner, T.U., Johansson, J.K., Kobberup, S., Wu, X., Brakebusch, C., and Semb, H. (2009). Cdc42-Mediated Tubulogenesis Controls Cell Specification. Cell 139, 791–801.

Kesavan, G., Lieven, O., Mamidi, A., Ohlin, Z.L., Johansson, J.K., Li, W.-C., Lommel, S., Greiner, T.U., and Semb, H. (2014). Cdc42/N-WASP signaling links actin dynamics to pancreatic cell delamination and differentiation. Development 141, 685–696.

Kharouta, M., Miller, K., Kim, A., Wojcik, P., Kilimnik, G., Dey, A., Steiner, D.F., and Hara, M. (2009). No mantle formation in rodent islets-The prototype of islet revisited. Diabetes Res. Clin. Pract. 85, 252–257.

Kilimnik, G., Kim, A., Jo, J., Miller, K., and Hara, M. (2009). Quantification of pancreatic islet distribution in situ in mice. Am. J. Physiol. Endocrinol. Metab. 297, E1331-8.

Kilimnik, G., Jo, J., Periwal, V., Zielinski, M.C., and Hara, M. (2012). Quantification of islet size and architecture. Islets 4, 167–172.

Kim, S.K., Hebrok, M., and Melton, D.A. (1997). Notochord to endoderm signaling is required for pancreas development. Development 124, 4243–4252.

Klein, A.M., and Simons, B.D. (2011). Universal patterns of stem cell fate in cycling adult tissues. Development 138, 3103–3111.

Knoblich, J.A. (2008). Mechanisms of Asymmetric Stem Cell Division. Cell 132, 583–597.

Kopinke, D., Brailsford, M., Shea, J.E., Leavitt, R., Scaife, C.L., and Murtaugh, L.C. (2011). Lineage tracing reveals the dynamic contribution of Hes1+ cells to the developing and adult pancreas. Development 138, 431–441.

Kopp, J.L., Dubois, C.L., Schaffer, A.E., Hao, E., Shih, H.P., Seymour, P. a, Ma, J., and Sander, M. (2011). Sox9+ ductal cells are multipotent progenitors throughout development but do not produce new endocrine cells in the normal or injured adult pancreas. Development 138, 653–665.

Kosanam, H., Prassas, I., Chrystoja, C.C., Soleas, I., Chan, A., Dimitromanolakis, A., Blasutig, I.M., Rückert, F., Gruetzmann, R., Pilarsky, C., et al. (2013). Laminin, gamma 2 (LAMC2): A Promising New Putative Pancreatic Cancer Biomarker Identified by Proteomic Analysis of Pancreatic Adenocarcinoma Tissues. Mol. Cell. Proteomics 12, 2820–2832.

Krijthe, J.H. (2015). Rtsne: T-Distributed Stochastic Neighbor Embedding using a Barnes-Hut Implementation.

Kumar, M., and Melton, D. (2003). Pancreas specification: A budding question. Curr. Opin. Genet. Dev. 13, 401–407.

Lammert, E., Cleaver, O., and Melton, D. (2001). Induction of pancreatic differentiation by signals from blood vessels. Science 294, 564–567.

Lawson, W.E., Polosukhin, V. V., Milstone, A.P., Egunova, S.M., Kulipanov, A.G., Tchuvakin, S.G., Massion, P.P., and Blackwell, T.S. (2007). Association of progressive structural changes in the bronchial epithelium with subepithelial fibrous remodeling: A potential role for hypoxia. Virchows Arch. 451, 793–803.

Li, H.J., Kapoor, A., Giel-Moloney, M., Rindi, G., and Leiter, A.B. (2012). Notch signaling differentially regulates the cell fate of early endocrine precursor cells and their maturing descendants in the mouse pancreas and intestine. Dev. Biol. 371, 156–169.

Li, X.Y., Zhai, W.J., and Teng, C.B. (2015). Notch signaling in pancreatic development. Int. J. Mol. Sci. 17, 1–19.

Li, Z., Manna, P., Kobayashi, H., Spilde, T., Bhatia, A., Preuett, B., Prasadan, K., Hembree, M., and Gittes, G.K. (2004). Multifaceted pancreatic mesenchymal control of epithelial lineage selection. Dev. Biol. 269, 252–263.

Lim, A., Shin, K., Zhao, C., Kawano, S., and Beachy, P.A. (2014). Spatially restricted Hedgehog signalling regulates HGF-induced branching of the adult prostate. Nat. Cell Biol. 16, 1135–1145.

Lindsay, T.H., Halvorson, K.G., Peters, C.M., Ghilardi, J.R., Kuskowski, M.A., Wong, G.Y., and Mantyh, P.W. (2006). A quantitative analysis of the sensory and sympathetic innervation of the mouse pancreas. Neuroscience 137, 1417–1426.

Livet, J., Weissman, T.A., Kang, H., Draft, R.W., Lu, J., Bennis, R.A., Sanes, J.R., and Lichtman, J.W. (2007). Transgenic strategies for combinatorial expression of fluorescent proteins in the nervous system. Nature 450, 56–62.

Lu, C.-K., Lai, Y.-C., Chen, H.-R., and Chiang, M.K. (2012). Rbms3, an RNA-Binding Protein, Mediates the Expression of Ptf1a by Binding to Its 3'UTR During Mouse Pancreas Development. DNA Cell Biol. 31, 1245–1251.

Ma, D.F., Sudo, K., Tezuka, H., Kondo, T., Nakazawa, T., Niu, D.F., Kawasaki, T., Mochizuki, K., Yamane, T., and Katoh, R. (2010). Polyclonal origin of hormone-producing cell populations evaluated as a direct in situ demonstration in EGFP/BALB/C chimeric mice. J. Endocrinol. 207, 17–25.

Van Der Maaten, L., Hinton, G., and van der Maaten, G.H. (2008). Visualizing Data using t-SNE.

Magenheim, J., Ilovich, O., Lazarus, A., Klochendler, A., Ziv, O., Werman, R., Hija, A., Cleaver, O., Mishani, E., Keshet, E., et al. (2011). Blood vessels restrain pancreas branching, differentiation and growth. Development 138, 4743–4752.

Martin, M., Gallego-Llamas, J., Ribes, V., Kedinger, M., Niederreither, K., Chambon, P., Dollé, P., and Gradwohl, G. (2005). Dorsal pancreas agenesis in retinoic acid-deficient Raldh2 mutant mice. Dev. Biol. 284, 399–411.

Marty-Santos, L., and Cleaver, O. (2016). Pdx1 regulates pancreas tubulogenesis and E-cadherin expression. Development 143, 1056–1056.

Mascré, G., Dekoninck, S., Drogat, B., Youssef, K.K., Brohée, S., Sotiropoulou, P.A., Simons, B.D., and Blanpain, C. (2012). Distinct contribution of stem and progenitor cells to epidermal maintenance. Nature 489, 257–262.

Masui, T., Swift, G.H., Deering, T., Shen, C., Coats, W.S., Long, Q., Elsässer, H.P., Magnuson, M.A., and MacDonald, R.J. (2010). Replacement of Rbpj With Rbpjl in the PTF1 Complex Controls the Final Maturation of Pancreatic Acinar Cells. Gastroenterology 139, 270–280.

Mellado-Gil, J., Rosa, T.C., Demirci, C., Gonzalez-Pertusa, J.A., Velazquez-Garcia, S., Ernst, S., Valle, S., Vasavada, R.C., Stewart, A.F., Alonso, L.C., et al. (2011). Disruption of hepatocyte growth factor/c-Met signaling enhances pancreatic β-cell death and accelerates the onset of diabetes. Diabetes 60, 525–536.

Miettinen, P.J., Huotari, M., Koivisto, T., Ustinov, J., Palgi, J., Rasilainen, S., Lehtonen, E., Keski-Oja, J., and Otonkoski, T. (2000). Impaired migration and delayed differentiation of pancreatic islet cells in mice lacking EGF-receptors. Development 127, 2617–2627.

Miller, K., Kim, A., Kilimnik, G., Jo, J., Moka, U., Periwal, V., and Hara, M. (2009). Islet formation during the neonatal development in mice. PLoS One 4.

Miralles, F., Czernichow, P., Ozaki, K., Itoh, N., and Scharfmann, R. (1999). Signaling through fibroblast growth factor receptor 2b plays a key role in the development of the exocrine pancreas. Proc. Natl. Acad. Sci. U. S. A. 96, 6267–6272.

Miyatsuka, T., Kosaka, Y., Kim, H., and German, M.S. (2011). Neurogenin3 inhibits proliferation in endocrine progenitors by inducing Cdkn1a. Proc. Natl. Acad. Sci. 108, 185–190.

Molotkov, A., Molotkova, N., and Duester, G. (2005). Retinoic acid generated by Raldh2 in mesoderm is required for mouse dorsal endodermal pancreas development. Dev. Dyn. 232, 950–957.

Morvaridi, S., Dhall, D., Greene, M.I., Pandol, S.J., and Wang, Q. (2015). Role of YAP and TAZ in pancreatic ductal adenocarcinoma and in stellate cells associated with cancer and chronic pancreatitis. Sci. Rep. 5, 16759.

Murtaugh, L.C., Stanger, B.Z., Kwan, K.M., and Melton, D.A. (2003). Notch signaling controls multiple steps of pancreatic differentiation. Proc. Natl. Acad. Sci. U. S. A. 100, 14920–14925.

Murtaugh, L.C., Law, A.C., Dor, Y., and Melton, D.A. (2005). Beta-catenin is essential for pancreatic acinar but not islet development. Development 132, 4663–4674.

Nakhai, H., Siveke, J.T., Mendoza-Torres, L., and Schmid, R.M. (2008). Conditional inactivation of Myc impairs development of the exocrine pancreas. Development 135, 3191–3196.

Ninov, N., Borius, M., and Stainier, D.Y.R. (2012). Different levels of Notch signaling regulate quiescence, renewal and differentiation in pancreatic endocrine progenitors. Development 139, 1557–1567.

Oike, Y., Ito, Y., Hamada, K., Zhang, X.-Q., Miyata, K., Arai, F., Inada, T., Araki, K., Nakagata, N., Takeya, M., et al. (2002). Regulation of vasculogenesis and angiogenesis by EphB/ephrin-B2 signaling between endothelial cells and surrounding mesenchymal cells. Blood 100, 1326–1333.

Pagliuca, F.W., and Melton, D.A. (2013). How to make a functional -cell. Development 140, 2472–2483.

Pagliuca, F.W., Millman, J.R., Gürtler, M., Segel, M., Van Dervort, A., Ryu, J.H., Peterson, Q.P., Greiner, D., and Melton, D.A. (2014). Generation of functional human pancreatic β cells in vitro. Cell 159, 428–439.

Pan, F.C., and Wright, C.V.E. (2011). Pancreas organogenesis: From bud to plexus to gland. Dev. Dyn. 240, 530–565.

Pan, F.C., Bankaitis, E.D., Boyer, D., Xu, X., Van de Casteele, M., Magnuson, M. a, Heimberg, H., and Wright, C.V.E. (2013). Spatiotemporal patterns of multipotentiality in Ptf1a-expressing cells during pancreas organogenesis and injury-induced facultative restoration. Development 140, 751–764.

Petzold, K.M., and Spagnoli, F.M. (2012). A System for ex vivo Culturing of Embryonic Pancreas. J. Vis. Exp.

Petzold, K.M., Naumann, H., and Spagnoli, F.M. (2013). Rho signalling restriction by the RhoGAP Stard13 integrates growth and morphogenesis in the pancreas. Development 140, 126–135.

Picelli, S., Faridani, O.R., Björklund, A.K., Winberg, G., Sagasser, S., and Sandberg, R. (2014). Full-length RNA-seq from single cells using Smart-seq2. Nat. Protoc. 9, 171–181.

Pierreux, C.E., Cordi, S., Hick, A.C., Achouri, Y., Ruiz de Almodovar, C., Prévot, P.P., Courtoy, P.J., Carmeliet, P., and Lemaigre, F.P. (2010). Epithelial: Endothelial cross-talk regulates exocrine differentiation in developing pancreas. Dev. Biol. 347, 216–227.

Pin, C.L., Rukstalis, J.M., Johnson, C., and Konieczny, S.F. (2001). The bHLH transcription factor Mist1 is required to maintain exocrine pancreas cell organization and acinar cell identity. J. Cell Biol. 155, 519–530.

Poliakov, A., Cotrina, M., and Wilkinson, D.G. (2004). Diverse roles of eph receptors and ephrins in the regulation of cell migration and tissue assembly. Dev. Cell 7, 465–480.

Pulkkinen, Mari-Anne, Spencer-Dene, Bradley, Dickson, Clive, Otonkoski, T. (2003). The IIIb isoform of fibroblast growth factor receptor 2 is required for proper growth and branching of pancreatic ductal epithelium but not for differentiation of exocrine or endocrine cells. Mech. Dev. 120, 167–175.

Puri, S., and Hebrok, M. (2007). Dynamics of embryonic pancreas development using real-time imaging. Dev. Biol. 306, 82–93.

Qu, X., Afelik, S., Jensen, J.N., Bukys, M.A., Kobberup, S., Schmerr, M., Xiao, F., Nyeng, P., Veronica Albertoni, M., Grapin-Botton, A., et al. (2013). Notch-mediated post-translational control of Ngn3 protein stability regulates pancreatic patterning and cell fate commitment. Dev. Biol. 376, 1–12.

Risau, W., and Flamme, I. (1995). Vasculogenesis. Annu. Rev. Cell Dev. Biol. 11, 73–91.

Rosenfield, S.M., Bowden, E.T., Cohen-Missner, S., Gibby, K.A., Ory, V., Henke, R.T., Riegel, A.T., and Wellstein, A. (2012). Pleiotrophin (PTN) Expression and Function and in the Mouse Mammary Gland and Mammary Epithelial Cells. PLoS One 7.

Rossi, J.M., Dunn, N.R., Hogan, B.L.M., and Zaret, K.S. (2001). Distinct mesodermal signals, including BMPs from the septum transversum mesenchyme, are required in combination for hepatogenesis from the endoderm. Genes Dev. 15, 1998–2009.

Rovira, M., Scott, S.-G., Liss, A.S., Jensen, J., Thayer, S.P., and Leach, S.D. (2010). Isolation and characterization of centroacinar/terminal ductal progenitor cells in adult mouse pancreas. Proc. Natl. Acad. Sci. U. S. A. 107, 75–80.

Roy, E., Neufeld, Z., Livet, J., Khosrotehrani, K. (2014). Concise Review : Understanding Clonal Dynamics in Homeostasis and Injury Through Multicolor Lineage Tracing. Stem Cells 32, 3046–3054.

Rukstalis, J.M., and Habener, J.F. (2007). Snail2, a mediator of epithelial-mesenchymal transitions, expressed in progenitor cells of the developing endocrine pancreas. Gene Expr. Patterns 7, 471–479.

Rukstalis, J.M., and Habener, J.F. (2009). Neurogenin3: a master regulator of pancreatic islet differentiation and regeneration. Islets 1, 177–184.

Sato, T., van Es, J.H., Snippert, H.J., Stange, D.E., Vries, R.G., van den Born, M., Barker, N., Shroyer, N.F., van de Wetering, M., and Clevers, H. (2011). Paneth cells constitute the niche for Lgr5 stem cells in intestinal crypts. Nature 469, 415–418.

Schaffer, A.E., Freude, K.K., Nelson, S.B., and Sander, M. (2010). Nkx6 transcription factors and Ptf1a function as antagonistic lineage determinants in multipotent pancreatic progenitors. Dev. Cell 18, 1022–1029.

Scheele, C.L.G.J., Hannezo, E., Muraro, M.J., Zomer, A., Langedijk, N.S.M., Oudenaarden, A. van, Simons, B.D., and Rheenen, J. van (2017). Identity and dynamics of mammary stem cells during 2 branching morphogenesis. Nature 542, 313-317.

Schnell, U., Cirulli, V., and Giepmans, B.N.G. (2013). EpCAM: Structure and function in health and disease. Biochim. Biophys. Acta - Biomembr. 1828, 1989–2001.

Seaberg, R.M., Smukler, S.R., Kieffer, T.J., Enikolopov, G., Asghar, Z., Wheeler, M.B., Korbutt, G., and van der Kooy, D. (2004). Clonal identification of multipotent precursors from adult mouse pancreas that generate neural and pancreatic lineages. Nat. Biotechnol. 22, 1115–1124.

Seymour, P.A., Bennett, W.R., and Slack, J.M. (2004). Fission of pancreatic islets during postnatal growth of the mouse. J Anat 204, 103–116.

Seymour, P.A., Freude, K.K., Tran, M.N., Mayes, E.E., Jensen, J., Kist, R., Scherer, G., and Sander, M. (2007). SOX9 is required for maintenance of the pancreatic progenitor cell pool. Proc. Natl. Acad. Sci. U. S. A. 104, 1865–1870.

Seymour, P.A., Shih, H.P., Patel, N.A., Freude, K.K., Xie, R., Lim, C.J., and Sander, M. (2012). A Sox9/Fgf feed-forward loop maintains pancreatic organ identity. Development 139, 3363–3372.

Shih, H.P., Kopp, J.L., Sandhu, M., Dubois, C.L., Seymour, P.A., Grapin-Botton, A., and Sander, M. (2012). A Notch-dependent molecular circuitry initiates pancreatic endocrine and ductal cell differentiation. Development 139, 2488–2499.

Shih, H.P., Wang, A., and Sander, M. (2013). Pancreas Organogenesis: From Lineage Determination to Morphogenesis. Annu. Rev. Cell Dev. Biol. 29, 81–105.

Shih, H.P., Panlasigui, D., Cirulli, V., and Sander, M. (2016). ECM Signaling Regulates Collective Cellular Dynamics to Control Pancreas Branching Morphogenesis. Cell Rep. 14, 169–179.

Smukler, S.R., Arntfield, M.E., Razavi, R., Bikopoulos, G., Karpowicz, P., Seaberg, R., Dai, F., Lee, S., Ahrens, R., Fraser, P.E., et al. (2011). The adult mouse and human pancreas contain rare multipotent stem cells that express insulin. Cell Stem Cell 8, 281–293.

Sneddon, J.B., Borowiak, M., and Melton, D.A. (2012). Self-renewal of embryonic-stem-cell-derived progenitors by organ-matched mesenchyme. Nature.

Snippert, H.J., van der Flier, L.G., Sato, T., van Es, J.H., van den Born, M., Kroon-Veenboer, C., Barker, N., Klein, A.M., van Rheenen, J., Simons, B.D., et al. (2010). Intestinal crypt homeostasis results from neutral competition between symmetrically dividing Lgr5 stem cells. Cell 143, 134–144.

Solar, M., Cardalda, C., Houbracken, I., Martín, M., Maestro, M.A., De Medts, N., Xu, X., Grau, V., Heimberg, H., Bouwens, L., et al. (2009). Pancreatic exocrine duct cells give rise to insulin-producing beta cells during embryogenesis but not after birth. Dev. Cell 17, 849–860.

Sonnenberg, E., Weidner, K., and Birchmeier, C. (1993). Expression of the met-receptor and its ligand, HGF-SF during mouse embryogenesis. EXS. 65, 381–394.

Spence, J.R., Lange, A.W., Lin, S.C.J., Kaestner, K.H., Lowy, A.M., Kim, I., Whitsett, J.A., and Wells, J.M. (2009). Sox17 Regulates Organ Lineage Segregation of Ventral Foregut Progenitor Cells. Dev. Cell 17, 62–74.

Stafford, D., and Prince, V.E. (2002). Retinoic acid signaling is required for a critical early step in zebrafish pancreatic development. Curr. Biol. 12, 1215–1220.

Stanger, B.Z., Tanaka, A.J., and Melton, D.A. (2007). Organ size is limited by the number of embryonic progenitor cells in the pancreas but not the liver. Nature 445, 886–891.

Strobel, O., Dor, Y., Alsina, J., and Stirman, A. (2007). In vivo lineage tracing defines the role of acinar-to-ductal transdifferentiation in inflammatory ductal metaplasia. Gastroenterology 133, 1999–2009.

Tarifeño-Saldivia, E., Lavergne, A., Bernard, A., Padamata, K., Bergemann, D., Voz, M.L., Manfroid, I., and Peers, B. (2017). Transcriptome analysis of pancreatic cells across distant species highlights novel important regulator genes. BMC Biol. 15, 21.

Thompson, N., Gesina, E., Scheinert, P., Bucher, P., and Grapin-Botton, A. (2012). RNA Profiling and Chromatin Immunoprecipitation-Sequencing Reveal that PTF1a Stabilizes Pancreas Progenitor Identity via the Control of MNX1/HLXB9 and a Network of Other Transcription Factors. Mol. Cell. Biol. 32, 1189–1199.

Thorel, F., Népote, V., Avril, I., Kohno, K., Desgraz, R., Chera, S., and Herrera, P.L. (2010). Conversion of adult pancreatic alpha-cells to beta-cells after extreme beta-cell loss. Nature 464, 1149–1154.

Trzpis, M., McLaughlin, P.M.J., de Leij, L.M.F.H., and Harmsen, M.C. (2007). Epithelial cell adhesion molecule: more than a carcinoma marker and adhesion molecule. Am. J. Pathol. 171, 386–395.

Tsai, Y.H., Hill, D.R., Kumar, N., Huang, S., Chin, A.M., Dye, B.R., Nagy, M.S., Verzi, M.P., and Spence, J.R. (2016). LGR4 and LGR5 Function Redundantly During Human Endoderm Differentiation. Cell Mol Gastroenterol Hepatol. 2, 648–662.e8.

Ventura, A., Kirsch, D.G., McLaughlin, M.E., Tuveson, D.A., Grimm, J., Lintault, L., Newman, J., Reczek, E.E., Weissleder, R., and Jacks, T. (2007). Restoration of p53 function leads to tumour regression *in vivo*. Nature 445, 661–665.

Villasenor, A., Chong, D.C., and Cleaver, O. (2008). Biphasic Ngn3 expression in the developing pancreas. Dev. Dyn. 237, 3270–3279.

Villasenor, A., Chong, D.C., Henkemeyer, M., Cleaver, O., Andrew, D.J., Ewald, A.J., Batlle, E., Henderson, J.T., Beghtel, H., Born, M.M. van den, et al. (2010). Epithelial dynamics of pancreatic branching morphogenesis. Development 137, 4295–4305.

Visvader, J.E., and Clevers, H. (2016). Tissue-specific designs of stem cell hierarchies. Nat. Cell Biol. 18, 349–355.

Wang, J., Kilic, G., Aydin, M., Burke, Z., Oliver, G., and Sosa-Pineda, B. (2005). Prox1 activity controls pancreas morphogenesis and participates in the production of “secondary transition” pancreatic endocrine cells. Dev. Biol. 286, 182–194.

Wang, S., Zhang, J., Zhao, A., Hipkens, S., Magnuson, M.A., and Gu, G. (2007). Loss of Myt1 function partially compromises endocrine islet cell differentiation and pancreatic physiological function in the mouse. Mech. Dev. 124, 898–910.

Wang, S., Hecksher-Sorensen, J., Xu, Y., Zhao, A., Dor, Y., Rosenberg, L., Serup, P., and Gu, G. (2008). Myt1 and Ngn3 form a feed-forward expression loop to promote endocrine islet cell differentiation. Dev. Biol. 317, 531–540.

Wang, S., Yan, J., Anderson, D. a, Xu, Y., Kanal, M.C., Cao, Z., Wright, C.V.E., and Gu, G. (2010). Neurog3 gene dosage regulates allocation of endocrine and exocrine cell fates in the developing mouse pancreas. Dev. Biol. 339, 26–37.

Weigelin, B., Bakker, G.-J., and Friedl, P. (2016). Third harmonic generation microscopy of cells and tissue organization. J. Cell Sci. 129, 245–255.

Wells, J.M., Esni, F., Boivin, G.P., Aronow, B.J., Stuart, W., Combs, C., Sklenka, A., Leach, S.D., and Lowy, A.M. (2007). Wnt/beta-catenin signaling is required for development of the exocrine pancreas. BMC Dev. Biol. 7, 4.

Westmoreland, J.J., Kilic, G., Sartain, C., Sirma, S., Blain, J., Rehg, J., Harvey, N., and Sosa-Pineda, B. (2012). Pancreas-specific deletion of Prox1 affects development and disrupts homeostasis of the exocrine pancreas. Gastroenterology 142, 999–1009.e6.

Wu, T.D., and Nacu, S. (2010). Fast and SNP-tolerant detection of complex variants and splicing in short reads. Bioinformatics 26, 873–881.

Wu, P.-C., Hsieh, T.-Y., Tsai, Z.-U., and Liu, T.-M. (2015). In vivo Quantification of the Structural Changes of Collagens in a Melanoma Microenvironment with Second and Third Harmonic Generation Microscopy. Sci. Rep. 5, 8879.

Xu, X., D'Hoker, J., Stangé, G., Bonné, S., De Leu, N., Xiao, X., Van de Casteele, M., Mellitzer, G., Ling, Z., Pipeleers, D., et al. (2008). Beta cells can be generated from endogenous progenitors in injured adult mouse pancreas. Cell 132, 197–207.

Yoshitomi, H., and Zaret, K.S. (2004). Endothelial cell interactions initiate dorsal pancreas development by selectively inducing the transcription factor Ptf1a. Development 131, 807–817.

Zhou, Q., Law, A.C., Rajagopal, J., Anderson, W.J., Gray, P.A., and Melton, D.A. (2007). A Multipotent Progenitor Domain Guides Pancreatic Organogenesis. Dev. Cell 13, 103–114.

Appendix A

This Thesis has contributed to the following manuscripts:

- “Defining lineage potential and fate behaviour during pancreas development.” Sznurkowska et al. 2017, in review
- “Deciphering islet morphogenesis with ubiquitous lineage tracing” Sznurkowska et al. 2017, manuscript in preparation

During the PhD I carried out research that has not been described in the thesis. My analysis of embryonic pancreata contributed to the following publication:

“Multi-site Neurogenin3 Phosphorylation Controls Pancreatic Endocrine Differentiation.” Azzarelli, Hurley, Sznurkowska et al. 2017, Dev. Cell.